

Final Report
FDOT Contract Number: BDV24-977-29

**Comparison of Standard Penetration Test (SPT) N-value with
Alternative Field Test Methods in Determining Moduli for
Settlement Predictions**



Principal Investigators: Manoj Chopra, Ph.D., P.E., Professor
Luis G. Arboleda-Monsalve, Ph.D., Assistant Professor

Project Manager: Larry Jones



University of Central Florida
Department of Civil, Environmental, and Construction Engineering
College of Engineering and Computer Science
Orlando, Florida 32816

September 2020

DISCLAIMER

The opinions, findings, and conclusions expressed in this publication are those of the authors and not necessarily those of the State of Florida Department of Transportation.

UNIT CONVERSIONS

APPROXIMATE CONVERSION TO SI UNITS

SYMBOL	WHEN YOU KNOW	MULTIPLY BY	TO FIND	SYMBOL
LENGTH				
in	inches	25.4	millimeters	mm
ft	feet	0.305	meters	m
yd	yards	0.914	meters	m
mi	miles	1.61	kilometers	km

SYMBOL	WHEN YOU KNOW	MULTIPLY BY	TO FIND	SYMBOL
AREA				
in²	square inches	645.2	square millimeters	mm ²
ft²	square feet	0.093	square meters	m ²
yd²	square yard	0.836	square meters	m ²
ac	acres	0.405	hectares	ha
mi²	square miles	2.59	square kilometers	km ²

SYMBOL	WHEN YOU KNOW	MULTIPLY BY	TO FIND	SYMBOL
VOLUME				
fl oz	fluid ounces	29.57	milliliters	mL
gal	gallons	3.785	liters	L
ft³	cubic feet	0.028	cubic meters	m ³
yd³	cubic yards	0.765	cubic meters	m ³

SYMBOL	WHEN YOU KNOW	MULTIPLY BY	TO FIND	SYMBOL
MASS				
oz	ounces	28.35	grams	g
lb	pounds	0.454	kilograms	kg
T	short tons (2000 lb)	0.907	megagrams (or "metric ton")	Mg (or "t")

SYMBOL	WHEN YOU KNOW	MULTIPLY BY	TO FIND	SYMBOL
TEMPERATURE				
°F	Fahrenheit	5 (F-32)/9 or (F-32)/1.8	Celsius	°C

SYMBOL	WHEN YOU KNOW	MULTIPLY BY	TO FIND	SYMBOL
FORCE and PRESSURE or STRESS				
lbf	pound force	4.45	newtons	N
lbf/in²	pound force per square inch	6.89	kilopascals	kPa
lbf	pound force	0.001	kip (kilopounds)	kip

APPROXIMATE CONVERSION TO IMPERIAL UNITS

SYMBOL	WHEN YOU KNOW	MULTIPLY BY	TO FIND	SYMBOL
LENGTH				
mm	millimeters	0.039	inches	in
m	meters	3.28	feet	ft
m	meters	1.09	yards	yd
km	kilometers	0.621	miles	mi

SYMBOL	WHEN YOU KNOW	MULTIPLY BY	TO FIND	SYMBOL
AREA				
mm²	square millimeters	0.0016	square inches	in ²
m²	square meters	10.764	square feet	ft ²
m²	square meters	1.195	square yards	yd ²
ha	hectares	2.47	acres	ac
km²	square kilometers	0.386	square miles	mi ²

SYMBOL	WHEN YOU KNOW	MULTIPLY BY	TO FIND	SYMBOL
VOLUME				
mL	milliliters	0.034	fluid ounces	fl oz
L	liters	0.264	gallons	gal
m³	cubic meters	35.314	cubic feet	ft ³
m³	cubic meters	1.307	cubic yards	yd ³

SYMBOL	WHEN YOU KNOW	MULTIPLY BY	TO FIND	SYMBOL
MASS				
g	grams	0.035	ounces	oz
kg	kilograms	2.202	pounds	lb
Mg (or "t")	megagrams (or "metric ton")	1.103	short tons (2000 lb)	T

SYMBOL	WHEN YOU KNOW	MULTIPLY BY	TO FIND	SYMBOL
TEMPERATURE				
°C	Celsius	1.8C+32	Fahrenheit	°F

SYMBOL	WHEN YOU KNOW	MULTIPLY BY	TO FIND	SYMBOL
FORCE and PRESSURE or STRESS				
N	newtons	0.225	pound force	lbf
kPa	kilopascals	0.145	pound force per square inch	lbf/in ²
kip	kip (kilopounds)	1000	pound force	lbf

TECHNICAL REPORT DOCUMENTATION PAGE

1. Report No. Draft Final	2. Government Accession No.	3. Recipient's Catalog No.	
4. Title and Subtitle Comparison of Standard Penetration Test (SPT) N-value with Alternative Field Test Methods in Determining Moduli for Settlement Predictions		5. Report Date September 2020	
		6. Performing Organization Code	
7. Author (s) Manoj Chopra and Luis G. Arboleda-Monsalve		8. Performing Organization Report No.	
9. Performing Organization Name and Address Department of Civil, Environmental, and Construction Engineering University of Central Florida		10. Work Unit No. (TRAIS)	
		11. Contract or Grant No. BDV24-977-29	
12. Sponsoring Agency Name and Address Florida Department of Transportation 605 Suwannee Street, MS 30 Tallahassee, FL 32366 – 6580		13. Type of Report and Period Covered Draft Final Report February 2018 – September 2020	
		14. Sponsoring Agency Code	
15. Supplementary Notes			
16. Abstract: In the determination of immediate settlements, the stiffness of the soil is a critical parameter. The selected value of the modulus of elasticity is typically obtained from published correlations using blow counts from standard penetration tests and tip or skin friction resistances from cone penetration tests. Other methods include the use of dilatometer, pressuremeter, and geophysical seismic tests. Numerous correlations can be used to calculate the modulus of elasticity of the soil. Due to the uncertainty in obtaining adequate elastic moduli for designs, engineers typically use conservative approaches to mitigate risks. Lack of knowledge of the most appropriate field test method and correlation to obtain accurate moduli causes the engineer typically to assign a conservative value, which often leads to overpredictions of ground surface settlements. A comprehensive evaluation of the methods used to determine the modulus of elasticity and calculate immediate settlements is necessary for the granular soil conditions in Florida. At a site at the University of Central Florida, full-scale tests were conducted to measure immediate settlements in a soil profile typical of Florida granular soil conditions. Three conical load tests and a comprehensive laboratory testing program were conducted, and the results are presented to understand the main variables involved in the geotechnical mechanisms that govern immediate settlements in Florida. Numerical finite element analyses were also conducted to provide guidance for researchers and practitioners on an alternative way of calculating immediate settlements using two constitutive models: hardening soil and hardening soil small, which can be easily calibrated from correlations with relative density of granular soil materials. The numerical model results matched well the measured values from conical load tests presented in this research.			
17. Key Word Settlements, elastic modulus, soil stiffness, field tests, triaxial tests		18. Distribution Statement No Restrictions.	
19. Security Classif. (of this report) Unclassified	20. Security Classif. (of this page) Unclassified	21. No. of Pages 263	22. Price

ACKNOWLEDGEMENTS

The researchers would like to thank the Florida Department of Transportation for its financial support to perform this research and the guidance from the project manager: Larry Jones. The FDOT drilling crew played an important role to accomplish the proposed tasks of this research project. This work would have not been possible without the strong commitment and dedication of the students at UCF: Sergio Marin, A. Felipe Uribe-Henao, Jaime A. Mercado, Alan Aparicio, and Sina Nassiri.

EXECUTIVE SUMMARY

The calculation of immediate settlements for the design of embankments and shallow foundations requires the determination of the loading conditions and stiffness of the underlying materials. In that calculation, the modulus of elasticity of the soil plays a very important role. The modulus of elasticity has been conventionally obtained from published correlations, mostly based on the results of field exploration in terms of standard penetration tests (SPT), cone penetration tests (CPT), dilatometer tests (DMT), pressuremeter tests (PMT), and geophysical seismic tests. Depending on the correlations used to calculate the modulus of elasticity to determine compressibility of the soil, a large scatter of the results of immediate settlement is expected. To solve this issue, engineers tend to adopt conservative approaches which can result in higher construction costs and, at times, in unnecessary ground improvements because lack of knowledge in the selection of such a parameter often leads to overpredictions of ground surface settlements. In this report, a comprehensive evaluation of the methods used to calculate stiffness parameters of the soil and a comprehensive review of the methods to calculate immediate settlements are presented for granular soil types specific to Florida.

A site at the University of Central Florida that has been extensively used in the past for research projects related to deep foundations was selected to conduct full-scale conical load tests to measure immediate settlements in a soil profile typical of Florida conditions. Schmertmann (1993) was the first proponent of a conical load test to measure soil compressibility on a scale between in situ plate and full-scale embankment tests. The method consisted of a gradually constructed cone-shaped mound of soil placed on the ground surface as short- and long-term soil stresses and ground movements are continuously monitored. Conical load tests represent a reliable field test procedure that at a relatively low construction cost, can accurately provide insight into the in situ compressibility characteristics of soils, rather than indirectly determining soil parameters only on the basis of strength field tests such as SPT, CPT, DMT, or PMT. A conical load test is advantageous because of its full-scale nature and because it typically applies pressures to the ground surface large enough to mobilize soil shear strains within the framework of immediate settlements. In addition, large influence zones in the vertical direction are generated in terms of vertical stresses. From this test, useful and realistic compressibility parameters can be obtained for the calculation of immediate settlements.

The site selected for the conical load tests was geotechnically characterized using numerous field tests from past research efforts and those recently made for the development of this project. These data, alongside a comprehensive laboratory testing program consisting of triaxial, constant rate of strain, x-ray diffraction, scanning electron microscope image tests, were used to reproduce soil behavior via finite element numerical simulations. Advanced constitutive soil models were employed to study immediate settlements at the proposed site where full-scale surcharge conical loads were applied. This report summarizes the main variables involved in the geotechnical mechanisms that govern immediate settlements in granular soils in Florida. The results presented herein provide guidance for practitioners and researchers in the area about the most suitable correlations for elastic modulus and immediate settlement procedures that compared well with the measured values with the conical load tests. Guidance on the calibration of constitutive soil

parameters for two soil models: hardening soil and hardening soil small are presented in this report. The models can be easily calibrated from correlations with relative density of the granular soil material and can be used to provide a more accurate alternative method of calculation of immediate settlements. The models presented in this report matched well those measured from conical load tests.

The following items describe the contents of this report and summarize the main findings:

1. A compilation of correlations for modulus of elasticity and immediate settlement methods found in the technical literature are presented herein. A comprehensive field and laboratory testing program is also presented to elucidate geomechanical properties that influence compressibility behavior of granular soils in Florida. The correlations presented herein for relative density, friction angle, small strain shear modulus, shear wave velocity, coefficient of earth pressure at rest, and elastic modulus can be used as the main input parameters for the computation of immediate settlements in granular soils in Florida. This was based on the assertive comparison between computed and measured values with the conical load tests.
2. An evaluation of variables that influence the settlement or compressibility response of soils when measured via conical load testing is presented. The conclusion is that this type of full-scale test constitutes a very practical soil-structure interaction problem, being the structure the conical load arrangement, where the relative stiffness of the participating components play an important role. The interaction between both systems (i.e., soils and conical load arrangement) for the calculation of immediate settlements depends greatly on the sequence of loading and strength-stress-strain characteristics of soils and applied loading.
3. Recommendations are provided for the proper selection of soil modulus depending on the expected strain levels during field or laboratory testing or during constructions. The authors found that for the calculation of elastic modulus, and in general for the determination of soil stiffness parameters, the strain level that the soil is subjected to causes a large impact in the computed settlements since soil stiffness decreases as a function of the mobilized strains due to the applied loading. The dependency of the soil stiffness on the strain level, which occurs for shear strains lower than 10^{-3} %, plays a very important role in the determination of ground deformations. The inclusion of small strain soil behavior in the design process plays an important role in the computation of settlements.
4. A detailed analysis is presented based on piezometric readings related to excess porewater pressure buildup as a result of applied surface loadings from the conical load tests. A clear distinction is made between changes in the hydrostatic porewater pressures and excess porewater pressures to assess the type and source of ground surface settlements. This is to corroborate not only the extent of vertical stress influence zones due to conical load testing but also to confirm that other time-dependent changes in volume such as consolidation settlements or secondary compression settlements were not measured. This way, the conclusions drawn in this report are only applicable to immediate settlement calculations. The numerical models also

confirmed that the measured settlements are mostly immediate in nature and are not related to primary consolidation or secondary compression.

5. Results of properly calibrated geotechnical models are presented. Those models reproduced reasonably well the conical load testing sequence of the field tests performed at the UCF site. Recommendations are provided for the calibration of constitutive soil model parameters, mainly as a function of the soil relative density, for the determination of immediate settlements in granular soils in Florida. This report lists useful correlations for the calibration of parameters for the soil models hardening soil and hardening soil small (i.e., HS and HSS), which can be optimized for local soil conditions and can be adapted to match laboratory testing programs.
6. The results computed with the HS model overpredicted the overall measured response. Larger computed vertical strains were mobilized using the HS model (i.e., a certain degree of conservatism was found when ignoring small strain soil behavior). For reliable predictions of ground deformations, the very small strain stiffness and its degradation should be considered in the numerical formulation.
7. The authors found that the following correlations for the calculation of elastic modulus provided conservative and good estimates of the soil stiffness when compared versus those measured with the conical load tests. Using the following correlations, if the input parameters come from reliable field tests, immediate settlement calculations should provide satisfactory results, particularly if those are supplemented and confirmed with well-calibrated numerical models:
 - i. Using the results of SPT tests: Webb (1969), Chaplin (1963), Papadopoulos and Anagnostopoulos (1987), Kulhawy and Mayne (1990), Bowles (1996), FHWA-IF-02-034.
 - ii. Using the results of CPT tests: Buisman (1940), DeBeer (1965), Bachelier and Perez (1965), Vesić (1970), Sanglerat (1972), DeBeer (1974), Schmertmann (1970), Schmertmann (1978).
 - iii. Using the results of DMT tests: Lutenegro and DeGroot (1995) and Bowles (1996).
8. The conical load testing procedure provided a relatively conservative estimate of the immediate settlements at the project site in relation to those computed with other published methods. The authors recommend the use of this type of test to confirm immediate settlements in geotechnical projects in Florida. Conical load tests constitute a straightforward, fast, and reliable way to confirm the amount of immediate settlements expected in a given project, as long as shallow loading conditions are applied and the expected mobilized strains in the project are in the same order of magnitude as those mobilized during the conical loading.

TABLE OF CONTENTS

DISCLAIMER	ii
UNIT CONVERSIONS	iii
TECHNICAL REPORT DOCUMENTATION PAGE	v
ACKNOWLEDGEMENTS	vi
EXECUTIVE SUMMARY	vii
LIST OF FIGURES	xv
LIST OF TABLES	xxi
CHAPTER 1 INTRODUCTION	1
1.1 Research Objectives and Scope of Work.....	2
CHAPTER 2 LITERATURE REVIEW	4
2.1 Methods for Estimating Immediate Settlements on Granular Soils	5
2.1.1 Elastic Half-Space Method	5
2.1.2 Method Proposed by Hough (1959).....	5
2.1.3 Additional Methods	7
2.2 Methods Reported by the FHWA: Geotechnical Engineering Circular No. 6	8
2.2.1 Method Proposed by Hough (1959).....	8
2.2.2 Method Proposed by D'Appolonia et al. (1968)	8
2.3 Additional Methods for Settlement Calculation	10
2.3.1 Method Proposed by Schmertmann (1970)	10
2.3.2 Method Proposed by Schmertmann et al. (1978).....	12
2.3.3 Method Proposed by Oweis (1979)	12
2.4 Additional Elastic Approaches Commonly Used in Practice	17
2.4.1 Method Proposed by Webb (1969)	17
2.4.2 Method Proposed by Tschebotarioff (1971)	17
2.4.3 Method Proposed by Poulos and Davis (1974).....	18
2.4.4 Method Proposed by Bowles (1987).....	19
2.4.5 Berardi et al. (1991)	21
2.4.6 Method Proposed by Papadopoulos (1992)	24
2.4.7 Method Proposed by Mayne and Poulos (1999).....	26

2.5 Methods for Computing Settlements on Granular Soils Based on Field Tests	28
2.5.1 Correlations Based on SPT Tests.....	29
2.5.1.1 Terzaghi et al. (1967).....	29
2.5.1.2 Meyerhof (1965).....	30
2.5.1.3 Teng (1962).....	30
2.5.1.4 Alpan (1964).....	30
2.5.1.5 Peck and Bazaraa (1969)	32
2.5.1.6 Parry (1985)	32
2.5.1.7 Schultze and Sherif (1973).....	34
2.5.1.8 Peck et al. (1974)	35
2.5.1.9 Meyerhof (1974).....	36
2.5.1.10 Arnold (1980).....	36
2.5.1.11 Burland and Burbidge (1985)	37
2.5.1.12 Anagnostopoulos et al. (1991)	37
2.5.2 Correlations Based on CPT Tests	38
2.5.2.1 DeBeer and Martens (1957).....	38
2.5.2.2 Meyerhof (1965).....	38
2.5.2.3 DeBeer (1965).....	39
2.5.3 Correlations Based on DMT Tests.....	39
2.5.3.1 Schmertmann (1986).....	39
2.5.3.2 Leonards and Frost (1988).....	40
2.6 Recommended Elastic Modulus Based on SPT, CPT, DMT, and PMT Correlations.....	42
CHAPTER 3 CONICAL LOAD FIELD TESTING PROGRAM.....	47
3.1 Summarized Soil Profile of Three Cone Locations	48
3.1.1 Conical Load Test, Site No. 1: (NE Corner).....	48
3.1.2 Conical Load Test, Site No. 2: (SW Corner)	49
3.1.3 Conical Load Test, Site No. 3: (SE Corner)	50
3.2 Installation of Field Instrumentation.....	51
3.2.1 Location of Piezometers and Spider Magnets	55
3.2.2 Settlement Plate and Pressure Cells.....	55
3.2.3 Magnetic Extensometers (Spider Magnets and Datum Magnets).....	56

3.2.4 Displacement Transducer at Cone 2	57
3.2.5 Inclinometers.....	58
3.3 Soil Sampling.....	58
3.4 Conical Load Testing Procedure.....	60
3.5 Field Measurements of Immediate Settlements.....	68
3.5.1 Results and Data Interpretation: Conical Load Test No. 1	68
3.5.1.1 Analysis of the Piezometric Readings	68
3.5.1.2 Analysis of the Conical Load Pressure Measured with Pressure Cells	70
3.5.1.3 Measured Settlement, Pressures, and Weights over Time	72
3.5.1.4 Excess Porewater Pressures versus Pressures and Settlements	73
3.5.1.5 Load-Deformation Behavior from Conical Load Test 1.....	74
3.5.1.6 Analysis of the Inclinometer Data	75
3.5.2 Results and Data Interpretation: Conical Load Tests No. 2 and 3.....	76
3.5.2.1 Analysis of Piezometric Readings: Test No. 3 (May 9, 2019)	77
3.5.2.2 Analysis of Conical Load Pressure Measured with Pressure Cells: Test No. 3 (May 9, 2019).....	78
3.5.2.3 Relationships Between Settlements, Pressures, and Weights over Time: Test No. 3 (May 9, 2019).....	80
3.5.2.4 Excess Porewater Pressures in Relation to Earth Pressures at Ground Surface: Test No. 3 (May 9, 2019).....	82
3.5.2.5 Load-Deformation Behavior in Conical Load Test 3	83
3.5.2.6 Analysis of Piezometric Readings: Test No. 2 (May 10, 2019)	83
3.5.2.7 Analysis of the Conical Load Pressure Measured with Pressure Cells: Test No. 2 (May 10, 2019).....	85
3.5.2.8 Relationships Between Measured Settlements, Pressures, and Weights over Time: Test No. 2 (May 10, 2019).....	87
3.5.2.9 Excess Porewater Pressures in Relation to Earth Pressures and Settlements: Test No. 2 (May 10, 2019).....	88
3.5.2.10 Load-Deformation Behavior Measured in Conical Load Test 2	90
3.5.2.11 Analysis of the Inclinometer Data: Test No. 2 (May 10, 2019)	91
3.5.3 Summary of Conical Load Tests No. 1, 2, and 3	92

3.5.3.1 Piezometric Readings.....	92
3.5.3.2 Conical Load Earth Pressure Measured with Pressure Cells	93
3.5.3.3 Measured Settlement, Pressures, and Weights over Time	95
3.5.3.4 Excess Porewater Pressures in Relation to Earth Pressures and Settlements	98
3.5.3.5 Load-Deformation Behavior from Conical Load Tests	99
CHAPTER 4 LABORATORY TESTING PROGRAM	101
4.1 Geology at the Project Site	101
4.1.1 Cypresshead Formation	101
4.1.2 Hawthorn Group	101
4.2 Geologic Soil Profile of the Site	102
4.3 Laboratory Testing Equipment	103
4.4 Laboratory Testing Program on Cypresshead Formation Soils.....	105
4.4.1 Index Property Test.....	105
4.4.2 Void Ratio Tests	106
4.4.3 Constant Rate of Strain Oedometer Test	107
4.4.4 Triaxial Testing Program	111
4.4.5 X-Ray Diffraction Tests.....	113
4.4.6 Microscopy Tests	114
4.4.7 Scanning Electron Microscopy Image Tests.....	116
4.5 Laboratory Testing Program on Hawthorn Group Soils.....	120
4.5.1 Index Property Tests	120
4.5.2 Incremental Loading Consolidation Tests	121
4.5.3 Constant Rate of Strain Consolidation Test.....	126
4.5.4 Triaxial Testing Program	132
4.5.5 X-Ray Diffraction Tests.....	135
4.5.6 Scanning Electron Microscopy Images	137
4.6 Comparison of Laboratory Versus Cone Penetration Test Results	139
4.6.1 Relative Density Calculation	140
4.6.2 Friction Angle Calculation.....	140
4.6.3 Coefficient of Consolidation.....	141
4.6.4 Hydraulic Conductivity.....	142

4.6.5 Constrained Modulus	143
4.6.6 Shear Wave Velocity and Small-Strain Shear Modulus	144
4.6.7 Undrained Shear Strength	144
4.6.8 Overconsolidation Ratio	145
4.6.9 Pre-consolidation Pressure	146
4.6.10 Coefficient of Earth Pressure at Rest	146
CHAPTER 5 RECOMMENDATIONS REGARDING CORRELATIONS AND NUMERICAL MODELING	148
5.1 Recommended Correlations for Relative Density Calculation	148
5.2 Recommended Correlations for Friction Angle (ϕ') Calculation	154
5.3 Recommended Correlations for Small-Strain Shear Modulus Calculation	156
5.4 Definition of Soil Profile and Parameters	162
5.5 Definition of Vertical Stress Influence Zone: Boussinesq Analysis	166
5.6 Calculation of Elastic Modulus from Published Correlations	166
5.7 Immediate Settlement Using Elastic Approaches and Field Test Correlations	170
5.8 Numerical Finite Element Simulations of Conical Load Tests	172
5.9 Results of the Numerical Simulations	179
5.9.1 Incremental Vertical Stress Variation due to Conical Load Tests	179
5.9.2 Distribution of Vertical Stresses and Settlement at the Ground Surface	181
5.10 Comparison of Computed Results Versus Field Measurements	187
CHAPTER 6 CONCLUSIONS AND RECOMMENDATIONS	189
6.1 Research Summary	189
6.2 Concluding Remarks and Recommendations	189
REFERENCES	194
APPENDIX A SURVEY RESULTS OF THE CURRENT PRACTICE IN FLORIDA	209
APPENDIX B PAPERS PRESENTED AT GEO-CONGRESS-ASCE	220

LIST OF FIGURES

Figure 2-1. Bearing capacity index versus corrected SPT. After Cheney and Chassie (2000)	7
Figure 2-2. Variation of correction factors for embedment and layer thickness as a function of footing geometry. After Christian and Carrier (1978).....	9
Figure 2-3. Modulus of compressibility versus average measured SPT blow count. After D'Appolonia et al. (1968).....	10
Figure 2-4. Strain influence factors. After Schmertmann et al. (1978)	12
Figure 2-5. Variation of settlement factors with the normalized depth. After Oweis (1979).....	13
Figure 2-6. Normalized elastic stiffness modulus in terms of the strain parameter, λ_i . After Oweis (1979).....	14
Figure 2-7. Variation of the influence factor α , with the normalized depth. After Oweis (1979)	15
Figure 2-8. Evaluation of drained Young's modulus from CPT for silica sands (Berardi et al. 1991).	16
Figure 2-9. Compression of the elastic material. After Tschebotarioff (1971)	18
Figure 2-10. Layer thickness correction factor, C_s , versus depth. After Tschebotarioff (1971)...	18
Figure 2-11. Variation of influence factor, i_c . After Rowe and Booker (1981).....	19
Figure 2-12. Variation of influence factor, I_F . After Bowles (1987)	20
Figure 2-13. Modulus number K_E versus N_1 . After Berardi et al. (1991)	22
Figure 2-14. Variation of K_E with relative settlement. After Berardi et al. (1991)	23
Figure 2-15. Flowchart for settlement calculations based on modulus number, K_E (Berardi et al. 1991)	24
Figure 2-16. Determination of settlement factor using the dimensionless coefficient, α . After Papadopoulos (1992)	25
Figure 2-17. Effect of foundation rigidity on centerpoint settlement. After Mayne and Poulos (1999).....	27
Figure 2-18. Displacement influence factor for flexible circular foundation on finite Gibson medium. After Mayne and Poulos (1999).....	28
Figure 2-19. Variation of the compressibility constant, α , based on the SPT blow count. After Alpan (1964)	31
Figure 2-20. Relative density chart from blow counts. After Coffman (1960)	32
Figure 2-21. Thickness correction factor for layer thickness (T). After Parry (1985).....	33
Figure 2-22. Influence factor chart from Schultze and Sherif (1973).....	35
Figure 3-1. Plan view of field tests performed at the UCF site	47
Figure 3-2. Summarized soil profile for conical load test No. 1 (NE corner)	49
Figure 3-3. Summarized soil profile for conical load test No. 2 (SW Corner).....	50
Figure 3-4. Summarized soil profile for conical load test No. 3 (SE Corner)	51
Figure 3-5. (a) Installation of piezometers in the ground using sacrificial tips, (b) drilling and grouting for installation of magnetic extensometers, (c) magnetic extensometer and datum magnet sensor, and (d-g) inclinometer casing installation.....	52
Figure 3-6. (a) Sacrificial tip used for piezometer installation, (b) piezometers at Cone 2, (c) piezometers in place, (d) installation of magnetic extensometers at Cone 3, (e) magnetic extensometer preparation, (f) use of water to avoid buoyancy at Cone 3. Pictures taken on April 8-10, 2019.....	53

Figure 3-7. (a) inclinometer casing installation, (b) installation of displacement transducer, (c-i) vibrating wire displacement transducer installation. Pictures taken on April 8-10, 2019	54
Figure 3-8. Field instrumentation location: (a) elevation view and (b) plan view	56
Figure 3-9. Soil sampling location for Cones 1 and 2	59
Figure 3-10. Sampling process of the Shelby tubes: (a) drilling, (b) extraction, and (c) wax sealing	59
Figure 3-11. Sampling process retrieved from the drill auger. (a) drilling, (b) extraction, and (c) wax sealing. Pictures taken on April 10, 2019	60
Figure 3-12. Equipment used in the conical load tests	61
Figure 3-13. Magnetic extensometer readings after first loading stage and soil volume control lines	61
Figure 3-14. Topographic survey equipment to control settlement of riser pipes	62
Figure 3-15. Inclinometer reading station at an intermediate conical load stage	62
Figure 3-16. Measurements of conical shape taken at different loading stages	63
Figure 3-17. Loading sequence after third riser pipe was coupled	63
Figure 3-18. Pictures of conical load testing sequence for Cone 3. Pictures taken on May 9, 2019	65
Figure 3-19. Sand cone density tests following ASTM D1556 standard. Pictures taken on May 22, 2019	67
Figure 3-20. (a) Measured total porewater pressure before, during, and after the test, (b) measured total porewater pressure during the test, and (c) only excess porewater pressure during the test	69
Figure 3-21. (a) Short-term pressure cell readings (i.e., from 0-8 and 8-35 hours) and (b) long-term pressure cell readings up to 40 days after test completion	70
Figure 3-22. Variation of normalized weights and pressures during the conical load test	71
Figure 3-23. (a) Pressure readings at pressure cells SC1 and SC2 compared to settlement vs. time, and (b) computed weight with volume compared to settlement vs. time	72
Figure 3-24. (a) Short-term settlement readings with the spider magnets at different depths, and (b) long-term settlement readings up to 36 days after test completion	73
Figure 3-25. Measured excess porewater pressures and pressures at the ground surface	73
Figure 3-26. Measured excess porewater pressures and settlement at the ground surface	74
Figure 3-27. Load-deformation behavior for Cone 1: (a) weight-settlement, and (b) stress-settlement	75
Figure 3-28. Lateral displacements in the soil at the edge of the conical load arrangement. A-A and B-B directions shown	76
Figure 3-29. Conical load test No. 3: (a) measured total porewater pressure before and after the test, (b) measured total porewater pressure during the test, and (c) excess porewater pressure during the test	78
Figure 3-30. Pressure cell SC1 readings at conical load test 3: (a) short-term pressure cell readings (i.e., from 0-7 and 20-48 hr.), and (b) long-term pressure cell readings up to 18 days after end of test	79
Figure 3-31. (a) Schematic sequence followed during conical load test 3, and (b) normalized weights and pressures during the conical load test	80
Figure 3-32. Settlement, pressure, and computed weights for the length of the test: (a) measured pressure and settlement behavior, and (b) computed weight and settlement behavior	81

Figure 3-33. Settlement vs. time measured with spider magnets: (a) short-term, and (b) long-term settlement readings up to 16 days after the end of test	82
Figure 3-34. Measured excess porewater pressures during the entire test in relation to earth pressures at the ground surface	82
Figure 3-35. Load-deformation behavior for Cone 1: (a) weight-settlement, and (b) stress-settlement	83
Figure 3-36. Conical load test No. 2: (a) measured total porewater pressure before and after the test, (b) measured total porewater pressure during the test, and (c) excess porewater pressure during the test	84
Figure 3-37. Pressure cells readings at conical load test 2: (a) short-term pressure cell readings (i.e., from 0-8 and 22-32 hours), and (b) long-term pressure cell readings up to 18 days after end of test.....	86
Figure 3-38. Schematic sequence followed during conical load test 2, and b) normalized weights and pressures during the conical load test.....	86
Figure 3-39. Settlement, pressure, and computed weights for the length of the test: (a) measured pressure and settlement, (b) computed weight and settlement behavior, (c) SC1 pressure readings related to settlements, and (d) computed weight in relation to settlements	87
Figure 3-40. Settlement with spider magnets: (a) short-term settlement readings and (b) long-term readings up to 15 days after the end of the test	88
Figure 3-41. Measured excess porewater pressures in relation to earth pressures at the ground surface: (a) clayey layer and (b) sandy layer	89
Figure 3-42. Measured excess porewater pressures and settlement at the ground surface measured with displacement transducer	90
Figure 3-43. Load-deformation behavior measured at conical load test. 2: (a) settlement versus weight, (b) settlement versus stress, (c) displacement transducer settlement versus weight, and d) displacement transducer settlement versus pressure at SC1	91
Figure 3-44. Lateral displacements in the soil at the edge of the conical load test	92
Figure 3-45. Conical load test 1 through 3: (a) long-term total porewater pressure, (b) total porewater pressure during the tests, and (c) excess porewater pressure during the test...	93
Figure 3-46. Pressure cell readings at conical load tests 1 to 3: (a) short-term pressure cell readings (i.e., from 0-7 and 23-48 hours) and (b) long-term pressure cell readings up to 18 days after end of the test	94
Figure 3-47. Normalized variation of weights and pressures during the conical load tests 1 through 3	95
Figure 3-48. Settlement, pressure, and computed weights over the test length: (a) pressure readings at pressure cells and settlement, and (b) computed weight and settlement.....	96
Figure 3-49. Magnetic extensometer readings at Cones 1 to 3 over the soil profile	97
Figure 3-50. Cones 1 and 2 measured excess porewater pressures and earth pressures at the ground surface.....	98
Figure 3-51. Cones 1 and 2 measured excess porewater pressures and settlement at the ground surface measured with magnetic extensometer and displacement transducer	99
Figure 3-52. Load-deformation behavior measured at cones 1 to 3: (a) settlement versus weight, (b) settlement versus stress, and (c) displacement transducer settlement versus stress..	100
Figure 4-1. Geologic soil profile at UCF test site location	102
Figure 4-2. Schematic view of the constant rate of strain equipment used in this project	104
Figure 4-3. Schematic view of triaxial testing system used in this project.....	104

Figure 4-4. Fine content effect on the void ratios: (a) sand layer at UCF site and (b) Cubrinovski and Ishihara's work (2002).....	107
Figure 4-5. Axial stress-strain behavior response for Cypresshead formation soils.....	109
Figure 4-6. Coefficient of volume compressibility during CRS testing.....	110
Figure 4-7. Constrained modulus during the CRS testing.....	110
Figure 4-8. Compression stress paths during the TX tests.....	112
Figure 4-9. Stress-strain response during the TX tests.....	112
Figure 4-10. Excess porewater pressure response during the TX tests.....	113
Figure 4-11. Phase angle intensity to identify mineral in XRD tests of soil samples at UCF site	114
Figure 4-12. Microscopy test of the Sample A1-B1.....	115
Figure 4-13. Microscopy test of the Sample A1-B2.....	115
Figure 4-14. Microscopy test of the Sample A1-B3.....	115
Figure 4-15. Microscopy test of the Sample A2-B2.....	116
Figure 4-16. Microscopy test of the Sample A2-B3.....	116
Figure 4-17. SEM image of sample A2-B2 at 50x.....	117
Figure 4-18. SEM image of sample A2-B2 at 67x.....	117
Figure 4-19. SEM image of sample A2-B2 at 92x.....	118
Figure 4-20. SEM image of sample A2-B2 at 150x.....	118
Figure 4-21. SEM image of sample A2-B2 at 200x.....	119
Figure 4-22. SEM image of sample A2-B2 at 203x.....	119
Figure 4-23. SEM image of sample A2-B2 at 250x.....	120
Figure 4-24. Axial stress-strain behavior of the Hawthorn group soils: (a) consolidation curves of NE Specimens and (b) consolidation curves of SW specimens.....	122
Figure 4-25. Coefficient of consolidation during the IL test: (a) coefficient of consolidation of NE specimens and (b) coefficient of consolidation of SW specimens.....	123
Figure 4-26. Coefficient of volume compressibility during the IL test: (a) coefficient of compressibility of NE specimens and (b) coefficient of compressibility of SW specimens.	124
Figure 4-27. Constrained modulus during the IL test: (a) constrained modulus of NE specimens and (b) constrained modulus of SW specimens.....	125
Figure 4-28. Hydraulic conductivity during the IL test: (a) hydraulic conductivity of NE specimens and (b) hydraulic conductivity of SW specimens.....	126
Figure 4-29. Axial stress-strain behavior response for Hawthorn group soils: (a) consolidation curves of NE specimens and (b) consolidation curves of SW specimens.....	127
Figure 4-30. Coefficient of consolidation during the CRS test: (a) coefficient of consolidation of NE specimens and (b) coefficient of consolidation of SW specimens.....	129
Figure 4-31. Coefficient of compressibility during the CRS test: (a) coefficient of compressibility of NE specimens and (b) coefficient of compressibility of SW specimens.....	130
Figure 4-32. Constrained modulus during the CRS test: (a) constrained modulus of NE specimens and (b) constrained modulus of SW specimens.....	131
Figure 4-33. Hydraulic conductivity during the CRS test: (a) hydraulic conductivity of NE specimens and (b) hydraulic conductivity of SW specimens.....	132
Figure 4-34. Triaxial stress paths followed during the triaxial tests.....	133
Figure 4-35. Stress-strain response during the triaxial tests.....	134
Figure 4-36. Excess porewater pressure response during the triaxial tests.....	134

Figure 4-37. Shear modulus degradation curves during the triaxial tests.....	135
Figure 4-38. Normalized shear modulus degradation curves during the triaxial tests.....	135
Figure 4-39. Phase angle intensity to identify minerals in XRD tests. (a) NE minerals and (b) SW minerals.....	136
Figure 4-40. XRD phase identification: (a) NE XRD results and (b) SW XRD results.....	137
Figure 4-41. SEM images of NE specimens: (a) sample B2-ST5 at 50 X (b) specimen B2-ST5 at 250 X, (c) sample B1-ST2 at 250 X, (d) sample B2-ST5 at 1 KX, and (e) sample B2-ST5 at 1 KX.....	138
Figure 4-42. SEM images of SW specimens: (a) sample B3-ST8 at 100 X, (b) sample B3-ST8 at 1 KX, (c) sample B3-ST8 at 1.25 KX, (d) sample B3-ST8 at 1 KX, (e) sample B4-ST11 at 350 X, and (f) sample B3-ST7 at 500 X.....	139
Figure 4-43. Relative density from CPTu tests.....	140
Figure 4-44. CPTu friction angle of the Cypresshead formation.....	141
Figure 4-45. Coefficient of consolidation from laboratory and dissipation tests.....	142
Figure 4-46. Hydraulic conductivity from laboratory and dissipation tests.....	143
Figure 4-47. Constrained modulus from laboratory and CPTu tests.....	143
Figure 4-48. Shear wave velocity and maximum shear modulus from laboratory and CPTu tests.....	144
Figure 4-49. Undrained shear strength from laboratory and CPTu.....	145
Figure 4-50. Overconsolidation ratio from laboratory and CPTu tests.....	145
Figure 4-51. Preconsolidation pressure from laboratory and CPTu tests.....	146
Figure 4-52. Coefficient of earth pressure at rest from laboratory and CPTu tests.....	147
Figure 5-1. Comparison between measured relative density and predicted using CPT correlations (Tanaka and Tanaka 1998).....	149
Figure 5-2. Variation of void ratio difference with the mean grain size of soils. From Cubrinovski and Ishihara (2001).....	152
Figure 5-3. Correlation between horizontal stress index from DMT and relative density for uncemented sands. From Marchetti et al. (2001).....	154
Figure 5-4. Shear moduli for sands at different relative densities. From Seed and Idriss (1970).....	158
Figure 5-5. Ratio of G_{SC} (G_0) from seismic cone penetration tests to E_D from DMT tests versus K_D for sandy soils. From: Tanaka and Tanaka (1998).....	160
Figure 5-6. Flowchart for evaluation of I_c based on the suggested iterative procedure by Robertson and Cabal (2015).....	161
Figure 5-7. Summarized soil profile at the project site showing the results of field tests, soil strength and stiffness parameters defined using the proposed correlations.....	165
Figure 5-8. Vertical stress profile for the definition of stress influence zone for the conical load arrangement.....	166
Figure 5-9. Computed values of E for both layers using published correlations with field tests (SPT, CPT, DMT).....	169
Figure 5-10 Average values of E for the topmost sandy layers one and two compared with the range of Young's modulus measured with the conical load tests.....	170
Figure 5-11. Computed immediate settlements using published methods and field test-based methods.....	171
Figure 5-12. Axisymmetric finite element model built in PLAXIS2D to reproduce the conical load tests performed at the UCF site.....	172

Figure 5-13. Conical loading soil cluster mesh built in a stage construction sequence.....	173
Figure 5-14. Computed response of sandy materials using numerically simulated: (a) drained triaxial compression test and (b) oedometer tests	176
Figure 5-15. Computed clay response numerically simulated: (a) undrained triaxial compression and (b) oedometer tests	177
Figure 5-16. Small strain soil behavior: (a) computed shear stiffness degradation curves for layers 1 and 2 and (b) normalized stiffness degradation curves of sandy materials published in the technical literature	178
Figure 5-17. Contours of cartesian vertical effective stress at the end of conical load testing (a) results using HS model and (b) results using HSS model	180
Figure 5-18. Variation of vertical effective stress with depth for the definition of conical load test influence zone with HS and HSS models	181
Figure 5-19. Variation of contact vertical stress with distance measured at the centerline of the cone versus that computed with HS and HSS models	182
Figure 5-20. Variation of conical load-induced settlement with distance measured at the centerline of the cone versus that computed with HS and HSS models	183
Figure 5-21. Contours of cartesian vertical strains at the final stage of conical loading: (a) results using HS model and (b) results using HSS model.....	184
Figure 5-22. Stiffness-strain behavior of soils with typical strain ranges for different testing techniques, geotechnical facilities, and areas of applicability (modified after Atkinson and Sallfors, 1991; Mair, 1993 ; Dowding, 2008. From: Zapata-Medina (2012)	185
Figure 5-23. Computed shear strain contours induced by conical load testing at final loading stage: (a) results computed with HS model and (b) results computed with HSS model	186
Figure 5-24. Contours of relative shear stresses (τ_{rel}) for the numerical models computed using: (a) HS model and (b) HSS model	187
Figure 5-25. Comparison between measured and computed immediate settlements	188
Figure A-1. Responses received for question 1.	212
Figure A-2. Responses received for question 2.	213
Figure A-3. Responses received for question 3.	214
Figure A-4. Responses received for question 4.	215
Figure A-5. Responses received for question 5.	216
Figure A-6. Responses received for question 6.	216
Figure A-7. Responses received for question 7.	217
Figure A-8. Responses received for question 8.	217
Figure A-9. Responses received for question 9.	218
Figure A-10. Responses received for question 10.	219

LIST OF TABLES

Table 2-1. Elastic shape and rigidity factors, EPRI (1983). From AASHTO LRFD-8	5
Table 2-2. Adjustment of E' for $\varepsilon_z > 0.1\%$	16
Table 2-3. Influence factor I_s for settlement calculations	21
Table 2-4. Influence factors from Schultze and Sherif (1973)	34
Table 2-5. Young's modulus correlations from SPT and CPT tests	42
Table 2-6. Young's modulus correlations from SPT and CPT tests (continuation)	43
Table 2-7. Young's modulus correlations from SPT and CPT tests (continuation)	44
Table 2-8. Young's modulus correlations from SPT and CPT tests (continuation)	45
Table 2-9. Young's Modulus correlations from DMT and PMT tests	46
Table 3-1. Summary of field tests performed at the location of conical load tests	48
Table 4-1. Results of index tests in topmost granular soils	105
Table 4-2: Parameters computed from gradation analysis	106
Table 4-3: Results of minimum and maximum void ratio for topmost granular soils	107
Table 4-4: Index properties from CRS tests	108
Table 4-5: Load-deformation and compressibility properties	109
Table 4-6: Index properties for triaxial tests in granular soils	111
Table 4-7. Specimen characteristics for XRD tests	113
Table 4-8. Index property test results for deep Hawthorn group soils	121
Table 4-9: Index properties from IL consolidation tests on deep Hawthorn group soils	121
Table 4-10: Load-deformation properties, preconsolidation pressure, and specimen quality designations for specimens tested in IL tests on deep Hawthorn group soils	122
Table 4-11. Index properties from CRS consolidation tests on deep Hawthorn group soils	127
Table 4-12: Load-deformation properties, preconsolidation pressure and specimen quality	128
Table 4-13: Index properties for triaxial tests on deep Hawthorn group soils	133
Table 4-14. Specimens characteristics for XRD tests	136
Table 4-15: Relative density correlated from CPTu tests	140
Table 4-16: Friction angle from TX tests and CPTu tests	141
Table 5-1. Summary of SPT correction factors. From Kulhawy and Mayne (1990)	153
Table 5-2. Physical properties of frozen samples tested (Hatanaka and Uchida 1996)	156
Table 5-3. Overconsolidated ratio exponent k. After Hardin and Drnevich (1972 b)	157
Table 5-4. Empirical relationships between G_{max} and in situ tests. From Kramer (1996)	159
Table 5-5. Summarized calculations of elastic modulus for the top two topmost granular soil layers at the project site (using SPT blow counts)	167
Table 5-6 Summarized calculations of elastic modulus for the top two topmost granular soil layers at the project site (using CPTu data)	168
Table 5-7. Hardening soil model parameters used in the numerical simulations	174
Table 5-8. Hardening soil small model parameters used in the numerical simulations	174
Table 5-9. Parameters used for the numerically simulated laboratory tests	175
Table 5-10. Small strain shear modulus parameters computed using HSS model	178
Table 5-11. Differences between numerically simulated G_{sec} and G_0	179
Table 5-12. Classification of predictions in geotechnical engineering. From Lambe (1973)	187
Table 6-1. Recommended soil parameters using hardening soil (HS) model	191
Table 6-2. Recommended equations for hardening soil small (HSS) model in terms of D_r	192

CHAPTER 1 INTRODUCTION

An understanding of the load-deformation behavior of soils is necessary for the design of embankments and shallow foundations. The determination of soil compressibility depends on the selection of stiffness parameters, mainly the soil stiffness properties in terms of the modulus of elasticity, which is widely used in current geotechnical practice. This parameter has been conventionally estimated via experimental correlations based on field tests, including standard penetration tests (SPT), cone penetration tests (CPT), dilatometer tests (DMT), and geophysical seismic wave propagation tests. Using the results of those tests to determine stiffness parameters and for the determination of ground deformations in granular soils for Florida-specific soil conditions was the main goal of this report. At times, design estimates made using conservative correlations calibrated from other soils around the world may lead to unnecessary ground improvements or larger foundations for the site-specific soil conditions of granular soils in Florida. The use of untested correlations for the soil conditions in Florida may cause overly conservative designs and might not match actual field performance. Computed settlements differ from actual field measurements of soil deformations because of lack of knowledge in the selection of stiffness and compressibility parameters of soils. And even if the soil modulus can be determined accurately, it does not guarantee accurate settlement predictions because computations were made using stiffness parameters that were defined for stress or strain levels different than the actual values mobilized for the specific project. Assessment of their accuracy and suitability for the local soil conditions were the main objectives of this project. The site used for testing the methods developed herein was located at the University of Central Florida (UCF), where the soil conditions are similar to many sites across the state of Florida.

The subsurface investigation program at the testing site started in 2003, and additional field exploration efforts were made to validate the research findings. The laboratory and field tests conducted in this research served as the basis for the site characterization used to summarize soil profiles corresponding to the location of each of three conical load tests. Those summarized soil profiles were used to define the instrumentation location plan and were used to conduct numerical finite element analyses for immediate settlement predictions. A detailed description of sensor installation methods is presented in this report, where the FDOT crew played an important role by contributing their experience of Florida soils. In this study, advanced laboratory tests are also conducted on samples retrieved from different depths at the project site. Soil samples tested in the laboratory provided insight into the geotechnical compressibility characteristics of the subsurface soils. The soil samples allowed the research team to: (i) understand fundamental soil behavior characteristics, including oedometer constant rate strain (CRS) and triaxial tests and (ii) evaluate intrinsic mineralogic and microscopic properties of the tested soils using x-ray diffraction and scanning electron microscope (SEM) image tests. The tests were conducted at the geotechnical engineering testing laboratory at UCF, and the results are part of this final report. The testing program results were used for a more accurate calibration of soil parameters and to provide recommendations regarding constitutive soil model parameters that can be used in various soil conditions in Florida.

Regarding the field instrumentation, a set of sensors used at each cone location is presented in this report. Recommendations on soil elastic modulus correlations and direct approaches for immediate settlement calculations leading to more accurate results for the project site are issued and validated with the finite element models presented herein. The soil parameters for the numerical models using hardening soil and hardening soil small models were calibrated based on correlations from field or laboratory tests. Conclusions are drawn regarding the most suitable settlement prediction methods for the conditions tested herein and recommendations are presented to highlight the importance of the considering soil nonlinearity and stiffness degradation considerations for the level of strains mobilized for specific projects. The results of a survey (see APPENDIX A) are also presented. The survey gathered information about the methods and procedures used by consulting companies in Florida on the broad topics of calculation of elastic modulus, immediate settlements, and on the use of numerical methods to validate preliminary design estimations of ground deformations.

1.1 Research Objectives and Scope of Work

The previous research reported by Chopra et al. (2003) and additional field testing program conducted herein were studied to determine three locations for conical load testing. Selection and location of the tests were planned according to the soil layers found in the subsurface exploration program. The influence stress zones considered for settlement estimations did not reach deep fine-grained soils and were mostly localized in the topmost granular materials, which were used to confirm the correlations of stiffness parameters to calculate immediate settlements. This project aimed at identifying the most appropriate correlations with field tests (mainly using SPT, CPT, and DMT) in order to obtain the most accurate values of soil stiffness that can be used to compute immediate settlements in the state of Florida. The research work plan was composed of six primary objectives, which are summarized below.

1. Assessment of the state-of-the-art for immediate settlement estimation from practitioners in Florida and in general practice: a survey was conducted to practitioners and district geotechnical engineers. The survey asked questions related to current practice in estimation of stiffness parameters and related computations of immediate settlements. The results of the survey are presented in APPENDIX A. In addition, a detailed review of technical literature related to current methods for calculation of soil stiffness parameters for their use in immediate settlement calculations is also presented based on correlations with SPTs and other field tests such as CPTs and DMTs. The technical review is presented in CHAPTER 2.
2. Conical load testing program at three field locations at the UCF testing site: conical load tests were conducted in three locations within the fenced UCF testing site to provide a safety protocol in the data acquisition. The three locations had a similar soil profile consisting mostly of granular soils with interbedded clay layers at larger depths close to the end of the conical loading influence zone. The results of the testing program are presented and analyzed in light of published correlations and methods presented in the technical review portion of this report. The field testing program in terms of the measured settlements, porewater pressures, lateral

movements, and contact pressures induced by the conical load arrangement are included in this report. The results of the conical load tests are presented in CHAPTER 3.

3. A laboratory testing program conducted in the geotechnical testing laboratory facilities at UCF: laboratory tests on soil samples retrieved from the field were conducted. These samples were tested at the UCF geotechnical testing laboratory under: oedometric incremental loading and constant rate of strain, advanced triaxial, X-Ray diffraction, and Scanning Electron Microscope tests. The results are used to provide the geotechnical intrinsic compressibility characteristics of the soils at the project site and for the definition of constitutive soil model parameters for the finite element simulations presented herein. The results are compared in relation the results of CPTu tests. The results of the laboratory testing program are presented in CHAPTER 4
4. Numerical modeling of conical load tests: advanced soil models are used to investigate the soil response to conical load tests. Conical load-induced ground surface settlements, soil stresses, shear strains, and vertical influence zones are computed using the numerical models, and are included in this report to describe the measured soil response. Recommendations about geotechnical modeling techniques are issued to calculate immediate settlements caused by surface loadings for projects in the state of Florida. This part of the research was developed to produce recommendations and practical guidelines regarding the soil parameters (mainly stiffness and strength parameters) necessary to compute immediate soil deformations. The results of the numerical modeling components of this research are presented in CHAPTER 5

CHAPTER 2 LITERATURE REVIEW

This chapter presents a technical review of wide range of analytical, empirical, and semi-empirical methods that can be used by practitioners to estimate ground surface settlements caused by shallow foundations on sandy soils. The discussion is subdivided into two categories – methods based on the theory of elasticity and methods based on correlations with field tests. The design of shallow foundations is based on the analysis of bearing capacity and settlement evaluations. Even though the latter usually governs the design, the scatter in the predictions is extensive due to the uncertainty in evaluating the soil parameters and the variety of methods for settlement calculations that are available in the geotechnical literature. A comprehensive review of the various methods used for settlement estimations is important to understand the variables and procedures presented in this report.

Shear stresses and the corresponding strains induced by external loading in soils such as sands, silts, or clays, are observed in the ground surface as changes in soil volume and vertical movements (i.e., settlements) occur. These vertical movements occur in two forms: immediate and time-dependent (i.e., consolidation) settlements. The latter is usually not included in the analyses presented herein due to large dissipation rate of excess porewater pressure observed in most sands, particularly when loadings are static. The concept of immediate settlements and the solutions based on the theory of elasticity are generally accepted by practitioners, particularly for soils comprised of granular materials. To include the nonlinearity of its stiffness degradation as shearing strains are mobilized, the stiffness parameters are either correlated from field tests for ranges of pressure commonly reached in geotechnical practice or are included as an influence factor. Studies of actual soil behavior have shown that both parameters are nonlinear and depend on the change in effective stress and stress history. Most geotechnical applications characterize soil behavior as elastic using Poisson's ratio and Young's modulus to represent in situ stiffness conditions. Additional parameters must be considered if the nonlinearity and plasticity of soils is a concern in the analysis. Otherwise, these parameters will not be able to produce reliable settlement predictions (Kulhawy and Mayne (1990). Poisson's ratio and Young's modulus can be measured from high-quality samples sheared using triaxial and/or oedometric testing devices. However, recovering "undisturbed" samples of granular soils from field testing is difficult. Thus, soil properties obtained using correlations derived from field test measurements such as: standard penetration test (SPT), cone penetration test (CPT), dilatometer (DMT), and pressuremeter tests (PMT), are needed to determine soil parameters representative of in situ soil conditions.

Analytical, empirical, and semi-empirical correlations have been widely studied by many researchers to calculate settlements (e.g., AASHTO standard (2017); Hough (1959); Briaud and Gibbens (1997), Briaud et al. (2000); Terzaghi et al. (1967); DeBeer and Martens (1957); Ménard and Rousseau (1962)) but given the inherent variability of soils, a unified methodology has not been accepted. Thus, it is common practice to estimate settlements with a combination of different methods that best resemble in situ soil conditions, and subject the final recommendations to limiting criteria from regulatory agencies and commercial codes [e.g., AASHTO standard (2017), FHWA-SA-02-054 (Kimmerling 2002), and NAVFAC (1986)].

2.1 Methods for Estimating Immediate Settlements on Granular Soils

A detailed literature review on the calculation of immediate settlements is presented in this section. Some of the reviewed methods also correspond to recommendations provided in the past by AASHTO (2017), NAVFAC (1986), and FHWA-SA-02-054 (Kimmerling 2002). AASHTO (2017) recommends the use of analytical methods based on the theory of elasticity for the calculation of settlements of footings on granular soils with negligible fine contents (i.e., clean sands). The following methods, reported in AASHTO (2017), use elastic half-space procedures and layered soil profiles as proposed by Hough (1959).

2.1.1 Elastic Half-Space Method

This method assumes a flexible footing and simplifies the soil profile within the influence zone of the footing as a homogeneous soil layer with infinite depth. The following equation was derived for a soil simplified as an elastic half-space:

$$s_e = \frac{[q_0(1 - \nu^2)\sqrt{A'}]}{144E_s\beta_z} \quad (1)$$

where:

- q_0 = applied vertical stress (ksf)
- A' = effective area of footing (ft²)
- β_z = elastic shape factor.
- ν = Poisson's Ratio
- E_s = Young's modulus of soil (ksi).

Table 2-1 lists the elastic shape and rigidity factors recommended by AASHTO LRFD-8 (2017). This specification recommends laboratory tests, field tests or field measurements to determine the elastic parameters. In addition, E_s can be determined between one-half or two-thirds of the footing width or using a weighted average value.

Table 2-1. Elastic shape and rigidity factors, EPRI (1983). From AASHTO LRFD-8

<i>L/B</i>	Flexible, β_z (average)	β_z Rigid
Circular	1.04	1.13
1	1.06	1.08
2	1.09	1.10
3	1.13	1.15
5	1.22	1.24
10	1.41	1.41

2.1.2 Method Proposed by Hough (1959)

This empirical method proposed by Hough (1959) is recommended by FHWA-SA-02-054 (Kimmerling 2002). It was developed for normally consolidated granular soils and it considers the

soil profile as a finite arrangement of layers within the influence zone of the footing. The influence zone considered by Hough (1959) extends up to 3 times the smallest footing dimension. The author recommended a maximum layer thickness of 10 ft. The modulus of elasticity plays an important role in the estimation of ground surface settlements. Methods based on layered soil profiles instead of uniform soil profiles lead to more accurate results.

$$s_e = \sum_{i=1}^n \Delta H_i ; \Delta H_i = H_c \left(\frac{1}{C'} \right) \log \left[\frac{(\sigma'_0 + \Delta \sigma'_v)}{\sigma'_0} \right] \quad (2)$$

where,

- s_e = settlement (ft)
- n = number of soil layers within the zone of stress influence of the footing
- ΔH_i = elastic settlement of layer i (ft)
- H_c = initial height of layer i (ft)
- C' = bearing capacity index = $(1 + e_0)/C_c$
- σ'_0 = initial vertical effective stress at the midpoint of layer i (ksf)
- $\Delta \sigma'_v$ = increase in vertical stress at the midpoint of layer i (ksf)

In absence of field and laboratory tests, Figure 2-1 shows a relationship between the bearing capacity index and the SPT blow count corrected at an energy efficiency of 60% as presented in Eq. (3).

$$N_1 = C_N N_{60} \quad (3)$$

where:

- N_1 = SPT blow count corrected for overburden pressure, σ'_v (blows/ft)
- C_N = $[0.77 \log_{10} (40/\sigma'_v)]$, and $C_N < 2.0$
- σ'_v = vertical effective stress (ksf)
- N_{60} = SPT blow counts corrected for hammer efficiency (blows/ft)

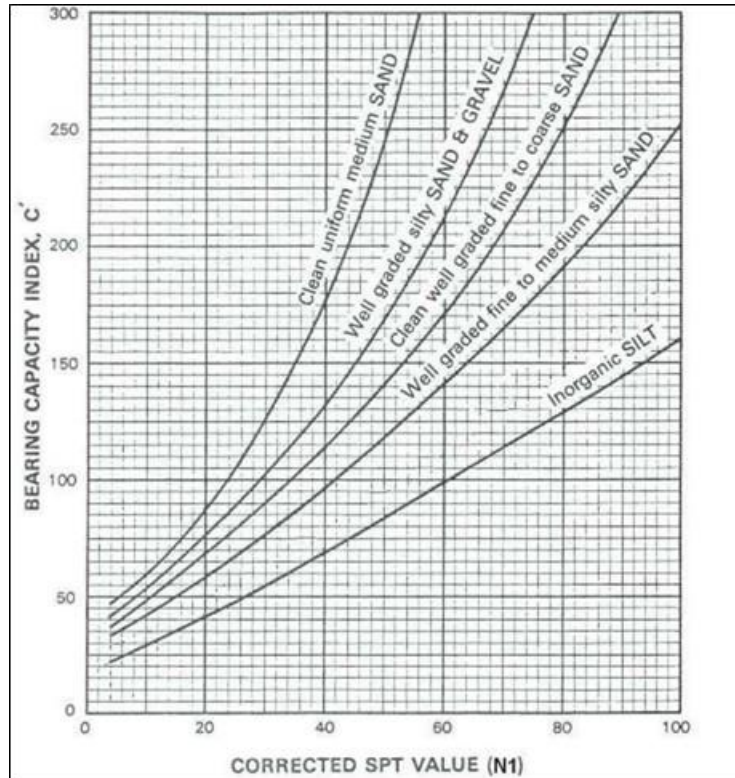


Figure 2-1. Bearing capacity index versus corrected SPT. After Cheney and Chassie (2000)

The thickness of the compressible soil could be obtained by an iterative procedure until $\Delta\sigma'_v/q$ is equal to 10% (Sargand et al. 2003), which is adopted as the influence zone for this project.

2.1.3 Additional Methods

AASHTO (2017) also recommended the following methods to determine the immediate settlements induced by shallow foundations:

- Terzaghi et al. (1967)
- Sowers (1979)
- U.S. Department of the Navy (1982)
- D'Appolonia et al. (1968)
- Tomlinson (1986)
- Gifford et al. (1987)

Further details for selected methods are presented in this chapter.

2.2 Methods Reported by the FHWA: Geotechnical Engineering Circular No. 6

The Federal Highway Administration, FHWA-SA-02-054 (Kimmerling 2002), reported a series of analytical and empirical methods to estimate immediate settlements for granular soils using elastic theories. Such theories must be carefully applied given the typical variability of soil conditions in sedimentary soil deposits. It is worth mentioning that immediate settlements based on analytical, empirical, or semi-empirical methods should be reliable, easy to implement, and should provide a good match versus measured values (Kimmerling 2002). The following analytical methods are recommended in this report to predict settlement in cohesionless soils.

2.2.1 Method Proposed by Hough (1959)

The method proposed by Hough (1959) is also adopted by the FHWA-SA-02-054 (Kimmerling 2002) for the estimation of immediate settlements as presented in Eq. (2). Recall that this method is based on a layered soil profile extended up to 3 times the smallest footing dimension. The author recommended a layer thickness thinner than 10 ft. The following equation is recommended by the FHWA-SA-02-054 (Kimmerling 2002) to correct the SPT blow count:

$$\frac{N_1}{N} = \frac{1}{\sqrt{\frac{\sigma'_{v0}}{95.76}}} \leq 2.0 \quad (4)$$

where:

- σ'_{v0} = initial vertical effective stress at the level of N (ksf)
- N_1 = SPT blow count corrected for overburden pressure, σ'_v (blows/ft)
- N = SPT blow counts corrected for hammer efficiency (blows/ft)

2.2.2 Method Proposed by D'Appolonia et al. (1968)

The method proposed by D'Appolonia et al. (1968) was derived in terms of sand compressibility parameters, footing geometry, and applied loading as presented in Eq. (5). In the study presented by D'Appolonia et al. (1968), a comparison with predictions from plate load tests, Meyerhof, Terzaghi and Peck methods, and SPTs were conducted. The author demonstrated that field observations were key to establish the basis for settlement prediction techniques.

$$\Delta H = \left(\frac{\Delta \sigma_v B_f}{M} \right) \mu_0 \mu_1 \quad (5)$$

where:

- ΔH = settlement in sand or sand and gravel
- $\Delta \sigma_v$ = applied stress beneath footing (in tsf)
- B_f = footing width
- μ_0 = correction factor for embedment
- μ_1 = correction factor for thickness of sand layer

M = modulus of compressibility of sand.
 M = $196 + 7.9(N)$ (in tsf) for normally loaded sand
 M = $416 + 10.9(N)$ (in tsf) for preloaded sand
 N = average uncorrected blow count between the base of the footing and a depth of B below the footing.

Figure 2-2 shows the variation of the correction factors for embedment and thickness as a function of the foundation geometry. This figure was presented by Christian and Carrier (1978).

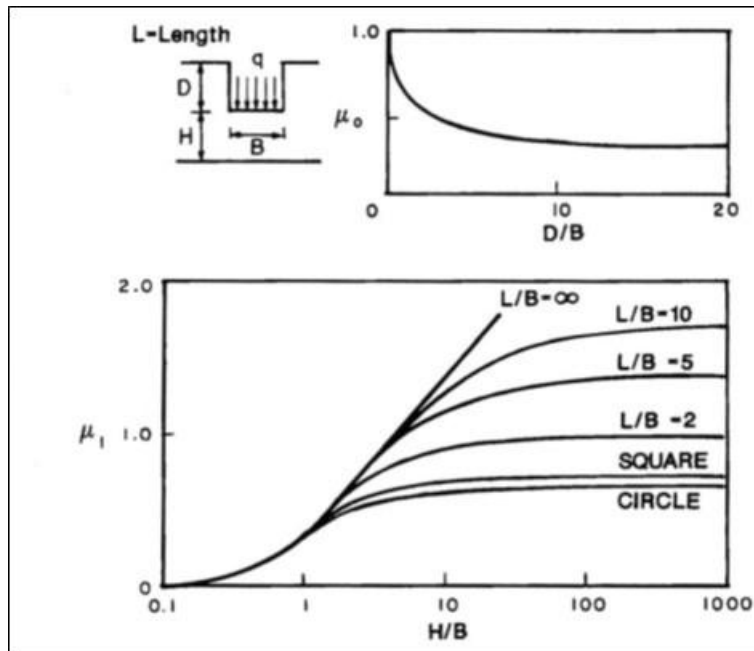


Figure 2-2. Variation of correction factors for embedment and layer thickness as a function of footing geometry. After Christian and Carrier (1978)

Figure 2-3 presents the modulus of compressibility versus the average measured SPT resistance at a depth B below footing expressed as blows per foot.

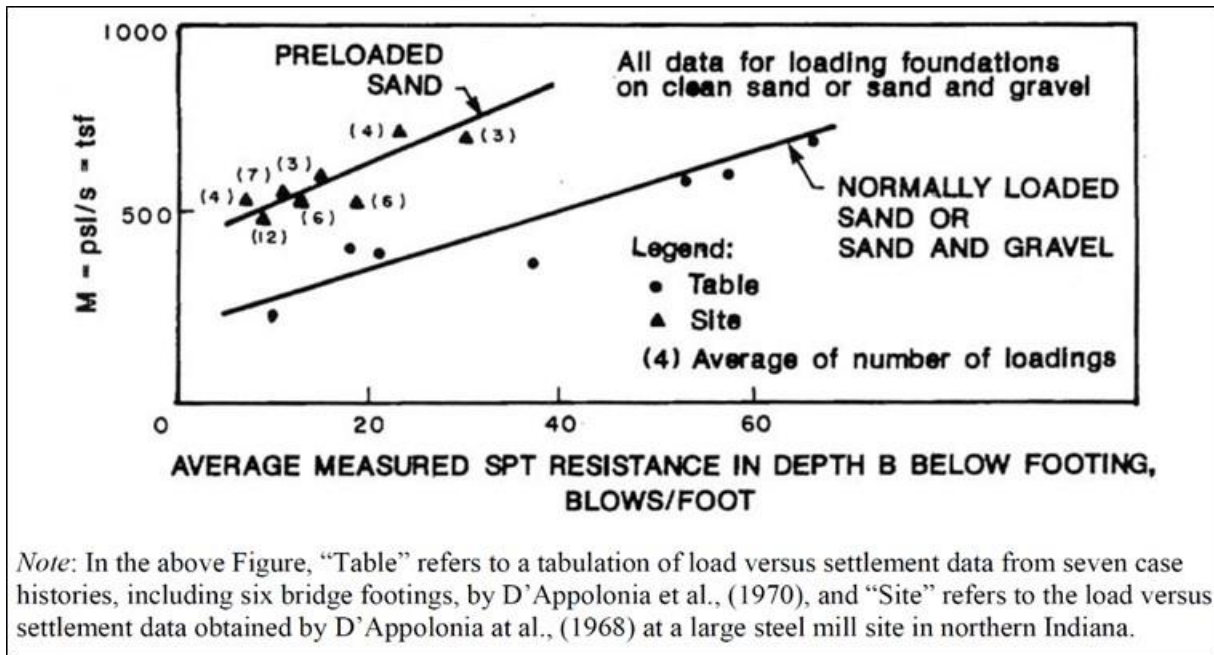


Figure 2-3. Modulus of compressibility versus average measured SPT blow count. After D'Appolonia et al. (1968)

2.3 Additional Methods for Settlement Calculation

2.3.1 Method Proposed by Schmertmann (1970)

The Schmertmann method (1970) is also recommended by FHWA HI-88-009. It uses a semi-empirical strain influence factor based on the theory of elasticity. The influence factor proposed by Schmertmann (1970), which describes the distribution with depth of load-induced vertical strains, is expressed in terms of the Poisson's ratio and two dimensionless factors that depend on the geometric location of the point considered in the soil mass. This method is based on the numerical integration of the strain influence factor to predict settlements, and assumes a uniform load distribution to determine the location of the vertical strains. Vertical strain distributions were determined via finite element simulations, experimental results, and previous studies on sandy soils. The author also performed finite element computer simulations to validate the method. The main equation of this method, which is also recommended by the FHWA HI-88-009, is as follows:

$$s = C_1 C_2 q \sum_{i=1}^n (I_z / E_s) z_i \quad (6)$$

where:

- s = settlement (in ft)
- q = footing stress (tsf)
- I_z = strain influence factor
- E_s = soil modulus (tsf)
- i = individual layer

- n = total number of soil layers
- z_i = thickness of individual layers (in ft)
- γ = unit soil weight (in pcf)
- D = depth of embedment
- C_1 = embedment correction factor = $1.0 - 0.5 (\gamma D/q) \geq 0.5$
- C_2 = creep correction factor = $1.0 + 0.2 \log (t/0.1)$
- t = time in years

For footings under axisymmetric conditions, the following recommendations were presented by Schmertmann (1970):

- E_s = $2 q_c$ modified to $E_s = 2.5 q_c$ in Schmertmann et al. (1978)
 - q_c = static cone bearing capacity (i.e., CPT tip resistance)
 - I_z = 0.1 at depth=0
 - I_z = 0 at depth = 2B
- Maximum I_z occurs at a depth of B/2 and has a value of:
- $$I_z = 0.5 + 0.1 [\Delta q / \sigma'_{vp}]^{0.5}$$

For footings under plane-strain conditions, the following recommendations were presented by Schmertmann (1970):

- E_s = $3.5 q_c$
 - q_c = static cone test bearing capacity (i.e., CPT tip resistance)
 - I_z = 0.2 at depth= 0
 - I_z = 0 at depth = 4B
- Maximum I_z occurs at a depth of B and has a value of:
- $$I_z = 0.5 + 0.1 [\Delta q / \sigma'_{vp}]^{0.5}$$
- Δq = net applied footing stress
 - σ'_{vp} = initial vertical effective stress at maximum I_z for each loading case

By the time that this method was proposed, Schmertmann (1970) indicated that a correction for the shape of the loaded area was not necessary given the uncertainties of plane-strain or axisymmetric loading conditions for various footing geometries (i.e., width-to-depth ratios of the footing base). Regarding loading effects near the footing, the author stated that in addition to the loading sequence (i.e., stress path followed), the solution should incorporate knowledge of soil nonlinearity, stress dependency, and stress-strain behavior. The correlation used for the elastic modulus was taken as the secant between 1 tsf and 3 tsf increment of a plate loading test (i.e., screw-plate test). From a total of 53 screw-plate and 12 rigid plate test results, 90% of the data were close to $2q_c$. This limit was later modified to 2.5. The good match was attributed by the author to the similarity of the cone penetration and the expansion of a cylindrical or spherical cavity as a result of a foundation loading.

2.3.2 Method Proposed by Schmertmann et al. (1978)

This method is based on the work developed by Schmertmann (1970). Figure 2-4 shows the strain influence factor diagrams presented by Schmertmann (1978) used for the numerical integration of the load-induced vertical strains. Eq. (6) and abovementioned recommendations can be used alongside with Figure 2-4 for the estimation of immediate settlements.

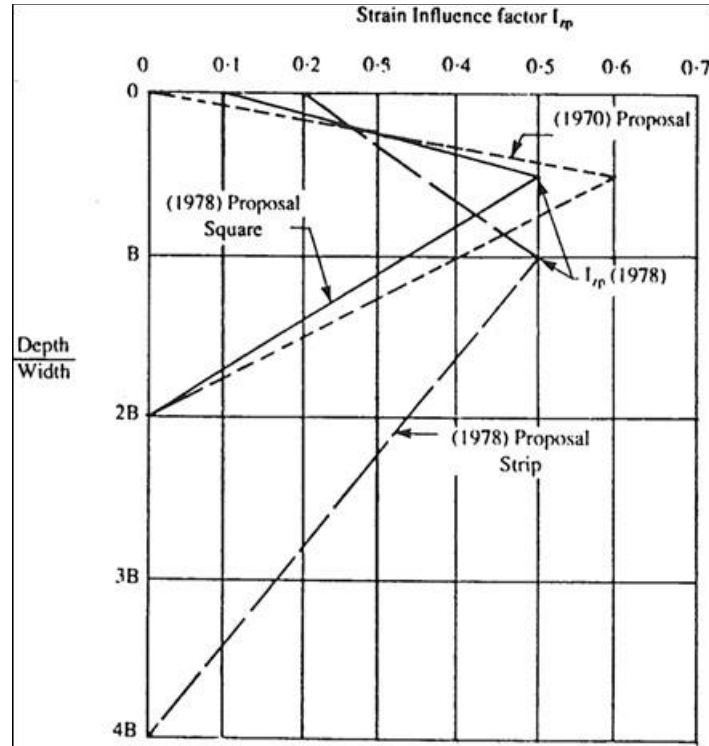


Figure 2-4. Strain influence factors. After Schmertmann et al. (1978)

2.3.3 Method Proposed by Oweis (1979)

This method considered the effects of mean normal effective stress, strain level, and initial compactness of sand on the calculation of settlements. The following equation was proposed by Oweis (1979) to account for the high variability of the elastic modulus with depth of soils by dividing the soil profile into multiple sublayers.

$$s = qB \sum_{i=1}^n (\psi_i / E_i) \quad (7)$$

where:

- s = settlement (ft)
- q = applied footing pressure (ksf)
- B = footing width (ft)
- i = individual layer

- n = total number of sublayers
- ψ_i = settlement factor of midpoint of sublayer i
- E_i = elastic stiffness modulus of sublayer i

Soil layers within the influence zone, defined by Oweis (1979) as two times the footing width, are recommended to be divided into at least four or five sublayers to improve the accuracy of the method. Figure 2-5 shows the settlement factor, F_i , varying with the normalized depth measured from the ground surface for different loading configurations as presented by Oweis (1979). The following equation alongside with Figure 2-5 were used to compute the settlement factor, ψ_i at the midpoint of the sublayer- i .

$$\psi_i = F_i - F_{i-1} \tag{8}$$

where:

- F_i = factor at the bottom of each soil layer
- F_{i-1} = factor at the top of each soil layer

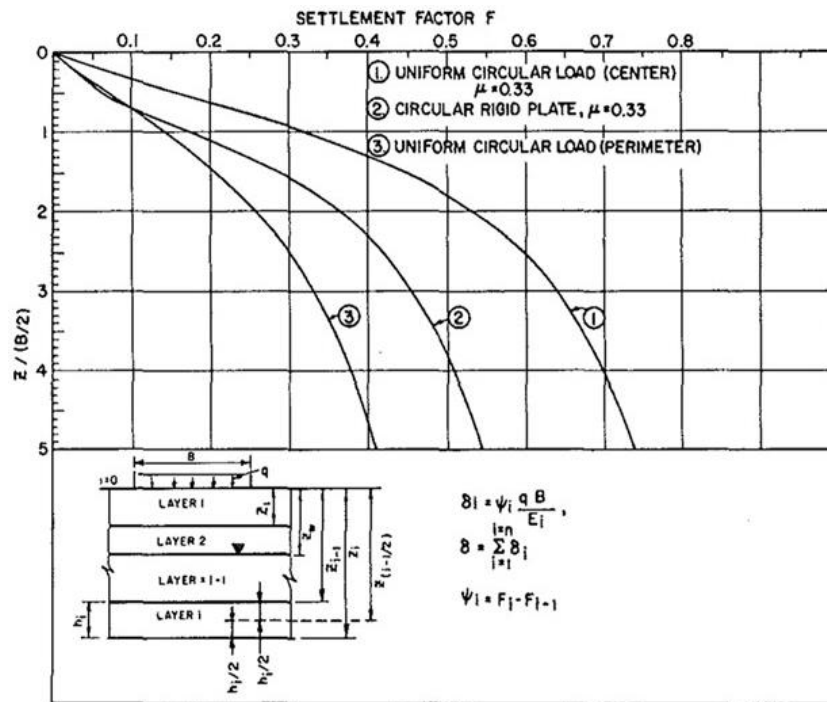


Figure 2-5. Variation of settlement factors with the normalized depth. After Oweis (1979)

Figure 2-6 shows the elastic stiffness modulus normalized to the maximum soil modulus corresponding to a strain level of 0.001% varying with the strain parameter, λ_i . This figure was presented by Oweis (1979) to properly calculate the elastic stiffness at the average strain in the sublayer- i as presented in Eq. (9).

$$\frac{E}{E_{max}} = \frac{\text{secant modulus } E \text{ at strain } (\epsilon_z)_{av.}}{\text{secant modulus } E \text{ at strain } 10^{-3}\%} \quad (9)$$

For each layer, the strain parameter, λ_i is calculated using:

$$\lambda_i = \frac{\psi_i q B}{z E_{max}} \quad (10)$$

- z = layer thickness (in ft)
- E_{max} = maximum soil modulus (in ksf) corresponding to a strain level of 0.001%
- $E_{max} = K_{max}(\sigma'_{mo} + \Delta\sigma'_m)^{0.5}$
- σ'_{mo} = effective stress at the midpoint of layer
- $\Delta\sigma'_m$ = effective stress caused by applied footing pressure at the midpoint of layer
- $K_{max} = 17.2(N_c)^{0.42}$
- N_c = overburden-corrected blow count

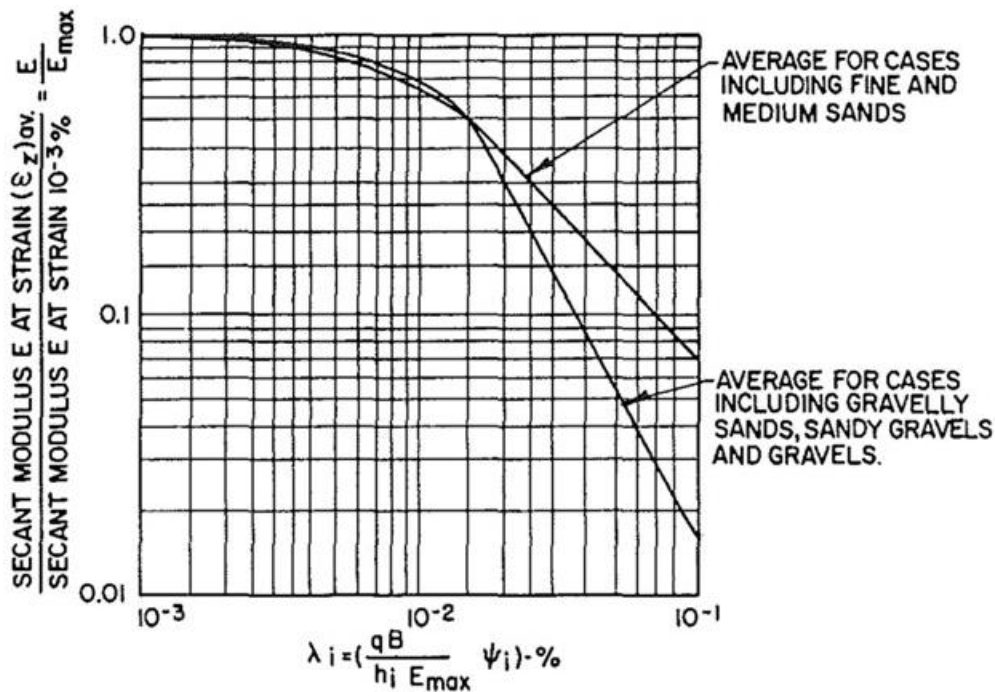


Figure 2-6. Normalized elastic stiffness modulus in terms of the strain parameter, λ_i . After Oweis (1979)

For each layer, Oweis (1979) stated that overburden-corrected SPT blow counts presented by Peck and Bazaraa (1969) should be used as follows:

$$N_c = \frac{4N}{1 + 2p'} \text{ for } p' < 1.5 \text{ ksf} \quad (11)$$

$$N_c = \frac{4N}{3.5 + 0.5p'} \text{ for } p' > 1.5 \text{ ksf} \quad (12)$$

where:

N_c = corrected blow count

N = field measured blow count

p' = effective overburden stress at the location of the blow count (in ksf)

The effective stress at the midpoint of each layer is calculated according to the following equation:

$$\sigma'_{mo} = \frac{1 + 2K_o}{3} p' \quad (13)$$

where,

K_o = at-rest coefficient of earth pressure (estimated)

p' = effective overburden stress at the layer midpoint

The effective stress resulting from the applied footing stress at the midpoint of each layer is:

$$\Delta\sigma'_m = \alpha q \quad (14)$$

where:

α = influence factor dependent on the depth and desired location of the calculation.

According to Oweis (1979), Figure 2-7 can be used to obtain the influence factor in terms of the normalized depth measured from the ground surface.

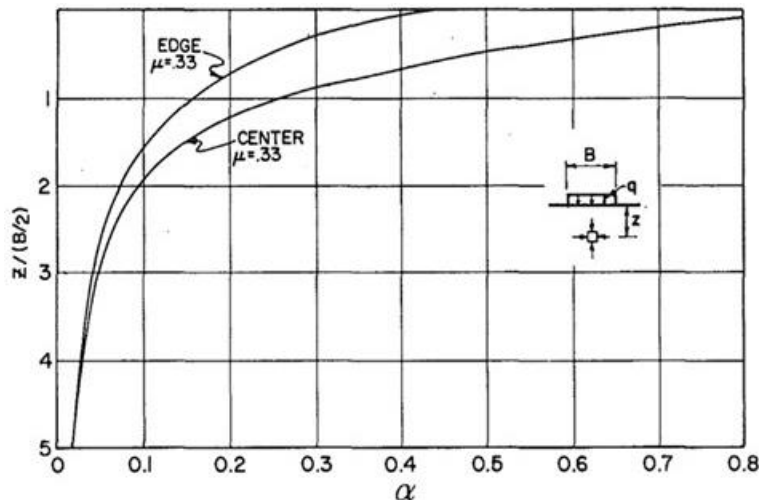


Figure 2-7. Variation of the influence factor α , with the normalized depth. After Oweis (1979)

Berardi et al. (1991) presented an alternative method to obtain the drained Young's modulus using CPT cone tip resistance data instead of SPT blow counts. This method is based on large- and small-scale laboratory tests conducted on reconsolidated silica sands and screw plate loading tests. Figure 2-8 presents the variation of the drained Young's modulus with the CPT tip resistance. This figure can be used alongside with Eq. (7) to estimate settlements caused by shallow foundations.

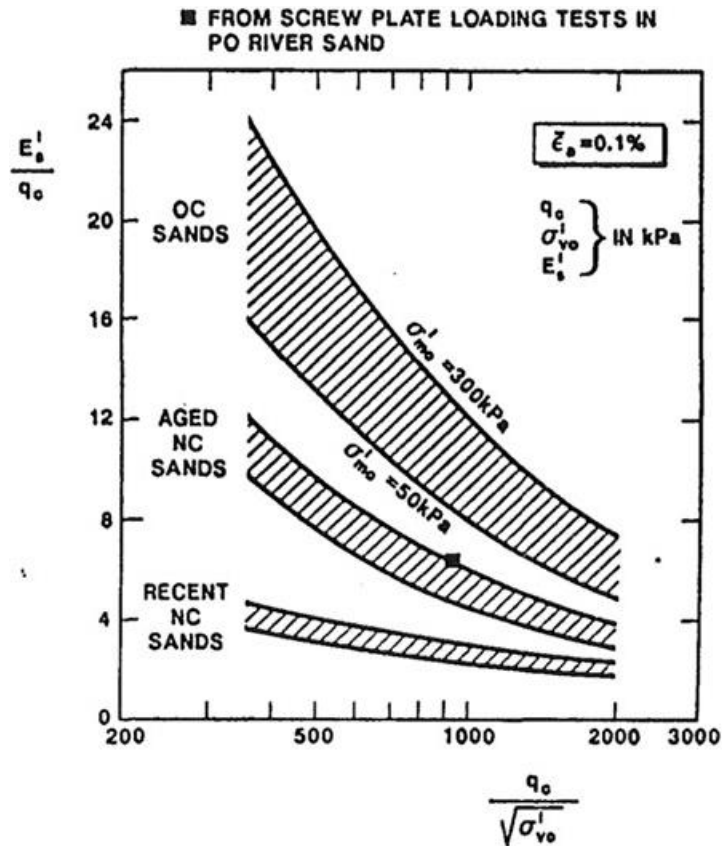


Figure 2-8. Evaluation of drained Young's modulus from CPT for silica sands (Berardi et al. 1991).

For uncontrolled granular fills and for NC cohesionless deposits, Berardi et al. (1991) recommended the reduction factors listed in Table 2-2 to correct the drained Young's modulus.

Table 2-2. Adjustment of E' for $\epsilon_z > 0.1\%$

$\frac{E'(\bar{\epsilon}_z = 0.25\%)}{E'(\bar{\epsilon}_z = 0.1\%)}$	$\frac{E'(\bar{\epsilon}_z = 0.50\%)}{E'(\bar{\epsilon}_z = 0.1\%)}$
0.65 to 0.75	0.50 to 0.60

2.4 Additional Elastic Approaches Commonly Used in Practice

2.4.1 Method Proposed by Webb (1969)

The following equation proposed by Webb (1969) considers layered soil profiles in the form of a summation of vertical stresses and elastic stiffness moduli.

$$s = \sum_i^n \left(\frac{\sigma_{zi}}{E} \right) \Delta Z_i \quad (15)$$

where,

- s = settlement (in ft)
- σ_{zi} = vertical stress in soil layer i produced by foundation stress q (in psf)
- ΔZ_i = thickness of layer i (in ft)
- E = soil Young's modulus (in psf)

Equations (16)-(18) as presented by Webb (1969) can be used to determine the Young's modulus of the soil from the uncorrected SPT blow counts, N for saturated silty sands, clayey sands, and sands with intermediate fine contents, respectively. These correlations were obtained from observations between SPT and field plate loading tests.

$$E = 5(N + 15) \quad (16)$$

$$E = 3.33(N + 5) \quad (17)$$

$$E = 4(N + 12) \quad (18)$$

2.4.2 Method Proposed by Tschebotarioff (1971)

The method proposed by Tschebotarioff (1971) were intended to estimate immediate settlements for square footings built on granular soils. Eqs. (19) and (20) were proposed for square and strip footings, respectively.

$$s = \frac{0.867qBC_s}{E} \quad (19)$$

$$s = \frac{2.0qB}{E} \log \left(1 + \frac{1.154H}{B} \right) \quad (20)$$

where,

- q = applied footing pressure
- B = footing width [or b as presented in Tschebotarioff (1971)]
- C_s = layer thickness correction factor
- E = Young's Modulus

Figure 2-9 shows the compression of the truncated pyramid of elastic material, considered by Tschebotarioff (1971). H is used in Figure 2-10 to compute the layer thickness correction factor as a function of depth.

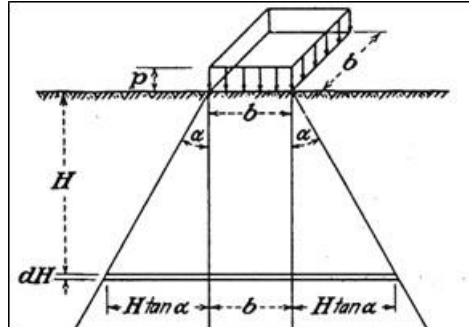


Figure 2-9. Compression of the elastic material. After Tschebotarioff (1971)

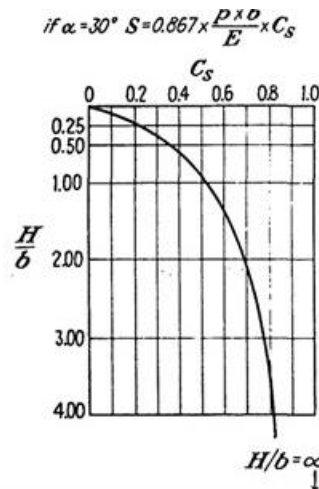


Figure 2-10. Layer thickness correction factor, C_s , versus depth. After Tschebotarioff (1971)

2.4.3 Method Proposed by Poulos and Davis (1974)

The method proposed by Poulos and Davis (1974) and included in the Canadian Foundation Engineering Manual (2006) is based on an elastic displacement solution which assumes soil as a homogeneous-isotropic and elastic material with finite layer thickness. The effects of the footing geometry, foundation roughness, foundation stiffness, and drainage conditions are included in the method. For circular footings, the following equation was proposed by Poulos and Davis (1974) to compute immediate settlements under uniform vertical pressure.

$$s = \frac{q_0 B i_c}{E_s} \quad (21)$$

where,

- s = settlement
- q_0 = applied net footing pressure
- B = footing width
- E_s = apparent modulus of elasticity
- i_c = influence factor

Figure 2-11 shows the influence factor as a function of the depth-to-footing width and Poisson's ratios proposed by Rowe and Booker (1981).

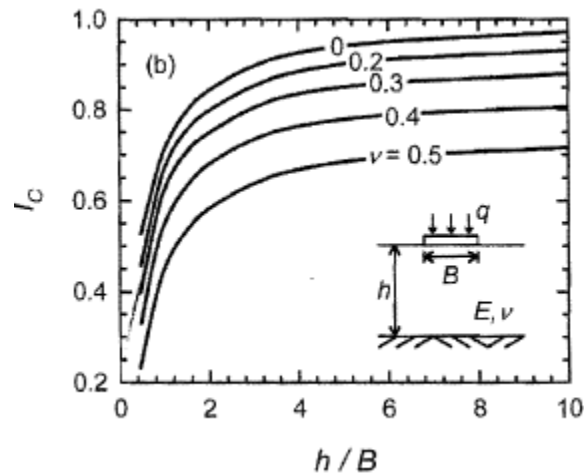


Figure 2-11. Variation of influence factor, i_c . After Rowe and Booker (1981)

The Canadian Foundation Engineering Manual (2006) stated that given the variability on soil conditions, geologic setting, type of foundation, and nature of loading, the selection of modulus of elasticity should be confirmed with empirical and semi-empirical correlations, laboratory tests, or field testing.

2.4.4 Method Proposed by Bowles (1987)

Bowles (1987) proposed the following equation for flexible and rigid shallow foundations built on predominant granular soils with variable water content.

$$s = q_0 B' \frac{1 - \mu^2}{E_s} m I_s I_F \quad (22)$$

where,

- s = settlement
- q_0 = intensity of contact pressure in units of E_s
- B' = least lateral dimension of contributing base area in units of s
- B' = $B/2$ for center; B for corner
- L' = $L/2$ for center; L for corner

- I_F = depth correction factor (computed below)
- I_s = Steinbrenner's influence factor (computed below)
- E_s = Modulus of elasticity = 2.5 to $3q_c$ in q_c units (for CPT) or $10(N+15)$ in ksf for SPT.
- μ = Poisson's ratio
- m = 4 at the footing center, 2 at edge, and 1 at the corner

Eqs. (23)-(25) were reported by Bowles (1987) to calculate the influence factors for flexible footings. In case of rigid foundations, the I_s factor can be used as 0.93. are calculated according to:

$$F_1 = \frac{1}{\pi} \left[M \ln \frac{(1 + \sqrt{M^2 + 1})\sqrt{M^2 + N^2}}{M(1 + \sqrt{M^2 + N^2 + 1})} + \ln \frac{(M + \sqrt{M^2 + 1})\sqrt{1 + N^2}}{M + \sqrt{M^2 + N^2 + 1}} \right] \quad (23)$$

$$F_2 = \frac{N}{2\pi} \tan^{-1} \left(\frac{M}{N(\sqrt{M^2 + N^2 + 1})} \right) \quad (24)$$

$$I_s = F_1 + \frac{1 - 2\mu}{1 - \mu} F_2 \quad (25)$$

where,

- M = L'/B'
- N = H/B'
- H = thickness of compressible stratum

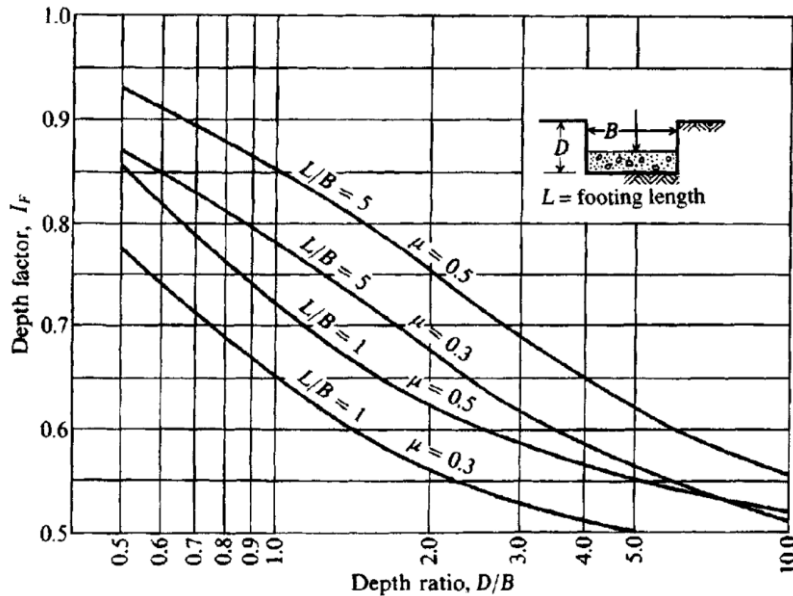


Figure 2-12. Variation of influence factor, I_F . After Bowles (1987)

The following procedure was recommended by Bowles (1987) to estimate the elastic stiffness modulus of the soil.

- Estimate q_0

- Convert round footings to equivalent squared footings
- Determine a point in the foundation base to estimate settlements.
- The stratum that is causing the settlement is: $Z=5B$
- Depth where a hard stratum is encountered. [Hard if $E_i > 10E_{i-1}$]
- Compute H/B' ratio using a constant $H=5B$
- Obtain I_s and I_F .
- Obtain the weighted average E using the following Eq. (26):

$$E_{s,av} = \frac{H_1 E_{s1} + H_2 E_{s2} + \dots + H_n E_{sn}}{H} \quad (26)$$

2.4.5 Berardi et al. (1991)

Berardi et al. (1991) revised the results of 200 cases published by Burland and Burbidge (1985) to propose some correlations to estimate the Young's modulus based on results from SPT and CPT, which are intended to be used in elastic settlement calculations. The authors also examined the problem of the depth of influence (assumed equal to B) at which the settlement should be computed. Factors such as anisotropy or fabric could not be included due to the simplification in the approach. The equation used is:

$$s = I_s \frac{qB}{E'} \quad (27)$$

s = settlement of foundation

B = width of foundation

q = net foundation pressure

E' = operational stiffness

I_s = influence factor that accounts for the shape and rigidity of the foundation, the Poisson's ratio (assumed in the original paper a value of 0.15), and H/B ratio where H is the thickness of the compressible stratum.

The I_s factor given in Table 2-3 is referred to the center of a rigid structural foundation.

Table 2-3. Influence factor I_s for settlement calculations

H/B	L/B					
	1	2	3	5	10	Circular
0.5	0.35	0.39	0.40	0.41	0.42	0.34
1.0	0.56	0.65	0.67	0.68	0.71	0.52
1.5	0.63	0.76	0.81	0.84	0.89	0.59
2.0	0.69	0.88	0.96	0.99	1.06	0.63

The drained Young's stiffness is:

$$E' = K_E P_a \left(\frac{\sigma'_{v0} + 0.5 \Delta \sigma'_v}{P_a} \right)^{0.5} \quad (28)$$

where,

$\Delta \sigma'_v$ = increment of the vertical stress under the center of the footing induced by the foundation pressure computed at a depth equal to B/2

P_a = atmospheric pressure. 1bar = 100 kPa

K_E = modulus number.

Berardi et al. (1991) based on the performance of 130 structures founded in silica sands and gravels presented a relationship between K_E and SPT blow count, N_1 . This relationship is presented in Figure 2-13. Note that N_1 can be calculated using the following equation reported in Berardi et al. (1991).

$$\bar{N}_1 = C_N \cdot \bar{N}_{SPT}; C_N = \frac{2}{1 + \sigma'_{v0}} \quad (29)$$

where,

σ'_{v0} = effective overburden stress at a depth equal to B/2 in kg/cm².

\bar{N}_{SPT} = average SPT blow-count within a depth of influence

\bar{N}_1 = average SPT blow-count normalized with respect to the effective overburden stress

C_N = correction factor

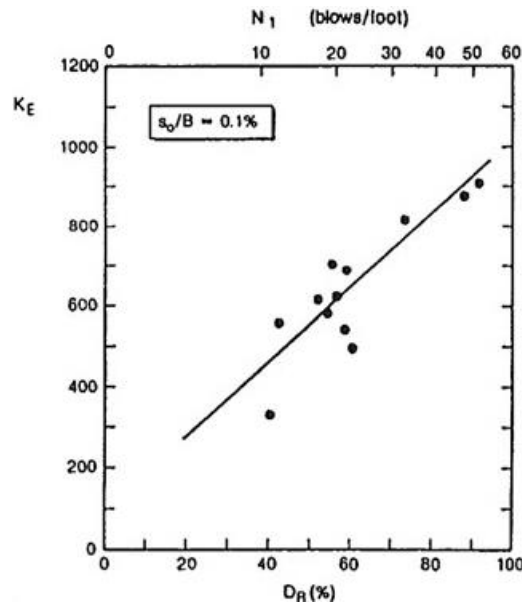


Figure 2-13. Modulus number K_E versus N_1 . After Berardi et al. (1991)

In addition, Figure 2-14 shows the loss of stiffness with relative settlement (i.e., axial strain).

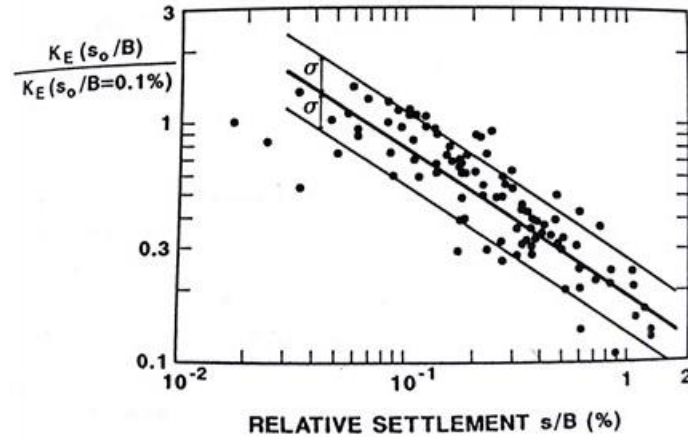


Figure 2-14. Variation of K_E with relative settlement. After Berardi et al. (1991)

Figure 2-15 presents the proposed procedure reported by Berardi et al. (1991) to estimate settlements using SPT blow counts [Eq. (28)] considering the modulus number, K_E to properly estimate the Young's modulus of the soil. The authors provide a list of factors that influence the stiffness to be considered in selecting E' as it is presented in the figure.

- Void ratio (e) or relative density (D_r)
- Average level of vertical strain ($\bar{\epsilon}_z$)
- Mean effective stress (σ'_m)
- Stress history (SH) of the deposit

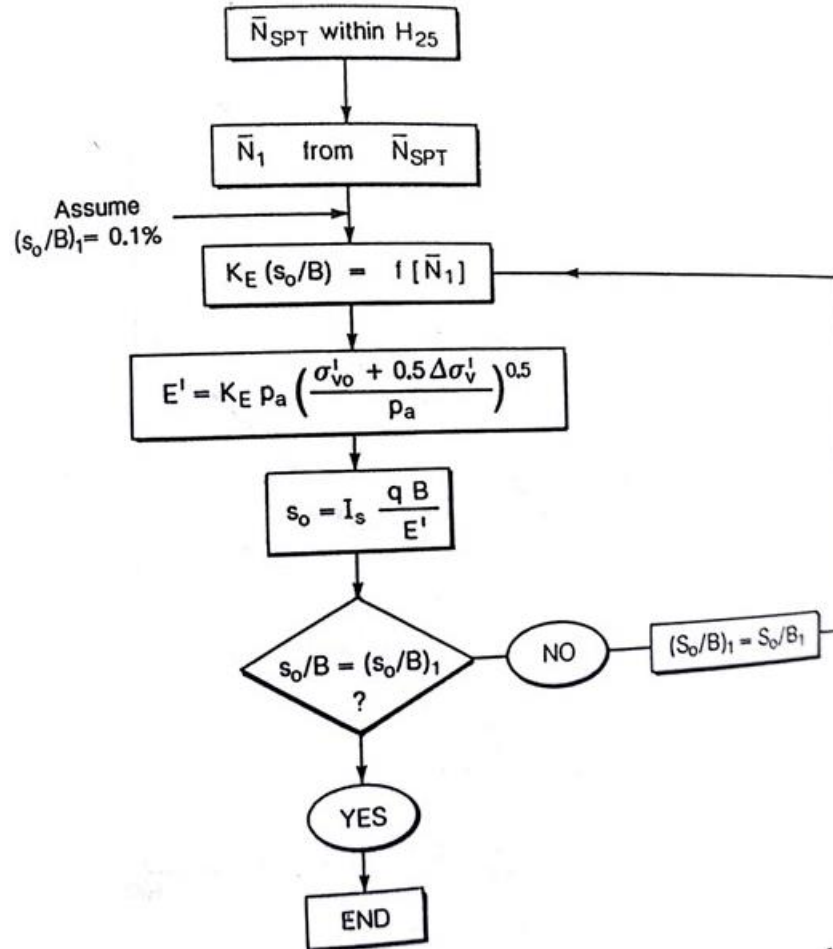


Figure 2-15. Flowchart for settlement calculations based on modulus number, K_E (Berardi et al. 1991)

2.4.6 Method Proposed by Papadopoulos (1992)

Papadopoulos (1992), based on measured stress-strain relationship, proposed a simplified method for the incremental stress variation and size of the influence zone for settlement calculations. Papadopoulos (1992) proposed the following equation taking into account the effects of nonlinearity of soil behavior by using a dimensionless factor, f . This correction factor depends on the soil stress history, foundation geometry, load conditions, and ratio constrained modulus-to-effective stress.

$$s = \left[\frac{qB}{E_s} \right] f \quad (30)$$

Where,

- s = settlement
- q = mean foundation pressure
- B = width of a rectangular foundation
- E_s = constrained modulus of the soil for the appropriate stress range

f = settlement factor which depends on soil stress history, geometry, loading and the relation between constrained modulus and effective stress.

Eq. (31) denotes a direct relationship between the constrained modulus and the effective stress (σ') for $\sigma' < 12.5$ ksf (600 kPa) proposed by Papadopoulos (1992). The constrained modulus, E_s is given by:

$$E_s = E_{s0} + \lambda \sigma' \quad (31)$$

where,

E_{s0} = constrained modulus for zero effective stress

λ = the rate of E_s with stress. $0 < \lambda < 3 \frac{E_{s0}}{\sigma'_0}$

Papadopoulos (1992) proposed the following equation as an alternative to Eq. (31):

$$E_s = 2.5 q_c \text{ and } E_s = 7.5 + 0.8N \text{ (MPa)} \quad (32a-b)$$

where:

q_c = CPT tip resistance

N = SPT blow count

According to Papadopoulos (1992), Figure 2-16 can be used to determine the settlement factor f in terms of mean foundation pressure, foundation width, unit weight of soil as it is expressed in Eq. (33). These variables were grouped in a dimensionless parameter, α and it denotes the horizontal axis of Figure 2-16 as proposed by the author.

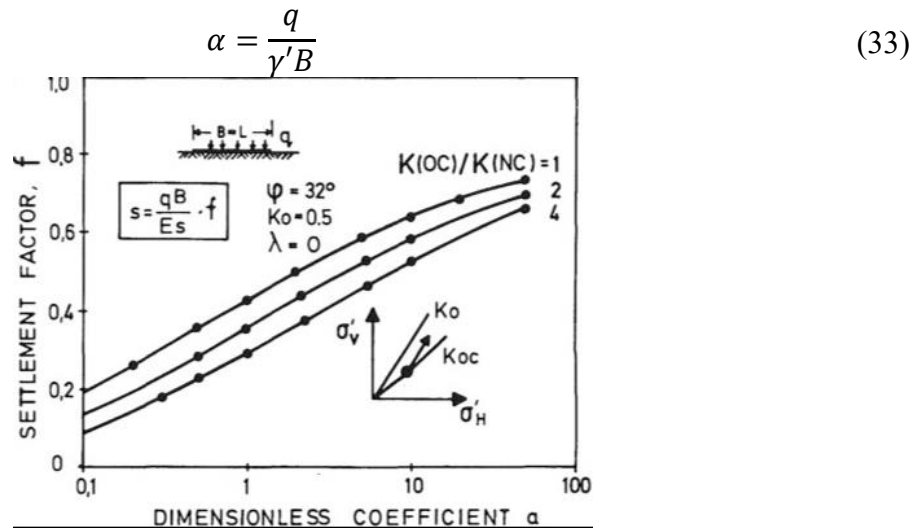


Figure 2-16. Determination of settlement factor using the dimensionless coefficient, α . After Papadopoulos (1992)

2.4.7 Method Proposed by Mayne and Poulos (1999)

Mayne and Poulos (1999) proposed Eq. (34) using displacement influence factors and numerical integration of elastic stress distributions to calculate the drained and undrained settlements of shallow foundations. This equation can be used to circular foundations on soils with Gibson profiles. Two correction factors to account for foundation rigidity and the embedment depth of the footing were included based on finite-element studies.

$$s = \frac{q \cdot d \cdot I_G \cdot I_F \cdot I_E \cdot (1 - \nu^2)}{E_0} \quad (34)$$

where,

- I_F = Foundation rigidity correction factor
- I_E = Embedment correction factor
- I_G = Displacement influence factor
- ν = Poisson's ratio (dimensionless)
- d = diameter of the footing (ft)
- t = footing thickness (ft)
- D_f = depth of embedment (ft)
- E_f = Elastic stiffness modulus of the foundation material (ksf)
- E_0 = Elastic stiffness modulus at the base of the footing (ksf)

Eqs. (35) and (36) were presented by Mayne and Poulos (1999) to compute the foundation rigidity and embedment correction factors, respectively.

$$I_F = \frac{\pi}{4} + \frac{1}{4.6 + 10K_F} = \frac{\pi}{4} + \frac{1}{4.6 + 10 \left(\frac{E_f}{E_0 + \frac{d}{2}k} \right) \left(\frac{2t}{d} \right)^3} \quad (35)$$

$$I_E = 1 - \frac{1}{3.5 \exp(1.22\nu - 0.4) \left(\frac{d}{D_f} + 1.6 \right)} \quad (36)$$

where, K_F is the foundation flexibility factor as presented in the following equation:

$$K_F = \frac{E_f}{E_s} \cdot (2t/d)^3 \quad (37)$$

where, E_s is elastic stiffness modulus of the soil computed at depth $z=d/2$.

According to Mayne and Poulos (1999), a rigid shallow foundation built on a semi-infinite soil continuum causes ground surface settlements approximately 22% lower than those obtained assuming a flexible shallow foundation. This effect is presented in Figure 2-17. The figure shows

the variation of the rigidity corrected factor with foundation flexibility factor reported by Mayne and Poulos (1999). The authors identified three categories: 1) flexible with $K_F < 0.01$, 2) intermediate flexibility with $0.01 \leq K_F \leq 10$, and 3) rigid with $K_F > 10$.

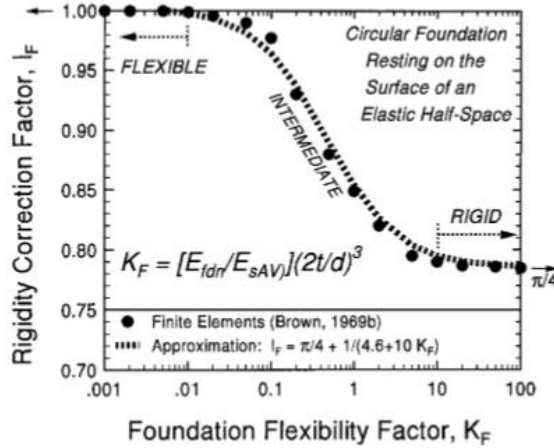


Figure 2-17. Effect of foundation rigidity on centerpoint settlement. After Mayne and Poulos (1999)

The following equations were proposed by Mayne and Poulos (1999) to compute the displacement influence factor for flexible and rigid shallow foundations.

$$I_G = \frac{1}{(1+0.68\beta^{-0.8})} \quad \text{for flexible footings} \quad (38)$$

$$I_G = \frac{1}{(1.27+0.75\beta^{-0.8})} \quad \text{for rigid footings} \quad (39)$$

where,

$$\beta = \text{Normalized Gibson Modulus} = \frac{E_0}{k_E d}$$

k_E = increase in the soil stiffness per unit depth (kips/ft³)

An updated set of solutions for the displacement influence factor I_G was proposed as a graphical solution for a flexible and smooth foundation presented in Figure 2-18:

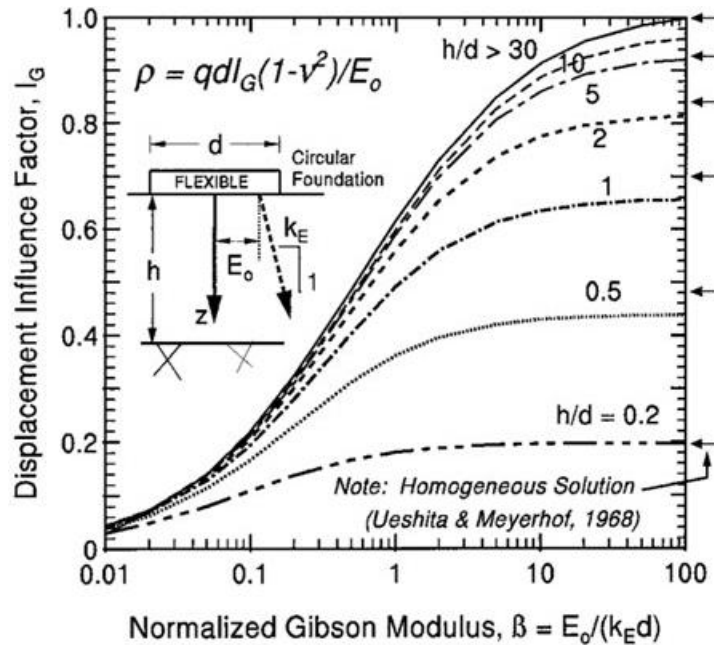


Figure 2-18. Displacement influence factor for flexible circular foundation on finite Gibson medium. After Mayne and Poulos (1999)

Finally, Mayne and Poulos (1999) proposed Eq. (40) to compute an equivalent diameter for immediate settlements in rectangular shallow foundations by using Eq. (34). The equivalent diameter of the footing can be written as:

$$d = \sqrt{\frac{4BL}{\pi}} \quad (40)$$

- d = equivalent diameter
- B = width of foundation
- L = length of foundation

2.5 Methods for Computing Settlements on Granular Soils Based on Field Tests

Empirical and semi-empirical methods proposed by several researchers [e.g., Terzaghi et al. 1967; Meyerhof (1965); Schmertmann (1986); Peck et al. (1974); among others] to correlate soil response with field measurements are widely used by practitioners to characterize the in situ conditions in addition to laboratory testing programs (i.e., triaxial and oedometer tests). In this section, correlations derived from SPT, CPT, PMT, and DMT data are presented to compute settlements. A summary of methods used to estimate the settlement and correlate the Young's modulus are listed at the end of this chapter. They, combined with the conical loading tests presented later in this report, will be used to issue recommendations of stiffness parameters and settlement calculations that best fit Florida soil conditions.

2.5.1 Correlations Based on SPT Tests

2.5.1.1 Terzaghi et al. (1967)

This method presented by Terzaghi et al. (1967) was derived for dry and moist sands based on SPT blow counts and surface loading tests. Eqs. (41)-(44) were presented by Terzaghi et al. (1967) for shallow foundations of width (B) smaller than 4 ft, larger or equal than 4 ft, rafts, and a general form, respectively.

$$s = \left(\frac{8q}{N}\right) (C_w C_d) \quad (41)$$

$$s = \left(\frac{12q}{N}\right) \left[\frac{B}{B+1}\right]^2 (C_w C_d) \quad (42)$$

$$s = \left(\frac{12q}{N}\right) (C_w C_d) \quad (43)$$

$$s = \left(\frac{3q}{N}\right) \left[\frac{2B}{B+1}\right]^2 (C_w C_d) \quad (44)$$

where,

s = settlement (inches)

q = net footing stress (in tsf)

N = uncorrected (field) blow counts

B = footing width (in ft)

W = depth of water table (in ft)

D = footing depth (in ft)

C_w = water correction. $C_w = 2 - (W/2B) \leq 2.0$ for surface footings; $C_w = 2 - 0.5 (D/B) \leq 2.0$ for fully submerged; and for embedded footings with $W \leq D$.

C_d = embedment correction. $C_d = 1 - 0.25 (D/B)$.

For dense saturated sands and fine-grained sands with silts, it is recommended to correct the blow counts, N, as follows:

$$N_c = 15 + 0.5 (N - 15) \text{ for } N > 15 \quad (45)$$

The correction for water table applies to cases where groundwater is at or above the base of the footing (i.e., fully submerged case). For partially submerged conditions (i.e., water located between D and D+B), a correction factor is required for surface footings only. In common practice, the water correction is often omitted from the settlement estimates using this method since the method is generally considered to be overly conservative (Lutenegger and DeGroot 1995).

2.5.1.2 Meyerhof (1965)

Meyerhof (1965) proposed Eqs. (46)-(48) for foundation layouts of $B \leq 4\text{ft}$, $B > 4\text{ft}$, and rafts, respectively.

$$s = \frac{4q}{N} \quad (46)$$

$$s = \left(\frac{6q}{N}\right) \left[\frac{B}{B+1}\right]^2 \quad (47)$$

$$s = \frac{6q}{N} \quad (48)$$

- s = settlement (in inches)
q = footing stress (in tsf)
N = uncorrected blow counts
B = footing width (in ft)

The author recommended an allowable bearing capacity equivalent to 1 inch of maximum ground surface settlement.

2.5.1.3 Teng (1962)

Using Terzaghi and Peck (1948), Teng converted the charts in this method into an equation:

$$s = \left[\frac{q}{720(N_c - 3)}\right] \left[\frac{2B}{B+1}\right]^2 \left(\frac{1}{C_w C_d}\right) \quad (49)$$

- s = settlement (inches)
q = net footing stress (in psf)
 N_c = corrected blow count
B = footing width (in ft)
 C_w = water table correction. $C_w = 0.5 + 0.5 (W/D)/(B) \geq 0.5$ for water at and below footing base
 C_d = embedment correction. $C_d = 1 + (D/B) \leq 2.0$
 $N_c = N [50/(p' + 10)]$ [blow count correction as Gibbs and Holtz (1957)]
 p' = effective overburden stress taken at $D + B/2$, in psi. $p' \leq 40$ psi.

2.5.1.4 Alpan (1964)

This method presented by Alpan (1964) is also included in the USACE (1990). It assumes a linear behavior for bearing pressures in the range of allowable bearing capacities, and can be used to estimate ground surface settlements based on foundation geometric configuration, applied pressure, and blow counts corrected by overburden pressure. The equation is expressed as:

$$s = s_0 \left[\frac{2B}{B+1}\right]^2 \left(\frac{m'}{12}\right) \quad (50)$$

where,

- s = settlement (in inches)
- s₀ = settlement of a 1ft² plate (in inches) = αq
- B = footing width (in ft)
- m' = shape correction factor. m'=(L/B)^{0.39} (USACE, 1990)

Note that the parameter s₀ can be computed as a product of a compressibility constant, α, and the foundation pressure, q, computed in tsf. The compressibility constant is determined based on the corrected blow count, N_c, as presented in Figure 2-19. The left hand side chart is used for blow counts between 5 and 50 and the right hand side chart for blow counts between 25 and 80. To account for the water table, Alpan (1964) recommended to duplicate the obtained settlement for small ratios of D/B. In case of D/B ratios near 1, the settlement should be increased by 50%.

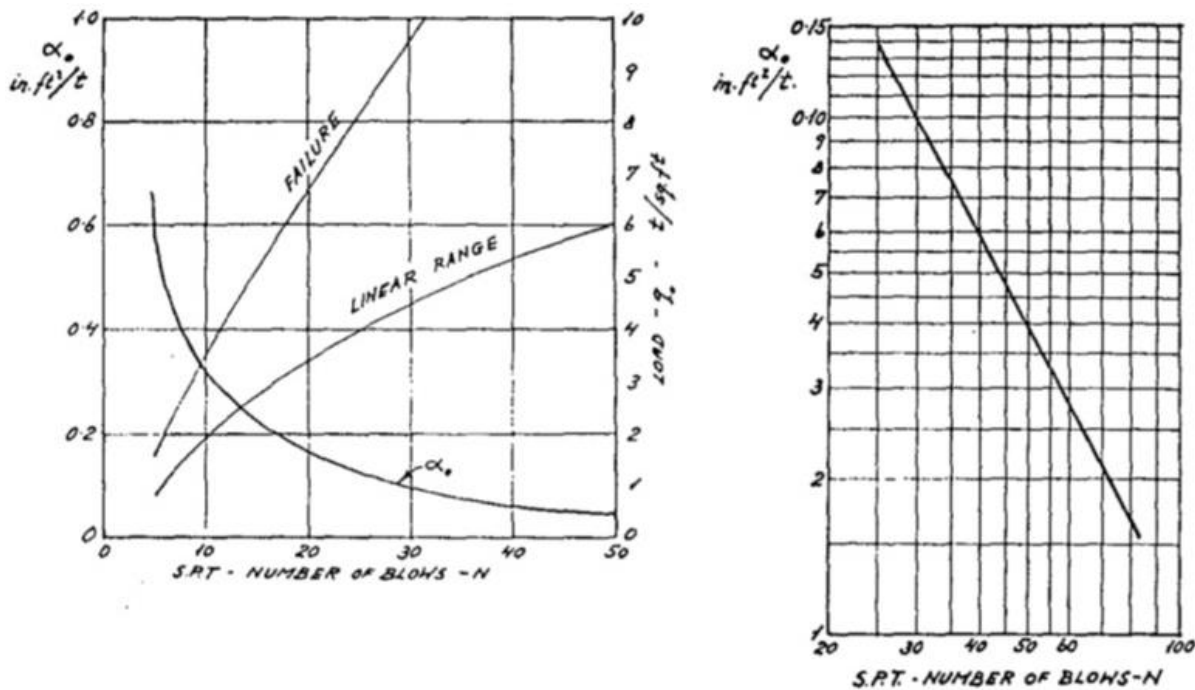


Figure 2-19. Variation of the compressibility constant, α, based on the SPT blow count. After Alpan (1964)

Figure 2-20 presents the corrected SPT blow count (N_c) reported by Alpan (1964) in terms of the relative density, D_r, and the effective overburden pressure for granular soils. Alpan (1964) proposed the following correction for blow counts greater than 15 for granular material with some fine contents:

$$N_c = 15 + 0.5(N - 15) \quad (51)$$

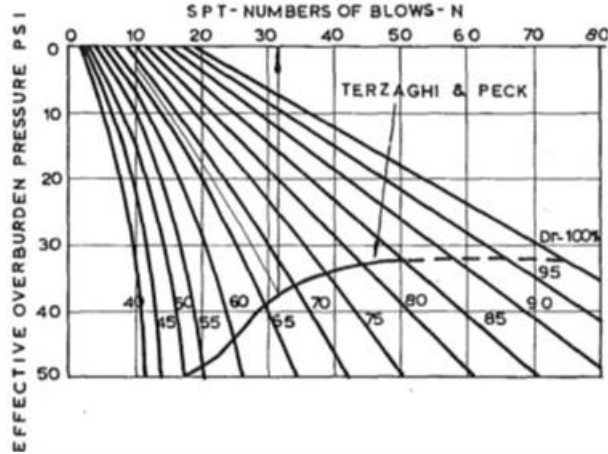


Figure 2-20. Relative density chart from blow counts. After Coffman (1960)

2.5.1.5 Peck and Bazaraa (1969)

This method is recommended by FHWA HI-88-009. It considers the effect of the overburden pressure on the blow counts, water table, and embedment depth. For settlement predictions, Eqs. (52)-(54) were proposed by Peck and Bazaraa (1969) for foundation geometries of $B \leq 4\text{ft}$, $B > 4\text{ft}$, and rafts, respectively.

$$s = \left[\frac{16q}{3N_c} \right] C_d C_w \quad (52)$$

$$s = \left[\frac{8q}{N_c} \right] \left[\frac{B}{B+1} \right]^2 C_d C_w \quad (53)$$

$$s = \left[\frac{8q}{N_c} \right] C_d C_w \quad (54)$$

where,

s = settlement (in inches)

q = footing pressure (in tsf)

N_c = corrected blow count

B = footing width (in ft)

C_d = embedment correction. $C_d = 1.0 - 0.4 [(\gamma D/q)]^{0.5}$

γ = soil total unit weight

C_w = water table correction. $C_w = \sigma_v / \sigma'_v$. If the water table is below $D + B/2$ $C_w = 1.0$.

σ_v = vertical total stress computed at $D + B/2$

σ'_v = vertical effective stress computed at $D + B/2$

$N_c = (4N)/(1+2\sigma'_v)$ for $\sigma'_v \leq 1.5$ ksf or $N_c = (4N)/(3.25+0.5\sigma'_v)$ for $\sigma'_v > 1.5$ ksf

2.5.1.6 Parry (1985)

Similar to D'Appolonia et al. (1970), this method was derived in terms of the sand compressibility, footing geometry, and applied load as presented in Eq. (55).

$$s = \alpha \left[\frac{qB}{N_m} \right] C_d C_w C_t \quad (55)$$

where,

- s = settlement (in inches)
- α = 0.25
- q = footing pressure (in tsf)
- B = footing width (in ft)
- N_m = weighted average of uncorrected N values between D and $D = 2B$
- C_d = embedment correction factor. $C_d = [1.3 (0.75 + D/B)]/[1 + 0.25 (D/B)]$
- C_w = water table correction factor. $C_w = 1 + (D_w)/(D + 3B/4)$ for $0 < D_w < D$ and $C_w = 1 + [D_w(2B + D - D_w)]/[2B(D + 0.75B)]$ for $0 < (D_w - D) < 2B$
- C_t = thickness correction factor for compressible sand layers.

The weighted average of SPT blow counts proposed by Parry (1985) is presented in Eq. (56). The author concluded that soil layers within $3B/4$ below the foundation would contribute with approximately 50% of the total settlements. The remaining 50% was associated with depths below $3B/4$.

$$N_m = \frac{3N_1 + 2N_2 + N_3}{6} \quad (56)$$

where,

- N_1 = Average N value until a depth of $3B/4$ from the footing base.
- N_2 = Average N value between depths $3B/4$ and $1.5B$ from the footing base.
- N_3 = Average N value below a depth of $1.5B$ from the footing base.

In addition, Figure 2-21 shows the variation of the thickness correction factors with the ratio thickness-to-footing width presented by Parry (1985) for soil layers made of compressible sandy soils.

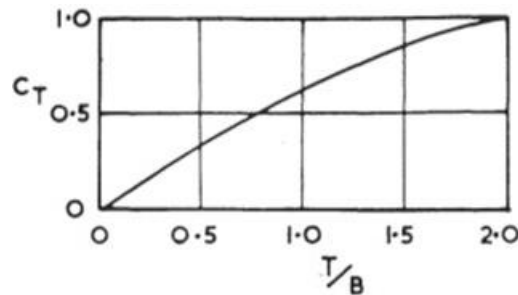


Figure 2-21. Thickness correction factor for layer thickness (T). After Parry (1985)

2.5.1.7 Schultze and Sherif (1973)

This method is based on measurements in 48 sites using the SPT results. The empirical equation proposed is:

$$s = \frac{Q \cdot F_c}{N^{0.87} C_d} \quad (57)$$

where,

- s = settlement (in cm)
- Q = gross footing pressure (i.e., surcharge is not subtracted) (in kg/cm²)
- F_c = influence factor based on footing geometry (in cm³/kg)
- N = uncorrected blow count (the USACE manual recommended to use the corrected N₆₀)
- C_d = embedment correction. C_d = 1 + 0.4 (D/B) ≤ 1.4

Table 2-4 and Figure 2-22 present the influence factors proposed by Schultze and Sherif (1973) in terms of the foundation geometrical configuration.

Table 2-4. Influence factors from Schultze and Sherif (1973)

D _v /B	L/B			
	1	2	5	100
1.5	0.91	0.89	0.87	0.85
1.0	0.85	0.73	0.69	0.55
0.5	0.52	0.48	0.43	0.39

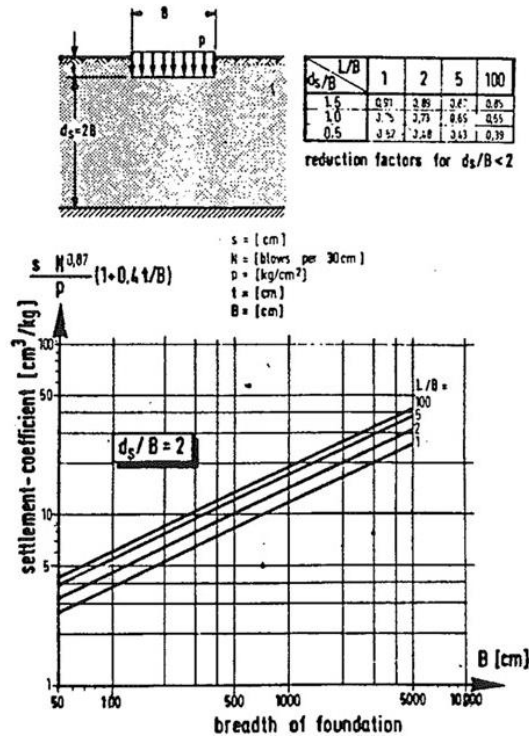


Figure 2-22. Influence factor chart from Schultze and Sherif (1973)

2.5.1.8 Peck et al. (1974)

This method proposed by Peck et al. (1974) employed the SPT blow count corrected with the overburden stress to estimate settlements caused by a shallow foundation as presented in Eqs. (58) and (59) for medium sized footings and rafts, respectively. This method also included a correction factor to account for the location of the groundwater table.

$$s = \frac{q}{0.11 \cdot N_c \cdot C_w} \quad (58)$$

$$s = \frac{q}{0.22 \cdot N_c \cdot C_w} \quad (59)$$

where

s = settlement (in inches)

q = footing stress (in tsf)

N_c = corrected blow count = $N C_n$

C_w = water table correction. $C_w = 0.5 + 0.5 (D_w / (D + B))$

C_n = $0.77 \log (20/p')$ (Overburden correction factor)

p' = effective overburden stress (in tsf) for the measured blow count at $D + B/2 \geq 0.25$ tsf

$2.0 > C_n > 1.5$ for overburden stresses less than 0.25 tsf in the upper 5 ft

2.5.1.9 Meyerhof (1974)

Meyerhof presented Eqs. (60) and (61) to estimate ground surface settlements based on SPT blow counts and foundation geometry for clean and silty sands, respectively:

$$s = \frac{q \cdot B^{1/2}}{2N} \cdot C_d \quad (60)$$

$$s = \frac{q \cdot B^{1/2}}{N} \cdot C_d \quad (61)$$

- s = settlement (in inches)
q = footing stress (in tsf)
B = footing width (in inches)
N = uncorrected blow count
C_d = embedment correction. C_d = 1 - 0.25 (D/B)

2.5.1.10 Arnold (1980)

This method proposed by Arnold (1980) is based on the relative density of the sand, D_r. The proposed equation is as follows:

$$s = 43.06B \sum_{z=0}^{2B} \Delta z \frac{\alpha \ln\left(\frac{1}{1 - Iq/Q}\right)}{[1 + (3.281B)^m]^2} \quad (62)$$

where,

- s = settlement (in mm)
B = footing width (in meters)
α = dimensionless constant. α = 0.032766 - 0.0002134 D_r
m = dimensionless constant. m = 0.788 + 0.0025 D_r
I = vertical strain influence factor
q = applied footing stress (kN/m²)
Q = hypothetical ultimate pressure (kN/m²). Q = 19.63 D_r - 263.3 (kN/m²)
Δz = individual layer thickness (in meters)
I = 1-0.5 (z/B) is related to depth below the footing at the midpoint of each layer

Arnold (1980) presented an additional equation to determine the relative density of sands in terms of the SPT blow count, N, and the total vertical stress, γH.

$$D_r = 25.6 + 20.37 \sqrt{\frac{1.26(N - 2.4)}{0.0203\gamma H + 1.36}} - 1 \quad (63)$$

2.5.1.11 Burland and Burbidge (1985)

This method, which is also presented in FHWA-SA-02-054, is based on 200 case histories considering load intensity, footing geometry, and influence zone below the footing base. Another important aspect that is taken into account is the consolidation stage of the sand (Lutenegger and DeGroot 1995).

$$s = 0.14 C_s C_I I_c \left(\frac{B}{B_r} \right)^{0.7} \frac{q'}{\sigma_r} B_r \text{ for NC soils} \quad (64)$$

$$s = 0.047 C_s C_I I_c \left(\frac{B}{B_r} \right)^{0.7} \frac{q'}{\sigma_r} B_r \text{ for OC soils and } q' \leq \sigma'_c \quad (65)$$

$$s = 0.14 C_s C_I I_c \left(\frac{B}{B_r} \right)^{0.7} \frac{q' - 0.67\sigma'_c}{\sigma_r} B_r \text{ for OC soils and } q' > \sigma'_c \quad (66)$$

where,

s = settlement (in mm)

C_s = shape factor. $C_s = [(1.25L/B)/(L/B) + 0.25]^2$

C_I = depth correction factor. $C_I = (H/Z_I)(2 - IH/Z_I) \leq 1.0$

I_c = soil compressibility index. $I_c = 1.71/(\bar{N}_{60})^{1.4}$ (for NC soils) or $I_c = 0.57/(\bar{N}_{60})^{1.4}$ (for OC soils)

\bar{N}_{60} = Average adjusted blow counts

B = footing width (in meters)

B_r = reference width ($B = 0.3$ m)

q' = net footing pressure (in kPa)

σ_r = reference stress. $\sigma_r = 100$ kPa

σ'_c = preconsolidation stress (in kPa)

L = footing length

B = footing width

H = depth from the bottom of the footing to the bottom of the compressible soil

Z_I = influence depth below footing. $Z_I = 1.4 (B/B_r)^{0.75} B_r$

Blow count values measured from the footing base to the depth of influence are corrected for energy efficiency. Burland and Burbidge (1985) recommended the used of Terzaghi and Peck (1948) for clayey or silty sand with $N_{60} > 15$. For gravelly sand or sandy gravel, the authors recommended multiplying N_{60} by 1.25.

2.5.1.12 Anagnostopoulos et al. (1991)

Based on statistical and regression analysis, Anagnostopoulos et al. (1991) presented the following equations for settlements:

$$s = \frac{0.57q^{0.94}B^{0.90}}{N^{0.87}} \text{ for } 0 < N < 10 \quad (67)$$

$$s = \frac{0.35q^{1.01}B^{0.69}}{N^{0.94}} \text{ for } 10 < N < 30 \quad (68)$$

$$s = \frac{604q^{0.90}B^{0.76}}{N^{2.82}} \text{ for } N > 30 \quad (69)$$

$$s = \frac{1.90q^{0.77}B^{0.45}}{N^{1.08}} \text{ for } B < 3 \text{ m} \quad (70)$$

$$s = \frac{1.64q^{1.02}B^{0.59}}{N^{1.37}} \text{ for } B > 3 \text{ m} \quad (71)$$

where,

- s = settlement (in mm)
- q = footing stress (in kPa)
- B = footing width (in meters)
- N = uncorrected blow count (mean value in B)

2.5.2 Correlations Based on CPT Tests

2.5.2.1 DeBeer and Martens (1957)

Based on the semi-empirical Terzaghi-Buisman method, the equation for calculating settlements is presented as follows:

$$s = \frac{2.3}{C} \log \frac{p'_0 + \Delta p'}{p'_0} H \quad (72)$$

where:

- s = settlement
- C = constant of compressibility
- p'_0 = effective overburden stress
- $\Delta p'$ = increment of stress at a given depth due to the footing pressure
- H = thickness of the layer
- C = $1.5q_c/p'_0$
- $\Delta p'$ = obtained using Boussinesq equation, $\Delta p' = (3q \cos^5\theta)/2\pi z^2$, for constant q_c , and using Buisman equation, $\Delta p' = (2P \cos^6\theta)/\pi z^2$, for variable q_c .

The influence zone was considered as the depth below the footing base where the change in vertical effective stress was equal to 10% of the applied surface pressure. This method is only applicable to NC sands.

2.5.2.2 Meyerhof (1965)

Meyerhof (1965) based on 20 case histories proposed Eq. (73) to predict the settlement for shallow foundations. The mean ratio of calculated to measured settlement was 1.25 higher for a settlement range of 0.3 to 3.3 in (Lutenegger and DeGroot 1995).

$$s = \frac{qB}{2q_c} \quad (73)$$

where:

- s = settlement (in ft)
- q = net foundation pressure (in tsf)
- B = footing width (in ft)
- q_c = average cone tip resistance over a depth equal to B below the footing (in tsf)

2.5.2.3 DeBeer (1965)

DeBeer and Martens (1957) presented the following equation:

$$s = \sum_{i=1}^N 1.535 \left(\frac{\sigma'_{v0i}}{q_{ci}} \right) \log \left[\frac{(\sigma'_{v0i} + \Delta\sigma'_v)}{\sigma'_{v0i}} \right] \Delta h_i \quad (74)$$

where,

- s = settlement (in meters)
- σ'_{v0i} = initial effective stress in the ith layer (in kPa)
- Δσ'_v = increase in effective pressure (in kPa)
- q_{ci} = cone tip resistance (in kPa)
- Δh_i = layer thickness (in meters)

2.5.3 Correlations Based on DMT Tests

2.5.3.1 Schmertmann (1986)

The following equation was presented by Schmertmann (1986). The author showed an average ratio of computed to predicted settlement of 1.18 based on sixteen cases.

$$s = \sum_{i=1}^n \left(\frac{\Delta\sigma'_v \cdot h_i}{M_i} \right) \quad (75)$$

where,

- Δσ'_v = effective stress increase at the mid-height of each layer. Any method to calculate the vertical stress increase is suitable.
- h_i = thickness of the ith layer.
- M = average modulus of soil for each layer from the DMT

Janbu (1963, 1967) expressed M as:

$$M = \frac{1 + e}{C_c} \ln \sigma'_v \quad (76)$$

where,

e = void ratio

C_c = compression index

For immediate settlements, E , is used as equivalent to the Young's modulus for sands ($M=E$). For cohesive soils $E = 0.75M$.

2.5.3.2 Leonards and Frost (1988)

This method proposed by Leonards and Frost (1988) combines CPT and DMT results and uses the following equation based on Schmertmann's expression:

$$s = C_1 q_{net} \sum_0^D I_z \Delta_z \left[\frac{R_z(OC)}{E_z(OC)} + \frac{R_z(NC)}{E_z(NC)} \right] \quad (77)$$

where,

C_1 = correction factor to take into account the effect of embedment

q_{net} = net increase contact pressure

D = thickness of the granular stratum

I_z = strain influence factor

Δ_z = height of the sublayer

$R_z(OC)$ = ratio of the stress increment corresponding to the OC portion in a given layer to the total increment of stress in that layer.

$R_z(NC)$ = ratio of the stress increment corresponding to the NC portion in a given layer to the total increment of stress in that layer.

$E_z(OC)$ = selected E-values corresponding to the OC portions.

$E_z(NC)$ = selected E-values corresponding to the NC portions.

The step-by-step procedure is described below:

- Divide the soil in layers.
- Determine the average q_c/σ'_{v0} ratio and K_D for each layer.
- Determine $K(OC)$ with the following equation:

$$K(OC) = 0.376 + 0.095K_D - 0.0017 \frac{q_c}{\sigma'_{v0}} \quad (78)$$

- Obtain ϕ_{ps} using Durgunoglu and Mitchell (1975) or Marchetti (1985) chart.
- Calculate ϕ_{ax} from:

$$\phi_{ax} = \phi_{ps} - \frac{\phi_{ps} - 32^\circ}{3} \quad (79)$$

- Determine:

$$OCR = \left[\frac{K(OC)}{1 - \sin\phi} \right]^{(1/0.8\sin\phi)} \quad (80)$$

- Calculate the initial vertical effective stress at the center of the layer
- Calculate the preconsolidation pressure:

$$p'_c = \sigma'_{v0} \cdot OCR \quad (81)$$

- Evaluate the stress increment at the center of the layer (assume 2:1 method)
- Calculate the final stress at the center of the layer as:

$$\sigma'_f = \sigma'_{v0} + \Delta\sigma' \quad (82)$$

- Determine:

$$R_z(OC) = \frac{(p'_c - \sigma'_{v0})}{(\sigma'_f - \sigma'_{v0})} \quad (83)$$

$$R_z(NC) = \frac{(\sigma'_f - p'_c)}{(\sigma'_f - \sigma'_{v0})} \quad (84)$$

- Determine $E_z(OC)$ and $E_z(NC)$ from E_D
- Determine the strain influence factor I_z from Schmertmann's method.
- Compute settlement

2.6 Recommended Elastic Modulus Based on SPT, CPT, DMT, and PMT Correlations

Using the results of in situ tests, it is possible to estimate the elastic properties (E , ν) of the soil. Since the variation of the Poisson's coefficient is not significant, only the correlations for the Young's modulus are presented. A compilation of correlations found in the technical literature are summarized in the following table:

Table 2-5. Young's modulus correlations from SPT and CPT tests

SOIL	SPT	CPT
Dry Sand	<p>Schultze and Melzer (1965): $E_s = (1/m_v) = \nu \sigma^{0.522}$ $\nu = 246.2 \log N - 263.4 \gamma \cdot t + 375.6 \pm 57.6$ $\gamma \cdot t =$ Overburden Pressure. Valid from $\gamma \cdot t = 0$ to 1.2 kg/cm^2. N in N_{30} Coefficient of correlation $R = 0.730$</p>	<p>Schultze and Melzer (1965): $E_s = (1/m_v) = \nu \sigma^{0.522}$ $\nu = 301.1 \log q_c - 382.3 \gamma \cdot t + 60.3 \pm 50.3$ $\gamma \cdot t =$ Overburden Pressure. Valid from $\gamma \cdot t = 0$ to 0.9 kg/cm^2. q_c in kg/cm^2 Coefficient of correlation $R = 0.778$</p>
Sand	<p>Trofimenkov (1974): $E_s = (350 \text{ to } 500) \log N, \text{ kg/cm}^2$ Webb (1969): $E = 4(N + 12), \text{ ton/ft}^2$ Chaplin (1963): $E_s^{4/3} = (44N), \text{ tsf}$ Denver (1982): $E_s = 7(N)^{0.5}, \text{ MPa}$ Clayton et al. (1985): $E_s = 3.5N \text{ to } 40N, \text{ MPa}$ Papadopoulos and Anagnostopoulos (1987): $E_s = 7.5 + 0.8N, \text{ MPa}$</p>	<p>Buisman (1940): $E_s = 1.5q_c$ Trofimenkov (1964): $E_s = 2.5q_c$ (lower limit) $E_s = 100 + 5q_c$ (Average) DeBeer (1965): $E_s = 1.5q_c$ Bachelier and Parez (1965): $E_s = \alpha q_c; \alpha = 0.8 - 0.9$ Vesić (1970): $E_s = 2(1 + D_R^2)q_c; D_R =$ relative density Gielly et al. (1969) Sanglerat et al. (1972): $E_s = \alpha q_c;$ $q_c < 50 \text{ bars } \alpha = 2; q_c > 100 \text{ bars } \alpha = 1.5$ DeBeer (1974b): Greek Practice $E_s = 1.5q_c; q_c > 30 \text{ kg/cm}^2$ $E_s = 3q_c; q_c < 30 \text{ kg/cm}^2$ Trofimenkov (1974): $E_s = 3q_c$ Thomas (1968): $E_s = \alpha q_c \alpha = 3 - 12$ Schmertmann (1970): $E_s = 2q_c$</p>

Table 2-6. Young's modulus correlations from SPT and CPT tests (continuation)

SOIL	SPT	CPT
Sand with fines	Kulhawy and Mayne (1990): $E/Pa=5N_{60}$ Webb (1969): $E = 3.33 (N + 5)$, tons/ft ² (Clayey saturated sands)	
Clean NC Sand	Kulhawy and Mayne (1990): $E/Pa=10N_{60}$	$E=2$ to $4 q_c$ Vesić (1970): $E=(1+Dr^2)q_c$
Clean OC Sand	Kulhawy and Mayne (1990): $E/Pa=15N_{60}$ Bowles (1996): $E_{(OCR)}=E_{NC}\sqrt{OCR}$, kPa $E_s=40,000+1,050N_{55}$, kPa	Bowles (1996): $E_s=6$ to $30 q_c$
Gravelly sand	Bowles (1996): $E_s=1,200(N_{55}+6)$, kPa $E_s=600(N_{55}+6)$, kPa (for $N_{55}\leq 15$) $E_s=600(N_{55}+6)+2,000$, kPa (for $N_{55}>15$)	
Young Uncemented silica sand		CPT Guide-2015: $E=\alpha_E(q_t-\sigma_{vo})$ $\alpha_E=0.015[10^{(0.55lc+1.68)}]$
Clayey sand	Bowles (1996): $E_s=320(N_{55}+15)$, kPa	Bowles (1996): $E_s=3$ to $6 q_c$ Bachelier and Parez (1965): $E_s= \alpha q_c$ $\alpha=3.8-5.7$
Silty sand		$E=1$ to $2 q_c$ Bachelier and Parez (1965): $E_s= \alpha q_c$ $\alpha=1.3-1.9$
Submerged fine to medium sand	Webb (1969): $E=5(N+15)$, tons/ft ²	
Submerged sand	Bowles (1996): $E_s=250(N_{55}+15)$, kPa	Webb (1969): $E_s= 2.5(q_c+30)$, tsf Bowles (1996): $E_s=F q_c$ $e=1.0$ $F=3.5$ $e=0.6$ $F=7.0$
Submerged clayey sand		Webb (1969): $E_s= 1.67(q_c+15)$, tsf
Silt with sand to gravel with sand	Begemann (1974): $E=40+C(N-6)$, kg/cm ² (for $N>15$) $E=C(N+6)$, kg/cm ² (for $N<15$) $C=3$ for silt with sand to 12 for gravel with sand	

Table 2-7. Young's modulus correlations from SPT and CPT tests (continuation)

SOIL	SPT	CPT
Gravel		Gielly et al. (1969) Sanglerat et al. (1972): $E_s = \alpha q_c$ $20 < q_c < 30 \text{ bars } 2 < \alpha < 4$ $q_c > 30 \text{ bars } 1.5 < \alpha < 3$
Sands, Sandy gravels	(FHWA-IF-02-034): $E = 1,200 (N_1)_{60}, \text{ kPa}$	Bogdanovic' (1973): $E_s = \alpha q_c$ $q_c > 40 \text{ kg/cm}^2$ $\alpha = 1.5$
Silty saturated sands		Bogdanovic' (1973): $E_s = \alpha q_c$ $20 < q_c < 40 \text{ kg/cm}^2$ $\alpha = 1.5-1.8$
Sand and silty saturated sands with silt		Bogdanovic' (1973): $E_s = \alpha q_c$ $5 < q_c < 10 \text{ kg/cm}^2$ $\alpha = 2.5-3.0$
NC Sands	Bowles (1996): $E_s = 500(N_{55} + 15), \text{ kPa}$ $= 7,000 \sqrt{N_{55}}$ $= 6,000 N_{55}$	Schmertmann et al. (1978): $E_s = 2.5 q_c \text{ L/B} = 1 \text{ to } 2$ $E_s = 3.5 q_c \text{ L/B} \geq 10$ Bowles (1996): $E_s = (2 \text{ to } 4) q_u$ $= 8,000 \sqrt{q_c}$
Silts, sandy silts, slightly cohesive mixtures	(FHWA-IF-02-034): $E = 400 (N_1)_{60}, \text{ kPa}$ Bowles (1996): $E_s = 300(N_{55} + 6), \text{ kPa}$	Bowles (1996): $q_c < 2,500 \text{ kPa } E'_s = 2.5 q_c$ $2,500 < q_c < 5,000 \text{ kPa } E'_s = 4 q_c + 5,000$
Clean fine to medium sands and slightly silty sands	(FHWA-IF-02-034): $E = 700 (N_1)_{60}, \text{ kPa}$	
Coarse sands and sands with little gravel	(FHWA-IF-02-034): $E = 1,000 (N_1)_{60}, \text{ kPa}$	
Not specified	Farrent (1963): $E = 7.5(1 - \nu^2) N, \text{ ton/ft}^2$ ν Poisson's ratio	
Soft clay		Bowles (1996): $E = 3 \text{ to } 8 q_c$ Bachelier and Parez (1965): $E_s = \alpha q_c \alpha = 7.7$
Soft silty clay		Meigh and Corbett (1969): $E_s = (1/m_v) = \alpha q_c$

Table 2-8. Young's modulus correlations from SPT and CPT tests (continuation)

SOIL	SPT	CPT
Low Plasticity Clays (CL)		Gielly et al. (1969) Sanglerat et al. (1972): $E_s = \alpha q_c$ $q_c < 7 \text{ bars } 3 < \alpha < 8$ $7 < q_c < 20 \text{ bars } 2 < \alpha < 5$ $q_c > 20 \text{ bars } 1 < \alpha < 2.5$
Low Plasticity Silts (ML)		Gielly et al. (1969) Sanglerat et al. (1972): $E_s = \alpha q_c$ $q_c > 20 \text{ bars } 3 < \alpha < 6$
Highly plastic silts and Clays (MH, CH)		Gielly et al. (1969) Sanglerat et al. (1972): $E_s = \alpha q_c$; $q_c < 20 \text{ bars}$; $2 < \alpha < 8$
Organic silts (OL)		Gielly et al. (1969) Sanglerat et al. (1972): $E_s = \alpha q_c$; $q_c < 12 \text{ bars}$; $2 < \alpha < 8$
Peat and organic clay (Pt, OH)		Gielly et al. (1969) Sanglerat et al. (1972): $E_s = \alpha q_c$ $q_c < 7 \text{ bars}$ $50 < w < 100 1.5 < \alpha < 4$ $100 < w < 200 1 < \alpha < 1.5$ $w > 200 0.4 < \alpha < 1$
Clayey silts		Bogdanovic' (1973): $E_s = \alpha q_c$; $10 < q_c < 20 \text{ kg/cm}^2$; $\alpha = 1.8-2.5$
Clays		Trofimenkov (1974): $E_s = 7q_c$

Table 2-9. Young's Modulus correlations from DMT and PMT tests

SOIL	DMT	PMT
Specified soils:		* $E=E_m^{1/\alpha}$ p_i =limit pressure at which the initial volume doubles.
Clean NC Sand		$7 < E_m/p_i < 12; \alpha=1/3$
Clean OC Sand		$E_m/p_i > 12; \alpha=1/2$
OC Sand and Gravel		$E_m/p_i > 10; \alpha=1/3$
NC Sand and Gravel		$6 < E_m/p_i < 10; \alpha=1/4$
OC Clay		$E_m/p_i > 16; \alpha=1$
NC Clay		$9 < E_m/p_i < 16; \alpha=2/3$
Weathered and remolded Clay		$7 < E_m/p_i < 9; \alpha=1/2$
OC Silt		$E_m/p_i > 14; \alpha=2/3$
NC Silt		$8 < E_m/p_i < 14; \alpha=1/2$
Non-specified	$E=(1-\nu^2)E_D$ Marchetti et al. (2001): $E=0.8M_{DMT}$ $M_{DMT}=R_M E_D$ for $0.2 < \nu < 0.3$ if $I_D \leq 0.6$ $R_M=0.14+2.36\log K_D$ if $I_D \geq 3$ $R_M=0.5+2\log K_D$ if $0.6 < I_D < 3$ $R_M=R_{M,0}+(2.5-R_{M,0})\log K_D$ with $R_{M,0}=0.14+0.15(I_D-0.6)$ if $K_D > 10$ $R_M=0.32+2.18\log K_D$ if $R_M < 0.85$ set $R_M=0.85$	

CHAPTER 3 CONICAL LOAD FIELD TESTING PROGRAM

Three conical load tests were performed in this study based on the testing procedure developed by Schmertmann (1993) to experimentally measure settlements, excess porewater pressures, and ground surface pressures from conical load tests, which are shown in this report to evaluate and validate the use of methods to predict settlements in Florida granular soils. A testing site with previous research efforts by the FDOT at UCF was selected to perform the conical load tests along with field testing and instrumentation. The subsurface soil stratigraphy and geotechnical characteristics used herein are based on existing field exploration data [i.e., standard penetration tests (SPTs) collected by Chopra et al. (2003)] and a new field testing program including cone penetration tests (CPTs), and flat dilatometer tests (DMTs). Figure 3-1 shows a schematic location of the three conical load tests and field exploration tests conducted in this project.

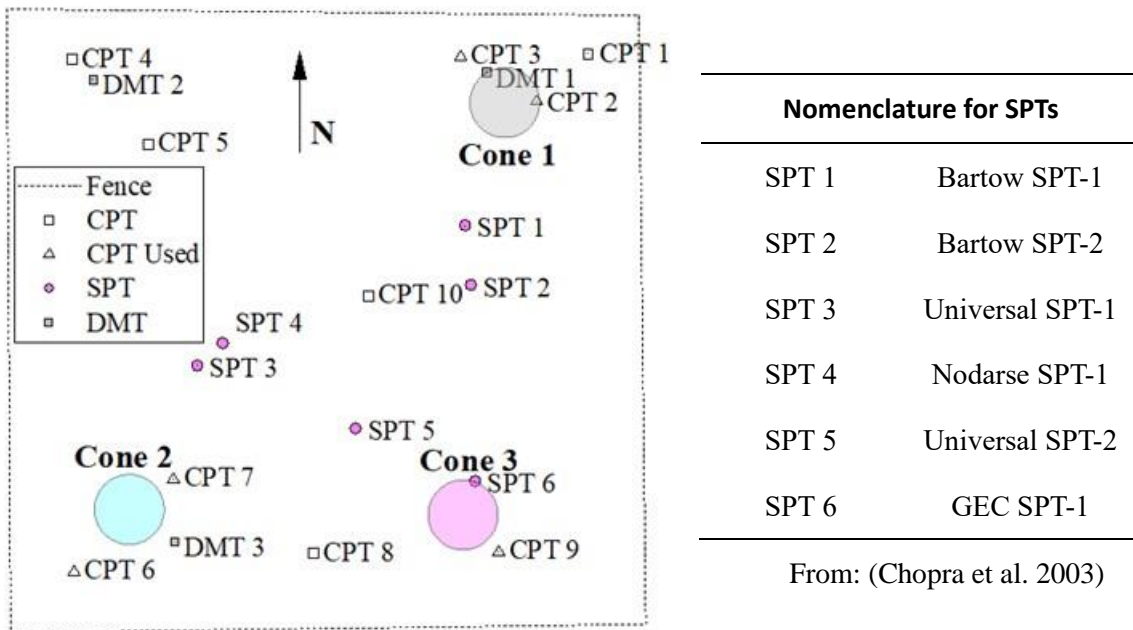


Figure 3-1. Plan view of field tests performed at the UCF site

Settlements in geotechnical engineering have three different components (Holtz and Kovacs 2011): (i) immediate or at times referred to as “elastic”, (ii) primary consolidation (i.e., time-dependent component caused by dissipation of excess porewater pressures), and (iii) secondary consolidation or creep. The immediate settlement is commonly misconceived as elastic settlement since it is usually estimated with the theory of elasticity, however from a soil behavior perspective, the immediate and elastic settlements should be treated separately. Since the predominant soils at the UCF site are granular silty sands and sandy silts, this report focuses on immediate settlement calculations and load-deformation characteristics of soils with large hydraulic conductivities. Consolidation and creep-controlled settlements, critical for clayey and organic soils, are almost negligible for the sandy soils tested in this project. To validate this assumption, a set of piezometers

was installed in the field to track the development and further dissipation of excess porewater pressures along with the rate of stresses and settlement.

The results of the conical load tests were used [in the project] to validate the use of theory of elasticity methods to describe the observed soil response. Two elastic soil stiffness parameters were used: modulus of elasticity (E) and Poisson’s ratio (ν). The calculation of E for soils [or shear modulus (G), which can be also computed from known expressions based on theory of elasticity] depends on the field or laboratory test used because the induced strain levels and shearing stress path in the soil are different for each test. For example, the small strain shear modulus (G_{max}) can be measured based on geophysics (i.e., non-destructive methods) once shear wave velocities are measured. Other tests such as CPTs or DMTs can be used to compute E or G values at larger strains, which tends to produce smaller moduli because those tests tend to mobilize larger shear strains. Proper selection of a soil modulus at the desired or expected strain level during field testing (or laboratory test) or during construction is key to avoiding large differences between computed and measured settlements in the field. This report shows later the typical strain levels induced by the conical load tests and provides guidance on the use of correlations suitable for Florida granular soils and groundwater level conditions for the calculation of settlement.

3.1 Summarized Soil Profile of Three Cone Locations

To define the field instrumentation location, a summarized soil profile for the proposed conical load test locations was developed using the results from field tests. A general diagram detailing the location of the conical load tests and field tests was presented in Figure 3-1. Table 3-1 summarizes the field tests used for each conical load test location within the UCF site. A total of six SPTs, reported in the FDOT report by Townsend et al. (2003), and field tests performed in this research were used for the summarized soil profiles. Generally, the predominant soil conditions at the UCF site consisted of surficial medium to dense sands on top of a silty clay material. Underlying the clayey soil layer, a medium-to-dense cemented sand was found. In the site, the groundwater table was found at a depth of approximately 3 ft. Since the surficial soils are sands and silty sands, immediate settlements were expected to be the main contribution to ground deformations due to conical load tests.

Table 3-1. Summary of field tests performed at the location of conical load tests

Cone No.	CPTu	SPT	DMT	Total
1	2	2	1	5
2	2	2	1	5
3	1	2	-	3
Total	5	6	2	13

3.1.1 Conical Load Test, Site No. 1: (NE Corner)

The first conical load test (i.e., Site No. 1 or Cone 1 in this report) was performed on the North-East of the UCF site. In Site No. 1, three CPTu and one DMT were performed. Data from SPT

tests performed by FDOT in 2003 were collected to enhance the definition of soil profile. The summarized soil profile at that corner was obtained from the analyses of the field tests shown in Figure 3-2. The NE corner of the site was characterized by a surficial 13 ft layer of medium to dense sand deposit. Below this topmost layer, medium-dense silty sands were found from approximately 13 to 33 ft. Underlying those two sandy layers, a 12 ft thick silty clay to clayey silt layer was found on top of a medium to dense silty cemented sand. Negligible stresses during the conical load tests were expected in the clay layer. The hydraulic characteristics of the relatively deep clayey soil found at the site simplified the lessons learned from the conical load testing program since the time-dependent porewater pressure response of the clay did not participate in the overall mechanisms of soil volume changes (i.e., negligible consolidation settlements were expected at the site).

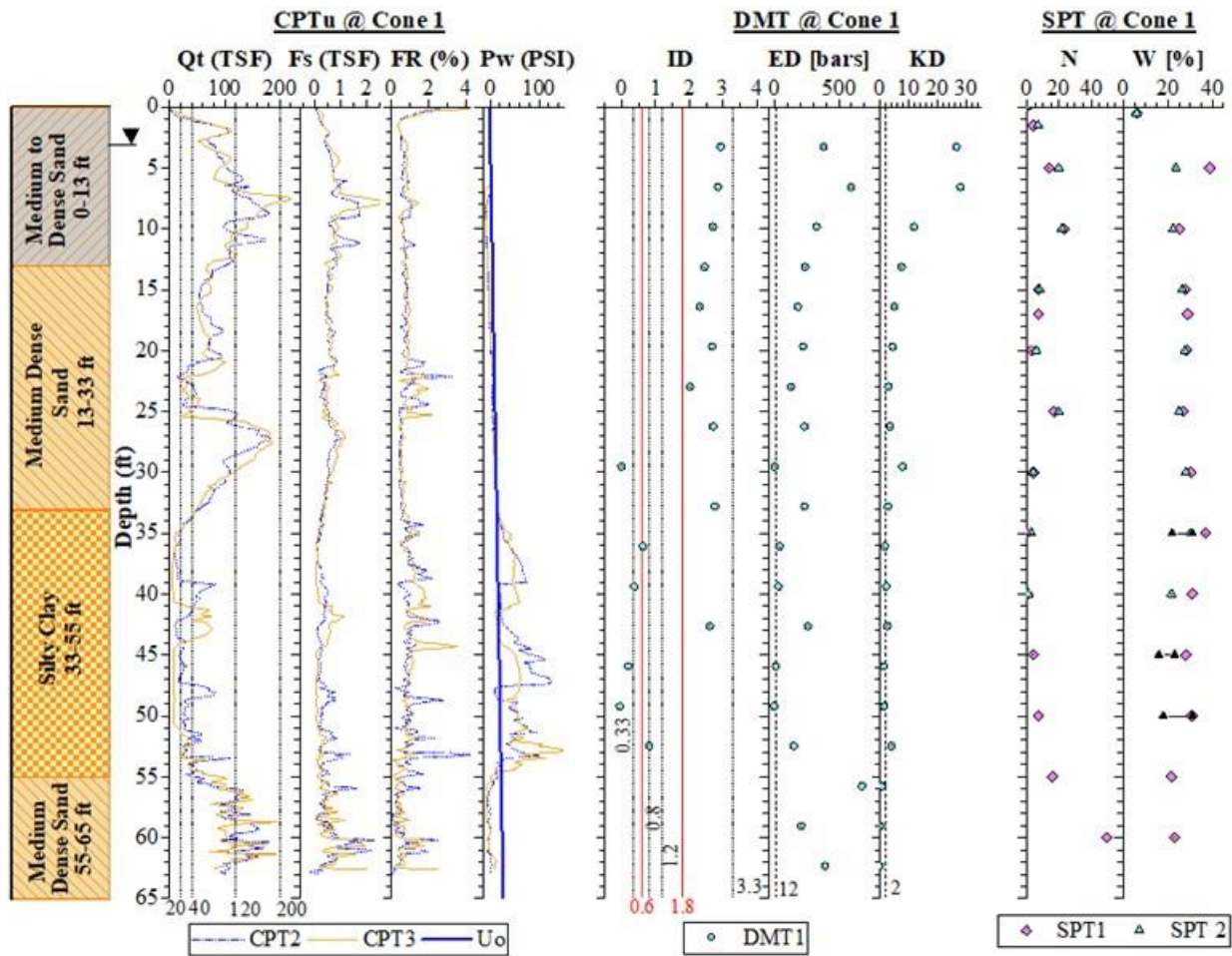


Figure 3-2. Summarized soil profile for conical load test No. 1 (NE corner)

3.1.2 Conical Load Test, Site No. 2: (SW Corner)

The second conical load test (i.e., Site No. 2 or Cone 2 in this report) was performed on the South-West of the UCF site. The summarized soil profile was obtained using two CPTu, one DMT, and two SPT tests presented in Figure 3-3. The Site No. 2 was characterized by a surficial medium-

dense sandy material on top of a loose sand at a depth from 25 to 33 ft. Underlying this layer, a 19-ft-thick clayey silt - silty clay layer was found. After an approximate depth of 52 ft, a layer of medium to dense cemented sand was found.

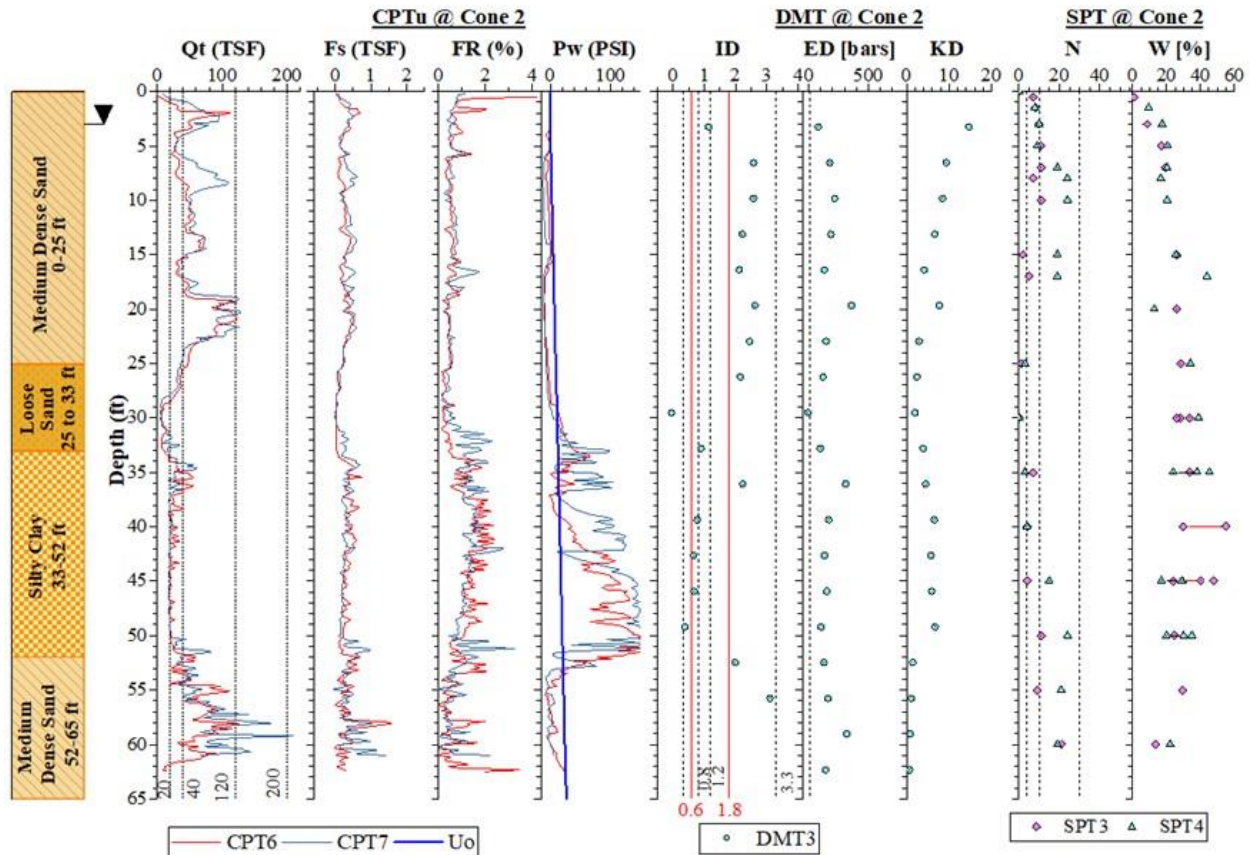


Figure 3-3. Summarized soil profile for conical load test No. 2 (SW Corner)

3.1.3 Conical Load Test, Site No. 3: (SE Corner)

The third conical load test (i.e., Site No. 3 or Cone 3 in this report) was performed on the South-East of the UCF site. The summarized soil profile at that corner was obtained from the analyses of one CPTu and two SPTs presented in Figure 3-4. The SE corner of the site was characterized by a surficial 30-ft-thick medium to dense silty sand to sandy silt on top of a silty clay layer with interbedded silty sands. After a depth of approximately 50 ft, medium to dense cemented sands were found.

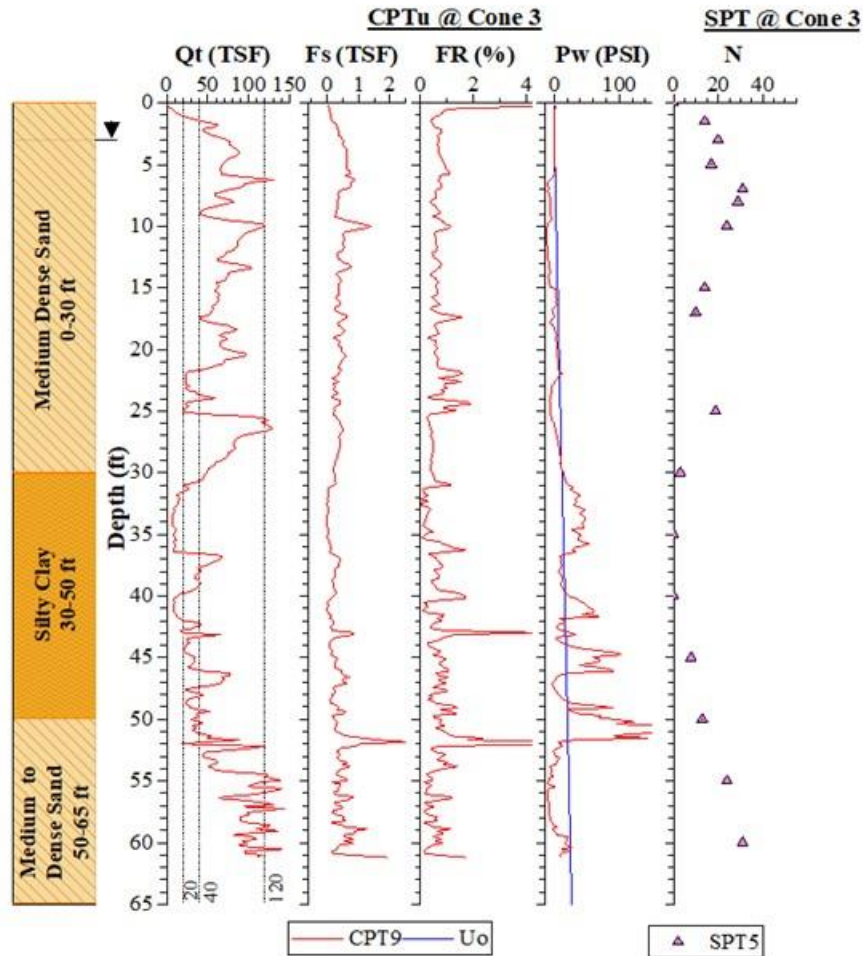


Figure 3-4. Summarized soil profile for conical load test No. 3 (SE Corner)

3.2 Installation of Field Instrumentation

The locations in depth and plan view of the field instrumentation and soil sampling were based on the previously defined soil profiles. Figure 3-5 shows photographs of the field instrumentation installation conducted at Cone 1. Three piezometers (PZ), five magnetic extensometers or spider magnets (SM), and one inclinometer (INCL) were installed by FDOT during the last week of August 2018. Piezometers were installed using sacrificial tips and hydraulically pushed with the drilling rig machine. Magnetic extensometers (i.e., spider magnets) were also installed in a grouted borehole with a continuous access tube passing through their center. Settlement plates were placed on top of the magnetic extensometer casing to obtain settlement readings at the center of the cone. Split spoon samples and Shelby tubes from two boreholes at test site No. 1 were retrieved. A laboratory testing program was conducted, and the results are presented in CHAPTER 5.



Figure 3-5. (a) Installation of piezometers in the ground using sacrificial tips, (b) drilling and grouting for installation of magnetic extensometers, (c) magnetic extensometer and datum magnet sensor, and (d-g) inclinometer casing installation

Figure 3-6 and Figure 3-7 shows additional pictures taken during the installation of field instrumentation at the other two cone locations. Four piezometers (three at Cone 2 and one at Cone 3), six spider magnets at each cone, one inclinometer, and one vibrating wire displacement transducer at Cone 2 were installed by FDOT during the second week of April 2019. During the installation of spider magnets, the casing was filled with water to avoid buoyancy. Five Shelby

tubes were retrieved along with six 5-gal buckets and two small jars of material from Cone 1 and Cone 2 to conduct the laboratory testing program.



Figure 3-6. (a) Sacrificial tip used for piezometer installation, (b) piezometers at Cone 2, (c) piezometers in place, (d) installation of magnetic extensometers at Cone 3, (e) magnetic extensometer preparation, (f) use of water to avoid buoyancy at Cone 3. Pictures taken on April 8-10, 2019



Figure 3-7. (a) inclinometer casing installation, (b) installation of displacement transducer, (c-i) vibrating wire displacement transducer installation. Pictures taken on April 8-10, 2019

3.2.1 Location of Piezometers and Spider Magnets

Figure 3-8 shows the location (elevation and plan view) of the piezometers, datum magnet, and spider magnets installed at test sites No. 1, 2, and 3. Three piezometers (Geokon Model 4500S-700 kPa) were installed at test site No. 1 (see Figure 3-1). The piezometers were located at an average distance of 5 ft from the center of the conical load and separated approximately 3 ft from each other. Three and one piezometers were installed at sites No. 2 and 3, respectively. These piezometers were also installed at an average distance of 3 ft from the center of the cone and separated approximately 2 ft from each other.

To measure porewater pressure variations during the conical load tests, the piezometers were installed in the medium to dense sands and silty clays at each location. During their installation at Cone 1, at approximately 35 ft depth, the hydraulic pushing system had to advance through a denser soil stratum to reach the desired depth. Data from piezometers were collected with a readout device before, during, and after the conical loading test. The raw data in *digits* was converted to engineering units of pressure using a second order polynomial equation provided with the sensor calibration sheets. The 16-channel data logger placed in the field was set to record readings at 3-minute intervals at Cone 1, and 2-minute intervals at Cones 2 and 3. During the conical loading process, data were collected every 30 seconds.

3.2.2 Settlement Plate and Pressure Cells

Settlement plates were installed at the center of the cone before the loading procedure was initiated. They were leveled after placing the topmost datum magnets that were only used at Cones 2 and 3. The steel riser pipes attached to the settlement plates were aligned with the magnetic extensometer casing to allow readings of the spider magnet sensors when lowering the magnetic extensometer probe through the steel riser pipes. The loading sequence started by connecting the first extension riser pipe of 5 ft to the settlement plate. As the loading progressed, two more 5-ft extensions were added at each cone to reach an approximate 14-ft-tall cone. Similar to the settlement plates, standard pressure cells were placed in contact with the natural ground. At Cone 1 location, two pressure cells were placed at 2 ft and 11 ft from the center of the cone. The pressure cells were used to quantify the variation of the vertical pressure and study the influence of the flexibility of the conical load arrangement. At Cone 2, two pressure cells were placed on the ground at a similar distance of approximately 2 ft. At Cone 3 only one pressure cell was used.

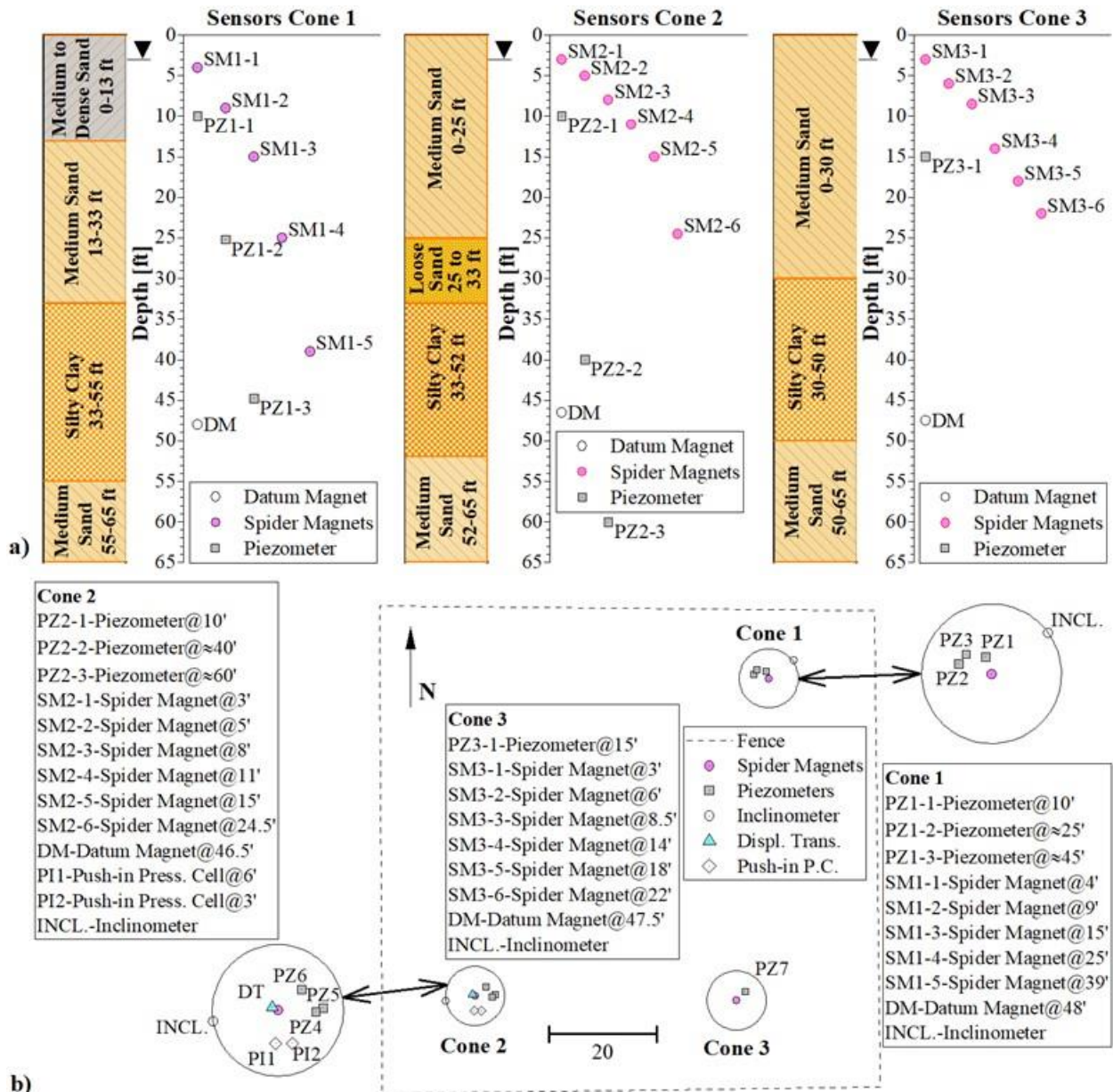


Figure 3-8. Field instrumentation location: (a) elevation view and (b) plan view

3.2.3 Magnetic Extensometers (Spider Magnets and Datum Magnets)

Spider magnet sensors were used in each conical load test to measure settlements at different depths at the center of the conical load arrangement. Three sets of magnetic extensometers were installed through casings in 6-inch boreholes and filled with a low strength grout. The boreholes were drilled to a target depth of 50 ft to ensure adequate anchorage for the setup since settlement readings are referenced to the bottom datum magnet. During the borehole drilling for the casing of magnetic extensometers and after reaching a depth of 40 ft (silty and sandy clay soil location), two soil samples with Shelby tubes were retrieved at depths 40-42.5 ft and 42.5-45 ft at Site No. 1. At Site No. 2, three Shelby tubes were taken at depths 37.5-40 ft, 40-47.5 ft, and 49-51.5 ft to target

the same clayey soil. The samples were carried to the UCF geotechnical laboratory to perform oedometric and triaxial tests under compression, extension, constant mean normal stress, and constant shearing loading and unloading stress paths. Test results are presented in CHAPTER 4.

The spider magnet sensors are labeled as SM followed by the number of the loading cone and a consecutive number from shallowest to the deepest (e.g., SM1-3 represents a spider magnet at Cone No. 1 and corresponds to the 3rd spider magnet installed from the ground surface). Spider magnets for Cones 2 and 3 were placed closer to the ground surface and an extra DM (not fixed) was placed underneath and in contact with the settlement plate. SM and DM readings were zeroed before the loading process initiated.

SM sensors were attached to a 1-inch PVC casing and placed at approximately the following depths from the ground surface: 4, 9, 15, 25, and 39 ft for Cone 1; 3, 5, 8, 11, 15, and 24.5 ft, for Cone 2; and 3, 6, 8.5, 14, 18 and 22 ft, for Cone 3. A datum magnet ring was placed at the bottom of each casing at a depth of 48 ft for Cone 1, 46.5 ft for Cone 2 and 47.5 ft for Cone 3 (see Figure 3-8a with label DM). The spider magnet sensors were tested to allow free relative displacement around the casing. A zero-baseline reading was taken immediately after installation to check whether the SMs were set at the target locations and no additional movements were caused during grout curing. Additional zero readings of the SMs and DMs were taken prior to the conical load test.

During the test, two readings were taken for each spider magnet, one when the probe was going down and one going up, and the average value was selected to estimate the movement at each sensor referenced with respect to the datum magnet. The reported accuracy of the spider magnets and probe for measuring settlements is approximately 1/4-inch.

3.2.4 Displacement Transducer at Cone 2

An additional borehole was drilled for the installation of a vibrating wire displacement transducer at Site No. 2. It was located approximately 2 ft away from the magnetic extensometer casing to avoid any damage during the installation process. This displacement transducer provides continuous settlement data as opposed to SMs. This sensor is equipped with a steel anchor rod installed at a depth of 51 ft (i.e., 50 ft steel rod plus 1 ft protective cap). The displacement transducer was anchored at the bottom of the borehole with a high strength grout (only at the lowest 10 ft of the borehole) as recommended by the manufacturer. During this procedure, the steel anchor rod and miscellaneous attachments were installed. The actual displacement transducer and protective cap were placed 7 days before the loading test started to avoid potential damage during the remaining sensor installation tasks. The topmost part of the protective cap of the sensor was placed underneath the settlement plate, thus the sensor recorded settlements triggered by downward movement of the settlement plate. Two additional soil samples with Shelby tubes were retrieved from this borehole at depths of 37.5-40 ft and 49-51.5 ft.

3.2.5 Inclinerometers

Inclinometers were installed at the edge of the 40-ft diameter conical loads (see in Figure 3-8b label INCL) in Site No. 1 and 2. The INCL locations were selected to avoid undesired movements during the conical tests. Similar to the SMs, 6-inch boreholes up to 40 ft and filled with low-strength grout were used to secure the casing in place. At Site No. 2, the INCL depth was reduced to 32.5 ft due to a soil cave-in issue during the installation. Two sets of horizontal grooves inside the casings, which are perpendicular to each other, were set in the radial and tangential direction of the projected conical loading. The A-A axis of the inclinometer was oriented toward the centerline of the cone before the grout hardened. The inclinometer readings were obtained in two directions: A-A and B-B axes which are the closest representation of the radial and tangential movements, respectively.

3.3 Soil Sampling

Figure 3-9 presents the locations of the soil sampling at different depths and the schematic plan view of sites No. 1 and 2. The soil sampling consisted of Shelby tubes and split spoon samples extracted from borings No. 1, 2 and 3, and 5-gal buckets retrieved from augered boreholes labeled as A1 and A2 in the figure. The procedure employed to extract soil samples from the conical load tests No. 1 and 2 is shown in Figure 3-10. Two split spoon samples were recovered from the first borehole (B1) at depths of 10 and 25 ft. Six thin-walled Shelby tubes were extracted at depths from 40 to 50 ft. An additional borehole was drilled to retrieve two more Shelby tube soil samples for laboratory testing at the UCF geotechnical laboratory. The Shelby tubes were taken from depths 40-42.5 ft and 45-47.5 ft. The bucket samples retrieved manually during the auger borings are labeled as *Buck.#* followed by their corresponding borehole number. Based on the visual observations, both soil samples had little or no organic material. SS1-B1 soil had medium to dark grey color and a sandy texture, while SS2-B1 had light grey color, sandy texture, and showed low plasticity at its natural moisture content.

Pictures of the Shelby tube and auger sampling process conducted at Site No. 1 and No. 2 are shown in Figure 3-11. Five Shelby tubes were successfully extracted at depths 37.5-52.5 ft and two additional boreholes were drilled to retrieve soil samples for laboratory tests.

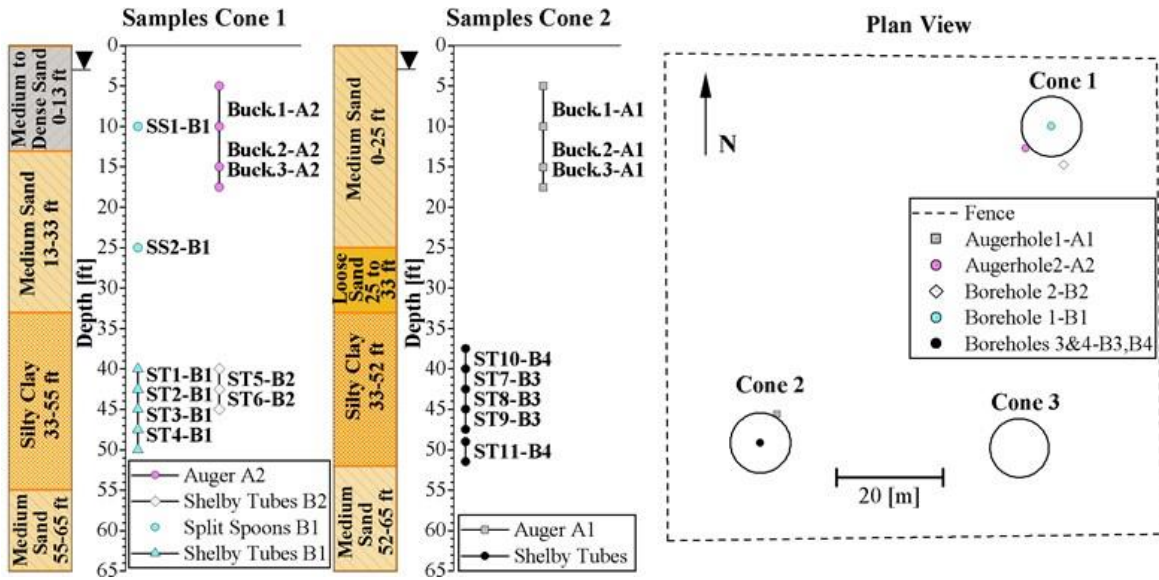


Figure 3-9. Soil sampling location for Cones 1 and 2



a)



b)



c)

Figure 3-10. Sampling process of the Shelby tubes: (a) drilling, (b) extraction, and (c) wax sealing



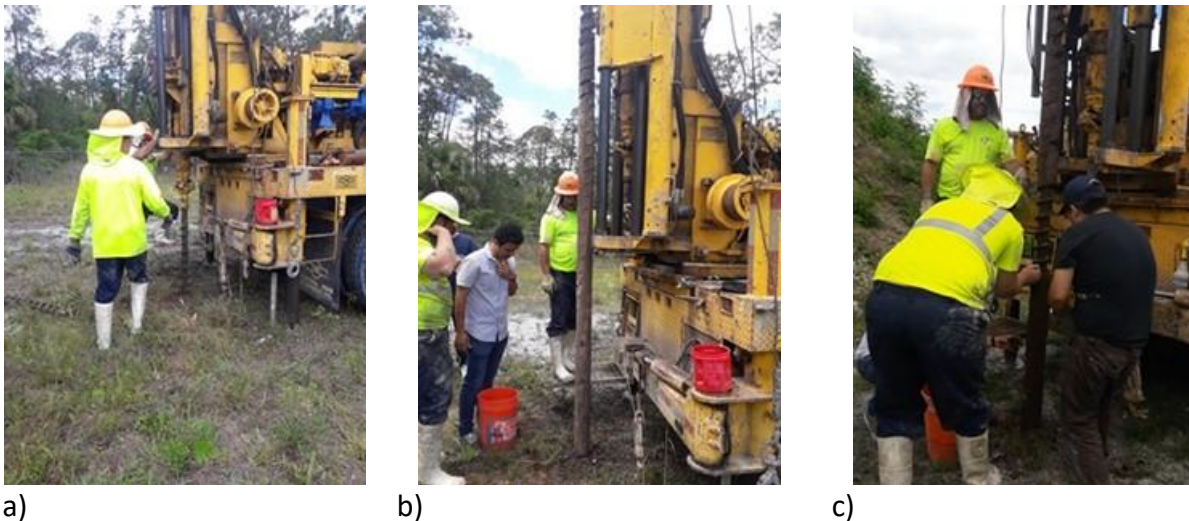


Figure 3-11. Sampling process retrieved from the drill auger. (a) drilling, (b) extraction, and (c) wax sealing. Pictures taken on April 10, 2019

3.4 Conical Load Testing Procedure

The conical load tests conducted in this research consisted of three 14-foot-high conical sand mounds built at an angle of repose for a granular fill of approximately 30 degrees. As a result, a base diameter of approximately 40 feet was obtained without compaction. A retro-excavator, wheel loader, and a bobcat were the equipment used to place the fill material as shown in Figure 3-12. The long reach of the retro-excavator allowed placement of the fill material without causing additional loading near the cone and without causing damage to the field instrumentation. The first conical load test was conducted on December 21, 2018. At Cone 1 location, four different sensors were previously installed: (i) one settlement plate, (ii) five spider magnets at different depths, (iii) two pressure cells placed at different distances from the center of the cone, and (iv) four piezometers installed at different depths. The settlement plate and spider magnets were employed to evaluate settlement prediction methods in this report, provide insight into predominant measured soil behavior, and evaluate the numerical models and proposed constitutive soil parameters for the Florida granular soil conditions studied herein. The pressure cells were installed to measure pressures induced by the conical load arrangement and were used to compute settlements. Piezometers measured any changes in porewater pressures induced by conical load test. These sensors were connected to a datalogger capable of taking automatic readings at the desired time step (i.e., 30 seconds during the loading procedure). The fill used during the loading process was mostly consisted of granular soil with some debris (bricks and boulders) retrieved from a stockpile at UCF.



Figure 3-12. Equipment used in the conical load tests

Reference lines were painted on the ground to control the volume of the loading soil at different stages of the conical load test. These lines were painted every 5 ft from the center of the cone, as is shown in Figure 3-13b. This process also helped to easily compute the load applied on the ground surface.



Figure 3-13. Magnetic extensometer readings after first loading stage and soil volume control lines

Settlements measured with the magnetic extensometers were also verified with survey equipment as shown in Figure 3-14. The riser pipes above the settlement plates were used to control the survey readings. Data readings were taken with the SMs and survey equipment several times during each loading stage to identify any sudden changes in the settlement data.



Figure 3-14. Topographic survey equipment to control settlement of riser pipes

Figure 3-15 shows the inclinometer reading process followed in the project. The readings were obtained in two directions; A-A and B-B directions to represent radial and tangential movements, respectively. A-A axis was oriented toward the center of the cone.



Figure 3-15. Inclinometer reading station at an intermediate conical load stage

Once the soil reached the top of a riser pipe, an extension was coupled to allow continuum settlement readings until the desired 14-ft-tall cone was reached as shown in Figure 3-16. After a new extension was coupled, the readings from the survey equipment and SMs were re-calibrated to account for the new length of the riser pipe. The plumbness of the settlement plate–riser pipe arrangement installed at the center of the cone was controlled at every stage and readings of the geometric shape and soil volume placed by the retro-excavator were tracked throughout the test.

The authors estimate approximate final conical soil volumes of 7335, 5734, and 5990 ft³ for Cones No. 1, 2, and 3, respectively.



Figure 3-16. Measurements of conical shape taken at different loading stages



Figure 3-17. Loading sequence after third riser pipe was coupled

Figure 3-18 shows the conical loading test sequence for Cones 2 and 3. The conical load test No. 3 was conducted on May 9, 2019 from 9:42 AM to 2:20 PM. The material used at this location was mostly moved from Cone 1 and from the material stockpile at UCF. Conical load test No. 2 was conducted on May 10, 2019 from 7:20 AM to 1:34 PM. Similar to Cone 1, the retro-excavator was placed far enough from the center of the cone. Before any load was induced in both testing locations, the effect of the excavator on the sensor readings was monitored to corroborate that significant changes in the settlements, porewater pressures, and lateral deformations were not caused by the weight of the equipment. The conical soil arrangement for different load increments was tracked by measuring the base circumference, the inclination of the slope from toe to top, the base and top radii, and the approximate height of the cone. The cone was built in small loading increments and given the conical loading shape, as the base of the cone expanded the pace to reach the final height was reduced. In summary, the variables monitored during conical load testing were:

- Cone volumes (diameter and height) at each loading stage. Weight of the cone was calculated using unit weights obtained from sand cone field tests.

- Hydrostatic porewater pressures (U_0) and excess porewater pressures (U_e) with piezometers installed at the project site.
- Ground surface settlements using separate systems: (i) survey equipment to track the elevation of settlement plate and riser pipes at the end of each loading increment, (ii) magnetic extensometers, and (iii) vibrating wire displacement transducer to continuously measure settlement (at Cone 2 only). Datum magnets were also installed and anchored at approximately 50 ft to serve as reference points for the settlement readings.
- Contact stresses applied by the conical soil loading at the ground surface measured with earth pressure cells. These readings were also used to calibrate numerical models presented in CHAPTER 5.
- Horizontal movements induced by the conical load tests using inclinometers.



Figure 3-18. Pictures of conical load testing sequence for Cone 3. Pictures taken on May 9, 2019



Figure 3-18 b. Pictures of conical load testing sequence for Cone 2. Pictures taken on May 10, 2019

Three sand cone density tests (ASTM D1556) per site were conducted as shown in Figure 3-19. From these tests, the average moist unit weight of the conical load was 100 pcf. This unit weight is used to compute the total weight of conical load material. The soil used was mostly classified based on the Unified Soil Classification System (USCS) as a poorly graded sand (SP). Samples for moisture content determination were taken from different locations around the perimeter of each conical load arrangement. The average measured moisture content was 6.4%. For cone 1, the moist unit weight and average water content were 100 pcf and 10%, respectively.

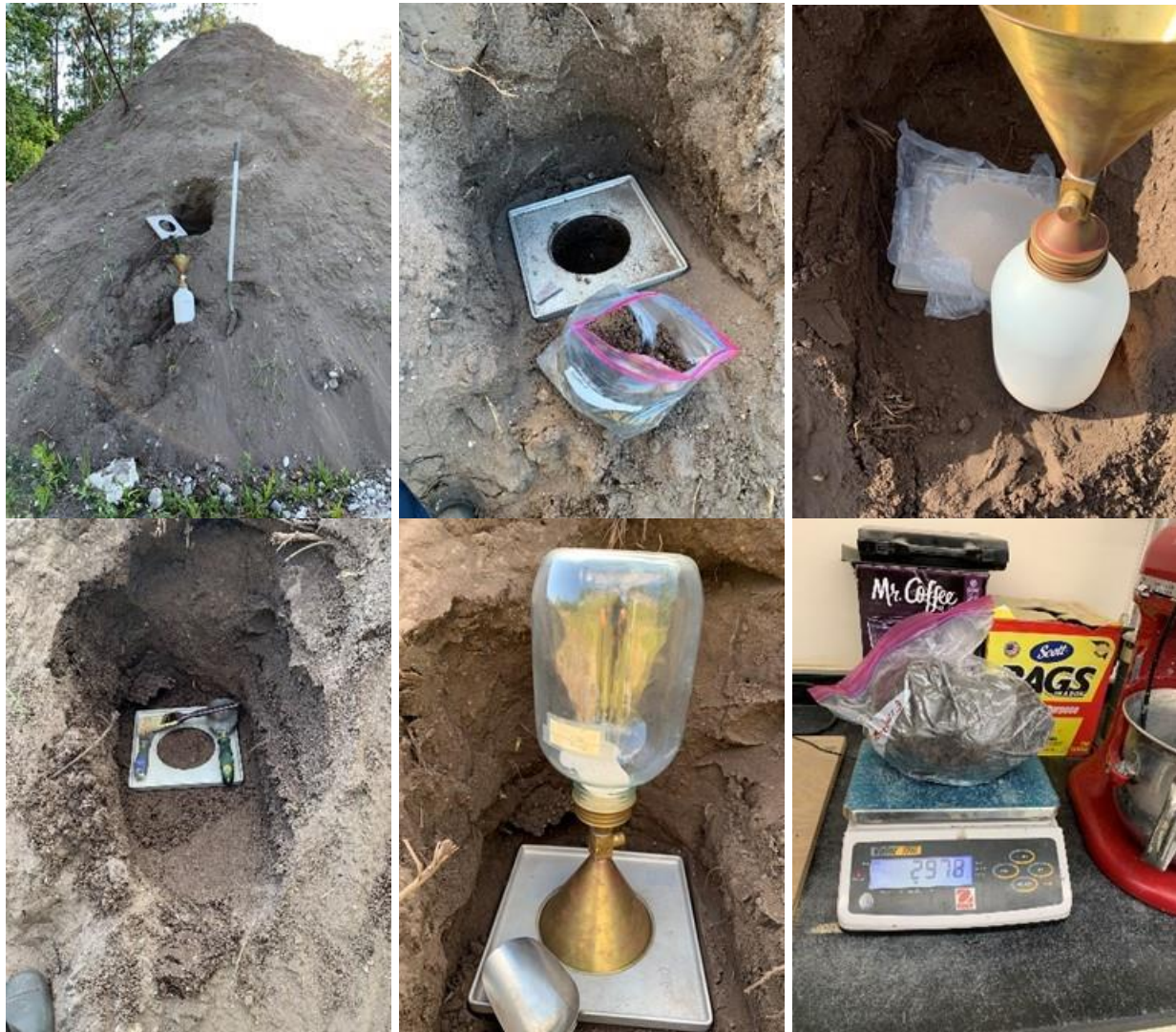


Figure 3-19. Sand cone density tests following ASTM D1556 standard. Pictures taken on May 22, 2019

3.5 Field Measurements of Immediate Settlements

3.5.1 Results and Data Interpretation: Conical Load Test No. 1

3.5.1.1 Analysis of the Piezometric Readings

Piezometer 1 (PZ1) and piezometer 2 (PZ2) were installed in the sandy material at depths of approximately 10 and 25 ft, respectively. Piezometer 3 (PZ3) was placed at a depth of 45 ft in the silty clay layer to study the potential excess porewater pressure build-up during the test, to determine the stress influence depth due to the conical load testing, and to confirm that consolidation settlements were not measured. Variation of water table over time and hydrostatic porewater pressures were measured with the piezometers installed at the site before any construction activities started. Figure 3-20 presents the results of the data collected with the piezometers at Cone 1. Figure 3-20a shows the total porewater pressure variation before, during, and after the conical load test (i.e., approximately three days of data are shown). The porewater pressure presented in the figure represents the total porewater pressure (i.e., addition of U_0 and U_e). Field instrumentation readings started to record data since the sensors were installed in August 2018. However, the information is presented in the figure only from approximately one day before the test started (i.e., December 20th 2018 at 00:00 am). The conical load test No. 1 is shown between the two vertical dashed lines in the figure. Results from PZ1 and PZ2 showed negligible variations in the porewater pressure during conical load test. However, PZ3 located in the clayey soil, showed a maximum excess porewater pressure ($U_{e, \max}$) of 60 psf (2.9 kPa). Figure 3-20b shows the porewater pressure readings for the three PZs used during the test. The time labeled as zero corresponds to 12/21/2018 at 8:14 am; ten minutes before the conical load test initiated. For comparison purposes, measured hydrostatic pressures are represented with dashed blue lines.

Changes in the U_0 before and after the conical load test were attributed to heavy local precipitation in the area. For example, the day before the test, PZ1 and PZ2 recorded a rapid increase in hydrostatic pressures due to an estimated precipitation of 3.65 inches at UCF. 1.88 inches of rain were also recorded the day of the test, which slightly increased the hydrostatic porewater pressures. The authors attribute those variations in the piezometer readings in the sandy soils to variations in hydrostatic pressures and not in excess porewater pressures, since the large hydraulic conductivity of those layers allows a rapid dissipation of U_e . It is important to separate changes in hydrostatic pressures and excess porewater pressures to assess the nature and source of ground surface settlements (i.e., immediate settlements versus time-dependent consolidation settlements).

Figure 3-20c shows the computed U_e attributed only to the conical load testing. U_e is computed by subtracting U_0 from the signal of porewater pressure during the test. Recall that piezometers were installed approximately 5 ft away from the center of the cone, which reduces the incremental vertical stress ($\Delta\sigma$) in the radial direction. However, the small value of excess porewater pressure (i.e., 60 psf) measured in the silty clay layer is not attributed to that radial-induced stress, but to the small vertical stress influence due to conical loading at the ground surface. This finding was confirmed with the Boussinesq-type analysis.

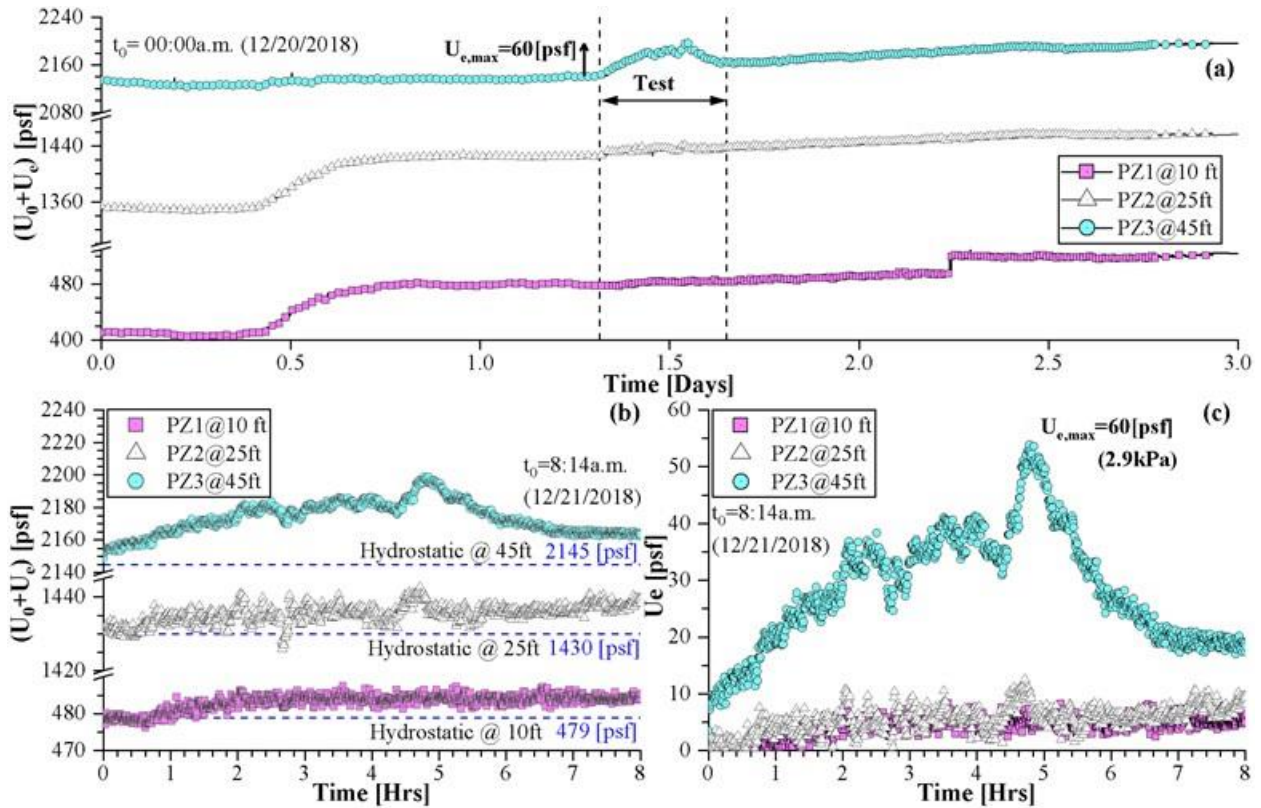


Figure 3-20. (a) Measured total porewater pressure before, during, and after the test, (b) measured total porewater pressure during the test, and (c) only excess porewater pressure during the test

Since excess porewater pressure and applied loading are related, Harr and Lovell (1963) presented a solution for the variation of vertical stress ($\Delta\sigma_z$) at the center of a conical shaped loading. The underlying assumption of this solution is that soils are isotropic, homogeneous, and elastic materials. The expression is as follows:

$$\sigma_z = p \left\{ 1 - \frac{1}{\left[\left(\frac{a}{z} \right)^2 + 1 \right]^{1/2}} \right\} \quad (85)$$

where p is the maximum vertical contact pressure under the center of the cone, a is the radius, and z is the depth below the base of the cone. Using the value of $p=1,400$ psf (measured with the pressure cell), $a= 20$ ft, and $z=45$ ft, the increase of vertical stress at that depth would be approximately 120 psf (or 5.7 kPa). This value represents only 4% of the vertical effective stress at that point. The excess porewater pressure due to the conical loading measured by PZ3 installed in the silty clay layer reasonably matched that computation.

3.5.1.2 Analysis of the Conical Load Pressure Measured with Pressure Cells

Figure 3-21 shows the data recorded with pressure cells at the ground surface from the conical load test. The initial zero readings were taken at 8:14 a.m. on December 21st (i.e., ten minutes before the test started). Figure 3-21a presents the pressure readings during the test (i.e., 0 to 8 hr) and a break in the horizontal axis is shown to present readings up to 35 hours. Figure 3-21b presents long-term readings up to 40 days after the test was completed. Recall that the pressure cells were located at 2 and 11 ft away from the center of the cone. Thus, differences in the pressure readings are mainly attributed to the low stiffness of the conical load arrangement. It would have been the same pressure if the conical loading were a rigid body built by compacting the cone at successive lift increments. In this test, the shape of the cone was controlled by the angle of repose of the material generated by the free fall of the soil deposited by the excavator.

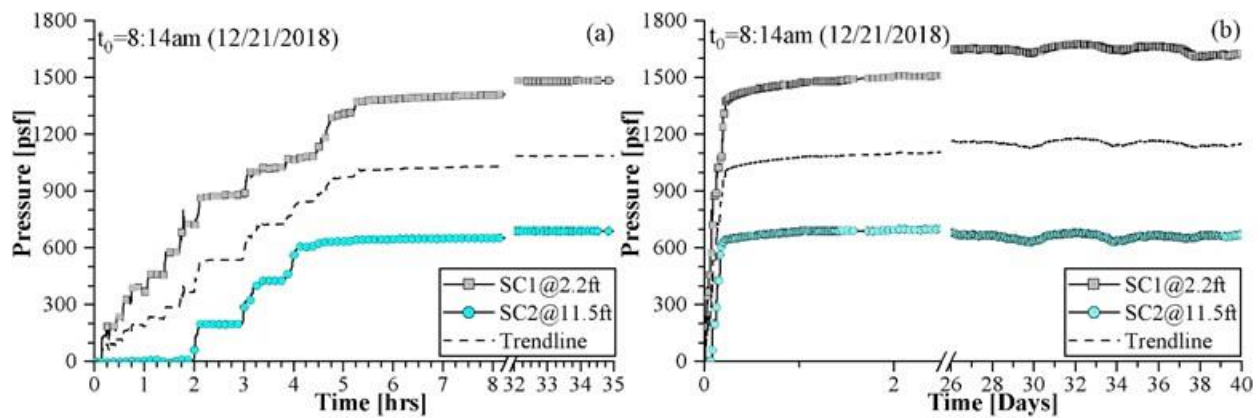


Figure 3-21.(a) Short-term pressure cell readings (i.e., from 0-8 and 8-35 hours) and (b) long-term pressure cell readings up to 40 days after test completion

Observe in the figure how pressure cell, SC1 measured an increase of pressure at a constant rate of approximately 450 psf per hour until the radius of the cone reached 11.5 ft and activated sensor SC2. As expected, the pressures on the cell located at 11.5 ft from the center of cone started to increase only after two hours. The loading sequence is reflected in the rates (i.e., slope in terms of pressure/time) and overall trends of the SC1 and SC2 pressure signals. These signals show that: (i) the distribution of pressures applied at the ground surface are not uniform, (ii) the conical loading is a deformable body that distributes the loads following different stress arching paths, and (iii) in the hypothetical case of a perfectly rigid conical loading arrangement, the stress would have been the same regardless of the pressure cell. Mayne and Poulos (1999) evaluated how the flexibility (or stiffness) of a foundation affects the magnitude of the resulting settlements. A similar result is inferred from the results presented herein but for a conical soil arrangement above the ground surface instead of a flexible foundation system.

Note also how the pressure readings at SC2 remained constant at approximately 600 psf even after 40 days (see Figure 3-21b). The inner cell SC1 showed an increase in the cell pressure of approximately 200 psf as a result of stress redistributions in the conical load arrangement. These

changes in the long-term pressures measured with the pressure cells are mainly attributed to: (i) variations of the density (i.e., moist unit weight) of the cone's material arising from rainfall-induced changes in the moisture content, (ii) redistribution of stresses and arching in the conical arrangement of soil above the ground surface, and (iii) densification and/or particle rearrangement of the conical load material and not of the underground soils as evidenced later in curves of settlement versus time.

To study the differences in the loading rates, Figure 3-22 shows normalized weights and pressures during the loading sequence. The data is normalized by dividing by the maximum weights or pressures reached in the test. The weights of the conical load were computed in two ways: (i) using the geometry of the cone measured at the end of each loading increment (the cone radius and height were tracked at the end of each loading increment), and (ii) the amount of buckets of material deposited in the conical arrangement (i.e., the excavator CAT325 had a bucket volume of approximately 1.16 m³) multiplied by the moist density of the material (i.e., 100 pcf as measured with sand cone tests). Each weight computation is labeled in the figure as “Comp. Weight (Geometry)” and “Comp. Weight (Volume)”, respectively. The results show similar results between both methods. It is important to note that in the original Schmertmann (1993) conical load paper, the author reported computed weights as opposed to stresses measured with pressure cells.

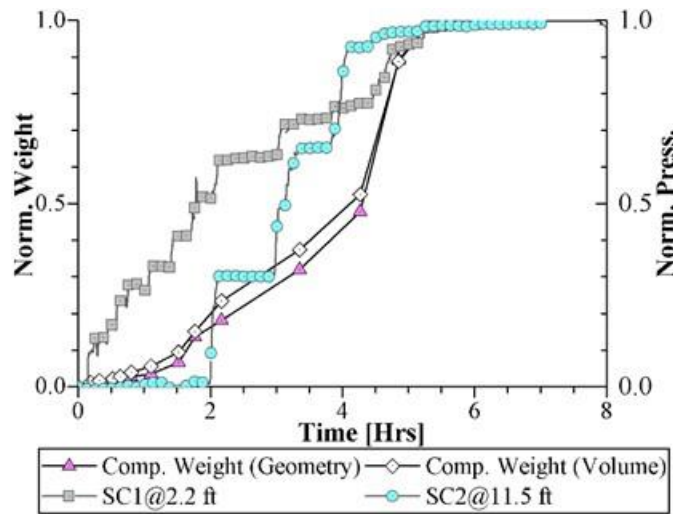


Figure 3-22. Variation of normalized weights and pressures during the conical load test

Measured values with pressure cells were used to parametrically study the influence of the flexibility/stiffness of the applied loading on the resulting conical-load induced settlement. In the hypothetical case of a rigid or infinitely stiff surface loading, both methods would be identical. Based on the studies performed by Mayne and Poulos (1999), the flexibility ratio of the structure and soil, highly influences the resulting magnitude of immediate settlements.

3.5.1.3 Measured Settlement, Pressures, and Weights over Time

Figure 3-23a shows the measured settlements and pressures for the duration of the test (i.e., eight hours). Figure 3-23b presents the measured settlements in relation to the computed weights applied at the ground surface. Settlements were computed using two different methods: (i) from changes in elevation of the settlement plate obtained with the survey equipment, and (ii) from the datum magnet anchored at 48 ft under the cone as shown in Figure 3-8a. Note how similar is the variation of settlement with the pressure over the same time. This confirms that stress measurements using SCs for conical loading are a better method to represent the load sequence and response of the soil. Therefore, stress redistributions of the conical load can be studied with pressure cells rather than using weights as originally proposed by Schmertmann (1993). Note that the rate of weight increment does not exactly follow the rate of settlement, demonstrating the arching effects and the importance of considering the stiffness of the applied loading.

Figure 3-24 shows the measured settlements using the magnetic extensometers (i.e., spider magnets) installed at different depths. Approximately 36 days after the test was completed, settlement readings were recorded to determine possible time-dependent variations caused by consolidation of the silty clay layers. The line labeled as “trendline”, corresponds to the average value of ground surface settlement presented in Figure 3-23. The spider magnets located at depths below 20 ft measured negligible displacement (i.e., less than a 1/4 of an inch). Figure 3-24b shows that settlement remained constant for 36 days after the test was completed. As shown in Figure 3-20c, small values of excess porewater pressure in the silty clay layer quickly dissipated after the test was completed. That finding, and the constant long-term settlement reading, confirms that the settlement measured was attributed to immediate instead of consolidation settlement.

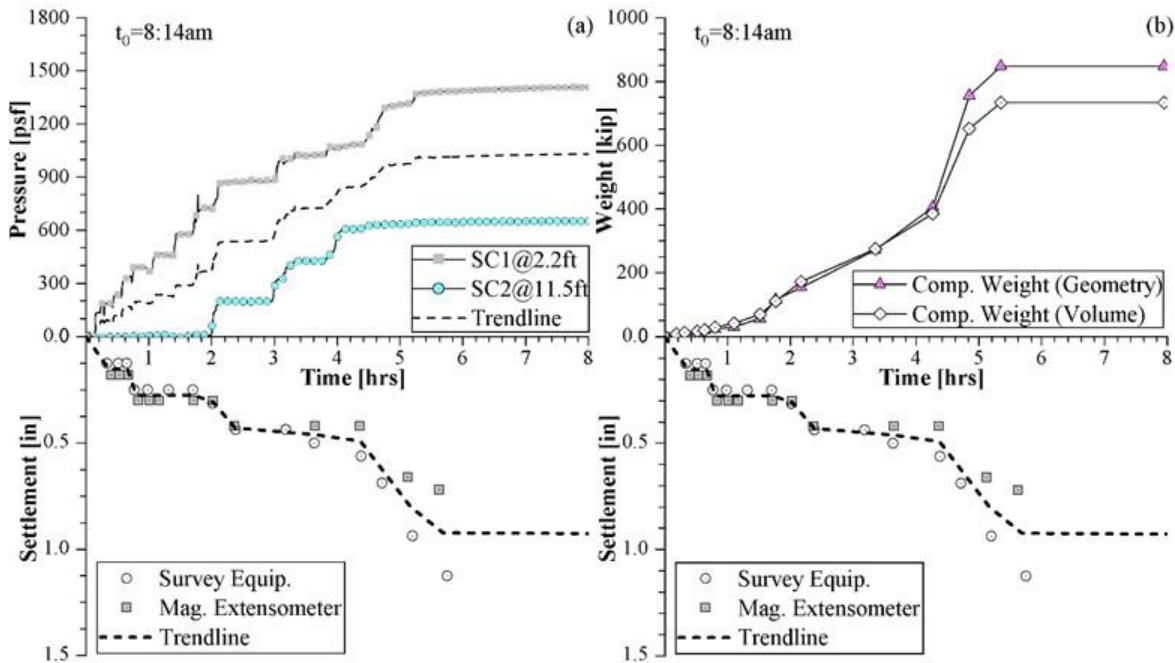


Figure 3-23. (a) Pressure readings at pressure cells SC1 and SC2 compared to settlement vs. time, and (b) computed weight with volume compared to settlement vs. time

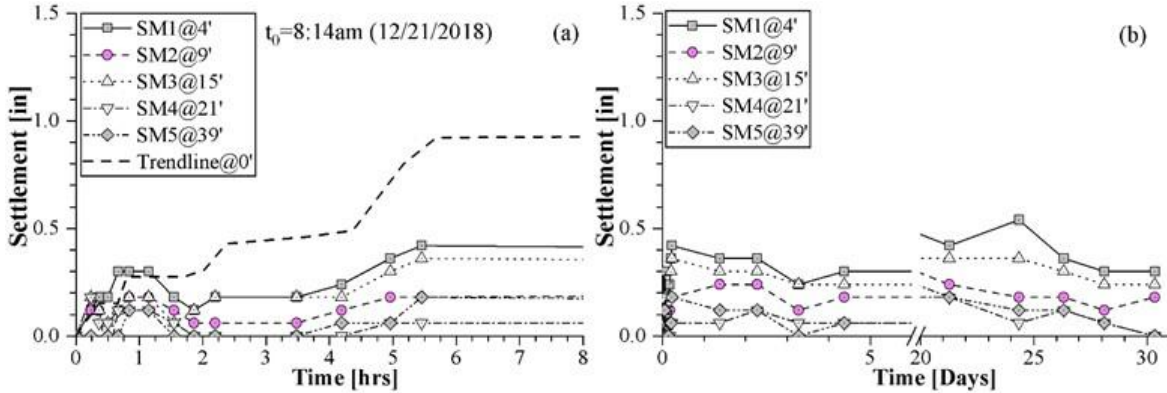


Figure 3-24. (a) Short-term settlement readings with the spider magnets at different depths, and (b) long-term settlement readings up to 36 days after test completion

3.5.1.4 Excess Porewater Pressures versus Pressures and Settlements

Figure 3-25 shows the excess porewater pressure and pressure readings versus time. Both graphs have the same initial time (i.e., the beginning of the test at 8:14 am on December 21, 2018). The general trend of the U_e for PZ3 is similar as the average pressure cell trend until the loading sequence was completed. Recall that PZ3 is located at the silty clay layer that has a low hydraulic conductivity. It is important to note also that U_e values at PZ1 and PZ2 are close to zero. The rate of the conical load was slow enough to allow water drainage in the silty-sand and sandy-silt layers. Recall that those surficial layers have large hydraulic conductivities, thus excess porewater pressures were not able to build up.

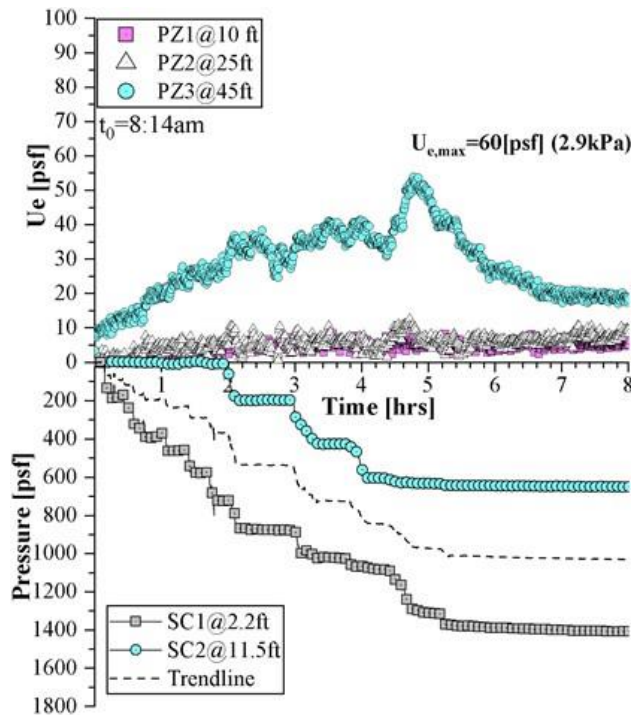


Figure 3-25. Measured excess porewater pressures and pressures at the ground surface

Figure 3-26 presents excess porewater pressures and settlement values over the test length. Note how the measured settlements in this Cone 1 were mainly immediate settlement. The maximum recorded immediate settlement was approximately 1 in. A peak excess porewater pressure of 60 psf was reached approximately 5 hr. after the test started. This coincides approximately with the end of the loading process that occurred approximately at that time (see Figure 3-25). The authors consider that consolidation settlements in the silty clay layer did not occur due to small induced U_e values (i.e., 60 psf or 3 kPa).

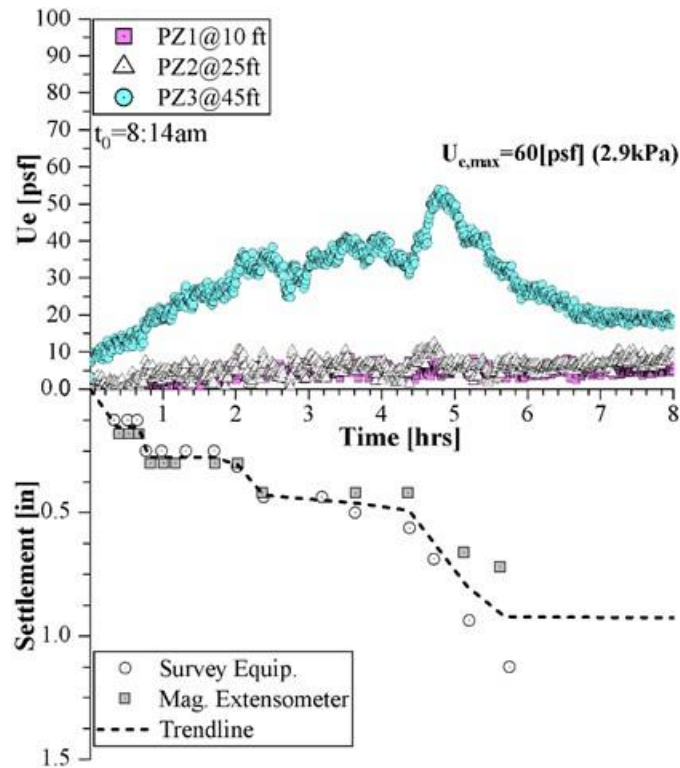


Figure 3-26. Measured excess porewater pressures and settlement at the ground surface

3.5.1.5 Load-Deformation Behavior from Conical Load Test 1

The soil load-deformation behavior induced by the conical load test is presented in Figure 3-27. Recall that settlements were measured using the magnetic extensometers and survey equipment. Figure 3-27a shows the weight-settlement behavior while Figure 3-27b shows the stress-settlement behavior with SC1 (located at approximately 2 ft from the cone center). Note how the behavior response changes with the load increments during the conical load test. The maximum load applied of 800 kips (1,500 psf in terms of stresses measured with SC1) resulted in a settlement of approximately 1 in. This settlement value is later in this report used to discuss settlement methods that best-fit the experimental results of this conical load test. This will also be used to calibrate soil parameters for the numerical simulations presented in CHAPTER 5.

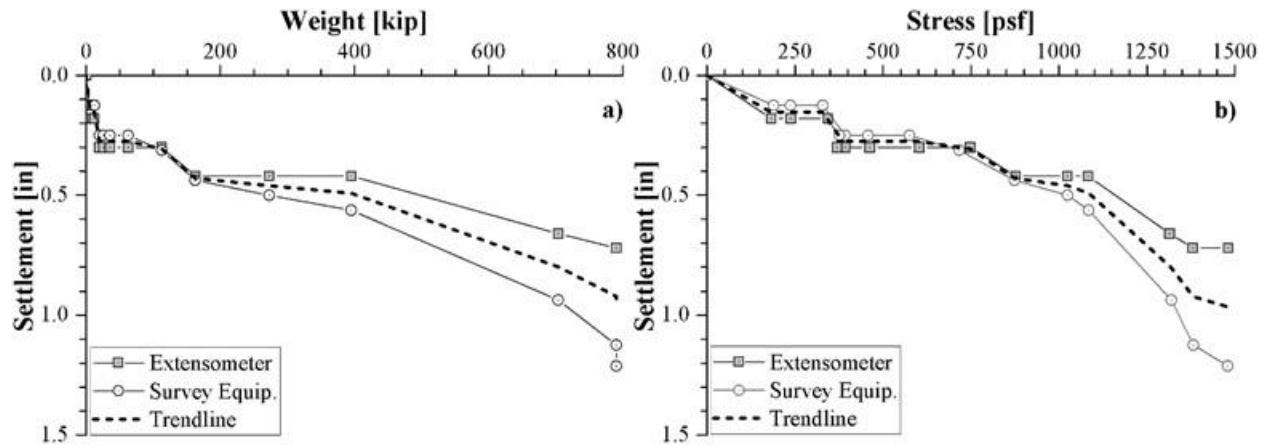


Figure 3-27. Load-deformation behavior for Cone 1: (a) weight-settlement, and (b) stress-settlement

Dividing the maximum settlement value of 1 in by the total height of the stress influence zone (i.e., 30 ft deep) produces an average vertical strain of 0.3%. The stress of 1,400 psf leads to a stiffness modulus of elasticity of approximately 470 ksf. Considering isotropic elasticity, proposed by Schiffman (1963) and later used by Schmertmann (1993), an estimation of the E can also be determined as follows:

$$E = \frac{p}{\delta} a(1 - \nu^2) \quad (86)$$

where p is the maximum vertical contact pressure under the cone axis, a is the base radius, ν is the Poisson's ratio, and δ is the settlement. Using the following input values of $p=1,400$ psf, $a=20$ ft, $\nu=0.3$ (assuming drained conditions), and $\delta=1$ in, the computed E is approximately 306 ksf. These results are compared later with values based on correlations using SPT, DMT and CPT results.

3.5.1.6 Analysis of the Inclinometer Data

Figure 3-28 shows the raw and zeroed lateral displacements measured with the inclinometer in the A-A and B-B directions, which correspond to the radial and tangential displacements, respectively. Recall from Figure 3-8 that the inclinometer was installed at the edge of the cone (i.e., at a distance of 20 ft with respect to the cone centerline). To zero the data in both directions, initial readings were taken before the test started. The raw data in both axes (A-A and B-B) show eight inclinometer readings taken throughout the test. The range of variation of the readings was very small. The conical loading test did not cause lateral displacements in the ground. Thus, the effect of an active wedge being developed downward in the soil capable of mobilizing a passive wedge and causing some lateral movements at that distance is negligible.

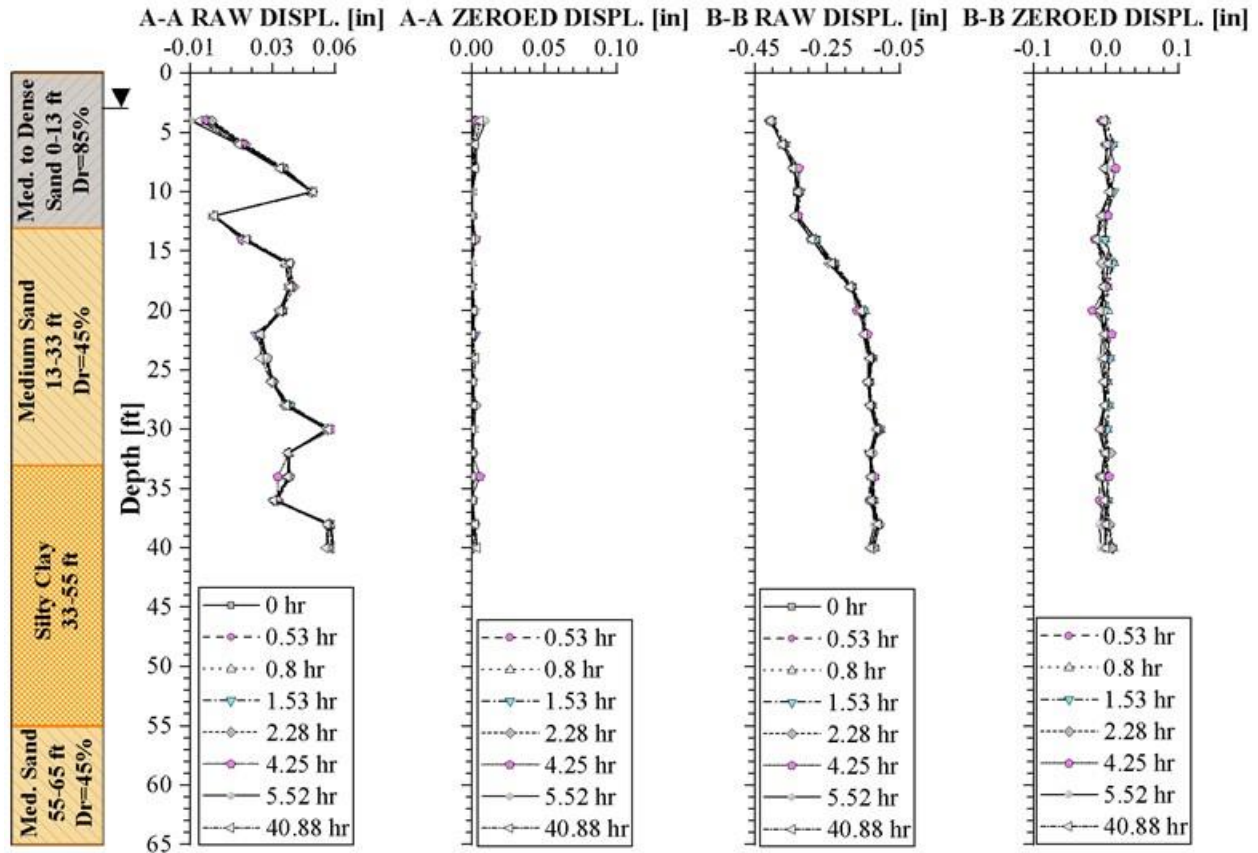


Figure 3-28. Lateral displacements in the soil at the edge of the conical load arrangement. A-A and B-B directions shown

3.5.2 Results and Data Interpretation: Conical Load Tests No. 2 and 3

The results and analysis of Cone 2 and 3 are presented in this section. For Site No. 2, SM2-1 through SM2-5 and PZ2-1 were placed in the surficial medium sand, SM2-6 was placed in the loose granular layer, PZ2-2 was placed in the silty clay layer, and PZ2-3 in the deepest sandy layer. For Site No. 3, SM3-1 through SM3-6 and PZ3-1 were placed in the surficial medium sand (recall that the first number in the labels shows the corresponding Cone and the second the order from top to bottom). In both cones, the datum magnets were installed at a depth of approximately 47 ft with respect to the ground surface. At this depth, with proper anchorage, zero movement of the datum magnet was expected.

As described in Cone 1, the vertical location and piezometric readings allow the estimation of water table depth and its seasonal fluctuations. Piezometers 1 at Cone 2 (PZ2-1) and 1 at Cone 3 (PZ3-1) installed at depths of approximately 10 and 15 ft, respectively, were placed in the sandy material (i.e., material with large hydraulic conductivity). These piezometers can be used to determine the variations of U_0 over time. Porewater pressure measurements taken with piezometer 2 at Cone 2 (PZ2-2), located at a depth of 40 ft in the silty clay layer were expected to have

minimum variations in the readings. PZ2-2 was installed with the dual purpose of: (i) studying potential excess porewater pressure build-up given the low hydraulic conductivity of the silty clay layer and (ii) assessing the depth of the vertical stress influence zone of the conical load test that can be used as a confirmation of Boussinesq-type analyses. Piezometer 3 at Cone 2 (PZ2-3) was installed at a depth of 60 ft to investigate whether downward groundwater flow was present at the site that could potentially alter the calculation of effective stresses.

3.5.2.1 Analysis of Piezometric Readings: Test No. 3 (May 9, 2019)

Figure 3-29 presents the results collected with PZ3-1. Figure 3-29a shows long-term porewater pressure variations and precipitation data. The latter was obtained from The Weather STEM Data Mining Tool at the University of Central Florida station (Orange Weather STEM, 2019). The sum of U_0 and U_e components, which represents the total porewater pressure, is presented in the figure. PZs were installed in April 2019; however, the information presented in the figure defines 05/01/2019 at 09:00 am as time zero (i.e., approximately eight days before the test started). A total of 16 days is shown to illustrate the variations of porewater pressures (U_0+U_e) before, during, and after the test was completed. The test duration is demarked with the two vertical dashed lines. Note how slight variations of porewater pressures were recorded during the test (see Figure 3-29b). In Figure 3-29b, zero time corresponds to 5/09/2019 at 9:42 am; when the conical loading at Cone 3 was initiated. Figure 3-29c presents a detailed plot of only U_e generated during the loading sequence.

Variations of U_0 before and after the test were attributed to water table variations due to the precipitation. Note the rapid increase in U_0 at approximately day 4 in Figure 3-29a due to a rainfall record of 1 in. During the day of the test, there was no precipitation recorded, thus a slight decrease in hydrostatic porewater pressures was measured with the piezometer. The authors attribute those decreases to slight variations in hydrostatic pressures rather than loading-induced excess porewater pressures, because of the large hydraulic conductivity of the medium dense silty sand layer where the piezometer was placed. Note how negligible the U_e computed for this test were (see Figure 3-29c). Measured variations of settlement in this test happened immediately and without the influence of time-dependent consolidation effects. Separation between hydrostatic and excess porewater pressures is necessary for an adequate evaluation of the type of settlement (i.e., either immediate or consolidation).

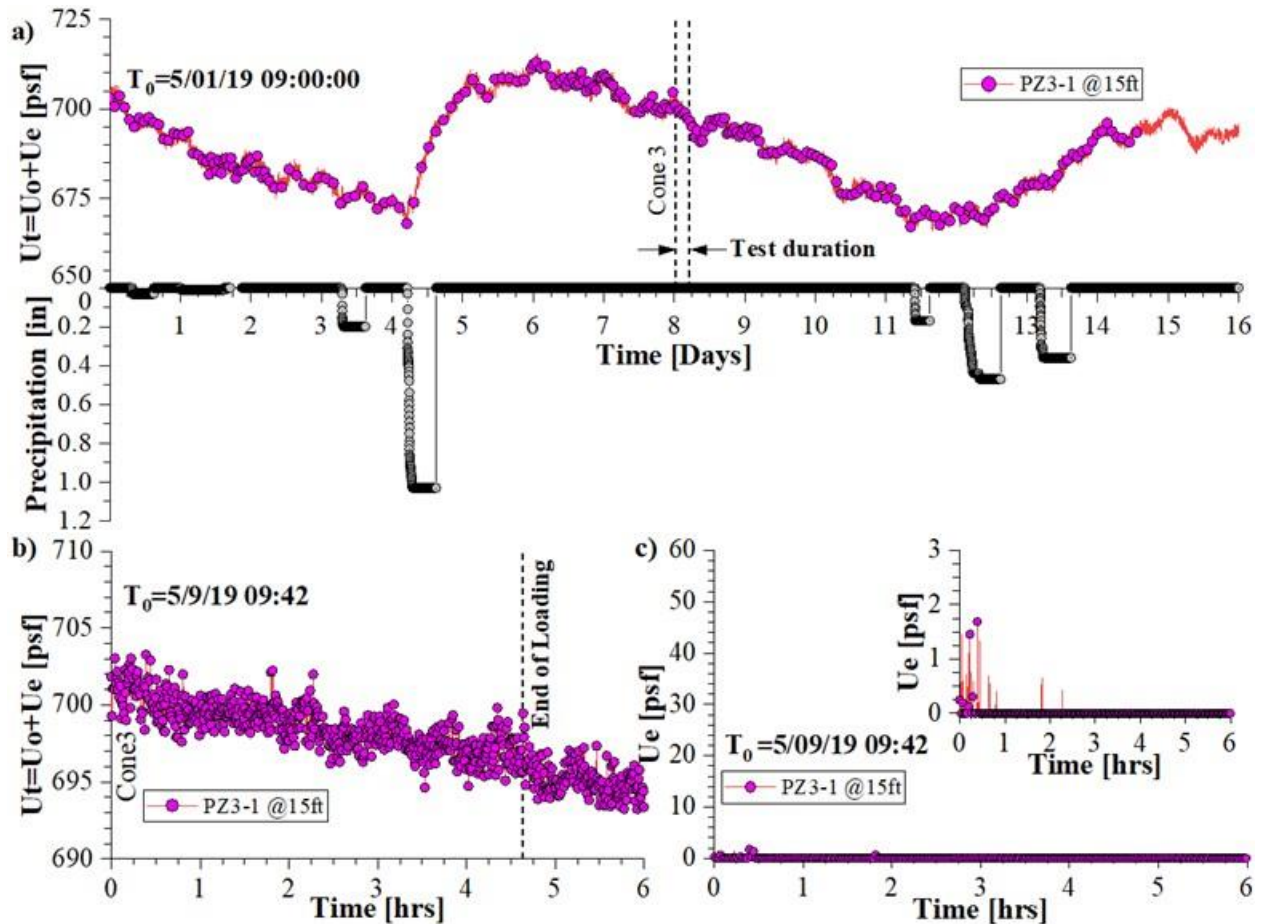


Figure 3-29. Conical load test No. 3: (a) measured total porewater pressure before and after the test, (b) measured total porewater pressure during the test, and (c) excess porewater pressure during the test

3.5.2.2 Analysis of Conical Load Pressure Measured with Pressure Cells: Test No. 3 (May 9, 2019)

Figure 3-30 shows pressures caused by the conical loading measured with pressure cells (SC) at the ground surface. Initial zero readings were taken before any load was applied and corresponded to 05/09/2019 at 9:42 a.m. Figure 3-30a presents pressure readings during the test (i.e., from 0 to 6.5 hr.) and a break in the horizontal axis is shown to present readings up to 48 hours. Figure 3-30b presents long-term readings up to 18 days after the test was completed. The pressure cell was located approximately 2-feet from the center of the cone. SC1 results show an increase of pressure at a constant rate of approximately 200 psf per hour until the radius of the cone reached approximately 14 ft, which occurred at $t=2.4$ hr. The loading sequence used during the test is reflected in the stepped loading rates of the SC1 pressure signal. The long-term pressure cell pressure readings, presented in Figure 3-30b, show a constant maximum value at approximately 800 psf. For Cone 3, as opposed to Cone 1, there were no variations in the moist unit weight of the fill due to rainfall-induced changes in moisture content. The slight increase in pressure can be attributed to some densification and/or particle rearrangement of the loading material.

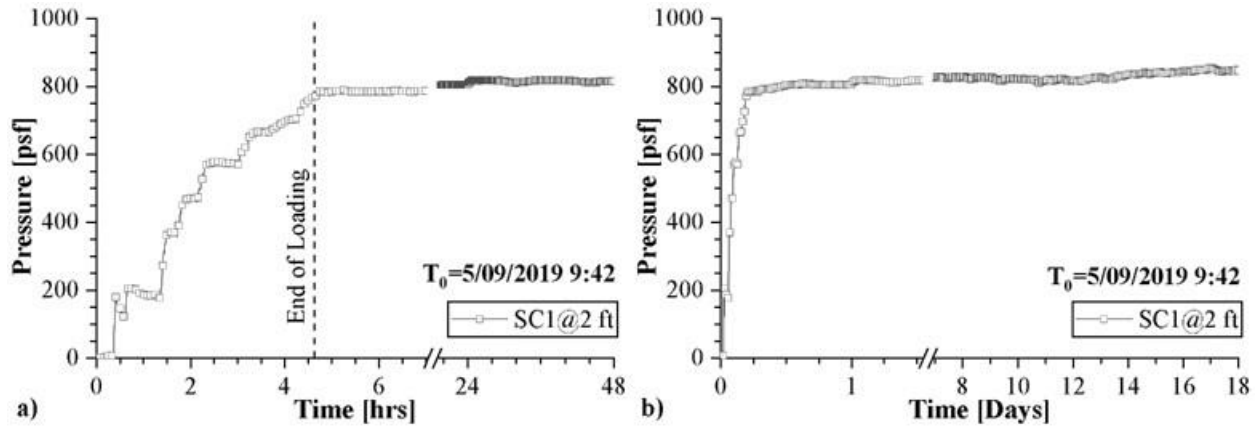


Figure 3-30. Pressure cell SC1 readings at conical load test 3: (a) short-term pressure cell readings (i.e., from 0-7 and 20-48 hr.), and (b) long-term pressure cell readings up to 18 days after end of test

Figure 3-31a shows a schematic geometry of the cone at different loading stages. Each stage is labeled with its corresponding order. This geometry was recreated from pictures and field measurements. Figure 3-31b presents normalized weights and pressures obtained during five hours of the loading sequence to assess the differences in the loading rates (i.e., computed weights vs. earth pressure cells with SC1). The vertical dashed line shows the time when the conical load test was completed. Weights and pressures were divided (i.e., normalized) by maximum weights or pressures reached at the end of the test. Similar to the results reported in Cone No. 1, the weight and pressure lines are not identical, which demonstrates that conical load did not act as a rigid body. Recall that Mayne and Poulos (1999) discussed that the relative stiffness of the loading in relation to the stiffness of the subjacent soil influences the resulting magnitude of immediate settlements.

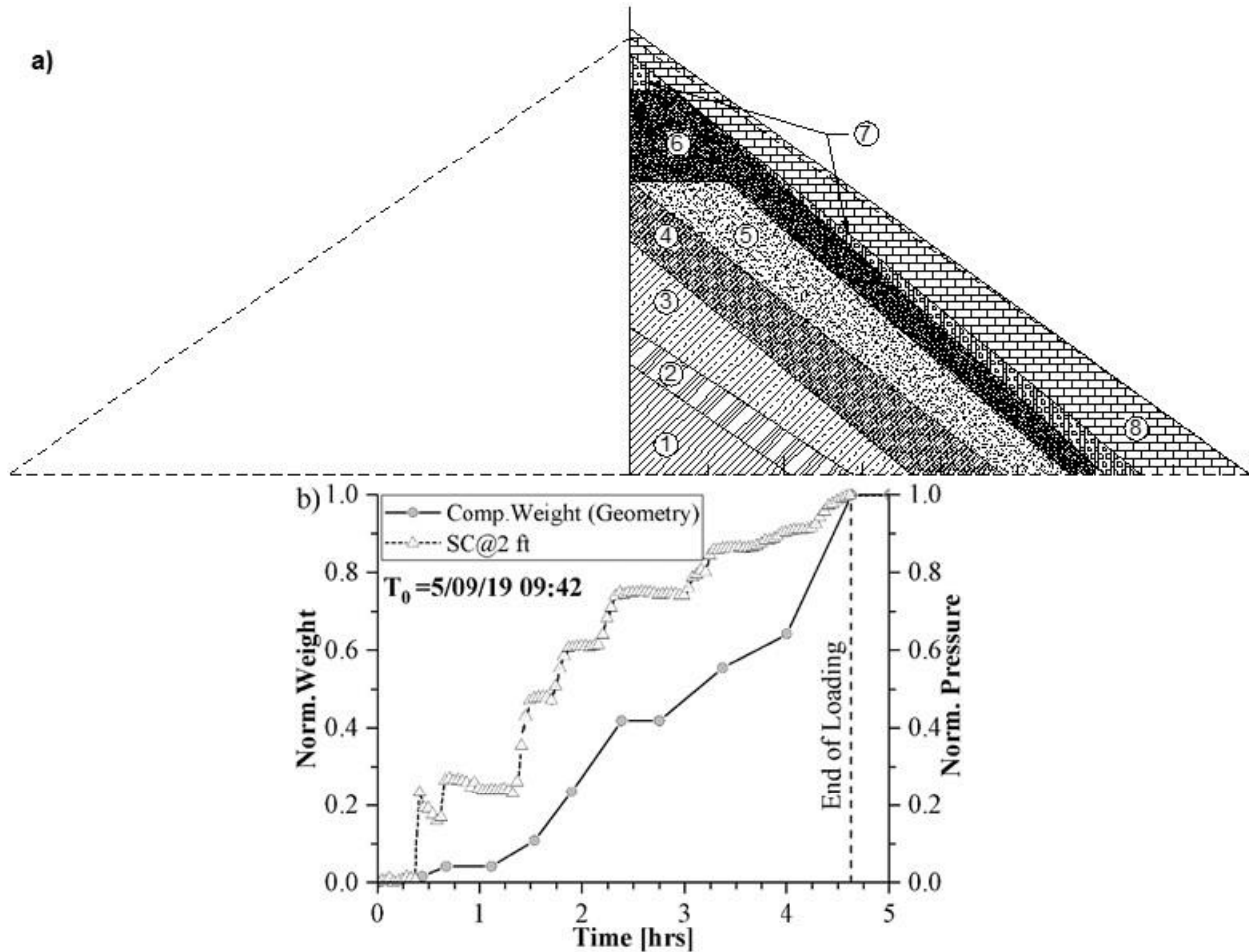


Figure 3-31. (a) Schematic sequence followed during conical load test 3, and (b) normalized weights and pressures during the conical load test

3.5.2.3 Relationships Between Settlements, Pressures, and Weights over Time: Test No. 3 (May 9, 2019)

Figure 3-32 presents measured settlements and pressures for the entire test (i.e., six hours) in relation to the weight and pressure applied. Note how similar the variation of settlement versus time is with respect to the applied pressure (see Figure 3-32a). Larger differences are observed when comparing the shape of weight and settlement for the length of the test (see Figure 3-32b). As demonstrated before, stress measurements using pressure cells are ideal for conical load test since the loading sequence and soil deformation response were more accurate than the computed weight results. Computed total weight does not follow the same trend as settlement over the same time, which confirms that soil arching effects, stress paths, and stiffness of the applied load cannot be evaluated using this method, but instead using data from pressure cells located on the ground surface.

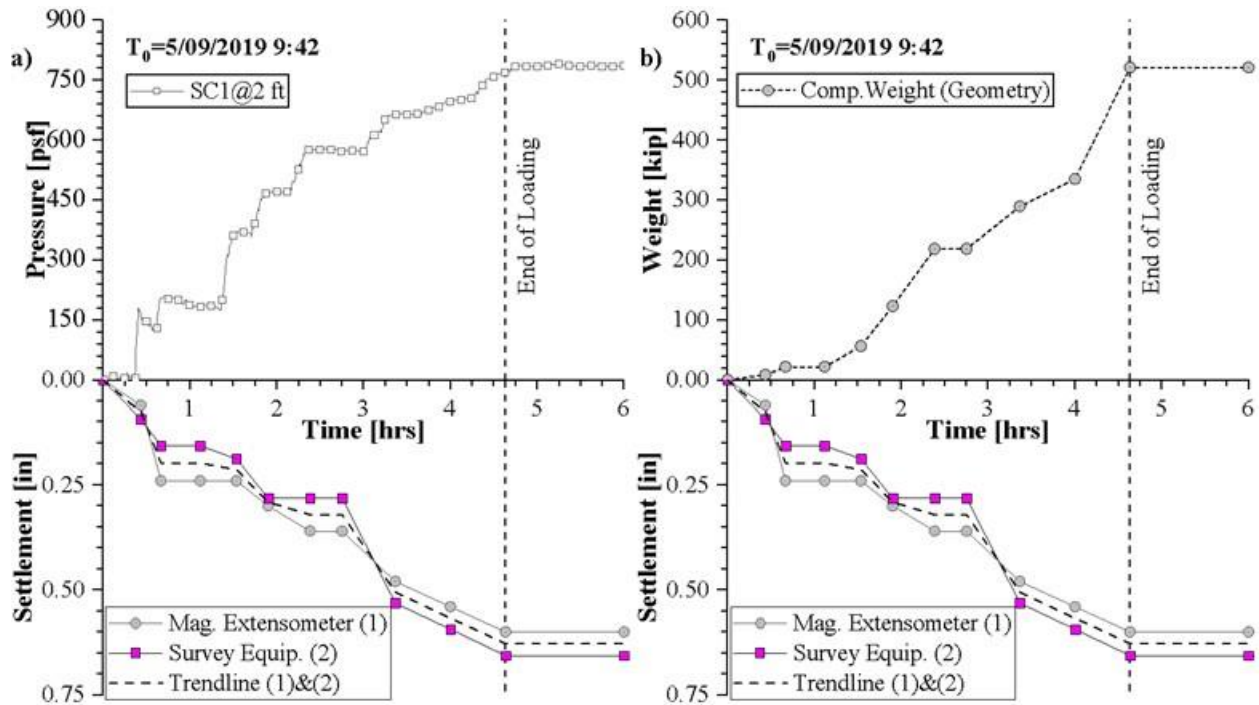


Figure 3-32. Settlement, pressure, and computed weights for the length of the test: (a) measured pressure and settlement behavior, and (b) computed weight and settlement behavior

Figure 3-33 presents measured settlements using the magnetic extensometers (i.e., spider magnets). Recall that two readings were taken for each spider magnet: one when the probe was going down and one going up, and the average value was used to compute the movement at each sensor. Settlement readings were collected until approximately 16 days after the test was completed to determine whether time-dependent behavior caused by consolidation of the silty clay layers occurred. The line labeled as “trendline” corresponds to the average value of ground surface settlement reported in Figure 3-32. Figure 3-33b shows how the settlement remained constant after the test was completed. Since no additional settlements were measured after the end of the test (i.e., long-term settlements are constant), the measured values can be attributed to immediate settlement. Changes in volume of the soil in the vertical direction (i.e., depth) are very small as reflected in negligible settlements even in the SMs located close to the ground surface.

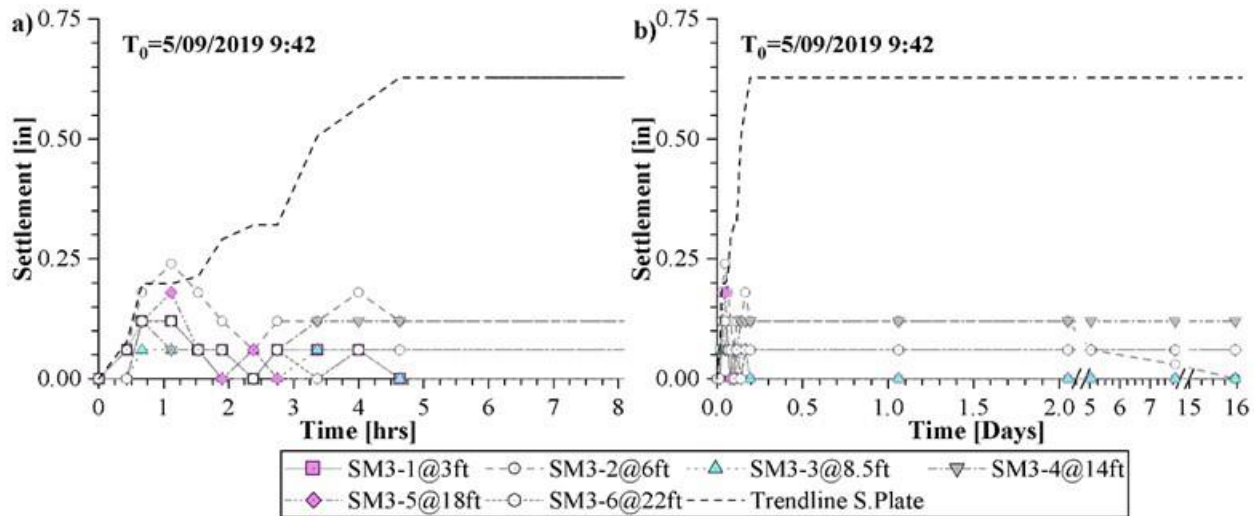


Figure 3-33. Settlement vs. time measured with spider magnets: (a) short-term, and (b) long-term settlement readings up to 16 days after the end of test

3.5.2.4 Excess Porewater Pressures in Relation to Earth Pressures at Ground Surface: Test No. 3 (May 9, 2019)

Figure 3-34 presents excess porewater pressures and earth pressure readings over the entire test. The initial time corresponds to the beginning of the test (i.e., 05/09/2019 at 9:42 am). The piezometer measured negligible excess porewater pressures. This is attributed to the large hydraulic conductivity of the sand layer where the PZ was installed, and because the rate of loading was not fast enough to buildup significant excess porewater pressures.

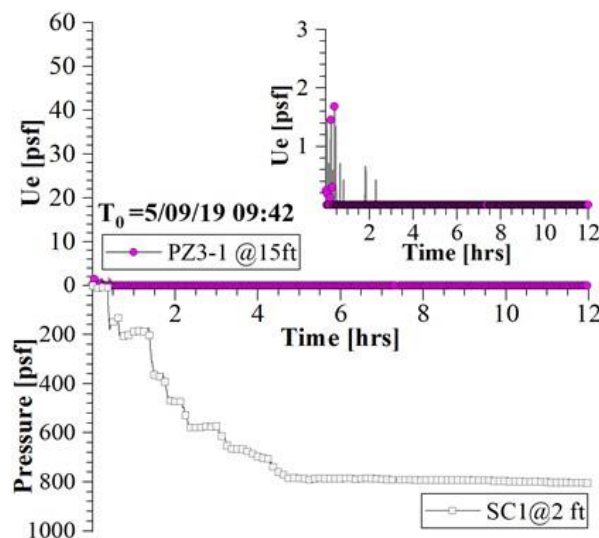


Figure 3-34. Measured excess porewater pressures during the entire test in relation to earth pressures at the ground surface

3.5.2.5 Load-Deformation Behavior in Conical Load Test 3

The load-deformation behavior caused by the conical load test located at the south-east of the UCF site (Cone 3) is summarized in Figure 3-35. The measured weight-settlement and stress-settlement behavior at the ground surface due to conical load test are shown in Figure 3-35a and b, respectively. Weight was computed using the volume of the soil material deposited by the excavator. Stresses were measured with SC1 located at the ground surface. The maximum load applied by the conical load test was 520 kips (or 900 psf in terms of earth pressure measured with SC1 near the center of the cone) and resulted in a maximum settlement of approximately 0.65 in. This experimental value will also be used later in this chapter to determine the best correlations for elastic moduli that match the results from the conical load testing program.

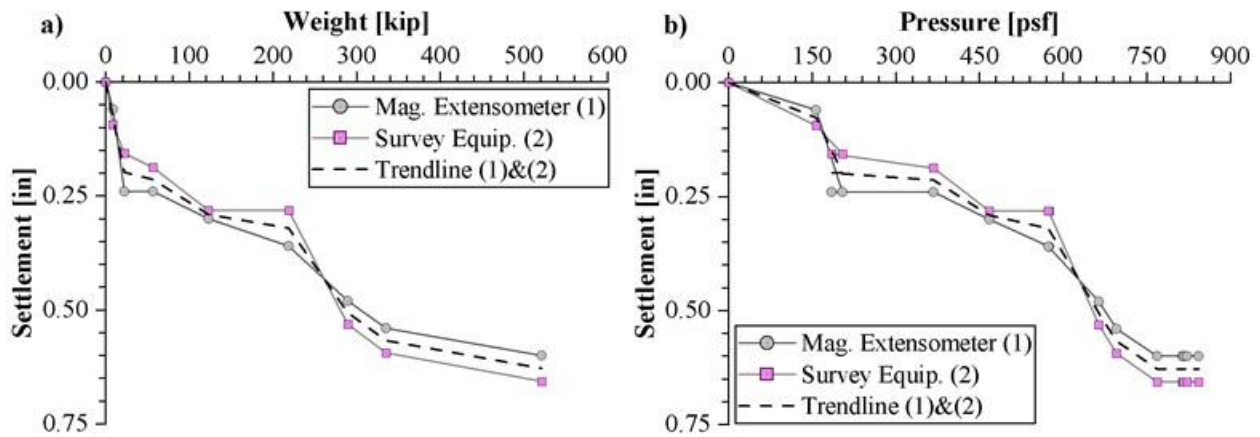


Figure 3-35. Load-deformation behavior for Cone 1: (a) weight-settlement, and (b) stress-settlement

If the maximum settlement value of 0.65 in is divided by the total height of the stress influence zone (i.e., 30 ft deep), an average vertical strain of 0.2% can be estimated. With an average stress of 780 psf, the stiffness modulus of elasticity of approximately 390 ksf can be computed. Using in Eq. (85) the following input values of $p=780$ psf, $a=20$ ft, $\nu=0.3$ (assuming drained conditions), and $\delta=0.65$ in, the computed E is approximately 300 ksf.

3.5.2.6 Analysis of Piezometric Readings: Test No. 2 (May 10, 2019)

Figure 3-36 presents the results of the piezometer data collected at Cone No. 2. Figure 3-36a presents the long-term porewater pressure variation and precipitation over time. The sensors were installed over the same time for Cone 3 in April 2019 and piezometric readings started to record since then. Data is shown from time zero (i.e., 05/01/2019 at 09:00 am, approximately eight days before the test started) up to 16 days, including the time when the tests were completed. Note that negligible U_e was generated during the test for PZ2-1 and PZ2-3. However, PZ2-2 recorded a $U_{e,max}$ of 50 psf during the test. Figure 3-36b shows the porewater pressure readings for the three PZs during the entire test. The time zero corresponds to 5/10/2019 at 7:20 am; when Cone 2 was initiated. Approximately one hour before Cone 2 started, a slight increase in porewater pressure was recorded due to the stockpiled material at the exterior north part of the cone (see Figure 3-18b).

At Cone 1 and 3, the loading material was not stockpiled because the excavator did the loading operations as the trucks were bringing material. That slight increase was also recorded by PZ2-3.

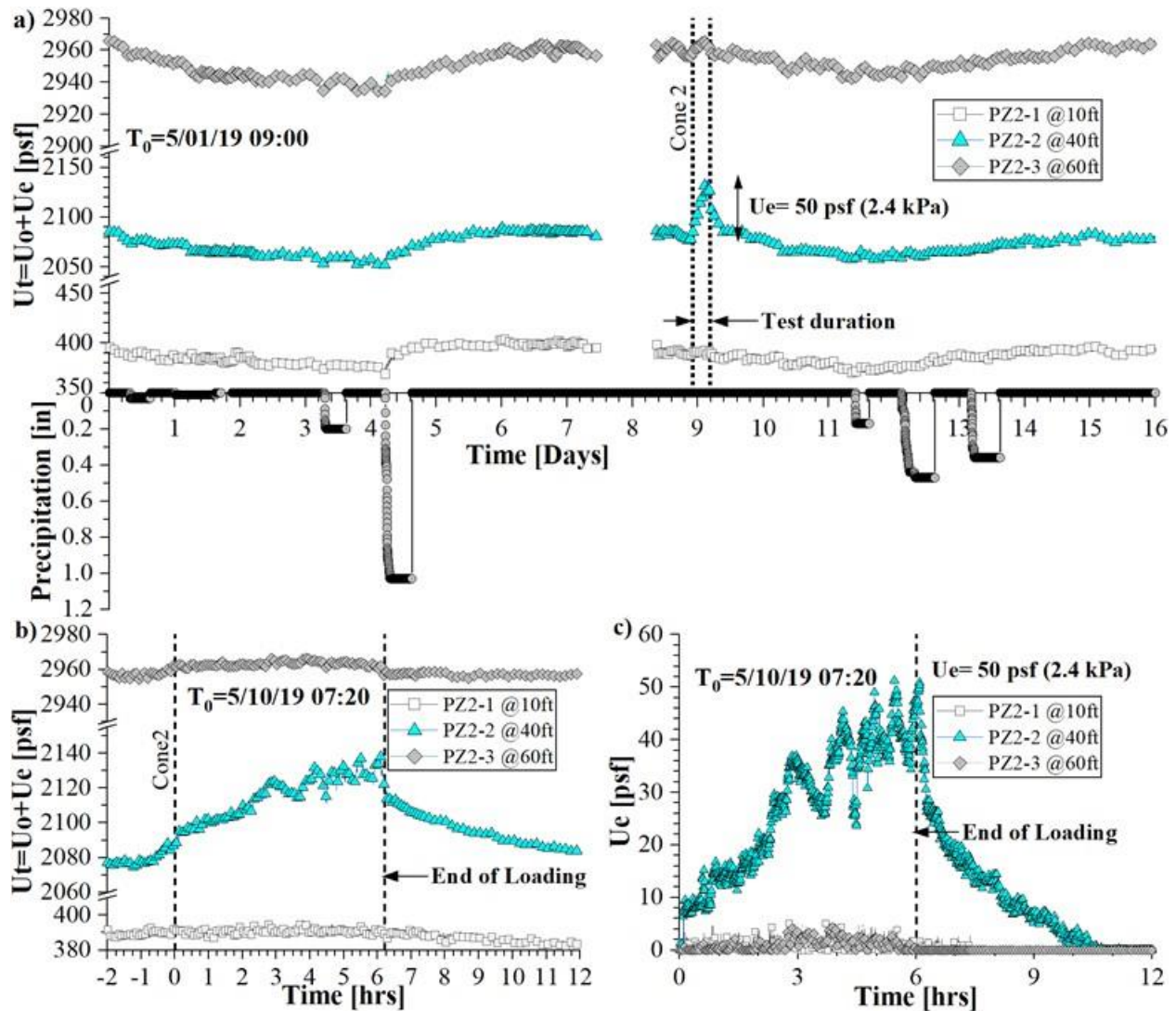


Figure 3-36. Conical load test No. 2: (a) measured total porewater pressure before and after the test, (b) measured total porewater pressure during the test, and (c) excess porewater pressure during the test

Fluctuation of hydrostatic porewater pressures before and after the test were attributed to the rain at the UCF site. Approximately at day 4 in Figure 3-36a, a slight increase in U_0 can be noted which coincides with an estimated rainfall of 1 inch (Orange Weather STEM, 2019). During the day of the test, there was not any precipitation recorded. Note how U_0 at the end of the test is slightly smaller compared to U_0 at the beginning of the test, except at PZ2-2 where dissipation of U_e was not completed until 6 hr. after the end of the test.

Figure 3-36c shows the excess porewater pressures only due to the conical load test 2. Recall that the piezometers were located approximately 3 feet away from the center of the cone; therefore, small incremental $\Delta\sigma$ caused by the conical load was expected which induced small excess porewater pressures. A $U_{e,max}$ value of 50 psf measured in the silty clay layer is not attributed to the radial dissipation of conical-induced stresses, since the conical loading placed at the ground surface barely stressed that soil layer.

Using the formulation proposed by Harr and Lovell (1963) to determine $\Delta\sigma_z$ at the axis of a conical shaped loading as presented for Cone 1, an increase of vertical stress 86 psf is calculated using the value of $p=810$ psf (measured with the pressure cells), $a=20$ ft, and $z=40$ ft, is (or 4 kPa). This value represents only 3.4% of the vertical effective stress at that point. The negligible U_e measured by PZ2-2 installed in the silty clay layer reasonably matched that computation.

3.5.2.7 Analysis of the Conical Load Pressure Measured with Pressure Cells: Test No. 2 (May 10, 2019)

Figure 3-37 presents pressure cell measurements at the ground surface due to the conical load test 2. The initial zero readings were taken at 05/10/19 at 7:20 a.m. (i.e., ten minutes before the test started and in the absence of any loading). Figure 3-37a presents earth pressure readings during the test (i.e., 0 to 8 hr.) and a break in the horizontal axis for readings up to 48 hours. Both pressure cells recorded an increase in pressure at a constant rate of approximately 250 psf per hour until the radius of the cone reached 13.7 ft. As expected, the shape of both pressure cell data is similar. Figure 3-37b shows the recorded long-term data up to 18 days after the test was completed. Recall that the earth pressure cells were located at two different positions with respect to the center of the cone (i.e., approximately 1.5 feet on the west and east sides of the cone). Note how in Figure 3-37b the pressure readings of the SC1 remained constant at approximately 700 psf after 18 days, but SC2 showed a decrease of the cell pressure of approximately 150 psf due to the redistribution of stresses in the test. The differences in the pressure readings of approximately 300 psf (14 kPa) at the end of the test were reduced in the long-term to approximately 200 psf (10 kPa). This confirms that the conical load was not acting as a rigid body.

Similar to Cone 3, Figure 3-38 shows the schematic loading increment sequence based on the recorded cone radius and height. In order to study the differences in the loading rates, Figure 3-38b presents normalized weights (calculated with the geometries presented in Figure 3-38a) and pressures obtained during the loading sequence. The weights and pressures are normalized by the maximum values reached after seven hours. For this cone, recall that the unit weight of the material was 87 pcf measured with sand cone tests. The normalized pressures SC1 and SC2 shown in Figure 3-38b are identical even though differences in their magnitude were previously presented in Figure 3-37a.

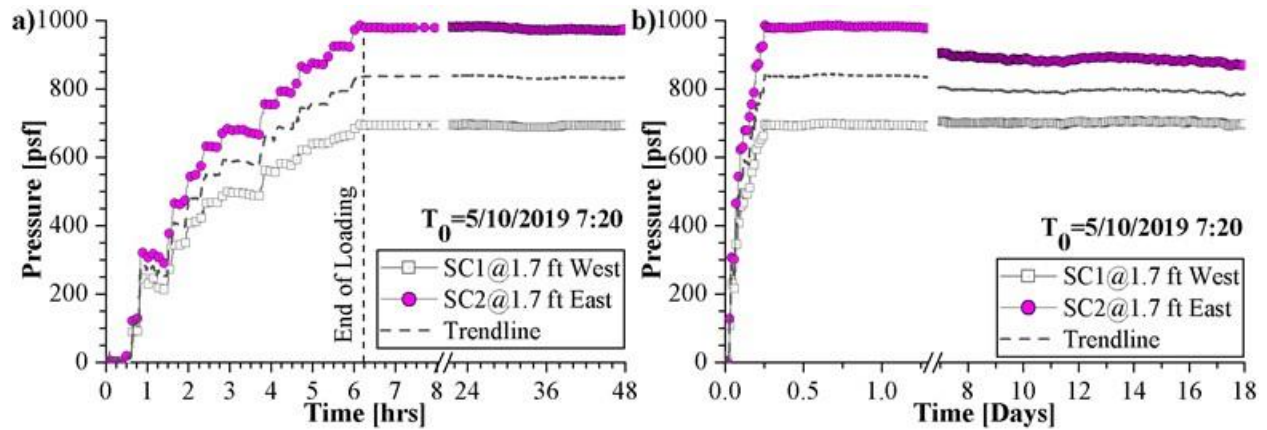


Figure 3-37. Pressure cells readings at conical load test 2: (a) short-term pressure cell readings (i.e., from 0-8 and 22-32 hours), and (b) long-term pressure cell readings up to 18 days after end of test

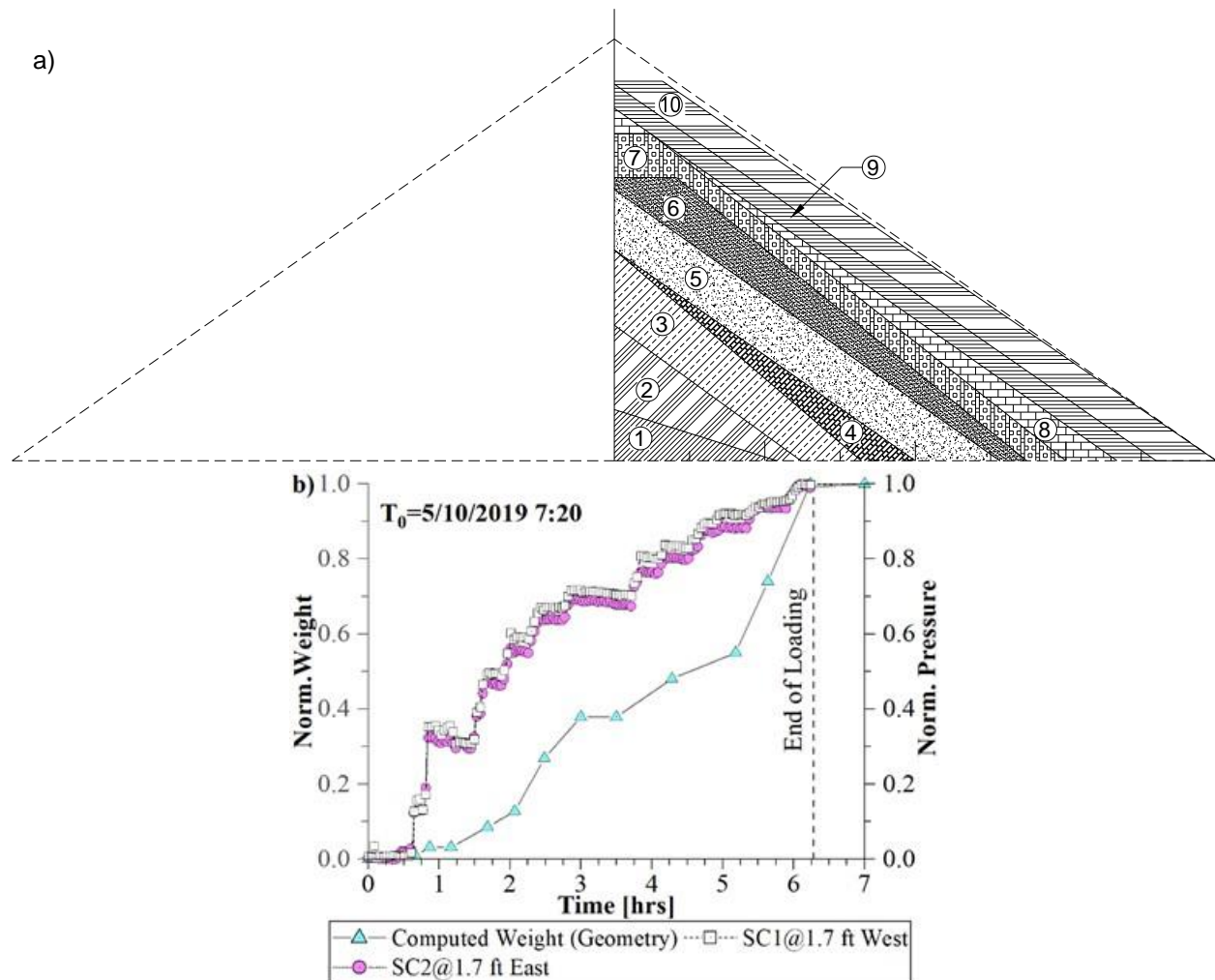


Figure 3-38. Schematic sequence followed during conical load test 2, and b) normalized weights and pressures during the conical load test

3.5.2.8 Relationships Between Measured Settlements, Pressures, and Weights over Time: Test No. 2 (May 10, 2019)

Figure 3-39a presents the measured settlements and pressures for the entire duration of the test (i.e., eight hours). Figure 3-39b presents the same measured settlements but in relation to the computed weights. The settlements measured in Cone 2 were recorded using the data from a vibrating wire displacement transducer installed under the settlement plate, survey equipment, and magnetic extensometer. Figure 3-39c presents a detailed view of the measured settlement from vibrating wire displacement transducer along with the SC1 pressure readings. Figure 3-39c shows the same settlements but in relation with the computed weight.

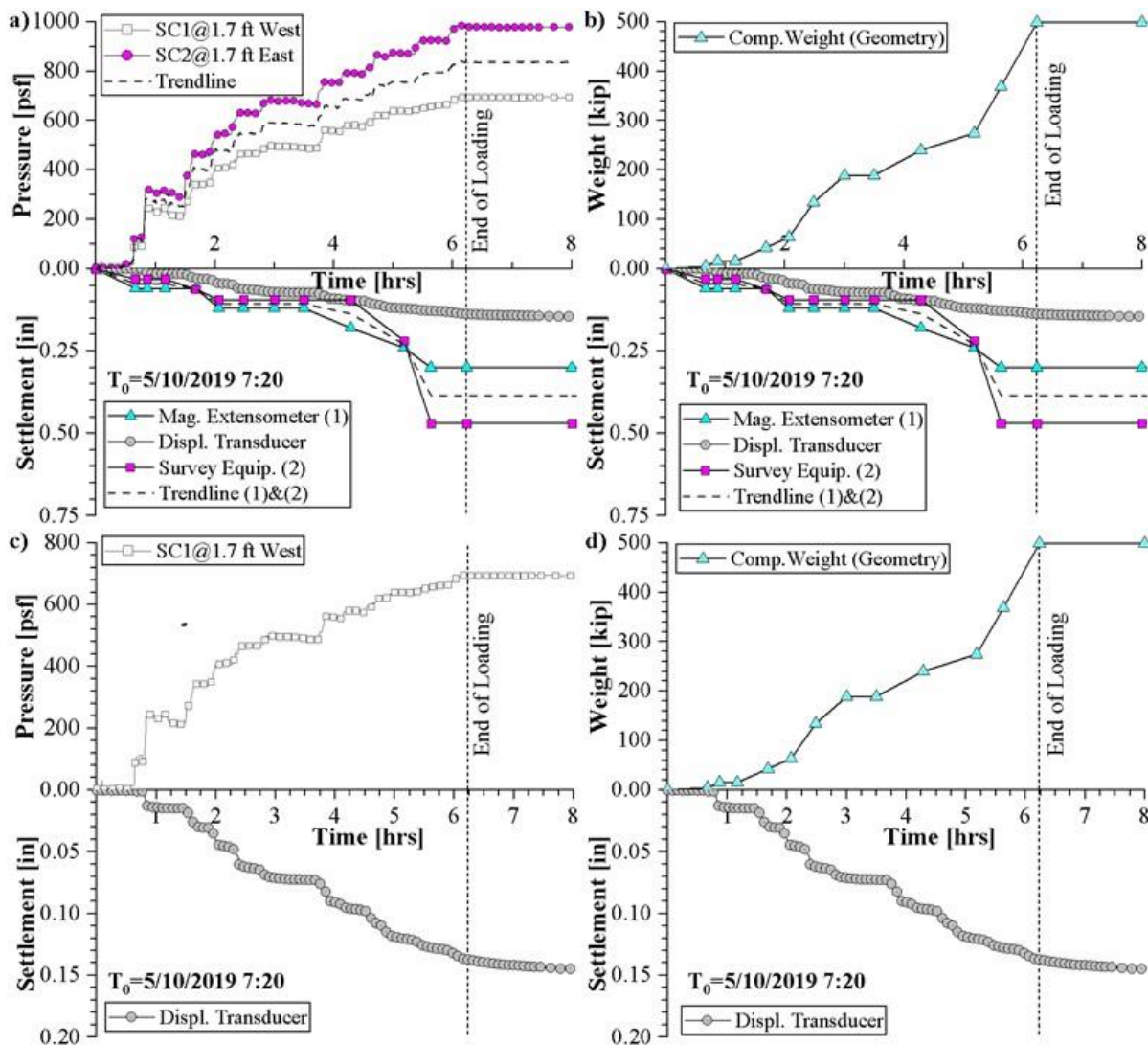


Figure 3-39. Settlement, pressure, and computed weights for the length of the test: (a) measured pressure and settlement, (b) computed weight and settlement behavior, (c) SC1 pressure readings related to settlements, and (d) computed weight in relation to settlements

It is intended to show the continuous readings of pressure and settlement with both sensors at the same side of the cone (West side) to identify the main differences in the results. The variation of settlement presented in Figure 3-39c is similar in shape to the variation of pressure for the entire test length (as opposed to weight data). This again confirms that measurements of pressures at the ground surface using pressure cells are more accurate when representing the loading sequence as oppose of the computed weight method.

Figure 3-40 presents the measured settlements using the magnetic extensometers. Settlement readings were collected until approximately 15 days after the test was completed to identify possible time-dependent variations caused by consolidation of silty clay layers found at a depth of 33 ft. The line labeled as “trendline” corresponds to the average value of ground surface settlement reported in Figure 3-39. In this case, the spider magnets recorded negligible displacements (i.e., less than 0.125 in.) which are very close to the accuracy of these types of instruments.

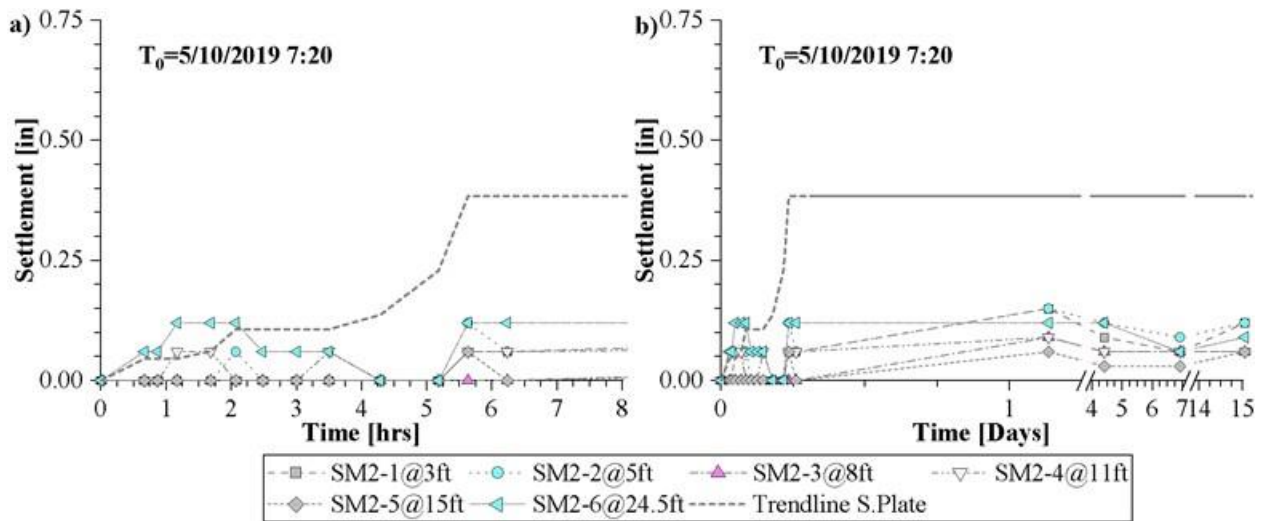


Figure 3-40. Settlement with spider magnets: (a) short-term settlement readings and (b) long-term readings up to 15 days after the end of the test

3.5.2.9 Excess Porewater Pressures in Relation to Earth Pressures and Settlements: Test No. 2 (May 10, 2019)

Figure 3-41 present the excess porewater pressure and earth pressure readings from the beginning of the test (i.e., 05/10/2019 at 7:20 am). In Figure 3-41a, the trend of U_e with PZ2-2 follows a similar pattern as the average pressure cell until the test was completed. Recall that the PZ2-2 is located at the silty clay layer. U_e values up to 50 psf were recorded for Cone 2 at the clayey-type layer. This layer was very lightly stressed by the conical loading. Figure 3-41b isolated the piezometric readings PZ2-1 and PZ2-3 showing negligible U_e variations. This suggests the presence of more granular deposits below the silty clay layer (estimated below 52 ft).

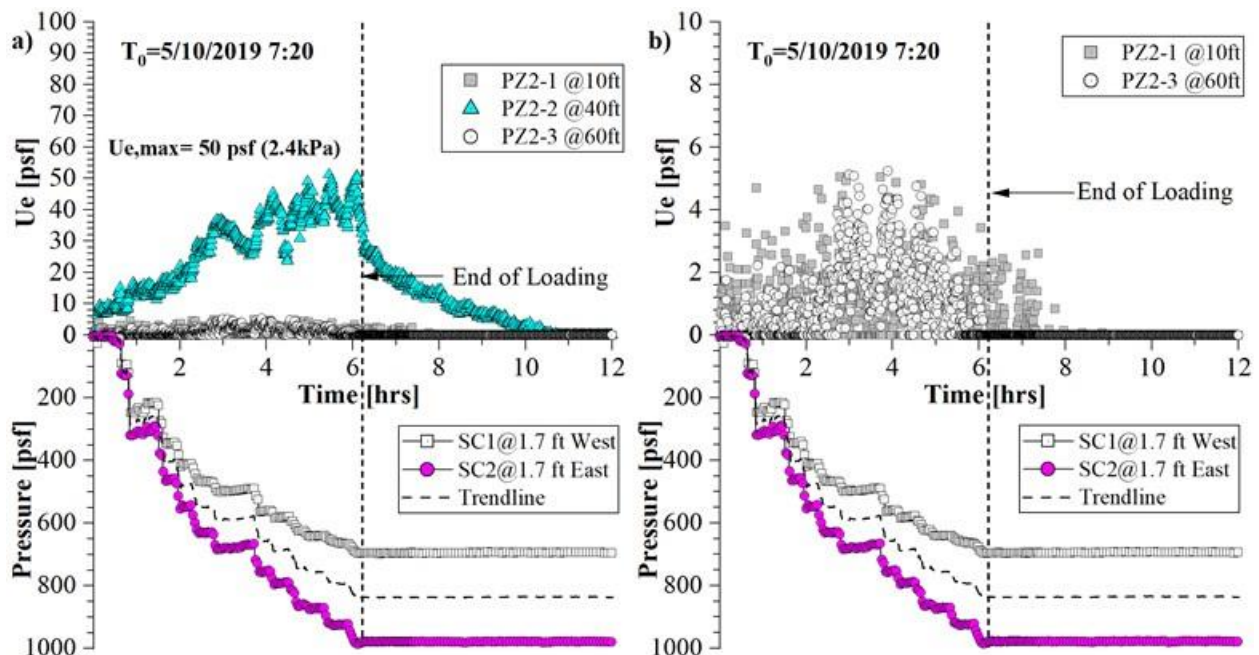


Figure 3-41. Measured excess porewater pressures in relation to earth pressures at the ground surface: (a) clayey layer and (b) sandy layer

Figure 3-42 presents excess porewater pressures and settlements measured with the vibrating wire displacement transducer. These figures along with Figure 3-34 and Figure 3-42 lead to the conclusions for all the Cones: (i) excess pore pressures did not build up in these sandy soil layers, (ii) the conical load was placed slow enough to allow U_e dissipation in the silty-sand and sandy-silt layers, and (iii) settlements measured in this test were immediate (and presumably elastic). The maximum immediate settlement measured in this test was 0.4 in at the center of the cone with survey equipment and spider magnets, and 0.15 in away from the center with vibrating wire displacement transducer.

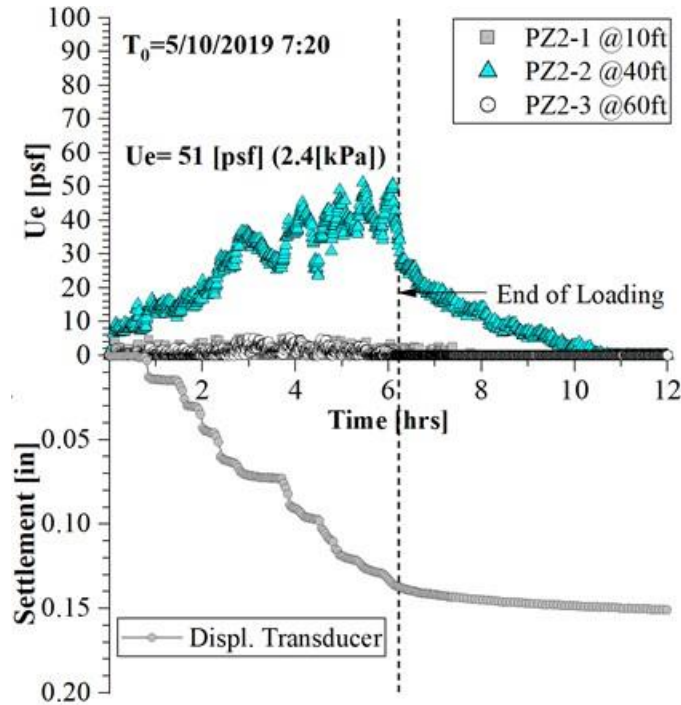


Figure 3-42. Measured excess porewater pressures and settlement at the ground surface measured with displacement transducer

3.5.2.10 Load-Deformation Behavior Measured in Conical Load Test 2

The soil load-deformation behavior induced by the conical load test 2 is presented in Figure 3-43. To plot the settlements from the displacement transducer related to computed weights, the weights at the end of each loading stage were divided between the number of intervals. The pairs made in the figure are based on the location of each sensor (i.e. displacement transducer versus SC1; SM and survey equipment versus SC2). Note how the recorded settlement from the vibrating wire displacement transducer is smaller than those recorded with other methods. This is attributed to the 2-ft distance apart from the center of the cone (i.e., where SM and survey equipment measured settlements).

Using an average stress of $p=800$ psf, $a=20$ ft, $\nu=0.3$ (i.e., drained conditions), and $\delta=0.5$ in., the computed E using equation (86), which was derived for a conical load arrangement assuming isotropic elasticity, is approximately 340 ksf. Based on Boussinesq analyses, the influence depth should be closer to 25 ft, and using this depth, an influence axial strain of 0.2% is computed based on uniaxial loading conditions. This way, the modulus of elasticity is computed as 380 ksf.

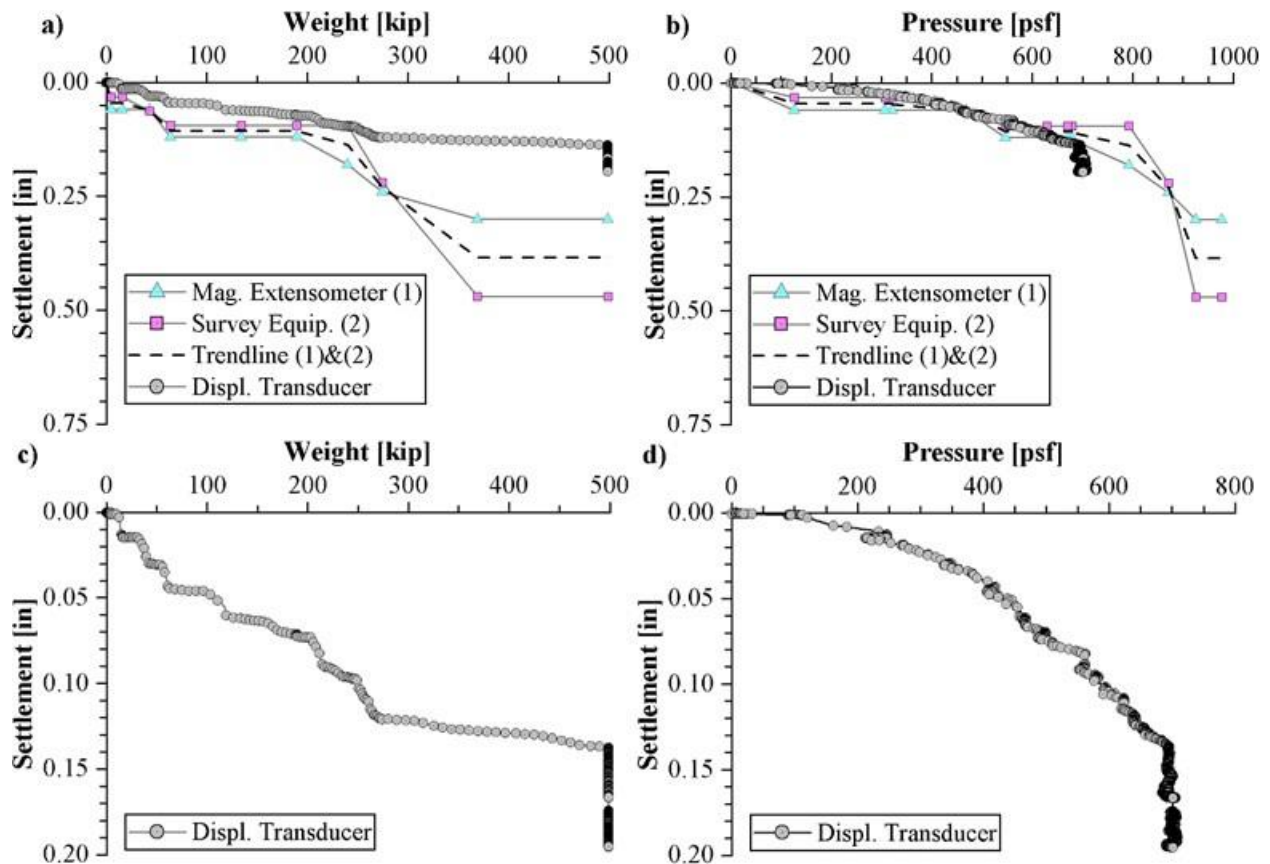


Figure 3-43. Load-deformation behavior measured at conical load test. 2: (a) settlement versus weight, (b) settlement versus stress, (c) displacement transducer settlement versus weight, and d) displacement transducer settlement versus pressure at SC1

3.5.2.11 Analysis of the Inclinometer Data: Test No. 2 (May 10, 2019)

Figure 3-44 presents the raw and zeroed lateral displacements measured with the inclinometer in the A-A and B-B directions which are close to the radial and tangential displacements, respectively. Recall that the inclinometer was installed at the edge of the cone (i.e., 20 ft from the centerline of the cone). Similar to Cone 1, initial readings were taken before the test started. Nine inclinometer readings were taken throughout this test. The range of variation of the readings is very small, which supports the conclusions drawn for Cone 1 that negligible lateral displacements caused by the conical load tests were induced.

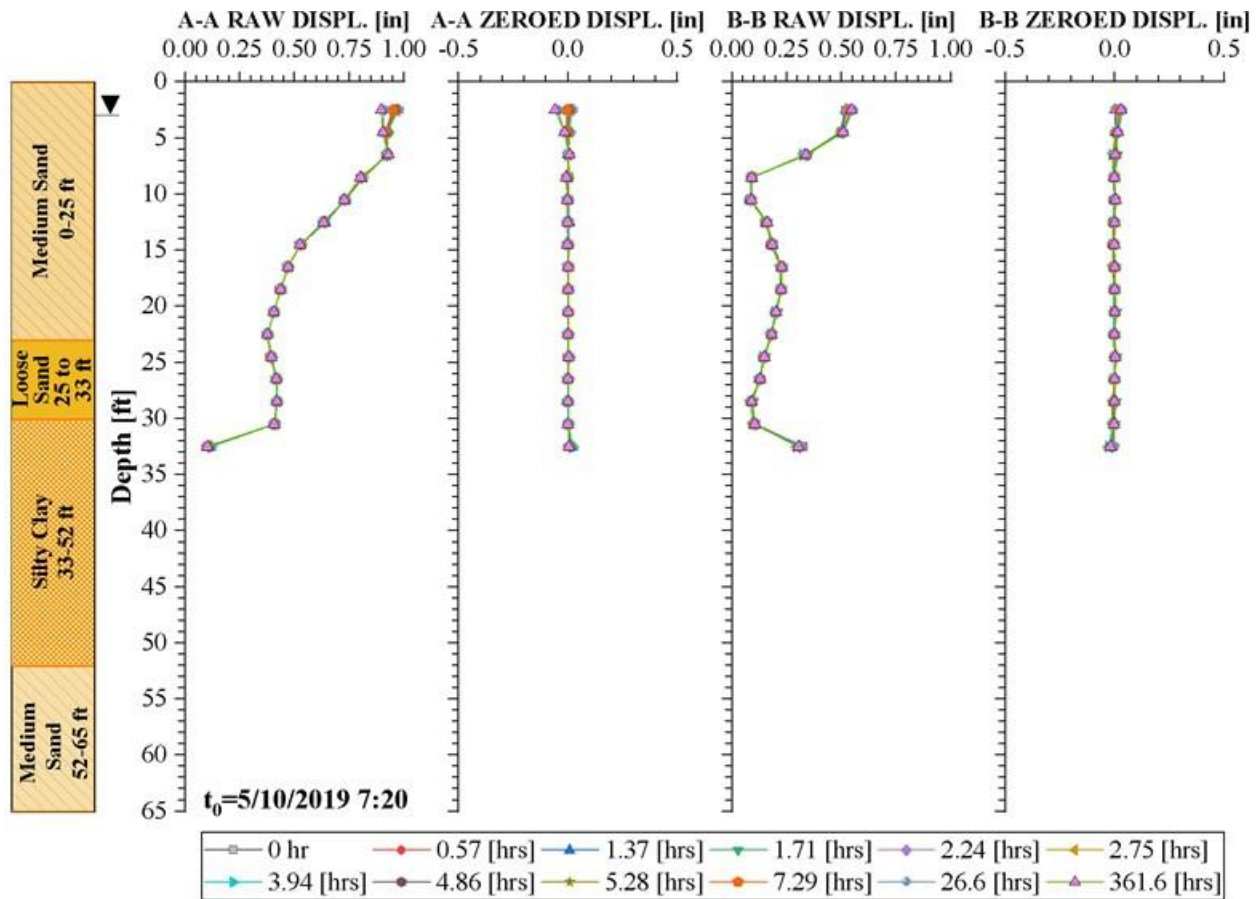


Figure 3-44. Lateral displacements in the soil at the edge of the conical load test

3.5.3 Summary of Conical Load Tests No. 1, 2, and 3

3.5.3.1 Piezometric Readings

Figure 3-45 presents the data collected with the piezometers for Cones 1 through 3. Figure 3-45a presents the long-term porewater pressure variation and precipitation over time. Each conical load test duration is presented within two verticals dashed, dotted, and dash-dotted lines, respectively. Figure 3-45b shows porewater pressure readings for the seven piezometers used during the tests. The zero time in Figure 3-45b corresponds to the start of the conical load test. Hydrostatic pressures are represented with dashed blue lines. The U_0 values were taken as the average value one hour before and after the test of the equilibrium porewater pressure readings. Variations in U_0 are attributed to water table changes due to precipitation as shown in Figure 3-45a. The effect on deeper soil layers (clay material) is not as perceptible as in the case of shallower granular material. Figure 3-45c presents the excess porewater pressures measured with PZ1-3 and PZ2-2 (installed in clayey layer). Even though PZ2-2 was placed 5 ft closer to the ground surface than PZ1-3, the U_e developed by Cone 1 is larger than the one measured on Cone 2, suggesting that the pressure applied by Cone 1 was larger.

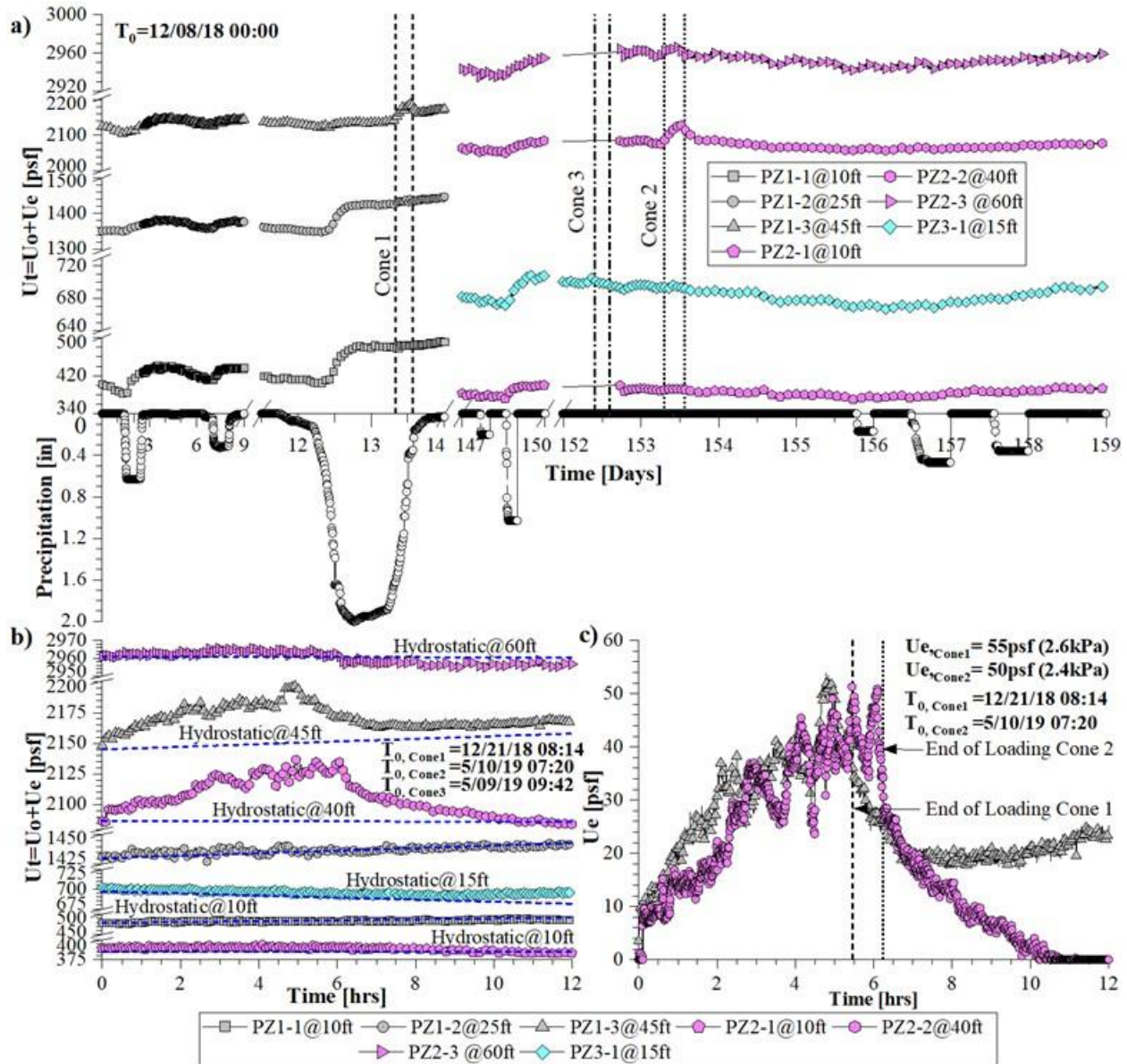


Figure 3-45. Conical load test 1 through 3: (a) long-term total porewater pressure, (b) total porewater pressure during the tests, and (c) excess porewater pressure during the test

3.5.3.2 Conical Load Earth Pressure Measured with Pressure Cells

Figure 3-46 shows recorded load-induced earth pressures with pressure cells at the ground surface. The initial zero readings were taken 10 min before the tests started and in the absence of any loading. Figure 3-46a presents pressure readings during the three tests (i.e., 0 to 7 hr.) and a break in the horizontal axis is shown to present readings up to 48 hours. The time when the tests were completed are demarked with vertical dashed lines. Figure 3-46b presents long-term readings up to 18 days after the tests were completed. The outputs of pressure cell correspond only to those sensors close to the center of each cone. A trendline for Cone 2 is used since both SCs were placed at the same distance from the center. Pressure readings at Cones 2 and 3 are considerably smaller

than at Cone No. 1. That is mainly attributed to the unit weight differences measured with sand cone tests (ASTM D1556): 87 pcf at Cones 2 and 3, and 100 pcf at Cone 1. Another difference was the water content of the fill material: 10% at Cone 1, and 6.4% at Cones 2 and 3. Differences in the conical volumes were also notable: 7,335, 5,734, 5,990 ft³ at Cones 1, 2, and 3, respectively. The long-term pressure reading changes were attributed to the following factors: (i) the variation of the moist density, (ii) redistribution of stresses and arching in the conical arrangement of soil above the ground surface, and (iii) densification and/or particle rearrangement of the conical load material.

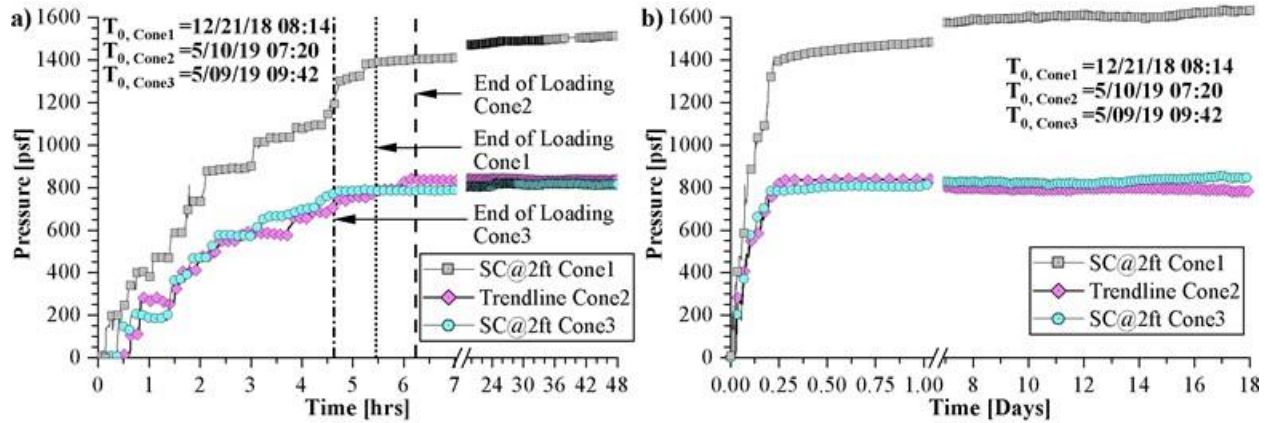


Figure 3-46. Pressure cell readings at conical load tests 1 to 3: (a) short-term pressure cell readings (i.e., from 0-7 and 23-48 hours) and (b) long-term pressure cell readings up to 18 days after end of the test

Differences in the loading rates for each conical load from pressure cells and computed weight are shown in Figure 3-47. The end of each test is demarked with vertical dashed lines, showing that all tests were completed in less than 7 hr at different rates.

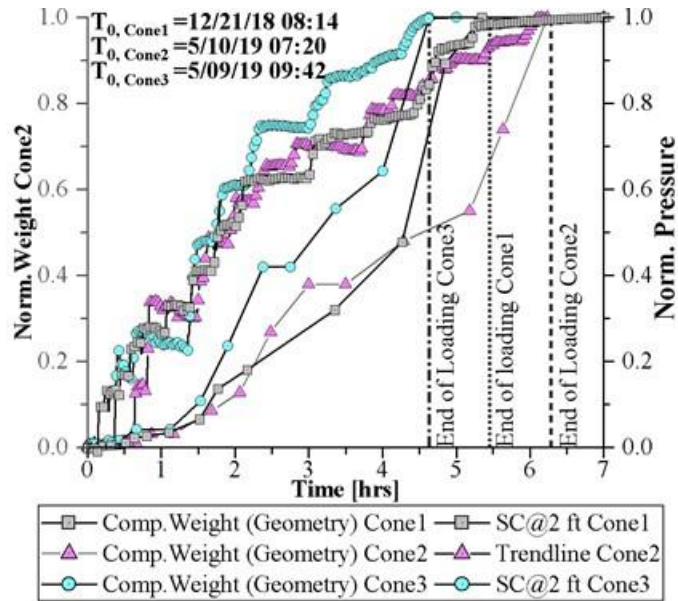


Figure 3-47. Normalized variation of weights and pressures during the conical load tests 1 through 3

3.5.3.3 Measured Settlement, Pressures, and Weights over Time

Figure 3-48a summarizes earth pressures and settlement for the entire length of the tests. Figure 3-48b presents the geometrically calculated weights and settlement over time. In both figures, the time when the tests were ended are demarked with vertical dashed lines. As explained earlier, using pressures rather than weights are preferable to evaluate the loading sequence and load-deformation behavior of soils in conical load tests.

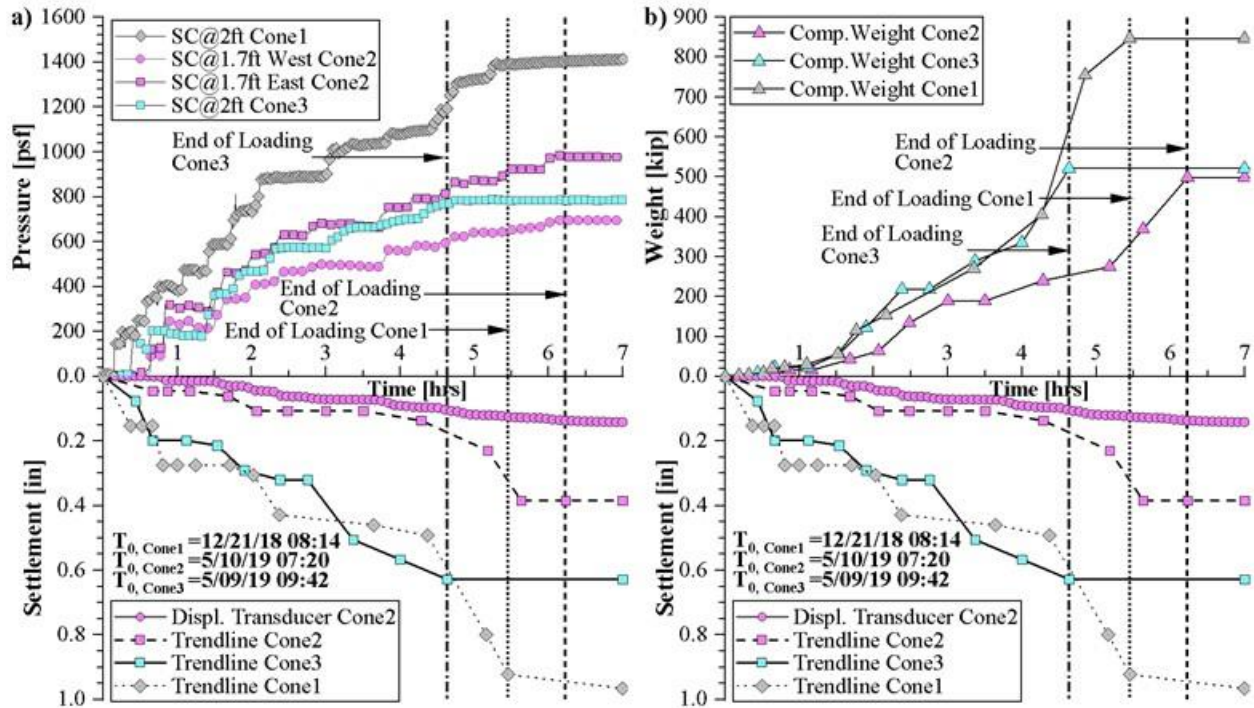


Figure 3-49 presents the recorded settlements with magnetic extensometers for the three conical load tests. Recall that the spider magnets were installed at different depths below the ground surface at the center of the conical test. Note that the recorded settlements in Cone 1 are larger when comparing the underground deformations for each load tests. Underground deformations at Cone 2 show measurements in the order of 0.06 in (1.5 mm) which is close to the smallest division for the measurement tape reel (1/100 ft). Thus, settlements were not discernable, and therefore, are considered zero below a depth of 15 ft.

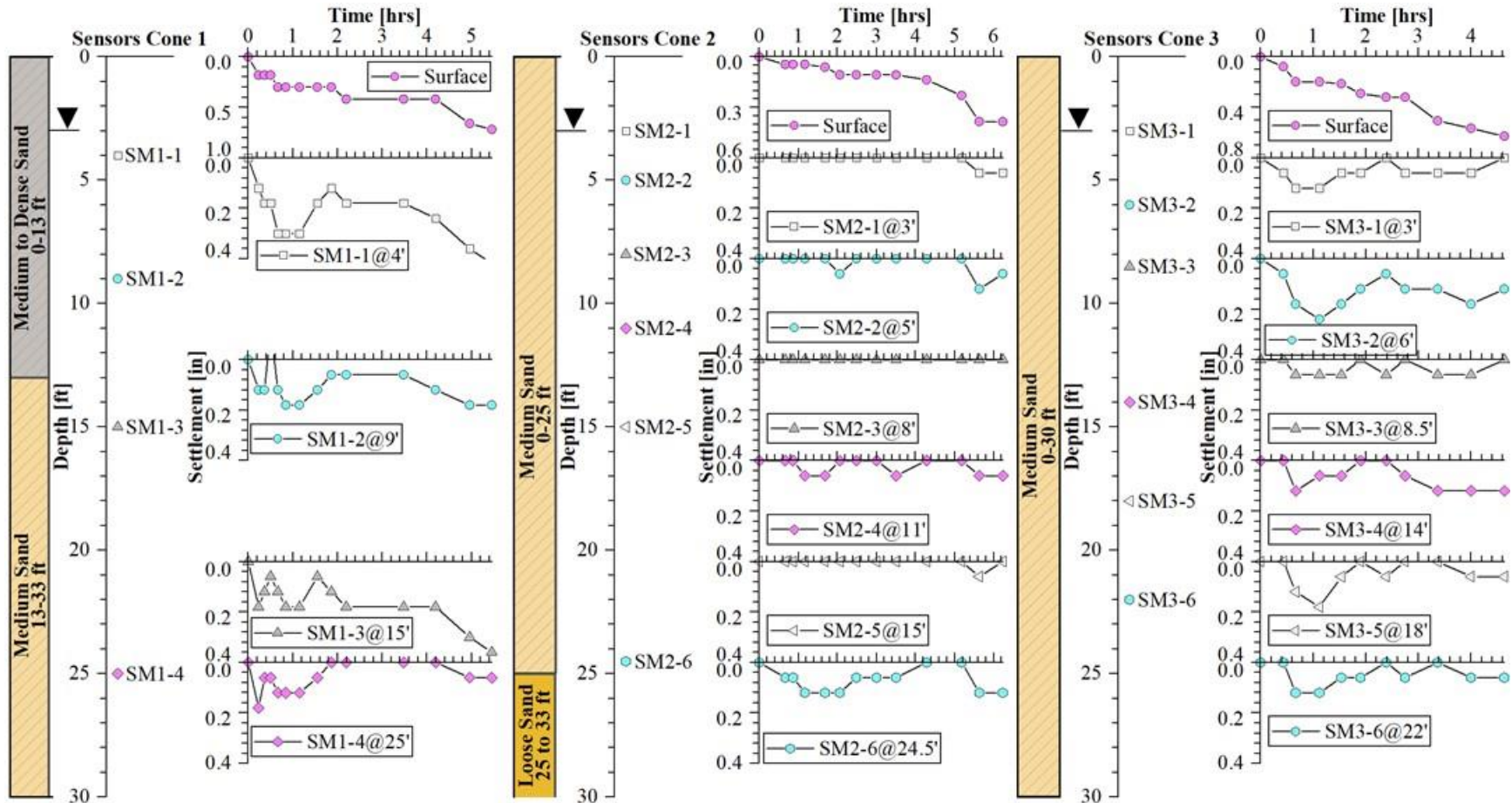


Figure 3-49. Magnetic extensometer readings at Cones 1 to 3 over the soil profile

3.5.3.4 Excess Porewater Pressures in Relation to Earth Pressures and Settlements

Figure 3-50 compares the excess porewater pressure readings for PZ1-3 and PZ2-2, and earth pressure readings at the same cones over time. Only PZ1-3 and PZ2-2 are reported in Figure 3-50 since the remaining piezometers were installed in sandy layers. The initial times for both cases correspond to the beginning of each test, and the maximum excess porewater pressures recorded at each test are indicated. Note that maximum excess porewater pressure between Cone 1 and 2 were similar at the clayey layer, even though the applied pressures were different. More interesting is that U_e at cone 1 was not completely dissipated during the test due to the large sustained pressure.

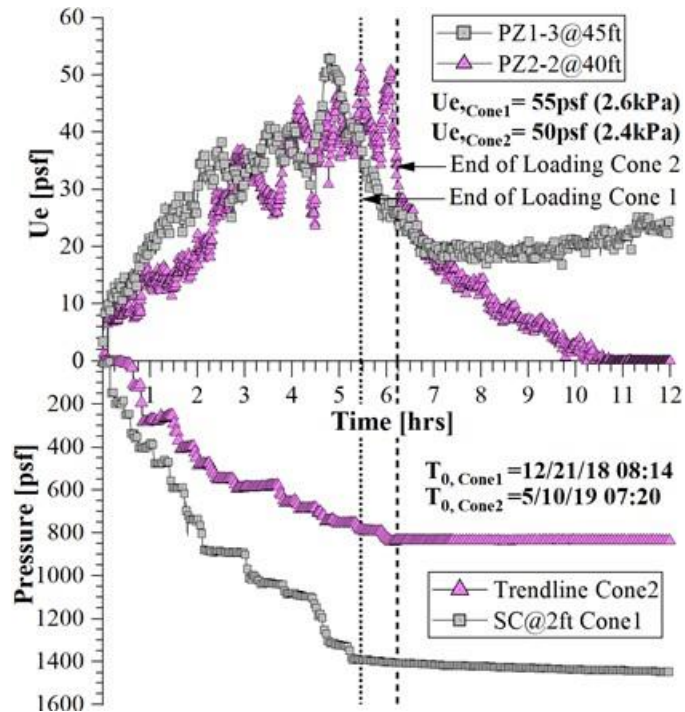


Figure 3-50. Cones 1 and 2 measured excess porewater pressures and earth pressures at the ground surface

Figure 3-51 relates the excess porewater pressures and settlements over time. Although excess porewater pressures presented in the figure are similar in magnitude, recall that PZ1-3 was installed deeper than PZ2-2, indicating that the applied load at Cone 1 was larger and assuming the spatial variability of soil properties of the clayey soil layer is not significant.

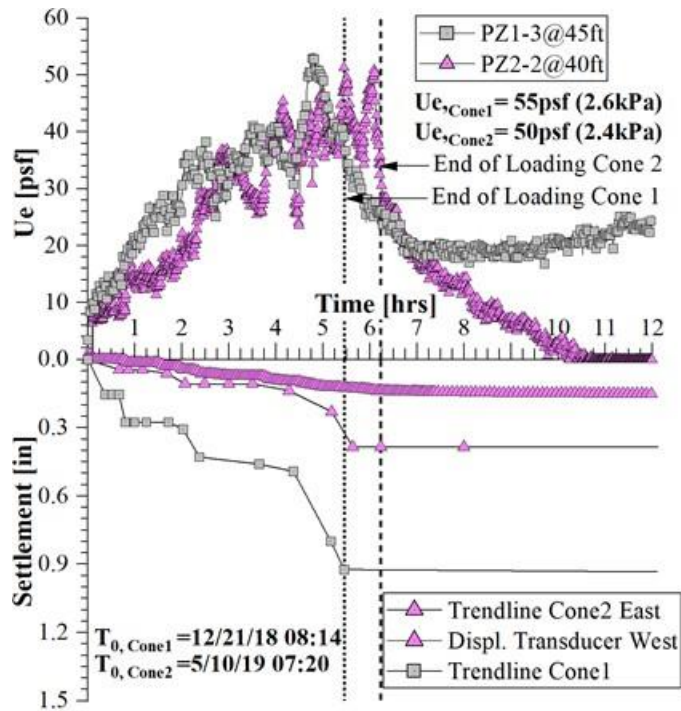


Figure 3-51. Cones 1 and 2 measured excess porewater pressures and settlement at the ground surface measured with magnetic extensometer and displacement transducer

3.5.3.5 Load-Deformation Behavior from Conical Load Tests

The load-deformation behavior of the soil caused by three conical load tests are presented in Figure 3-52. As previously discussed, both figures present two different settlement readings at Cone No. 2 labeled “Displ. Transducer” and “Trendline Cone2.” The figure shows similar load-settlement behaviors for each conical load test, even though the amount of measured settlements differs between each test. Note that pressures up to 1500 psf were applied causing settlements up to 1 in.

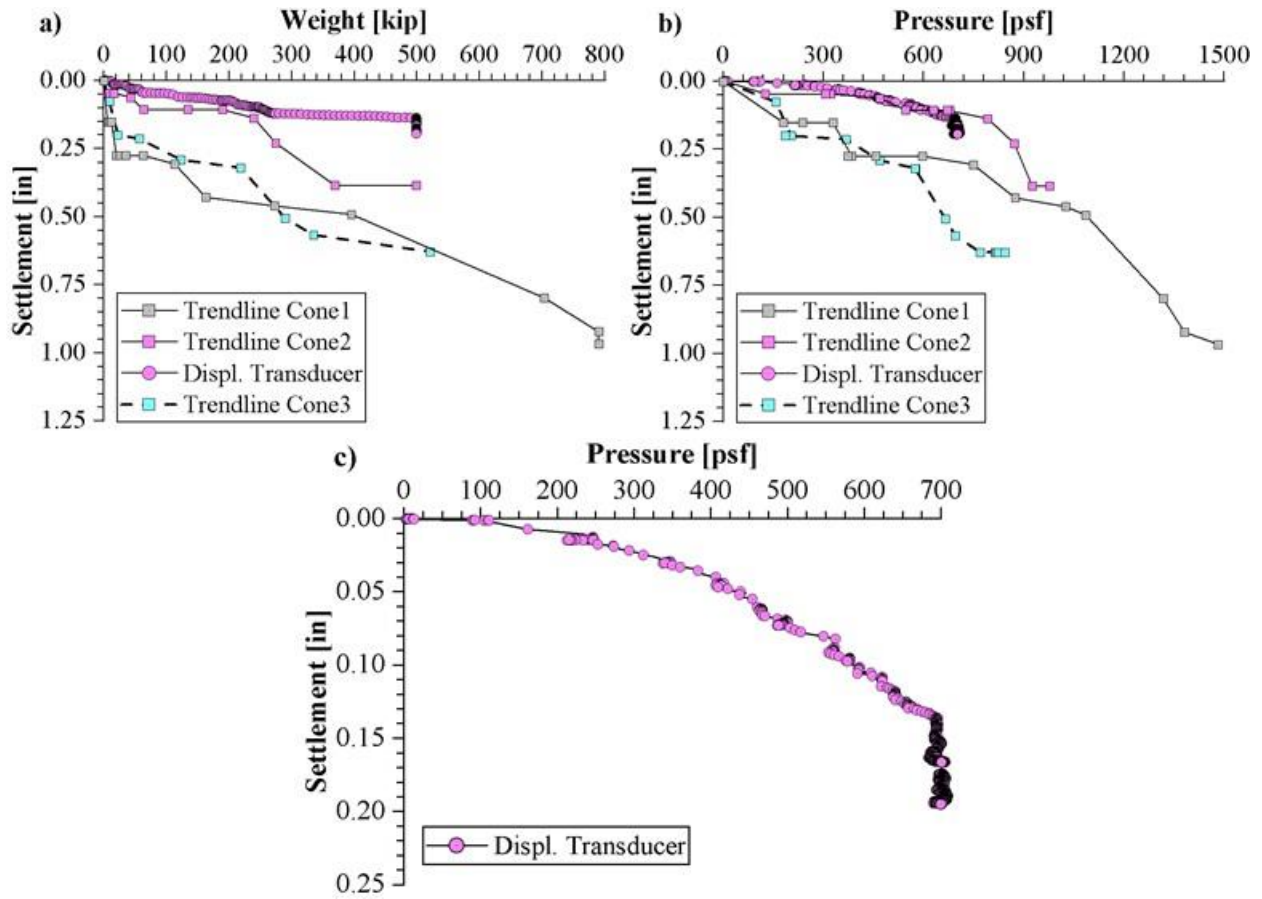


Figure 3-52. Load-deformation behavior measured at cones 1 to 3: (a) settlement versus weight, (b) settlement versus stress, and (c) displacement transducer settlement versus stress

CHAPTER 4

LABORATORY TESTING PROGRAM

Two experimental programs were designed to evaluate soil properties and mechanical behavior of the soils at the UCF site in terms of compressibility, stiffness, and strength of the two geological formations [i.e., Cypresshead Formation and Hawthorn Group (Fountain 2009)] that are present in the area of study. Soil mechanical properties were estimated from field tests and compared to those obtained with the laboratory test results.

4.1 Geology at the Project Site

4.1.1 Cypresshead Formation

The Cypresshead formation, formed during the late Pliocene to early Pleistocene, overlies either the undifferentiated Hawthorn Group or the Peace River formation of the Hawthorn group in central and southern peninsular Florida (Fountain 2009). Its extension comprises Dorchester County in South Carolina, southeastern Georgia and central Highlands, and Highlands County in Florida (Scott 1992). The depositional environment still remains unclear due to the mixed evidence found in this formation, which suggests that siliciclastic sediments were deposited in a mix of shallow-water marine and coastal environments (Fountain 2009). The lithology indicates siliciclastic sediments, predominately quartz and clay minerals, reddish brown to reddish orange, unconsolidated to poorly consolidated, fine to very coarse-grained, clean to clayey sands. Feldspar, mica, and heavy minerals are present in minor amounts. Sediments vary from poorly to well-sorted and angular to subrounded, with induration generally poor to non-indurated (Scott 2001; Fountain 2009; Fountain et al. 2009). Typically, the cementing agent is clay although iron oxide is known to appear. In areas where the Cypresshead formation outcrops, kaolinite is characteristically present whereas illite and smectite are dominant when the formation is overlain by another stratum (Scott 1992; Fountain et al. 2009).

4.1.2 Hawthorn Group

The Hawthorn Group, constituted by interbedded and intermixed carbonate and siliciclastic sediments and variable occurrence of phosphate grains, is a very complex geologic unit. Research on lithostratigraphy indicates heterogeneity of the formation along the state of Florida, and in some cases within a few feet in individual strata (Scott 1988; Puri and Vernon 1972; Pirkle 1956; Missimer 2002). The variability can be explained considering the depositional and environmental controls exerted by sea-level fluctuations and geologic structures in the peninsular Florida. The deposition of siliciclastic sediments, provided by the gradual erosion of the Appalachian mountains via streams and rivers onto the Florida platform was controlled by the Georgia channel system, limiting the siliciclastic deposition and allowing carbonate deposition during the Paleogene. The uplift in the Appalachians dramatically increased the supply of siliciclastic sediments in the late Oligocene to the early Miocene, infilling the Georgia channel system until covering the Florida platform (Upchurch et al. 2019; Scott 1988, 1990). In addition, the sea-level fluctuations during the Miocene controlled the extent of deposition, diminishing when dropping the sea level. Fluctuations in the Aquitanian, Burdigalian, Serravallian and Tortonian in combination with the

geologic structures, as Sanford High, Ocala, St. Johns, and Brevard platforms, created the distributional pattern that composes the Hawthorn Group (Vail and Mitchum 1979; Scott 1988).

The Hawthorn Group is composed of different formations which vary depending on the zone within Florida. In central Florida, the area between the Sanford High and Ocala platform, consisted of a thin layer of Hawthorn sediments and exhibit more variation in its composition when compared to surrounding formations. Thus, the area is classified herein as Undifferentiated Hawthorn Group (Scott 1988). The lithology indicates small content of phosphate, sediments from light olive gray and blue gray in un-weathered sections to reddish brown in deeply weathered sections, poorly to moderately consolidated clayey sands to silty clays (Scott 2001). The change in porewater pressure and soil structure caused by the sea-level fluctuations, delayed consolidation (aging) and occurrence of carbonate minerals, respectively, which are the principal mechanisms for the pre-consolidation pressures of the Hawthorn sediments (Bjerrum 1967; Kenney 1964).

4.2 Geologic Soil Profile of the Site

The geologic soil profile of the testing site is illustrated in Figure 4-1 and is composed of three layers. The deepest layer is part of the Ocala Limestone, which consisted of nearly pure limestones and occasional dolostones (Scott 2001). Although the seasonal fluctuation of the water table showed phreatic levels that vary from one foot to deeper locations, the water table level was encountered at 3 ft from the ground surface.

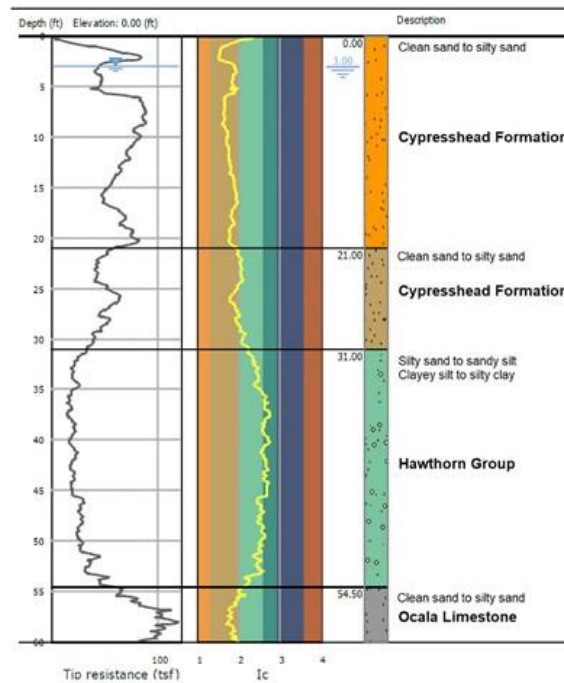


Figure 4-1. Geologic soil profile at UCF test site location

4.3 Laboratory Testing Equipment

A laboratory testing program at the UCF site was developed using cutting-edge geotechnical testing equipment to assess the properties and mechanical behavior of the soil samples retrieved from the project site. Conventional laboratory tests (i.e., gradation, water content, specific gravity, and consistency limits), consolidation tests using incremental loading (IL) and constant rate of strain (CRS), triaxial tests, X-ray diffraction and microscopy tests, and scanning electron microscopy (SEM) tests were performed at UCF geotechnical research laboratory facilities. Following ASTM standards, different soil laboratory characterization tests were performed: (i) natural water content following ASTM D2216 (2010); (ii) soil gradation and hydrometer tests following method B of the ASTM D6913 (2017) and ASTM D7928 (2017); (iii) specific gravity tests following ASTM D854 (2014); and iv) Atterberg limits tests following ASTM D4318 (2017).

Mechanical behavior and compressibility characteristics of the soils at the UCF site were determined using consolidation and triaxial tests. Incremental loading consolidation tests were performed following ASTM D2435 (2011), which correspond to an axial stress-controlled testing procedure. Axial deformations are recorded at each loading stage. Generally, IL tests last more than 24 hours since the standard load increment duration should exceed the time required to complete primary consolidation. As the ASTM standard states, this method does not use back pressure to saturate the soil specimen. Thus, saturation may not always be reached and cannot be quantified before the test starts. Most of those limitations can be addressed when performing a consolidation test with a CRS device like the one used in this testing program. CRS testing allows practitioners to obtain compressibility properties of the soils, improving several deficiencies of the classical Consolidometer devices. The time required to complete an oedometer test is significantly reduced because of the continuous measurement of excess porewater pressures, reducing the time necessary to reach primary consolidation. Saturation using a CRS device can be easily accomplished, quantified, and maintained during the test due to the addition of a pore pressure transducer. CRS allows continuous measurement of the excess porewater pressure throughout the test, which cannot be measured with most conventional oedometer devices (Mercado et al. 2018).

Figure 4-2 presents a schematic view of the consolidation CRS equipment used in this project to study the compressibility characteristics of the soils at the UCF site. This device was manufactured by *GDS Instruments, Ltd.* It is equipped with an internal submersible load cell with a capacity of 10 kN. One and two-way drainage patterns can be accomplished with this device. Usually, in a consolidation test the bottom valve is closed during the test, thus only drainage occurs through the top of the sample (i.e., one-way drainage pattern). A pore pressure transducer connected at the base of the chamber allows a continuous reading of excess porewater pressures when loading the sample. Cell pressures and changes in volume can be easily controlled by the GDS Enterprise Level Pressure/Volume Controller (ELDPC) with a pressure range from 0 to 1 MPa and a volumetric capacity of 200 cm³. An external linear variable differential transducer (LVDT) is used to measure the vertical displacement of the piston. The software used to setup the tests and process data allows an automatic continuous data collection throughout the test.

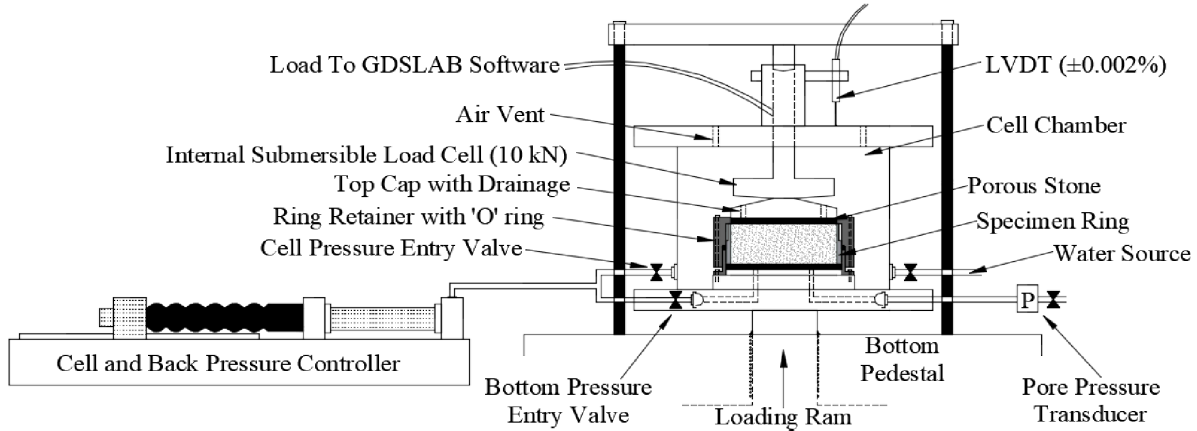


Figure 4-2. Schematic view of the constant rate of strain equipment used in this project

Figure 4-3 shows the schematic view of the triaxial testing system and internal instrumentation used to assess the mechanical behavior and stiffness-strength properties of the soils at the UCF site. This equipment was also manufactured by *GDS Instruments, Ltd.* The cell of this device has a capacity of 2 MPa and an internal dynamic actuator capable of inducing axial forces and deformations up to 10 kN and 100 mm, respectively. Two pressure/volume controllers adjust the cell pressure and volume changes. Pore pressure transducers connected at the base of the pedestal continuously read porewater pressures during the test. Internal instrumentation was also used during the tests consisting of Hall Effects (HE) transducers directly placed on the specimens to control local axial and radial deformations in the soil samples. Bender elements (BE) were installed at the top and bottom of the sample to monitor small-strain shear modulus associated with propagated shear waves during the test.

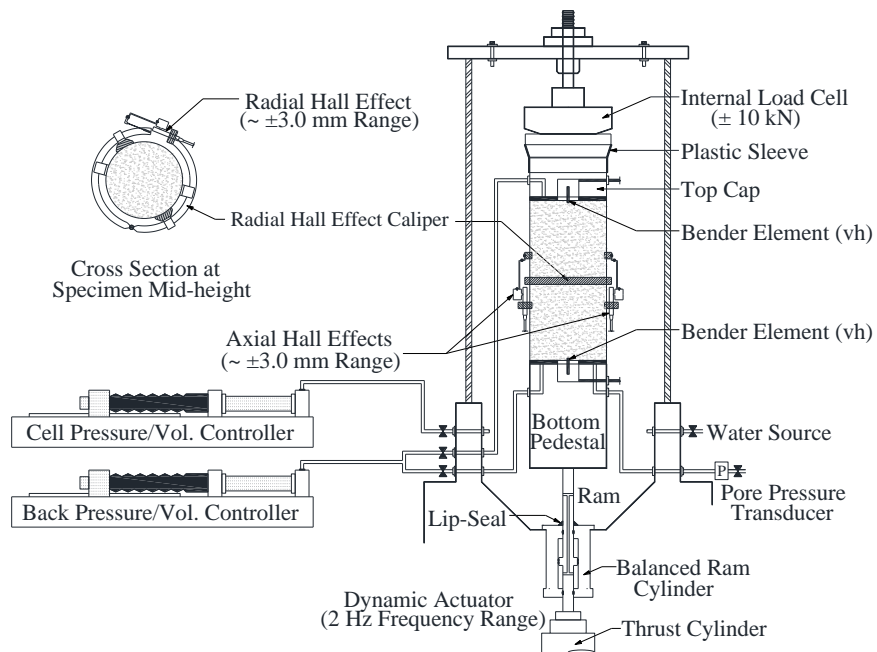


Figure 4-3. Schematic view of triaxial testing system used in this project

Visual examination of the soils was performed with a digital compound microscope manufactured by OMAX® to observe particle size and shape. To assess the internal composition and internal structure of the soil at the UCF site, X-ray diffraction (XRD) and SEM tests were performed at the UCF Advanced Material Processing and Analysis Center (AMPAC) facilities. XRD tests were used to determine the crystal structure and lattice parameters of materials present at the site. *X'Pert HighScore Plus® v.3.0.0* by PANalytical® was also used to perform the readings for the XRD test and using the Joint Committee on Powder Diffraction Standards (JCPDS) database, phase identification was performed to determine the minerals in the soil samples. SEM image tests were performed with the Zeiss ULTRA-55 FEG device. This is an electrostatic device that allows the microscope to image magnetic materials without distortion by a magnetic field. It can deliver high resolution images even with low voltages. It is equipped with Naby Electron Beam Lithography System that acquire information and detect elements as light as Boron. This is useful for soils with different compositions like the ones found at the project site.

4.4 Laboratory Testing Program on Cypresshead Formation Soils

4.4.1 Index Property Test

The laboratory test results presented in this section are based on the retrieved samples described in CHAPTER 3. Recall that soil samples were retrieved from boreholes at the southwest (SW) and northeast (NE) of the UCF testing site. Initially the samples were characterized to determine their index properties as summarized in Table 4-1.

Table 4-1. Results of index tests in topmost granular soils

Loc.	Sample	Depth [ft]	w_n^a [%]	Sand ^b [%]	Fines ^b [%]	Silt ^c [%]	Clay ^c [%]	G_s^d	LL ^e [%]	PL ^e [%]	Classification ^f
SW	A1-J1	2.50	17	-----	-----	-----	-----	-----	-----	-----	-----
SW	A1-B1	7.50	27	82.6	17.4	1.1	16.3	2.650	NP	NP	SM
SW	A1-B2	12.50	30	86.3	13.6	1.9	11.8	2.662	NP	NP	SM
SW	A1-B3	16.25	28	64.6	35.3	4.8	30.4	2.661	NP	NP	SM
NE	A2-J1	2.50	19	-----	-----	-----	-----	-----	-----	-----	-----
NE	A2-B1	7.50	23	85.8	14.2	-----	-----	2.629	NP	NP	SM
NE	A2-B2	12.50	28	88.5	11.4	1.8	9.6	2.659	NP	NP	SP-SM
NE	A2-B3	16.25	32	85.1	14.8	4.2	10.6	2.654	NP	NP	SM

Note: SW: Southwest. NE: Northeast. NP: Non-plastic.

^aNatural water content performed by Method A of the ASTM D2216 (2010).

^bGradation performed by Method B of the ASTM D6913 (2017).

^cGradation performed according to the ASTM D7928 (2017).

^dSpecific gravity performed by method A of the ASTM D854 (2014).

^eConsistency limits performed by procedure 2, method A (LL) and procedure 1 (PL) of the ASTM D4318 (2017).

^fClassification by the Unified Soil Classification System (ASTM D2487 2017).

Natural water content, gradation analyses, hydrometer, specific gravity (G_s), Atterberg limits were used to characterize the materials. Soils were classified using the Unified Soil Classification System (USCS). All samples tested on Cypresshead formation soils were classified as silty sands (SM) based on USCS. However, note that the clay content is larger than the silt in the soil samples according to hydrometer tests. Most of the samples have a sand content larger than 80%, except the A1-B3 with approximate 65% of sands. Non-plastic content in the fine sand was found with consistency limits performed to the material passing Sieve No 40 (425 μm) [i.e., Liquid limit (LL) and Plastic limit (PL) could not be determined]. The measured G_s values for these samples were consistently between 2.650 and 2.662; however, a slightly lower G_s of 2.629 in sample A2-B1 was measured in the test, suggesting the presence of organic alluvial mud which was confirmed based on the brown color of the sample (i.e., visual inspection). This sample was not considered in the subsequent tests.

Shape parameters obtained from the gradation analyses are summarized in Table 4-2. Gradation results on the coarse-grained fraction indicate a predominant presence of fine sands (< 425 μm). A uniform grain size distribution in the coarse and fine fractions was also observed in the gradation tests. Note that sample A1-B3 has a larger fine-grained fraction than the other samples. Coefficients of uniformity and curvature were computed based on the gradation tests. Consistent values were measured among the samples.

Table 4-2: Parameters computed from gradation analysis

Location	Sample	Depth [ft]	D_{10}^a	D_{30}	D_{50}	D_{60}	C_u	C_c
SW	A1-B1	7.50	0.060	0.100	0.122	0.133	2.211	1.244
SW	A1-B2	12.50	0.070	0.097	0.119	0.128	1.837	1.046
SW	A1-B3	16.25	0.052	0.070 ^b	0.087	0.096	1.844	0.983
NE	A2-B2	12.50	0.071	0.114	0.138	0.153	2.145	1.191
NE	A2-B3	16.25	0.068	0.095	0.118	0.129	1.887	1.021

Note: SW: Southwest. NE: Northeast.

^aEstimated by extrapolating the sand fraction.

^bEstimated by extrapolating the sand fraction.

4.4.2 Void Ratio Tests

Minimum and maximum void ratios (i.e., e_{min} and e_{max} , respectively) were measured using different test methods, such as tamping, air pluviation, and water sedimentation. In tamping compaction (T) tests, the specimens were manually compacted in three layers with a stainless cylindrical tamper of 270 g in a rigid stainless ring. Tamper has a diameter of 1.25 in (3.175 mm) and a height of 1.725 in (4.380 mm). A variation of the proposed method by Lade et al. (1998) was used for the air pluviation (AP) test. To determine e_{min} , 50 g of sand were poured into a graduated 1,000 mL cylinder and tapped eight times with a small rubber hammer. This process was repeated until filling the cylinder with 600 g of sand (12 layers). Excessive force was not applied to avoid particle crushing. To determine e_{max} , a graduated sealed cylinder with 300 and 600 g of sand, was turned upside down very slowly (i.e., around 60 s to rotate 180°) allowing the particles to gently settle. In

water sedimentation (WS) tests, 150 g of sand were placed into a graduated cylinder with water by keeping the funnel outlet as close as possible to the water level. Each test method was repeated at least three times per sample. Table 4-3 summarizes the results of e_{min} and e_{max} of each sample and test. Assumed values were chosen based on the maximum and minimum results among all the samples since similar results were obtained. Recall the large fines content in the A1-B3 sample; thus, different void ratios were assumed for this soil sample. Figure 4-4 shows the fine contents effects on void ratios. According to Cubrinovski and Ishihara (2002), when fine content in a soil is larger than 30%, the void ratio significantly increases.

Table 4-3: Results of minimum and maximum void ratio for topmost granular soils

Location	Sample	Depth [ft]	Tamping	Dry Pluviation		Water Sedimentation		Assumed		Range
			e_{min}	e_{min}	e_{max}	e_{max}	e_{max}	e_{min}	e_{max}	
SW	A1-B1	7.50	0.757	0.766	1.283	1.333	1.340	0.72	1.42	0.70
SW	A1-B2	12.50	0.726	0.750	1.252	1.306	1.312	0.72	1.42	0.70
SW	A1-B3	16.25	0.837	0.849	1.463	1.487	1.726	0.83	1.73	0.90
NE	A2-B2	12.50	0.724	0.750	1.278	1.320	1.392	0.72	1.42	0.70
NE	A2-B3	16.25	0.744	0.761	1.318	1.343	1.419	0.72	1.42	0.70

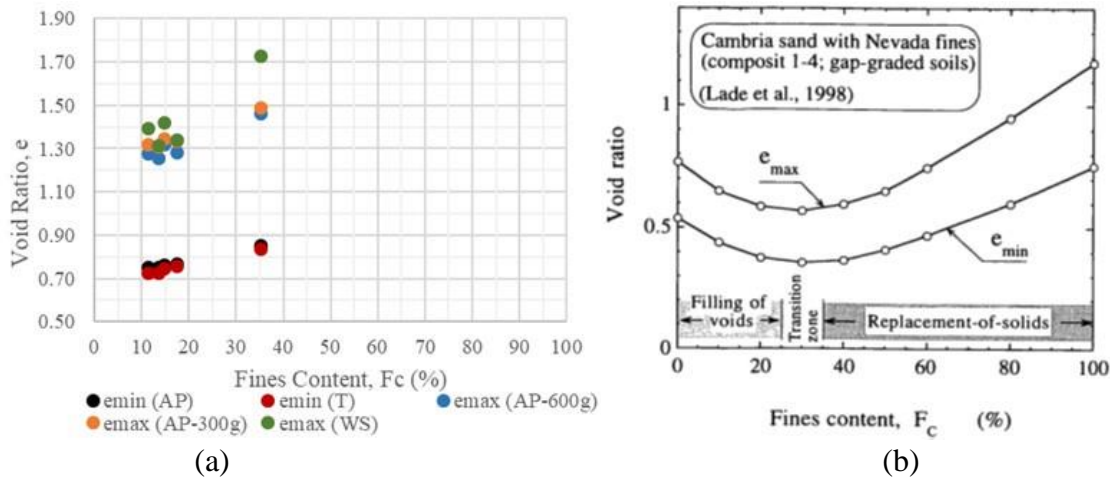


Figure 4-4. Fine content effect on the void ratios: (a) sand layer at UCF site and (b) Cubrinovski and Ishihara's work (2002)

4.4.3 Constant Rate of Strain Oedometer Test

To evaluate the compressibility properties for the surficial sandy layer, CRS oedometer tests were conducted. The tests were performed following the recommendations of the ASTM D4186 (2012). The specimens were prepared to fit the stainless-steel ring dimensions (i.e., height of 0.87 in - 22 mm- and diameter of 1.97 in -50 mm-). Dry pluviation method was used to place the specimens in the ring to reach different relative density (D_r) initial values. Table 4-4 summarizes the strain rate and index properties used in the CRS tests after specimen saturation. Saturation was accomplished by applying backpressure in a ramp to reach up to 6.3 ksf (300 kPa) and verified by

monitoring the excess porewater pressure increment rate (less than 15 s) once the chamber pressure was increased in 0.52 ksf (25 kPa). Note that this is not necessarily a Skempton B-value check. Saturation using CRS device can be maintained during the test due to the addition of a pore-pressure transducer at the base of the CRS cell. After saturation, loading and unloading stages were performed under strain-controlled conditions at constant rates of 1 and 10% per hr. Subsequently, a creep stage was performed before applying load reversal by keeping constant the effective stress in the sample.

Table 4-4: Index properties from CRS tests

Location	Sample	Specimen	Strain Rate [%/hr.]	Depth [ft]	e	D_r [%]	ρ_d [lb/ft ³]	γ_d [pcf]
SW	A1-B1	CRS-1-10P	10	7.50	0.893	75	87.27	87.28
SW	A1-B1	CRS-2-10P	10	7.50	0.803	88	91.58	91.61
SW	A1-B2	CRS-3-10P	10	12.50	0.951	67	85.03	85.05
SW	A1-B2	CRS-4-10P	10	12.50	1.035	55	81.53	81.55
SW	A1-B2	CRS-5-1P	1	12.50	1.003	60	82.84	82.88
SW	A1-B3	CRS-6-10P	10	16.25	1.078	72	79.78	79.83
NE	A2-B2	CRS-7-10P	10	12.50	0.854	81	89.40	89.44
NE	A2-B2	CRS-8-10P	10	12.50	1.238	26	74.04	74.10
NE	A2-B2	CRS-9-1P	1	12.50	0.955	66	84.78	84.79

Note: SW: Southwest. NE: Northeast.

Compressibility behavior curves in terms of axial strain and vertical effective stress are shown in Figure 4-5. Slight differences are observed in the results among most of the samples, where the obtained axial strains range between 11 and 15%. However, specimens CRS-6-10P and CRS-8-10P showed more compressible behavior, with approximate axial strains ranging from 19% to 22%, respectively. Note that specimen CRS-6-10P has a large fine content percentage (i.e., sample A1-B3) which increased compressibility according to Cubrinovski and Ishihara's (2002). Large compressibility of specimen CRS-8-10P is attributed to the small initial relative density.

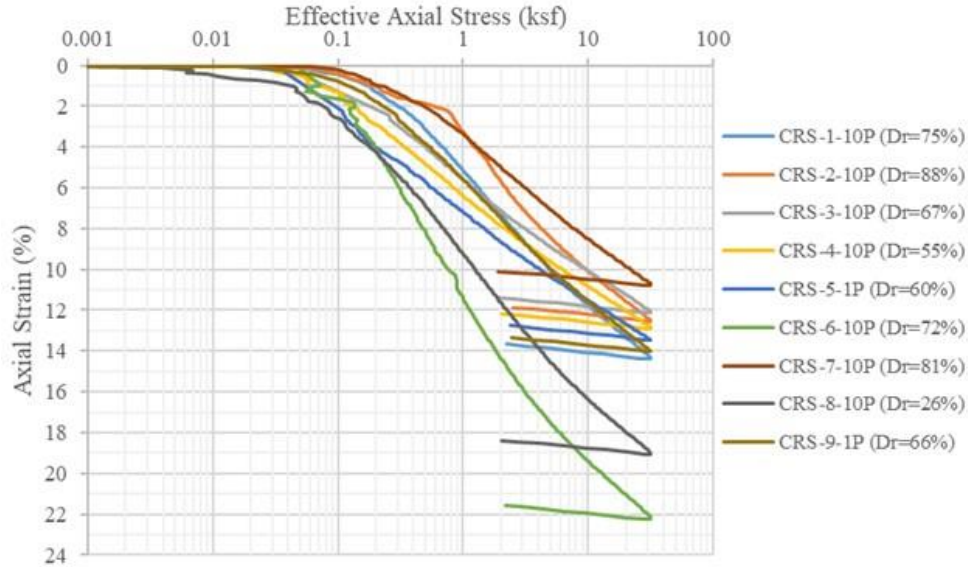


Figure 4-5. Axial stress-strain behavior response for Cypresshead formation soils

Load-deformation properties from CRS tests are shown in Table 4-5. To quantify the compressibility behavior of the samples, compression (C_c) and recompression (C_r) indices were computed. C_c values from 0.08 to 0.17 were calculated for the specimens used herein. Mesri and Vardhanabhuti (2009) presented typical C_c values for granular materials between 0.01 to 1.0. Usually, the larger the C_c values the larger the compressibility of the material. Recompression behavior among the specimens showed negligible differences based on C_r values.

Table 4-5: Load-deformation and compressibility properties

Location	Sample	Specimen	Strain Rate [%/hr.]	Depth [ft]	D_r [%]	C_c	C_r	C_r/C_c
SW	A1-B1	CRS-1-10P	10	7.50	75	0.119	0.012	0.10
SW	A1-B1	CRS-2-10P	10	7.50	88	0.115	0.012	0.10
SW	A1-B2	CRS-3-10P	10	12.50	67	0.088	0.012	0.14
SW	A1-B2	CRS-4-10P	10	12.50	55	0.093	0.013	0.14
SW	A1-B2	CRS-5-1P	1	12.50	60	0.088	0.013	0.15
SW	A1-B3	CRS-6-10P	10	16.25	72	0.177	0.013	0.07
NE	A2-B2	CRS-7-10P	10	12.50	81	0.090	0.011	0.12
NE	A2-B2	CRS-8-10P	10	12.50	26	0.157	0.013	0.08
NE	A2-B2	CRS-9-1P	1	12.50	66	0.114	0.012	0.11

The coefficient of volume compressibility in relation to the stress level during loading for each specimen is shown in Figure 4-6. This coefficient of volume compressibility showed a decreasing trend as the loading increases. At low effective axial stresses, samples usually tend to have large values of coefficient of volume compressibility since the strain levels are large. As the effective stress increases, and with a constant rate of strain, the coefficient tends to be small.

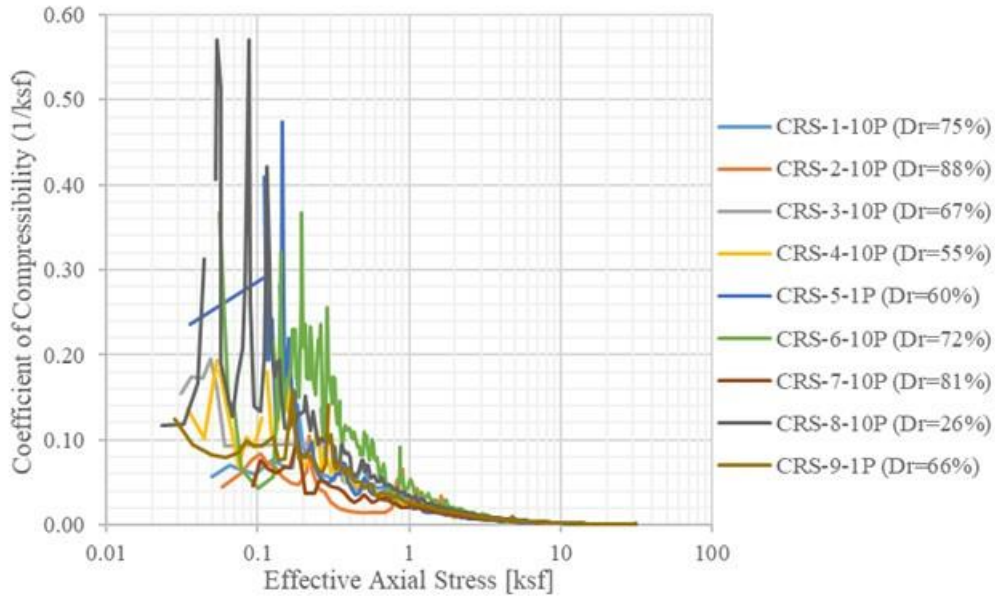


Figure 4-6. Coefficient of volume compressibility during CRS testing

Figure 4-7 presents the constrained modulus computed for the CRS tests. This modulus is typically computed by taking the reciprocal of the coefficient of volume compressibility. For CRS tests, this modulus generally increases during the loading stage. Note the overall upward trend of the computed modulus for all CRS tests. Maximum values from 1250 to 1650 ksf were computed at the end of the tests.

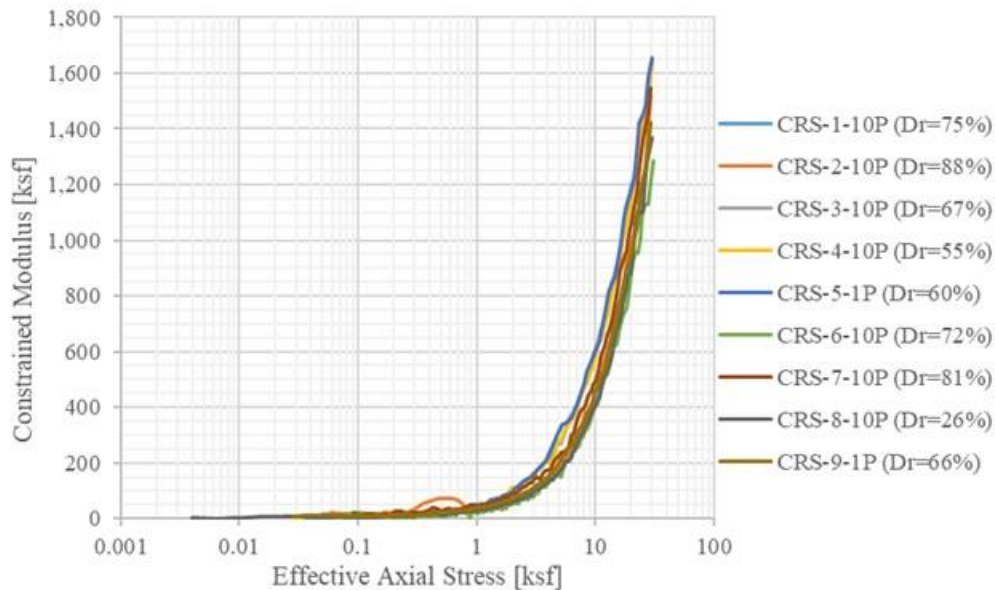


Figure 4-7. Constrained modulus during the CRS testing

4.4.4 Triaxial Testing Program

To evaluate stiffness and strength properties of the topmost sandy layer at the UCF site, triaxial (TX) tests were performed. Specimens of 5.5 in (140 mm) in height and 2.75 in (70 mm) in diameter were reconstituted in a split mold by dry deposition. D_r was achieved via tapping the mold on opposite sides with a small rubber hammer. Saturation was accomplished by replacing air in the voids with CO₂ during 30 min, passing volumes of de-aired water to fill the voids and applying backpressure in a ramp to reach up to 6.3 ksf (300 kPa). Skempton B-values over 0.98 were obtained for all specimens during saturation. Consolidation stages were performed under stress-controlled conditions at constant rate of 1 kPa/min. Despite the effort to target a specific D_r , test specimens changed in volume rapidly, always reaching D_r values larger than 60% before shearing. Specimens were loaded to different effective mean normal stresses (p') under K_0 conditions. A creep stage of 30 min was applied before shearing. All the specimens were sheared under strain-controlled conditions at constant rate of 10%/hr. in undrained conditions (CK_0 -UTXC in the table). Table 4-6 summarizes the test characteristics and index properties of the TX tests.

Figure 4-8, Figure 4-9, and Figure 4-10 present the stress paths, stress-strain behaviors, and porewater pressures, respectively, for the specimens tested herein. The TX test results clearly showed a dilative response among the samples despite the different target p' values. Note that all samples after failing, followed the same slope (i.e., failure line). From the tests, an effective friction angle of 33° was calculated from the stress path using $\phi' = \sin^{-1} [3M / (6+M)]$, where M is the slope of the failure line. A cohesion intercept was not found for these specimens. Note in the stress-strain response how the samples reached different peak deviator stress which is highly influenced by the cell pressure and target p' values. Negative porewater pressures in the soil samples confirms the dilative characteristics of the soils at the UCF site.

Table 4-6: Index properties for triaxial tests in granular soils

Loc.	Sample	Specimen	Depth [ft]	Type of test	Target p' [ksf]	Strain Rate [%/hr]	e	D_r [%]	ρ_d [lb/ft ³]	γ_d [pcf]
SW	A1-B2	TX-1	12.50	CK_0 -UTXC	5.22	10	0.962	65	84.53	84.54
SW	A1-B2	TX-2	12.50	CK_0 -UTXC	5.22	10	0.866	79	88.90	88.93
SW	A1-B2	TX-3	12.50	CK_0 -UTXC	10.45	10	0.788	90	92.77	92.81
SW	A2-B2	TX-4	12.50	CK_0 -UTXC	31.34	10	0.787	90	92.83	92.88

Note: CK_0 -UTXC: K_0 -Consolidation Undrained Triaxial Compression test.

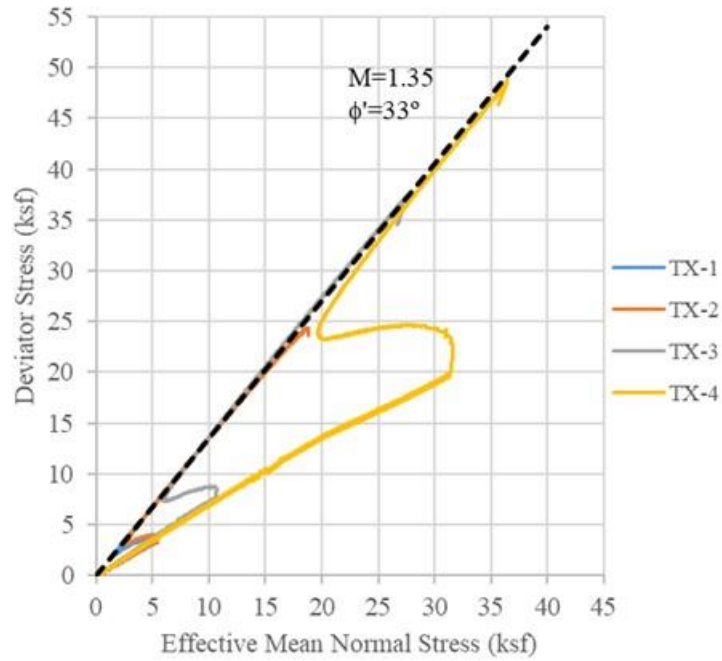


Figure 4-8. Compression stress paths during the TX tests

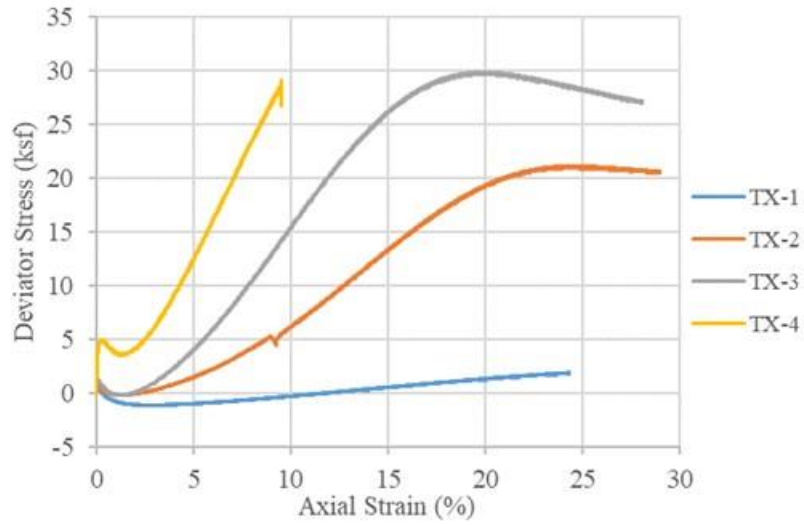


Figure 4-9. Stress-strain response during the TX tests

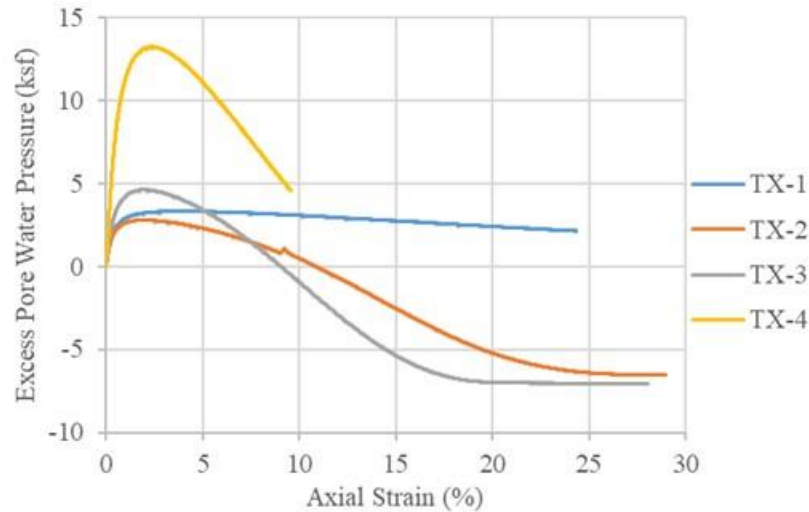


Figure 4-10. Excess porewater pressure response during the TX tests

4.4.5 X-Ray Diffraction Tests

To identify the internal composition of the soils tested herein, three samples were selected (i.e., one from the Cone 1 and two from the Cone 2 locations) to perform XRD tests. Table 4-7 summarizes the soil specimen locations and depths used for the XRD tests. Figure 4-11 shows the intensity of minerals in the soil at different phases. Readings between specimens showed a good correlation. The sample UCF_A1_B1_XRD1 was used to illustrate phase identification. Note the large intensity (i.e., large content) of quartz in all soil samples (i.e., sandy soils) between 20° and 30°. Kaolinite mineral was also found in the sample in small quantities. Recall that these sandy soil samples contain between 10 and 20% of fines (i.e., silt and clay). Minerals found in XRD tests coincide with minerals found in Florida cover materials (Upchurch et al. 2019) and the lithology described earlier in this chapter.

Table 4-7. Specimen characteristics for XRD tests

Location	Sample	Depth [ft]	XRD [test]
SW	A1-B1	7.50	1
SW	A1-B2	12.50	1
NE	A2-B2	12.50	1

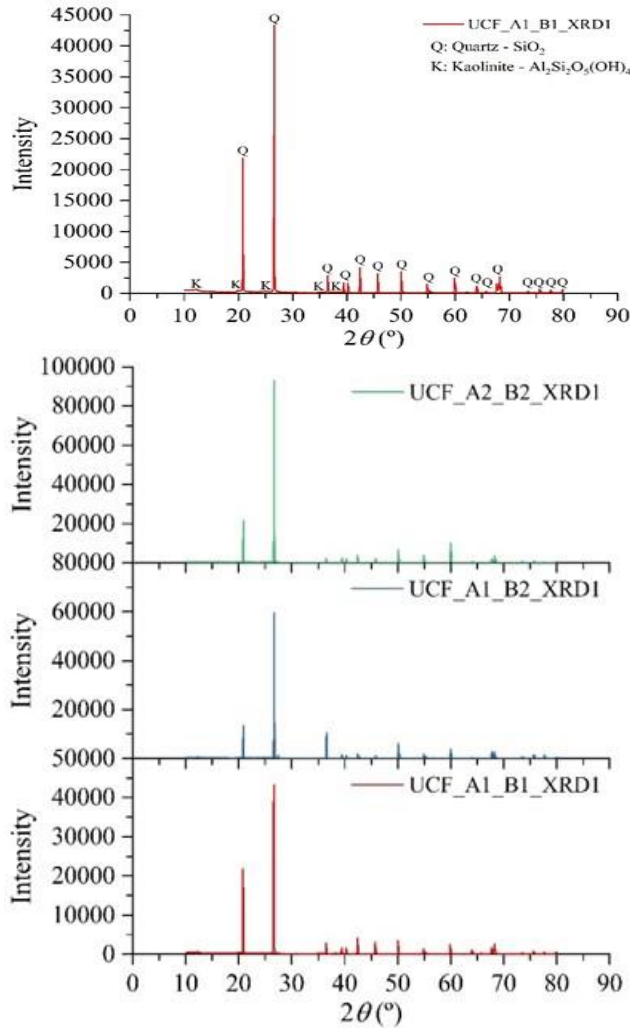


Figure 4-11. Phase angle intensity to identify mineral in XRD tests of soil samples at UCF site

4.4.6 Microscopy Tests

Visual inspection of the soil samples was conducted with microscopy tests. Figure 4-12 through Figure 4-16 present pictures from the microscopy tests of the sandy samples. Magnifications of 4x and 10x were used to detail shapes of the soil grains. Results showed particles of relatively plane sides with rounded to sharp edges, indicating angularity of the coarse-grained fraction from subangular to angular according to ASTM D2488 (2017). In general, the soil particles were found to be smaller than 475 μm , which indicates that samples are mostly fine sands. Particles smaller than 75 μm can be seen in the pictures in less quantities, which confirms the presence of silts and clays. These results from microscopy tests match the lithology description of the Cypresshead formation.

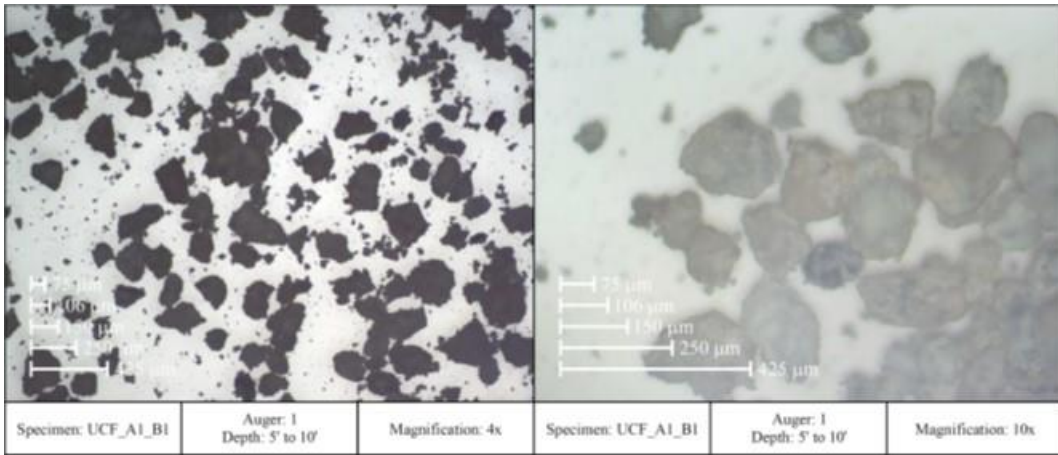


Figure 4-12. Microscopy test of the Sample A1-B1

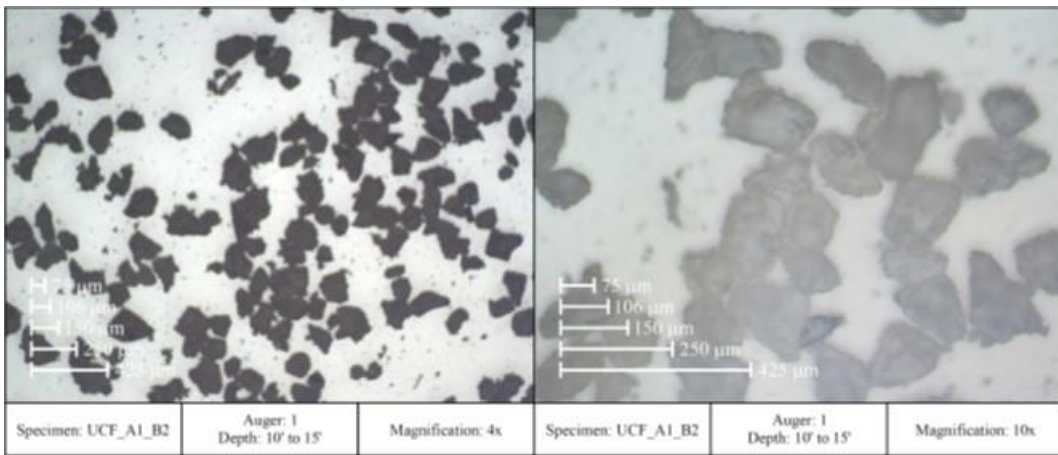


Figure 4-13. Microscopy test of the Sample A1-B2

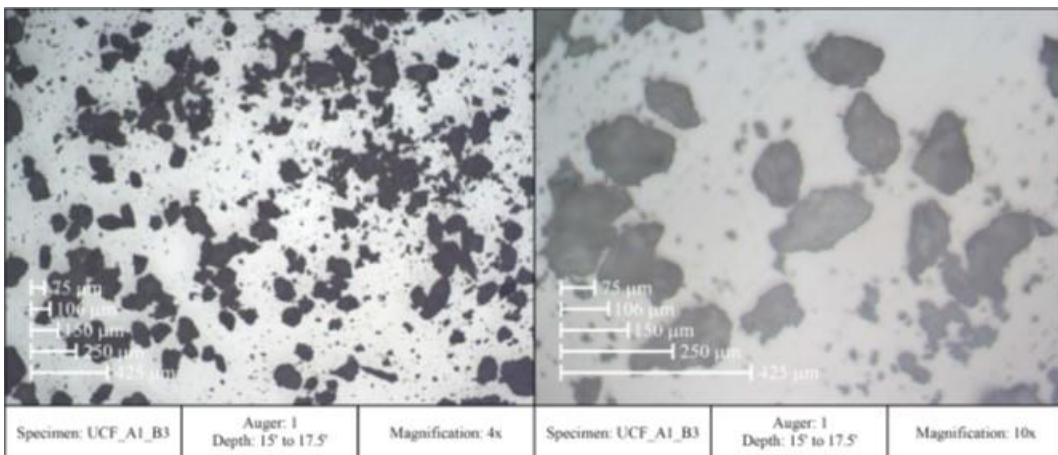


Figure 4-14. Microscopy test of the Sample A1-B3

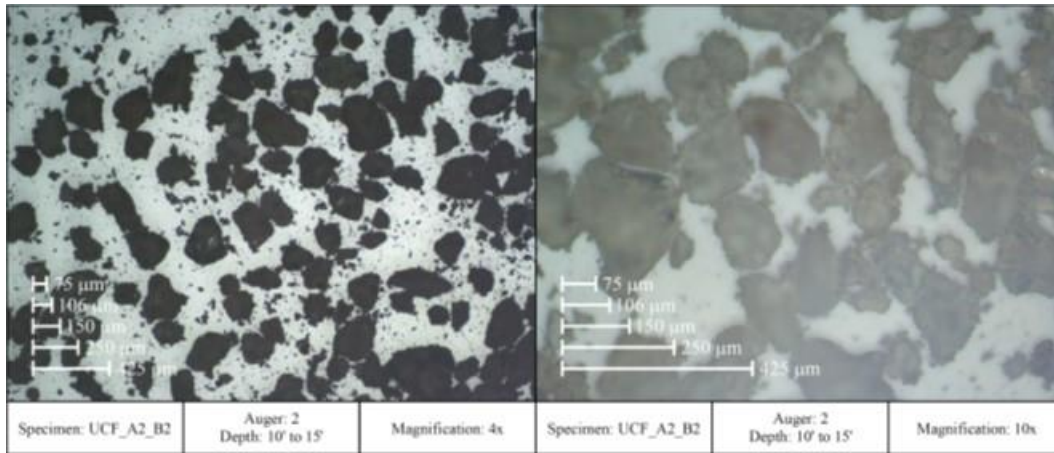


Figure 4-15. Microscopy test of the Sample A2-B2

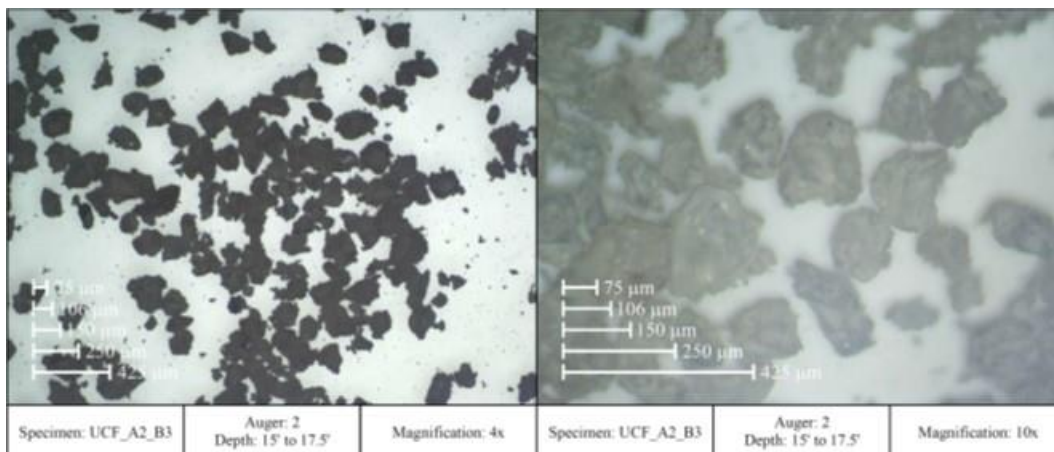


Figure 4-16. Microscopy test of the Sample A2-B3

4.4.7 Scanning Electron Microscopy Image Tests

Advanced visual examination and structure assessment of sample A2-B2, extracted at approximately 12.5 ft, were performed with SEM image tests. Figure 4-17 through Figure 4-23 show the SEM image tests where particle size, shapes, and internal structure were observed. Pictures with magnification between 50x and 250x were taken to the soil sample. Results show fine sand particles of relatively plane sides with rounded to sharp edges, indicating an angularity of the coarse-grained fraction from subangular to angular according to the ASTM D2488 (2017). Images with larger magnification, can show internal structure of the soil. Bonding between sandy particles can be noted from the figures. This bonding between particles is attributed to the presence of kaolinite, which was also found in the XRD tests. These results from SEM image tests match the lithology description of the Cypresshead formation.

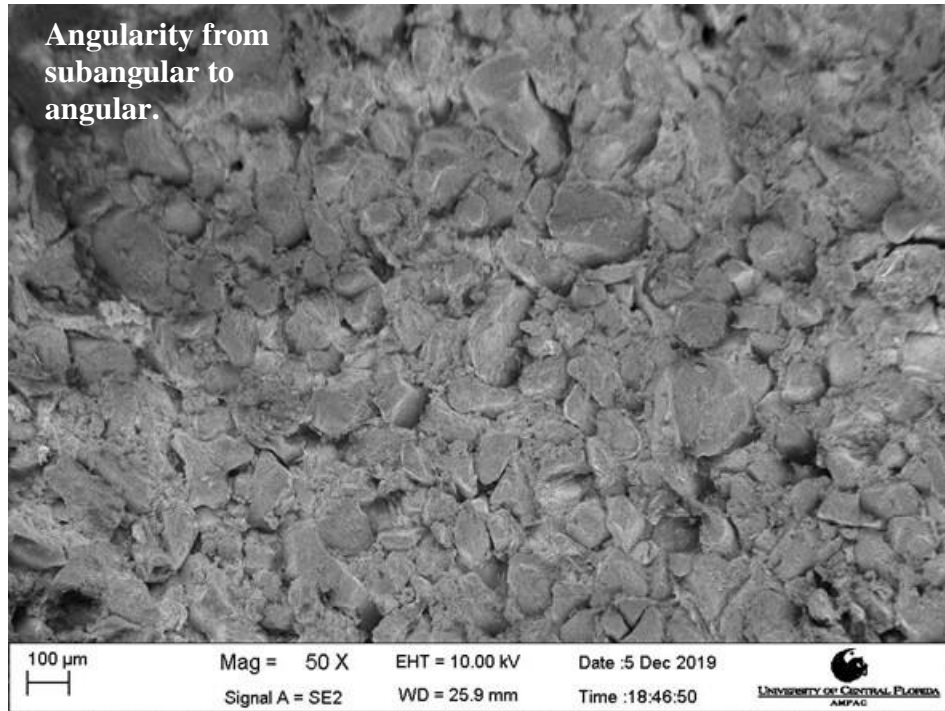


Figure 4-17. SEM image of sample A2-B2 at 50x

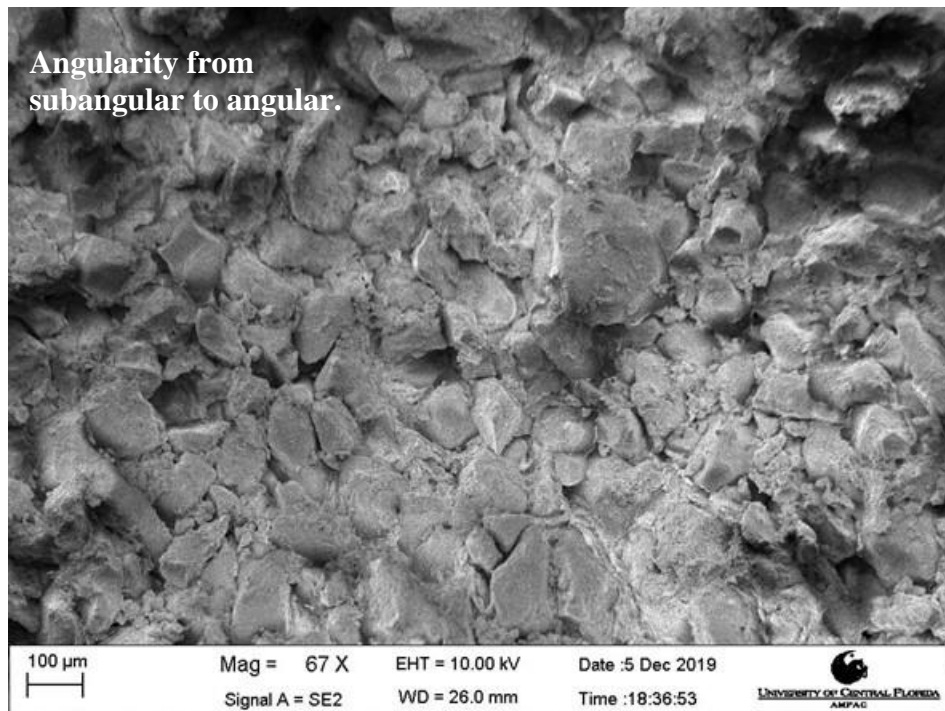


Figure 4-18. SEM image of sample A2-B2 at 67x

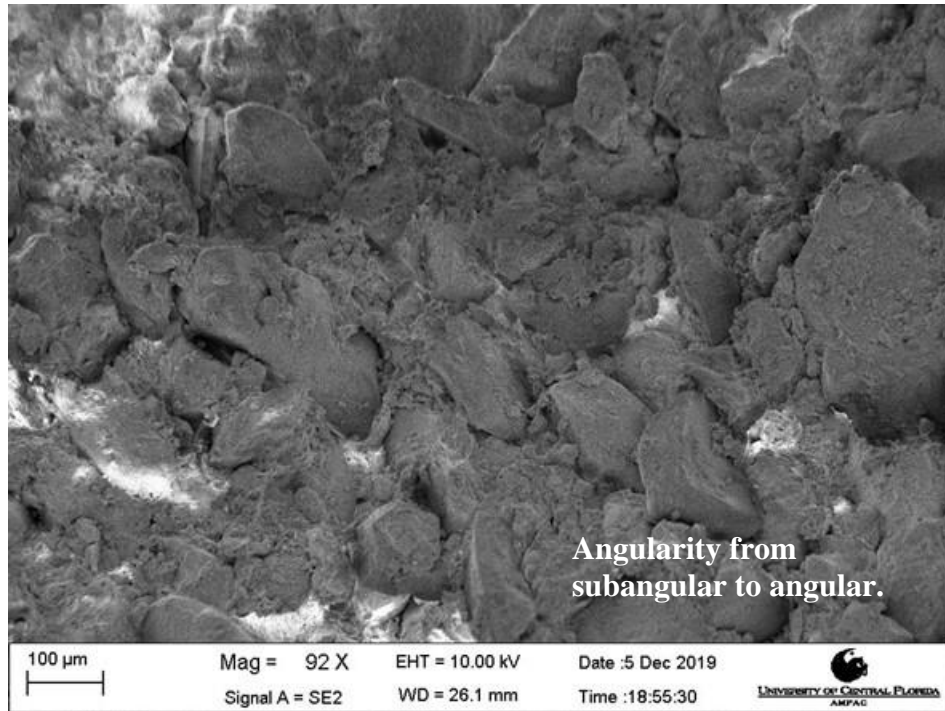


Figure 4-19. SEM image of sample A2-B2 at 92x

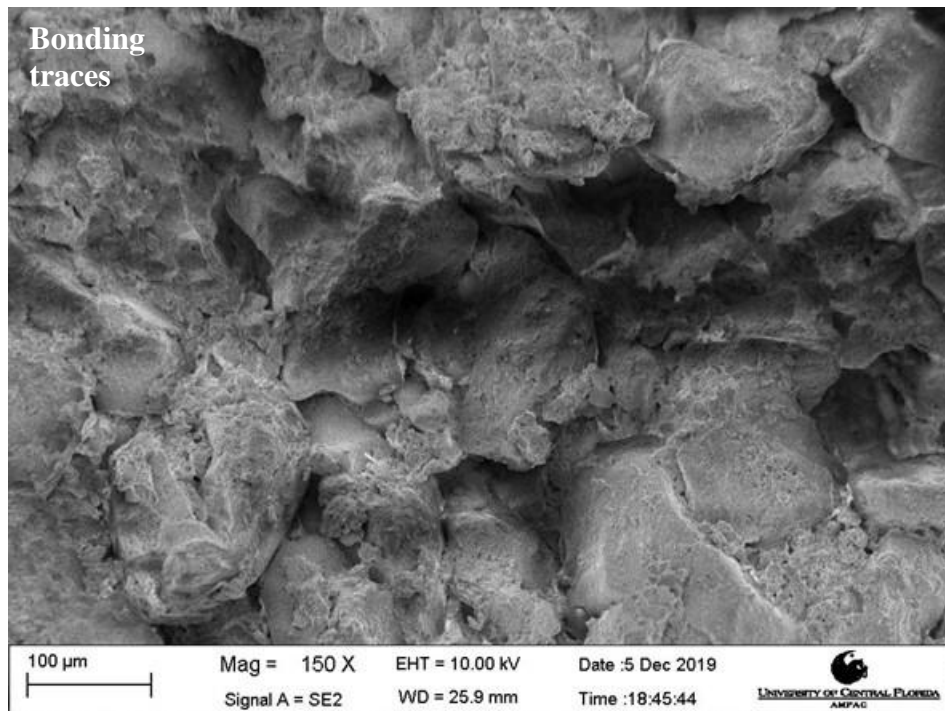


Figure 4-20. SEM image of sample A2-B2 at 150x

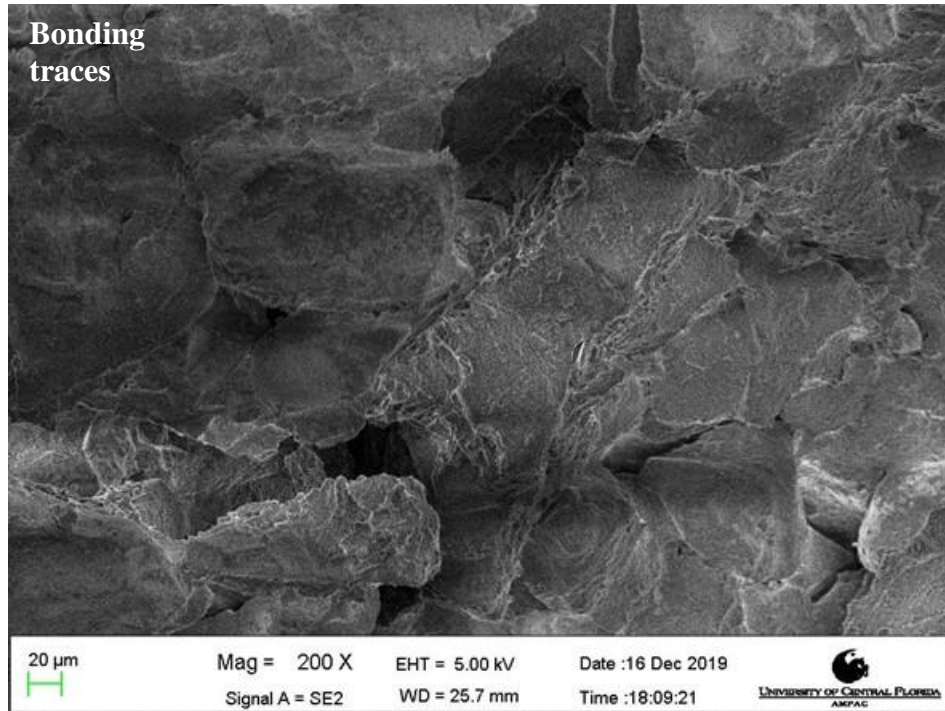


Figure 4-21. SEM image of sample A2-B2 at 200x

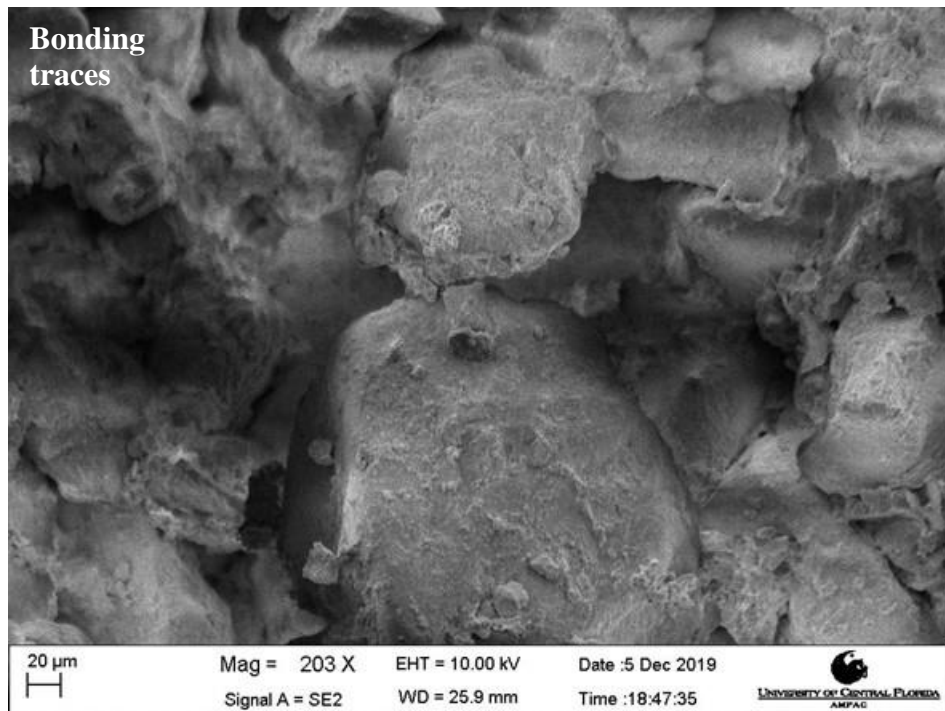


Figure 4-22. SEM image of sample A2-B2 at 203x

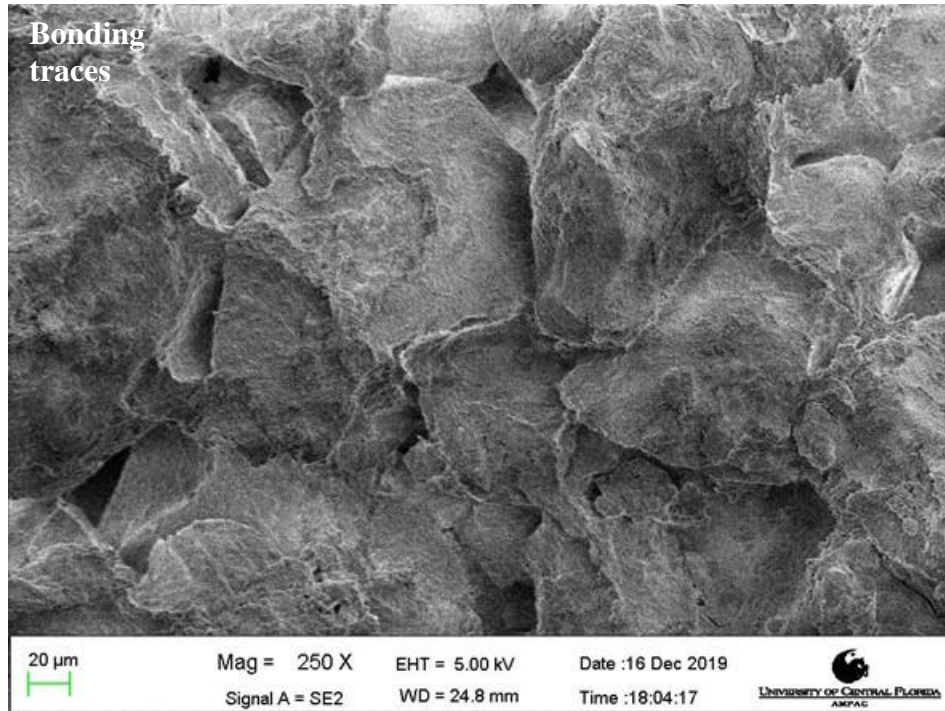


Figure 4-23. SEM image of sample A2-B2 at 250x

4.5 Laboratory Testing Program on Hawthorn Group Soils

The laboratory test results presented in this section are based on the samples retrieved from the UCF site, specifically from soil samples extracted from the Hawthorn Group with thin-walled Shelby tubes at the NE and SW sides of the UCF testing site. Laboratory tests performed for the Hawthorn Group used the same equipment and procedures followed for the Cypresshead formation soils.

4.5.1 Index Property Tests

Table 4-8 summarizes the index property tests performed for each soil sample retrieved with Shelby Tubes. Note that different results were obtained for the Hawthorn Group soils in relation to those of the Cypresshead formation, which is in agreement with the lithology of the group. Silty sands (i.e., SM) and low and high plasticity clays (i.e., CL and CH, respectively) were found using USCS based on consistency limits. Note that the presence of fine sand ($< 425 \mu\text{m}$) in soil samples influences the estimation of the consistency limits, since the tests were performed with material passing the Sieve No. 40 ($425 \mu\text{m}$). This also influenced the soil classification with USCS. Samples located at the SW side, were mainly high plasticity clays with large liquid limits. The soil located at the NE side is mainly classified as a silty sand. G_s values for all the samples were between 2.71 and 2.77. Note how the natural water content is between LL and PL, which may indicate that the clays are normally to lightly over-consolidated.

Table 4-8. Index property test results for deep Hawthorn group soils

Location	Shelby Tube	Depth [ft]	w_n^a [%]	Sand ^b [%]	Silt ^b [%]	Clay ^b [%]	G_s^c	LL^d [%]	PL^d [%]	Classification ^f
NE	B1-ST1	41.3	27	32.6	11.6	55.7	2.729	22 ^e	17 ^e	CL-ML
NE	B1-ST2	43.8	30	85.6	2.5	11.8	2.713	NP ^e	NP ^e	SM
NE	B1-ST3	46.3	29	80.7	3.3	15.9	2.730	19 ^e	17 ^e	SM
NE	B1-ST4	48.8	----	64.6	6.1	29.3	2.716	18 ^e	15 ^e	SM
NE	B2-ST5	41.3	30	93.6	1.7	4.6	2.708	NP ^e	NP ^e	SP-SM
NE	B2-ST6	43.8	29	63.1	9.8	27.1	2.733	22 ^e	17 ^e	SC-SM
SW	B3-ST7	41.3	69	16.3	50.6	33.2	2.767	83	35	CH
SW	B3-ST8	43.8	64	11.2	44.4	44.4	2.749	82	28	CH
SW	B3-ST9	46.3	52	16.7	50.3	33.0	2.741	42 ^e	20 ^e	CL
SW	B4-ST10	38.8	57	30.7	44.6	24.7	2.762	62	24	CH
SW	B4-ST11	50.3	65	15.5	54.4	30.1	2.765	85	30	CH

^aNatural water content performed by method A of the ASTM D2216 (2010).

^bGradation performed by method B of the ASTM D6913 (2017) and ASTM D7928 (2017).

^cSpecific gravity performed by method A of the ASTM D854 (2014).

^dConsistency limits performed by procedure 1, method A (LL) and procedure 1 (PL) of the ASTM D4318 (2017).

^eConsistency limits performed by procedure 2, method A (LL) and procedure 1 (PL) of the ASTM D4318 (2017).

^fClassification by the Unified Soil Classification System (ASTM D2487 2017).

4.5.2 Incremental Loading Consolidation Tests

One-dimensional consolidation tests using incremental loadings were performed in a conventional apparatus based on ASTM D2435 (2011) method B. Specimens of 0.79 in (20.0 mm) in height and 2.5 in (63.5 mm) in diameter were hand-trimmed and placed in a fixed stainless-steel ring. A load increment ratio of 1.0 was used to complete the IL tests. Table 4-9 summarizes index properties of the samples used for the IL tests.

Table 4-9: Index properties from IL consolidation tests on deep Hawthorn group soils

Location	Specimen	w [%]	e	S [%]	ρ_d [lb/ft ³]	γ_d [pcf]	ρ [lb/ft ³]	γ [pcf]
NE	B1-ST1-IL1	31.0	0.958	88.3	86.84	86.89	113.74	113.82
NE	B1-ST2-IL1	31.5	0.884	96.6	89.71	89.76	117.99	118.02
NE	B1-ST3-IL1	32.8	0.946	94.6	87.40	87.47	116.05	116.11
NE	B2-ST6-IL1	29.0	0.827	95.7	93.21	93.26	120.24	120.25
SW	B3-ST7-IL2	69.4	2.021	95.0	57.06	57.10	96.70	96.70
SW	B3-ST8-IL1	89.8	2.528	97.6	48.57	48.57	92.14	92.18
SW	B3-ST9-IL1	42.2	1.284	90.1	74.79	74.80	106.31	106.37
SW	B4-ST10-IL1	55.3	1.611	94.8	65.92	65.95	102.38	102.36
SW	B4-ST10-IL2	57.9	1.730	92.4	63.05	63.09	99.57	99.56

The compressibility behavior in terms of axial stress-strain relationships for the soil samples is shown in Figure 4-24. The figure presents vertical strains instead of void ratios since the results can be compared directly regardless of the initial D_r . Maximum axial strains between 10% and 15% were measured for the sandy-type soils; however, clayey-type soils showed larger axial strains (i.e., between 20% and 40%) for the same stress levels.

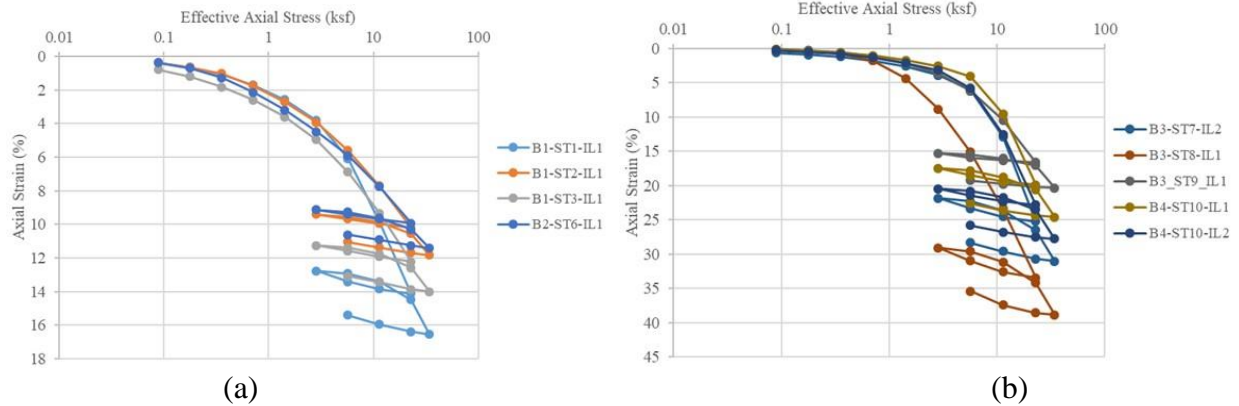


Figure 4-24. Axial stress-strain behavior of the Hawthorn group soils: (a) consolidation curves of NE Specimens and (b) consolidation curves of SW specimens

Load-deformation properties, including preconsolidation pressures and specimen quality designations, are shown in Table 4-10. C_c values from 0.13 to 0.26 were computed for the sandy-type soil specimens. For clayey-type soils, C_c values from 0.47 to 1.16 were computed. According to Kulhawy and Mayne (1990), clays with a high degree of compressibility have C_c values larger than 0.4. Preconsolidation pressures (σ'_p) were estimated using the strain energy method (i.e., also known as Work Method) proposed by Becker et al. (1987). This method is based on the cumulative strain energy during the test. σ'_p values between 4.4 and 6.1 ksf were computed, showing a lightly over-consolidated material when compared to the in situ effective stress in terms of overconsolidation ratio (OCR). The specimen quality based on the criteria by Andresen and Kolstad (1979) and Lunne et al. (2006) was estimated for each sample, finding fair to poor and good to poor quality for each method, respectively. These are typical sample quality designations for samples extracted from Shelby tubes as opposed to high-quality block sample methods.

Table 4-10: Load-deformation properties, preconsolidation pressure, and specimen quality designations for specimens tested in IL tests on deep Hawthorn group soils

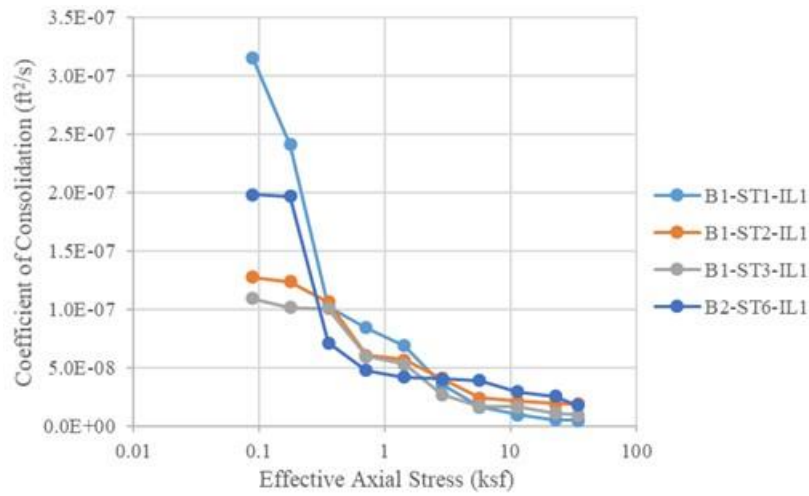
Location	Specimen	C_c	C_r	σ'_{v0} [ksf]	σ'_p [ksf]	OCR	Andresen & Kolstad (1979)	Lunne et al. (2006)
NE	B1-ST1-IL1	0.265	0.029	2.30	4.60	2.0	C	2
NE	B1-ST2-IL1	0.162	0.018	2.40	4.80	2.0	C	3
NE	B1-ST3-IL1	0.190	0.023	2.51	4.80	1.9	D	3
NE	B2-ST6-IL1	0.139	0.018	2.40	5.43	2.3	D	3
SW	B3-ST7-IL2	1.160	0.110	2.30	6.06	2.6	C	3
SW	B3-ST8-IL1	1.148	0.165	2.40	4.39	1.8	D	3
SW	B3-ST9-IL1	0.473	0.033	2.51	5.64	2.3	C	3
SW	B4-ST10-IL1	0.831	0.070	2.19	6.06	2.8	C	2
SW	B4-ST10-IL2	0.875	0.069	2.19	5.43	2.5	C	2

Note: NE: Northeast. SW: Southwest.

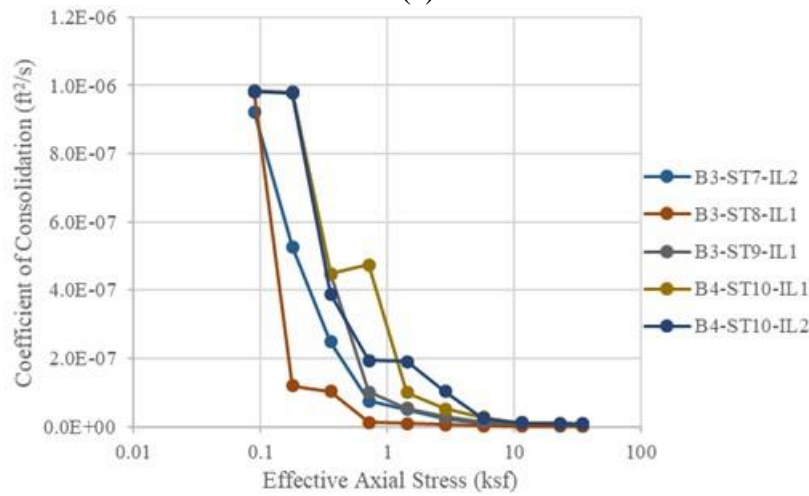
Andresen & Kolstad (1979): A: very good to excellent, B: good, C: Fair, D: Poor, E: very poor.

Lunne et al. (2006): 1: very good to excellent, 2: good to fair, 3: poor, 4: very poor.

Figure 4-25 through Figure 4-28 show the compressibility behavior of the specimens under IL tests. The coefficient of consolidation (c_v) showed very small values when large stresses are applied to the specimens. The coefficient of volume compressibility showed a decreasing trend as the loading increases. At low effective axial stresses, samples usually tend to have large values of coefficient of volume compressibility since the strain levels are significantly large for the applied loading. Note how the computed constrained modulus for the sandy-type soils is significantly larger than those computed for the clayey-type soil (i.e., values up to 350 ksf and 1,000 ksf for the clays and sands, respectively) located at SW corner of the UCF site. Hydraulic conductivity (k) computed from the IL tests, showed results approximately between 1×10^{-8} and 1×10^{-7} ft/s.

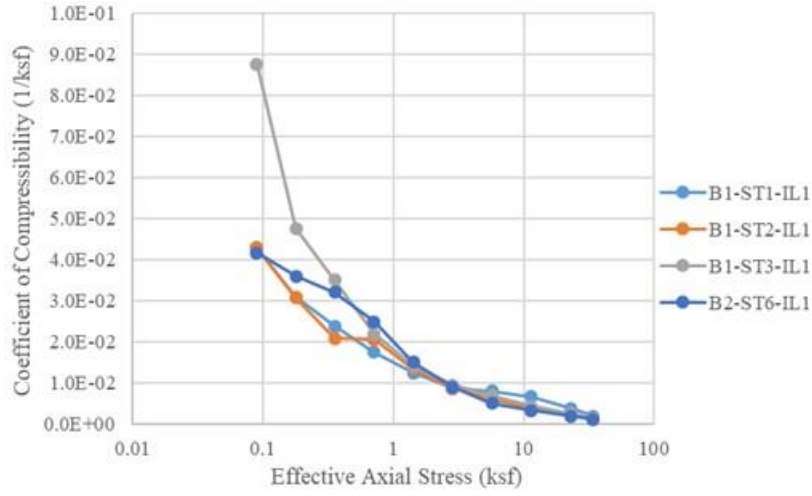


(a)

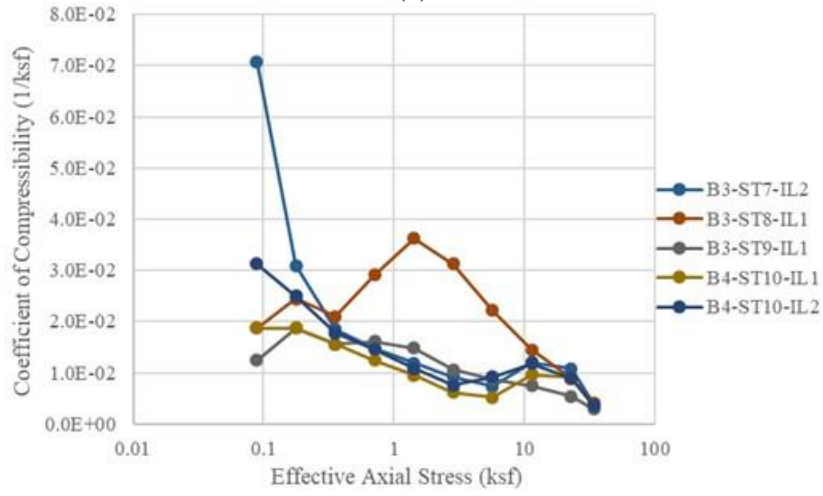


(b)

Figure 4-25. Coefficient of consolidation during the IL test: (a) coefficient of consolidation of NE specimens and (b) coefficient of consolidation of SW specimens

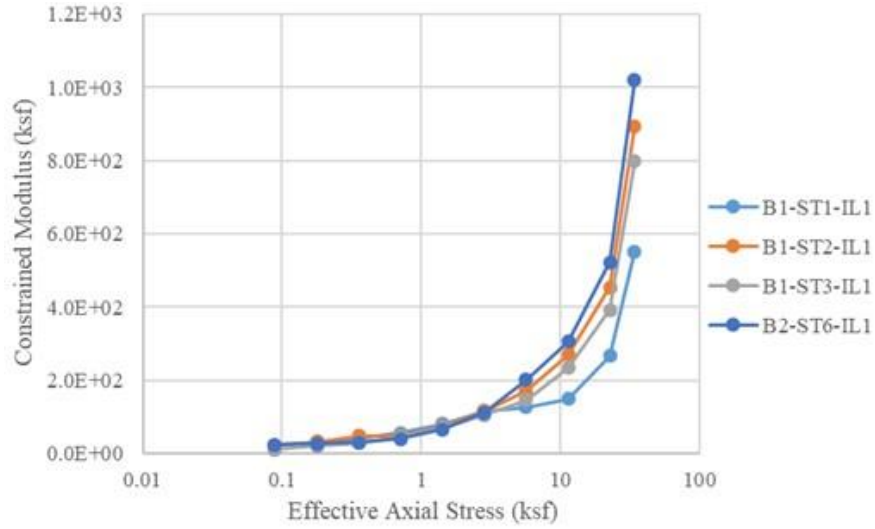


(a)

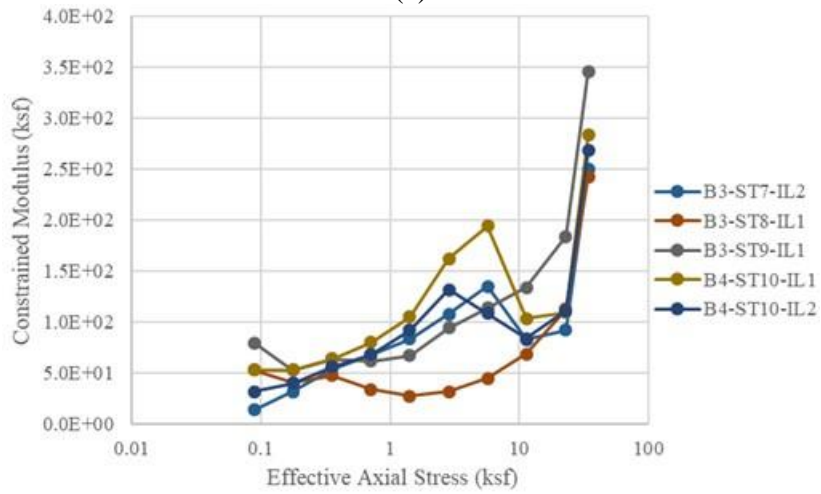


(b)

Figure 4-26. Coefficient of volume compressibility during the IL test: (a) coefficient of compressibility of NE specimens and (b) coefficient of compressibility of SW specimens.

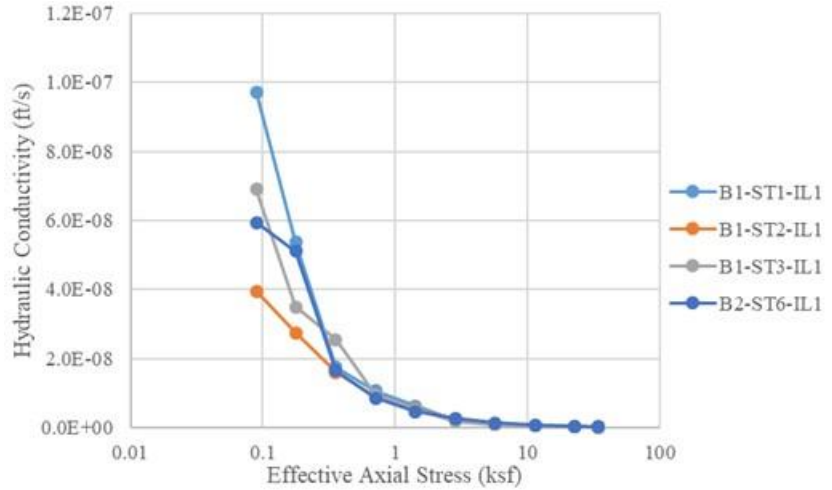


(a)

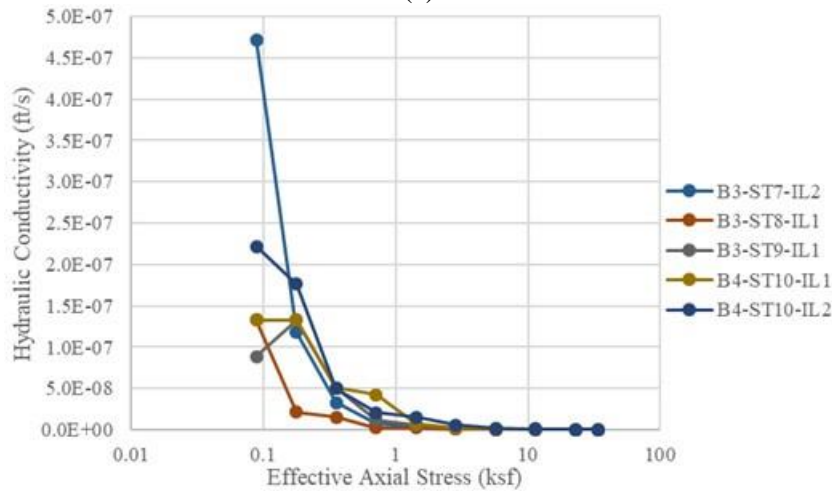


(b)

Figure 4-27. Constrained modulus during the IL test: (a) constrained modulus of NE specimens and (b) constrained modulus of SW specimens



(a)



(b)

Figure 4-28. Hydraulic conductivity during the IL test: (a) hydraulic conductivity of NE specimens and (b) hydraulic conductivity of SW specimens

4.5.3 Constant Rate of Strain Consolidation Test

CRS consolidation tests were conducted to specimens retrieved from the Hawthorn Group. Table 4-11 summarizes the strain rate and index properties used in the CRS tests after specimen saturation. Saturation was performed by applying backpressure in a ramp to reach up to 4.2 ksf (200 kPa) and verified by measuring the excess porewater pressure increment rate (i.e., less than 15 s) once the chamber pressure was increased to 0.52 ksf (25 kPa). After saturation, loading and unloading stages were performed under strain-controlled conditions at constant rates of 1, 5, and 10%/hr. A creep stage was performed before applying load reversal.

Table 4-11. Index properties from CRS consolidation tests on deep Hawthorn group soils

Location	Specimen	w [%]	e	S [%]	ρ_d [lb/ft ³]	γ_d [pcf]	ρ [lb/ft ³]	γ [pcf]
NE	B1-ST1-CRS1-5P	39.6	1.128	95.8	79.91	79.96	111.56	111.59
NE	B1-ST1-CRS2-1P	51.2	1.467	95.2	68.92	68.94	104.25	104.27
NE	B1-ST1-CRS3-1P	29.4	0.933	86.1	87.96	87.98	113.87	113.89
NE	B1-ST3-CRS1-1P	31.6	0.917	93.9	88.71	88.74	116.74	116.75
NE	B1-ST3-CRS2-5P	32.8	0.960	93.2	86.84	86.83	115.24	115.29
NE	B1-ST3-CRS3-10P	31.7	0.927	93.2	88.27	88.30	116.24	116.24
SW	B3-ST7-CRS1-1P	86.9	2.524	95.3	48.94	48.95	91.46	91.48

Axial stress-strain behavior of samples tested in CRS conditions are shown in Figure 4-29. As the IL test results showed, smaller axial strains were measured for the sandy-type soil when compared to the clayey-type specimens. Figure 4-29a shows a maximum axial strain of 25% for the CL soil at the NE site. The CRS tests showed larger axial strains as the fine content increases in the sample. Recall that excess porewater pressures can be continuously measured during the test. Specimens reached an excess pressure ratio of approximately 3% at different times (including the clayey-type soil).

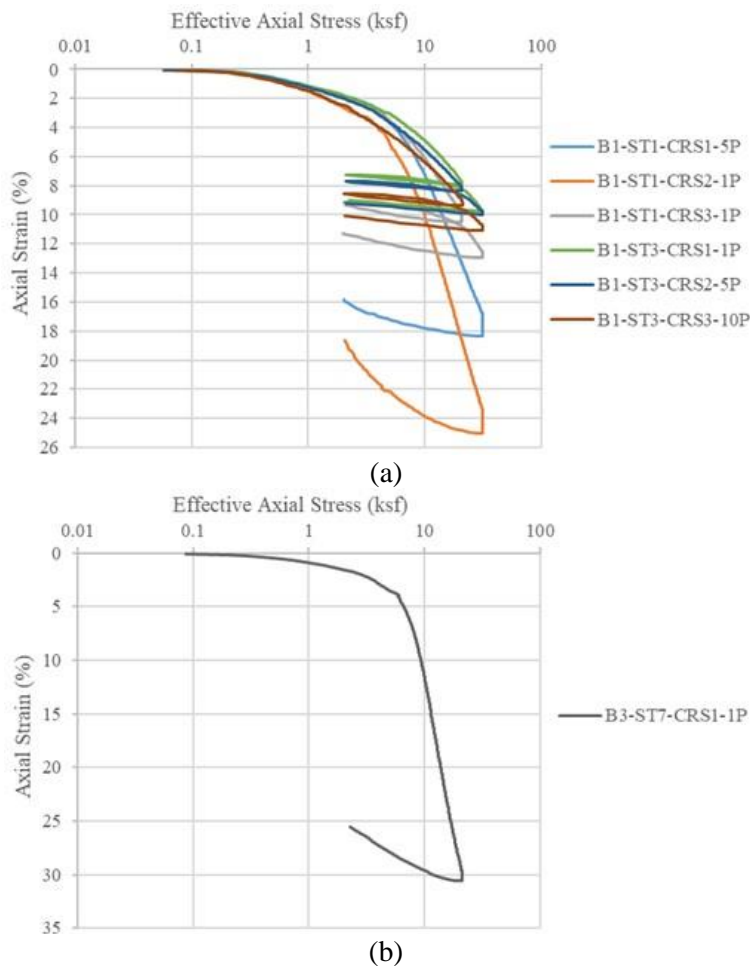


Figure 4-29. Axial stress-strain behavior response for Hawthorn group soils: (a) consolidation curves of NE specimens and (b) consolidation curves of SW specimens

Load-deformation properties, pre-consolidation pressures, and specimen quality designations are shown in Table 4-12. Note the consistent C_c values for the sandy-type soils, however, as the fine content is larger the C_c value increased. Note the large value for the B3-ST7-CRS1-1P specimen (i.e., CH soil specimen) of 1.716, indicating a high degree of compressibility according to Kulhawy and Mayne (1990). σ'_p values between 5.4 and 7.1 ksf were computed with the strain energy method. Based on the OCR, the Hawthorn Group is an over-consolidated deposit. The specimen quality based on the criteria by Andresen and Kolstad (1979) and Lunne et al. (2006) was good to fair, and very good to poor quality for each method respectively.

Table 4-12: Load-deformation properties, preconsolidation pressure and specimen quality

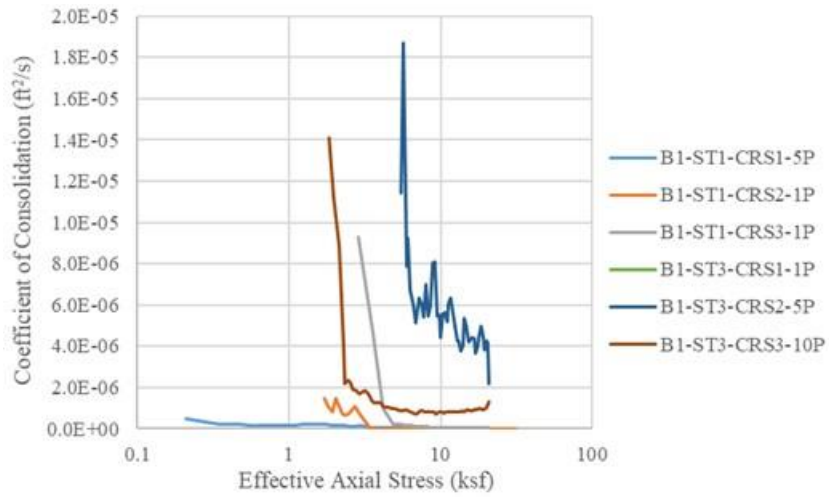
Location	Specimen	C_c	C_r	σ'_{v0} [ksf]	σ'_p [ksf]	OCR	Andresen & Kolstad (1979)	Lunne et al. (2006)
NE	B1-ST1-CRS1-5P	0.413	0.035	2.30	6.89	3.0	B	2
NE	B1-ST1-CRS2-1P	0.674	0.091	2.30	6.89	3.0	C	2
NE	B1-ST1-CRS3-1P	0.236	0.028	2.30	6.48	2.8	C	2
NE	B1-ST3-CRS1-1P	0.187	0.014	2.51	6.48	2.6	C	2
NE	B1-ST3-CRS2-5P	0.155	0.014	2.51	5.64	2.3	C	2
NE	B1-ST3-CRS3-10P	0.160	0.017	2.51	5.43	2.2	C	3
SW	B3-ST7-CRS1-1P	1.716	0.203	2.30	7.10	3.1	B	1

Note: NE: Northeast. SW: Southwest.

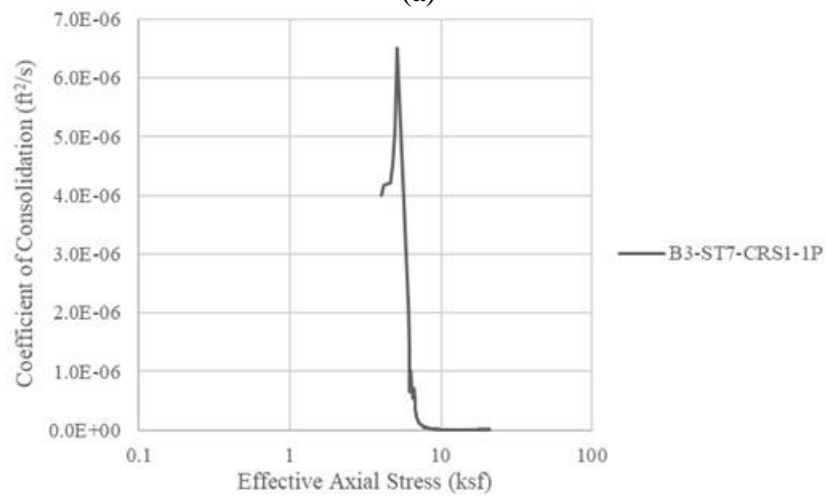
Andresen & Kolstad (1979): A: very good to excellent, B: good, C: Fair, D: Poor, E: very poor.

Lunne et al. (2006): 1: very good to excellent, 2: good to fair, 3: poor, 4: very poor.

Figure 4-30 through Figure 4-33 show the compressibility properties for soils in the Hawthorn Group. c_v values computed for the CRS test are larger than those obtained from the IL consolidation tests. This is attributed to the continuous application of strains in the CRS tests. Recall that c_v indicates the rate of consolidation of the soil. The coefficient of volume compressibility showed a decreasing trend as the loading increases. However, for the clay sample, the volume compressibility increased with larger axial stresses. This is attributed to the high degree of deformability that clays in this site have when large axial stresses are applied. The computed constrained modulus for the sandy-type soils are larger than those computed for the clayey-type soil (i.e., values up to 275 ksf and 350 ksf for the clays and sands, respectively). k values computed from the CRS tests were approximately 1×10^{-7} ft/s.

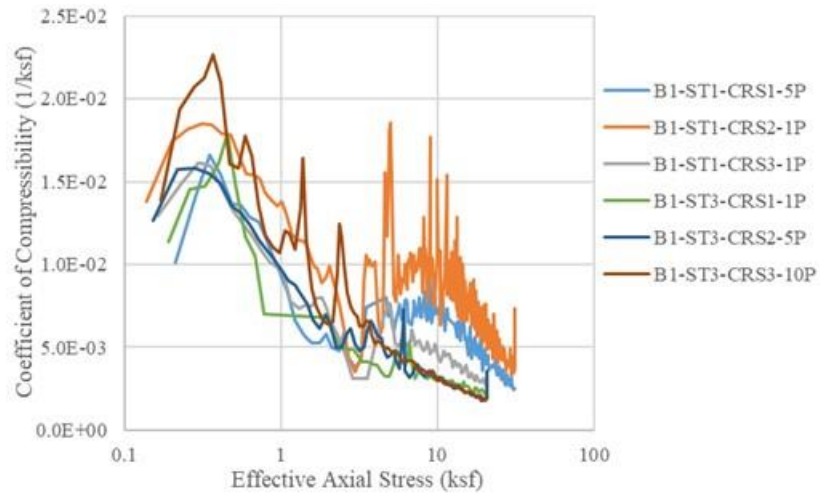


(a)

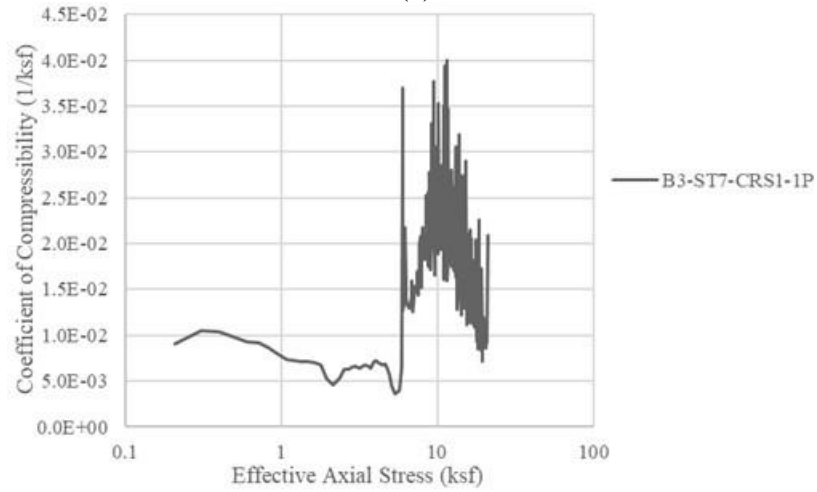


(b)

Figure 4-30. Coefficient of consolidation during the CRS test: (a) coefficient of consolidation of NE specimens and (b) coefficient of consolidation of SW specimens

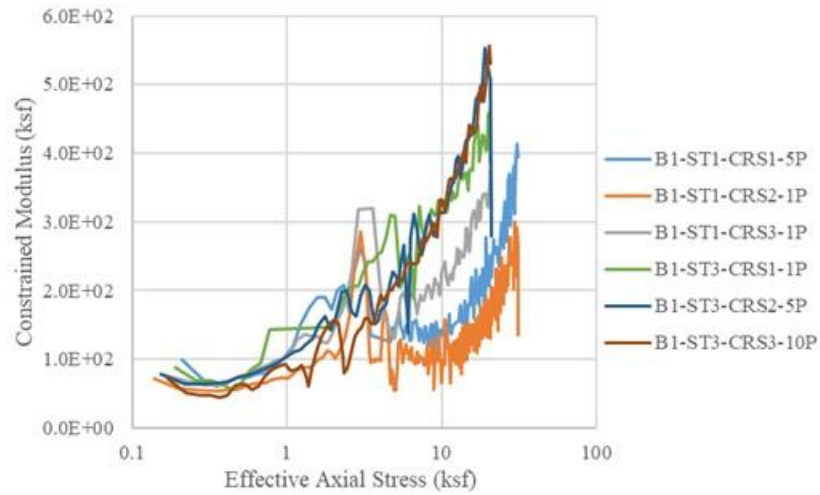


(a)

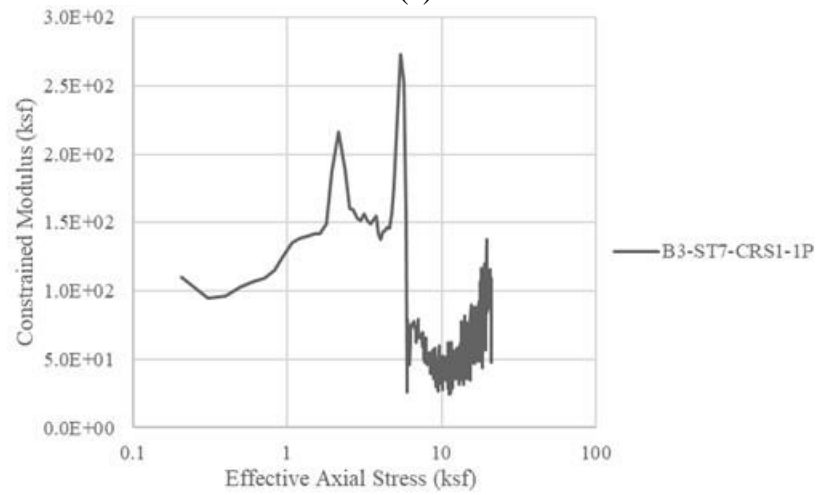


(b)

Figure 4-31. Coefficient of compressibility during the CRS test: (a) coefficient of compressibility of NE specimens and (b) coefficient of compressibility of SW specimens

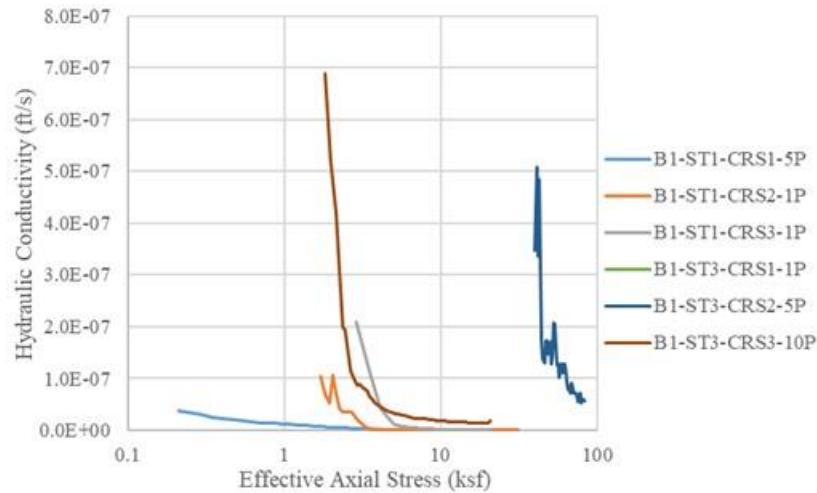


(a)

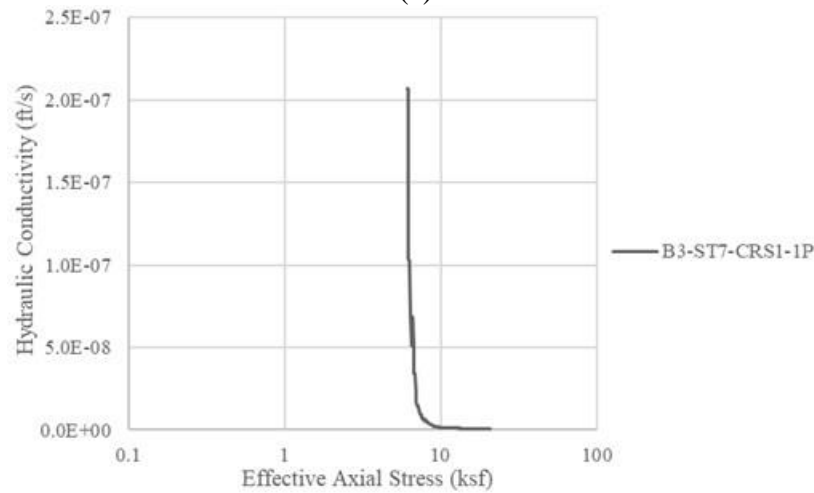


(b)

Figure 4-32. Constrained modulus during the CRS test: (a) constrained modulus of NE specimens and (b) constrained modulus of SW specimens



(a)



(b)

Figure 4-33. Hydraulic conductivity during the CRS test: (a) hydraulic conductivity of NE specimens and (b) hydraulic conductivity of SW specimens

4.5.4 Triaxial Testing Program

For the Hawthorn Group, triaxial tests with local instrumentation, bender elements, and Hall Effect transducers were conducted. Specimens of 5.9 in (150 mm) in height by 2.8 in (70 mm) in diameter were hand-trimmed and mounted in the triaxial cell. A pair of bender elements were installed in the top cap and base pedestal to measure shear wave velocities during the tests. A pair of axial and radial Hall Effect transducers were attached to the specimen to measure local displacements. Saturation was performed under a constant confinement stress equal to the residual effective stress, which was estimated by a porewater pressure measurement technique to reduce the disturbance caused by swelling (Ladd and Lambe 1964; Cho et al. 2007). Reconsolidation was conducted following three different stress paths, CK₀-UTXC, CA-UTXC and CIA-UTXC, with a constant load rate of 1.0 psf/min (0.05 kPa/min). After reconsolidation, a drained creep was performed under constant stress to avoid the influence of continued deformations at the end of reconsolidation when measuring stiffness response at very small strains (Clayton et al., 1992; Santagata et al.,

2005). Specimens were sheared in undrained conditions following triaxial compression paths. Strain controlled shearing was conducted with a strain rate of 0.2%/h until the axial strain was approximately 1%, then a strain rate of 0.5%/h was applied until the specimen reached failure. Table 4-13 summarizes test conditions and index properties from the TX tests.

Table 4-13: Index properties for triaxial tests on deep Hawthorn group soils

Loc.	Shelby Tube	Specimen	w [%]	e	S [%]	ρ_d [lb/ft ³]	γ_d [pcf]	ρ [lb/ft ³]	γ [pcf]
SW	B3-ST8	CK ₀ -UTXC	64.3	1.798	98.3	0.981	9.62	1.611	15.80
SW	B3-ST9	CA-UTXC	52.2	1.506	94.9	1.092	10.71	1.661	16.29
SW	B4-ST11	CIA-UTXC	58.2	1.688	95.3	1.027	10.07	1.624	15.93

Note: SW: Southwest. CK₀: K₀-consolidation. CA: Anisotropic consolidation. CIA: Isotropic and anisotropic consolidation. UTXC: Undrained triaxial compression.

Figure 4-34, Figure 4-35 and Figure 4-36 presents the stress paths, stress-strain behaviors and excess porewater pressures, respectively, for the specimens tested herein. The TX test results displayed contractive behavior. From the tests, an effective friction angle of 31° was calculated from the stress paths. Effective cohesion intercept of 0.17 ksf was found for these specimens. Excess porewater pressure up to 1.2 ksf was measured in the tests.

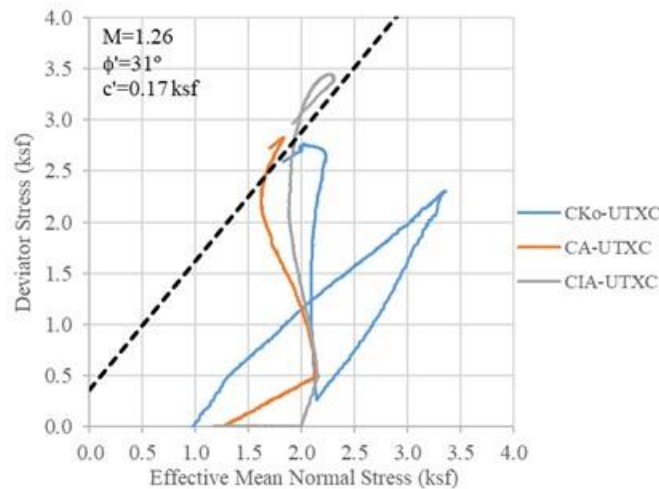


Figure 4-34. Triaxial stress paths followed during the triaxial tests

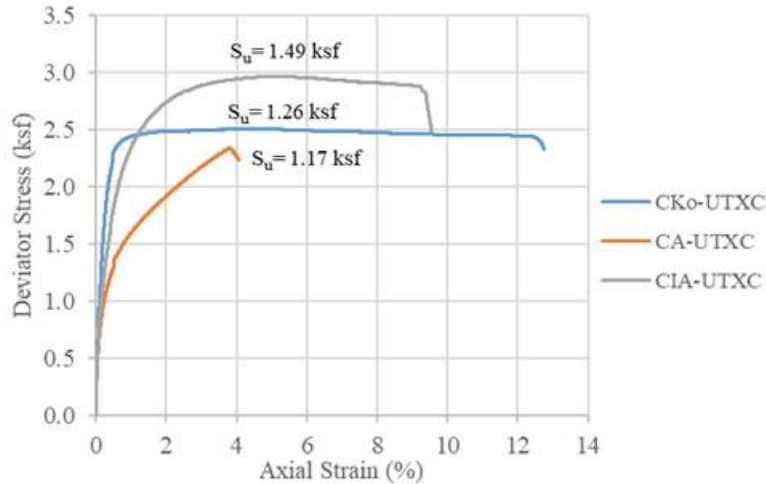


Figure 4-35. Stress-strain response during the triaxial tests

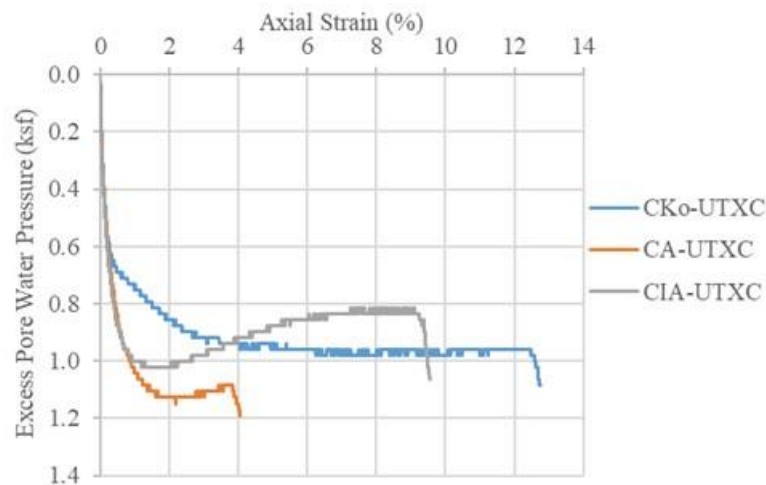


Figure 4-36. Excess porewater pressure response during the triaxial tests

Figure 4-37 shows the shear modulus degradation curves obtained from the bender element sensors during the triaxial loading stage. Figure 4-38 shows normalized shear modulus curves. Bender elements are used to estimate the variation of shear modulus during the triaxial loading based on the propagation of shear waves through the sample. Note the shear modulus degradation as the shear strain increases. For practical purposes, this is important to determine the adequate shear modulus depending on the shear strain level expected for the project.

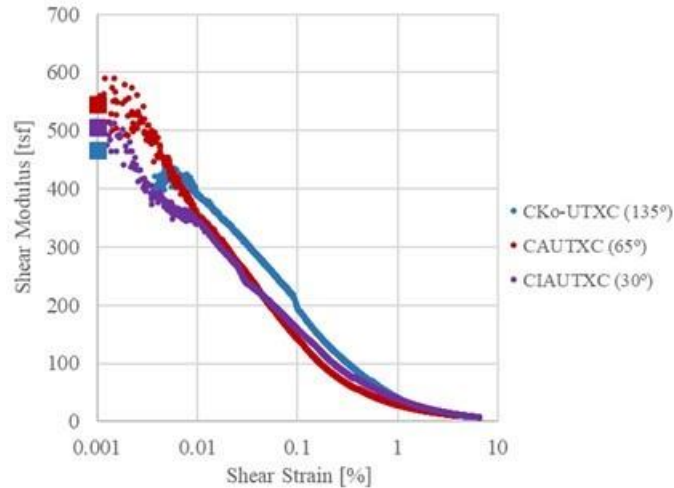


Figure 4-37. Shear modulus degradation curves during the triaxial tests

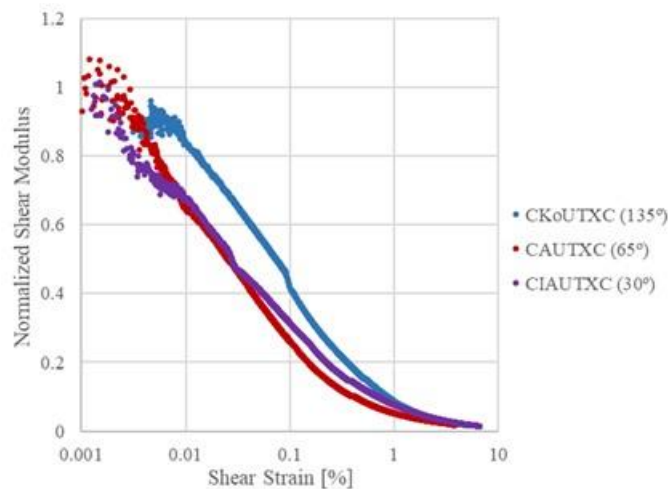


Figure 4-38. Normalized shear modulus degradation curves during the triaxial tests

4.5.5 X-Ray Diffraction Tests

To identify the internal composition of the soils tested, four soil samples retrieved with Shelby Tubes were selected to perform XRD tests (i.e., two from the NE and two from SW side of the UCF site). Table 4-14 shows the soil specimen locations and depths used for the XRD tests. Figure 4-39 and Figure 4-40 show the intensity of minerals in the soil at different phases. Differences in the response were observed depending on the sample location. The samples UCF_B1_ST2_XRD1 and UCF_B4_ST11 were used to illustrate phase identification from the NE and SW samples, respectively. A large variety of minerals, such as: quartz, calcite, aragonite, microcline, and kaolinite, were found in soils located at the SW corner of the UCF site. Minerals found in XRD tests coincide with minerals found in Florida cover materials (Upchurch et al. 2019) and lithology of the project site. The presence of carbonate minerals in SW specimens can explain the soil behavior observed in the consolidation tests reflected in higher void ratios than specimens at the NE side.

Table 4-14. Specimens characteristics for XRD tests

Location	Shelby Tube	Depth [ft]	XRD [test]
NE	B1-ST2	43.75	2
NE	B2-ST5	41.25	2
SW	B3-ST8	43.75	2
SW	B4-ST11	50.25	2

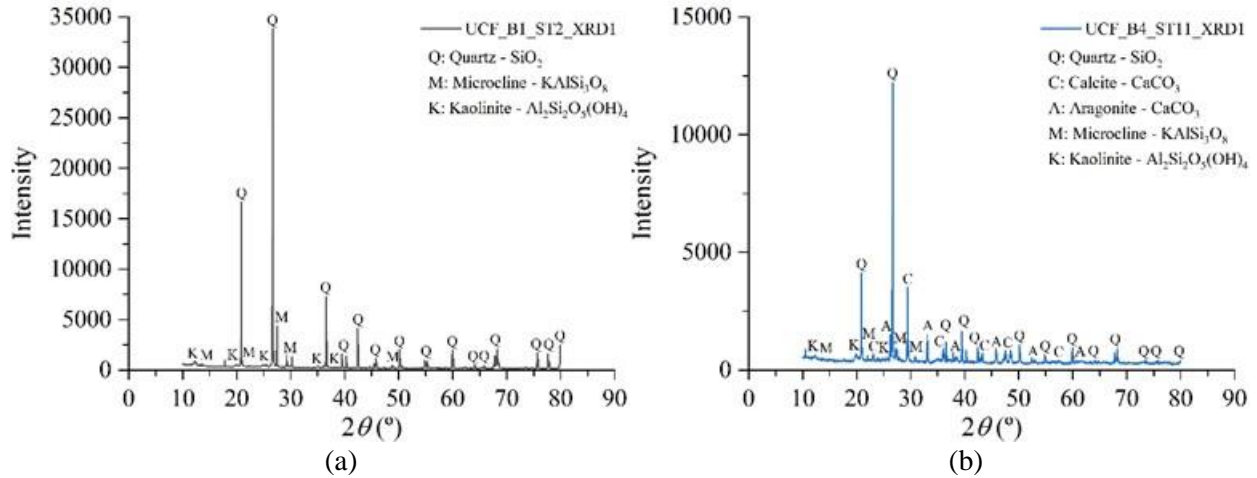


Figure 4-39. Phase angle intensity to identify minerals in XRD tests. (a) NE minerals and (b) SW minerals

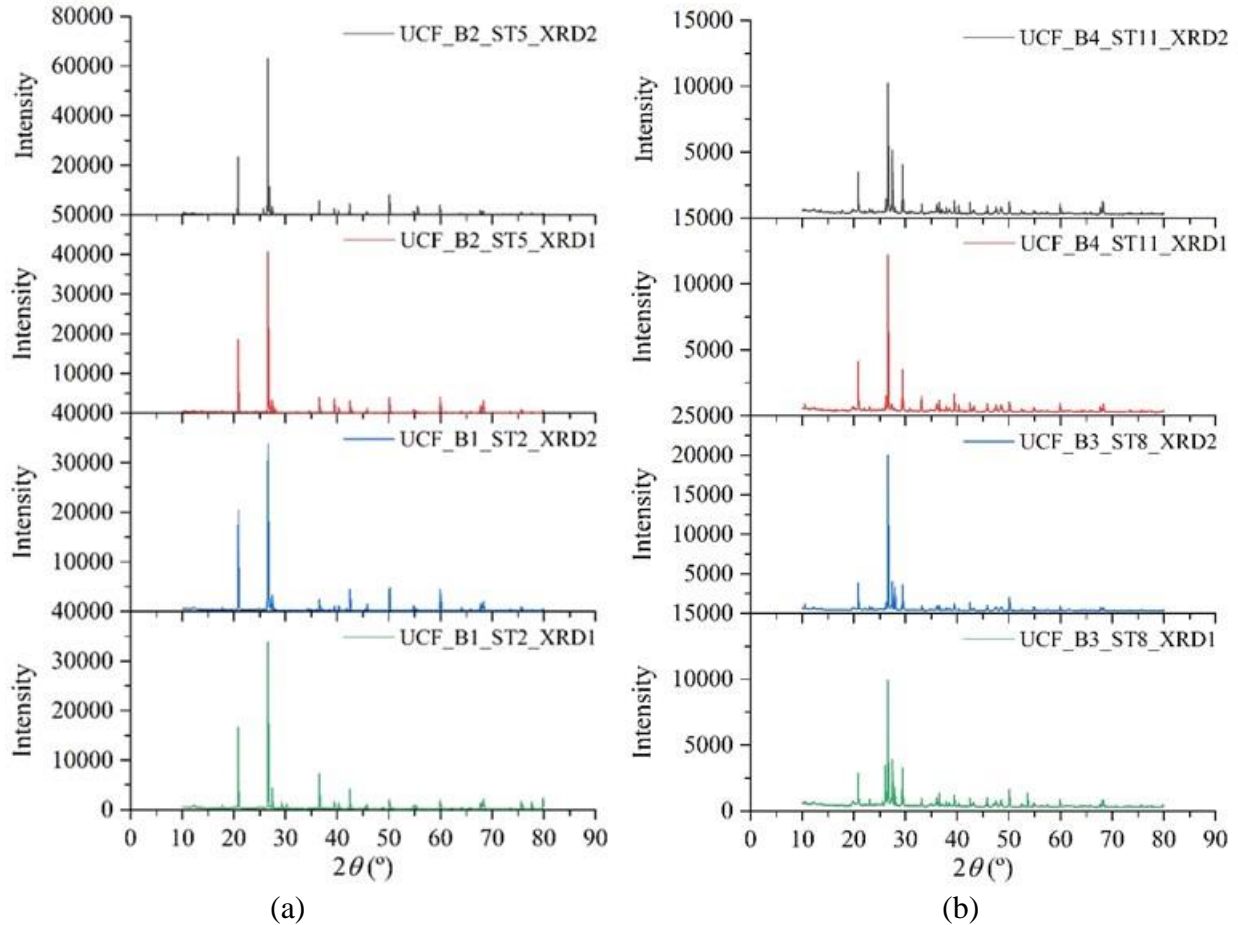


Figure 4-40. XRD phase identification: (a) NE XRD results and (b) SW XRD results

4.5.6 Scanning Electron Microscopy Images

Advanced visual examination and structure assessment of six soil samples retrieved with Shelby Tubes (i.e., three from the NE and three from SW of the testing site), were performed with SEM tests. Figure 4-41 and Figure 4-42 show the SEM image tests where particle sizes, shapes, and internal structure were observed. Images with magnification between 100x and 5,000x were taken to the soil samples. Results from NE specimens show a soil structure composed mainly of fine sand particles of relatively plane sides with rounded to sharp edges. The angularity of the coarse-grained fraction is classified as subangular to angular according to the ASTM D2488 (2017). These NE specimens (i.e., generally silty and clayey sands) are bonded by flat sheets (phyllosilicates) between particles with presence of kaolinite based on XRD results, and a minor porosity when compared to the SW specimens. Results from SW specimens show a soil structure composed mainly of flat sheets (phyllosilicates), with presence of kaolinite, calcite and aragonite based on XRD results and cementation between particles. Large porosity structures were noted in SW specimens with the SEM results. These results from SEM tests coincide with the lithology description of the Hawthorn Group.

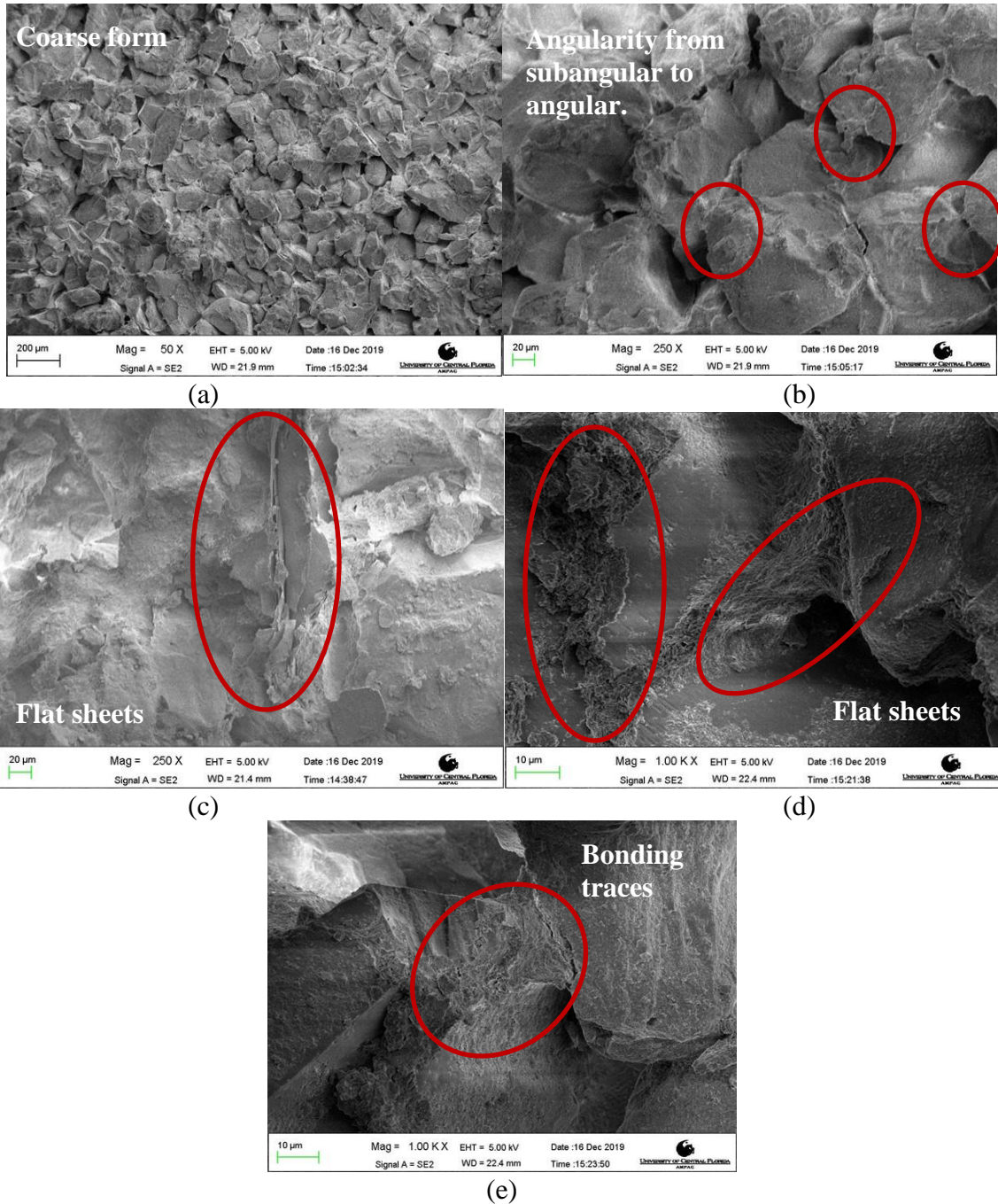
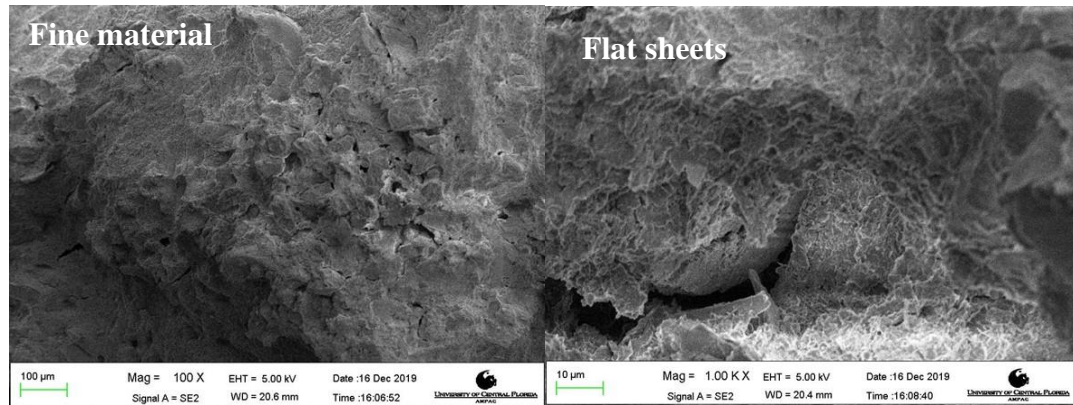
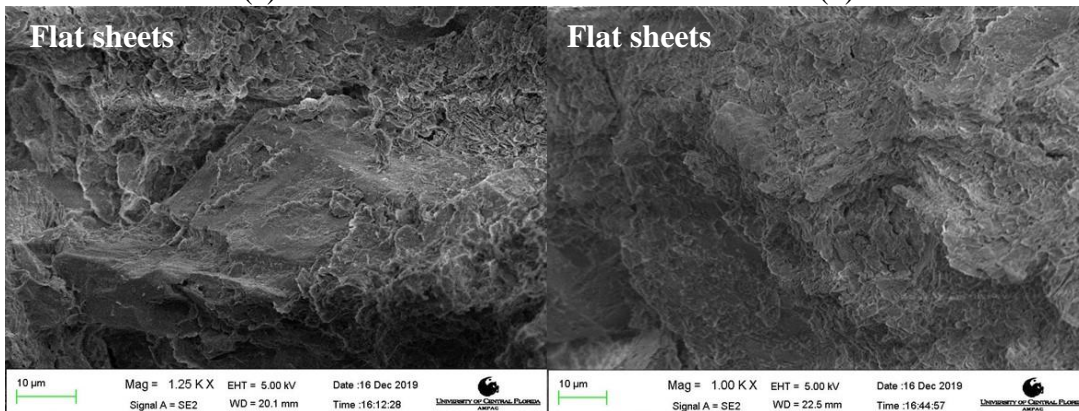


Figure 4-41. SEM images of NE specimens: (a) sample B2-ST5 at 50 X (b) specimen B2-ST5 at 250 X, (c) sample B1-ST2 at 250 X, (d) sample B2-ST5 at 1 KX, and (e) sample B2-ST5 at 1 KX



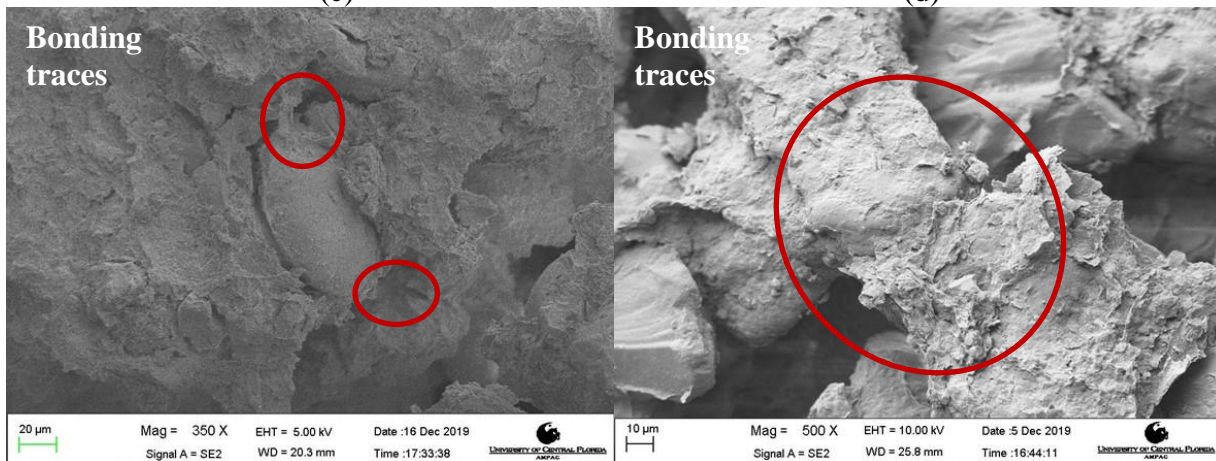
(a)

(b)



(c)

(d)



(e)

(f)

Figure 4-42. SEM images of SW specimens: (a) sample B3-ST8 at 100 X, (b) sample B3-ST8 at 1 KX, (c) sample B3-ST8 at 1.25 KX, (d) sample B3-ST8 at 1 KX, (e) sample B4-ST11 at 350 X, and (f) sample B3-ST7 at 500 X

4.6 Comparison of Laboratory Versus Cone Penetration Test Results

Based on cone penetration tests with porewater pressure measurement (CPTu) performed by FDOT at the testing site, soil laboratory results are compared with the results of field tests. Recall

that the main advantages of CPTu are the fast and continuous profiling of the soil. The comparison is established in terms of: relative density, friction angle, coefficient of consolidation, hydraulic conductivity, constrained modulus, shear modulus, undrained shear strength, over-consolidation ratio, and pre-consolidation pressure.

4.6.1 Relative Density Calculation

Relative density (D_r) was estimated as a function of the normalized cone resistance (Q_{tn}) as suggested by Robertson and Cabal (2014). The constant C_{dr} was assumed 300 due to the particle sizes found in the laboratory test results (mainly fine sands). The results are illustrated in Table 4-15 and Figure 4-43.

Table 4-15: Relative density correlated from CPTu tests

Depth [ft]	Description	D_r [%]
0 to 21	CPTu Averaged	61*
21 to 31	CPTu Averaged	42*

Note: *Based on geometric mean of CPT data

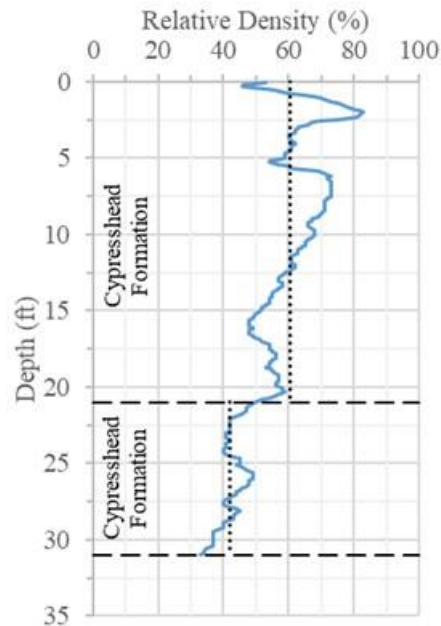


Figure 4-43. Relative density from CPTu tests.

4.6.2 Friction Angle Calculation

Friction angle (ϕ') was calculated from the normalized cone resistance (Q_{tn}) relationship suggested by Kulhawy and Mayne (1990). Figure 4-44 shows the continuous friction angle of the soil profile up to 31 ft. Table 4-16 summarized the computed average friction angles for the

Cypresshead formation and compared to the friction angle obtained from triaxial tests. The soil profile was divided at 21 ft due to a change in strength and relative density. A maximum difference of 5° was observed between TX tests conducted on Cypresshead formation soils and CPTu tests at the surficial sand layers.

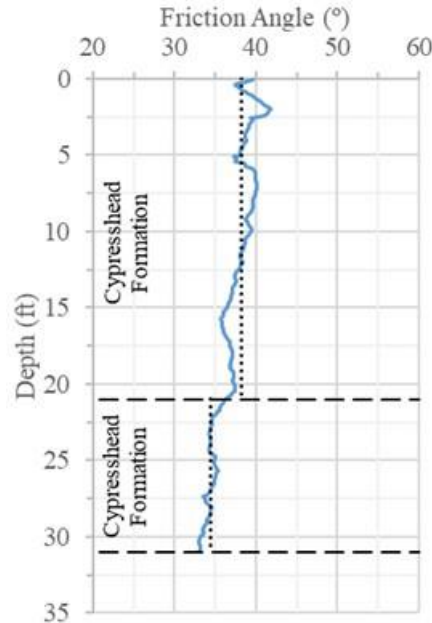


Figure 4-44. CPTu friction angle of the Cypresshead formation

Table 4-16: Friction angle from TX tests and CPTu tests

Depth [ft]	Description	ϕ' [°]
0 to 21	CPTu Averaged	38*
21 to 31	CPTu Averaged	34*
0 to 17.5	Triaxial tests on CF soils	33

Note: *Based on geometric average of CPTu profiles. CF: Cypresshead Formation

4.6.3 Coefficient of Consolidation

c_v was estimated from dissipation tests using the relationship proposed by Robertson et al. (1992) for CPTu tests. An anisotropic permeability ratio of 5 (Baligh and Levadoux 1986) was used to develop the dissipation tests. Dissipation tests are usually performed in clayey-type soils, since the excess porewater pressure generated around the cone may be large. This test allows dissipation of excess porewater pressures to calculate the rate of dissipation as a function of c_v . Figure 4-45 shows the computed c_v values for the IL, CRS, and dissipation field tests in relation the sample depth. Recall that only one CRS test generated enough excess pore pressure before the in situ vertical effective stress was reached, thus the results may not be considered accurate for samples tested at the same stress (i.e., observe the scatter in the figure). According to Robertson (2010), if the time corresponding to 50% consolidation (t_{50}) is less than 30s, the cone penetration can be considered

as partially drained, thus the theoretical solution provided by Teh and Houlsby (1991) may yield inaccurate results. Only one field dissipation test had a t_{50} larger than 30 s (i.e., $t_{50} = 361$ s), showing an approximate c_v value of 1×10^{-5} . The other tests had a t_{50} less or approximately equal to 30 s.

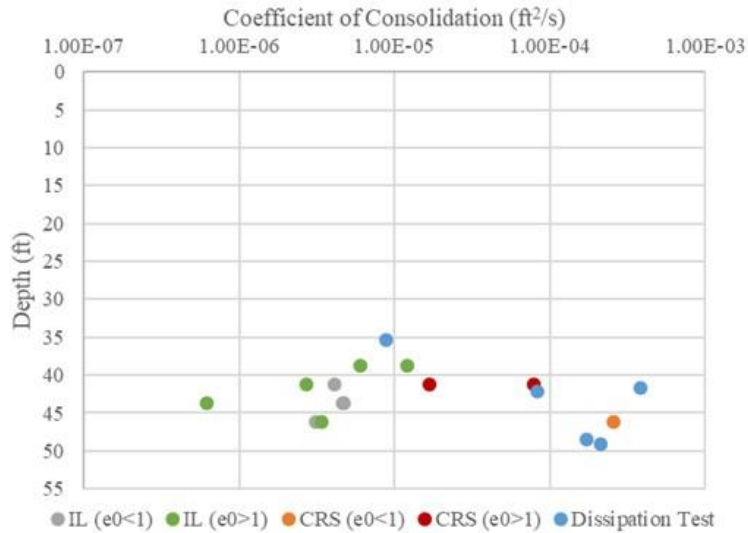


Figure 4-45. Coefficient of consolidation from laboratory and dissipation tests

4.6.4 Hydraulic Conductivity

Vertical hydraulic conductivity (k_v) was estimated from dissipation tests with an anisotropic permeability ratio of 5 (Baligh and Levadoux 1986). Figure 4-46 shows the variation of hydraulic conductivity with depth. k_v values were computed using the CPT soil behavior type (SBT) charts proposed by Robertson (2010) for the field dissipation tests. The hydraulic conductivity and coefficient of consolidation are highly related to the consolidation process. Results from laboratory and field tests match reasonably well. k_v values were computed between 1×10^{-7} and 1×10^{-9} ft/s. These results suggest that drainage at that elevation is controlled by the fines content in the samples.

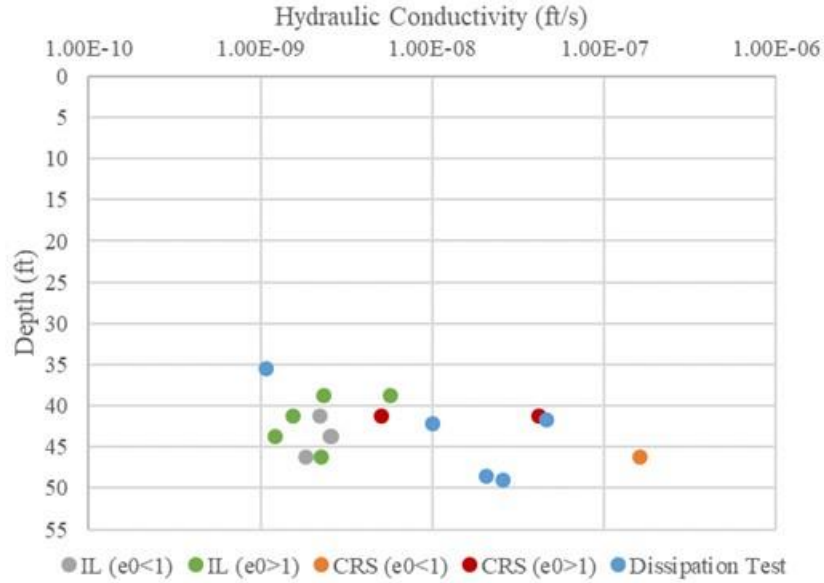


Figure 4-46. Hydraulic conductivity from laboratory and dissipation tests

4.6.5 Constrained Modulus

Figure 4-47 shows the constrained modulus (M) estimated as a function of the mechanical response measured during CPTu tests (Mayne 2007) and laboratory test results. Estimation of M using CPTu depends on the soil plasticity and natural water content. Note how the moduli computed from CRS and IL are close to M computed from the CPTu tests, despite the scatter shown in the figure. At depths between 37 and 47 ft, the laboratory tests measured approximate M values up to 100 tsf.

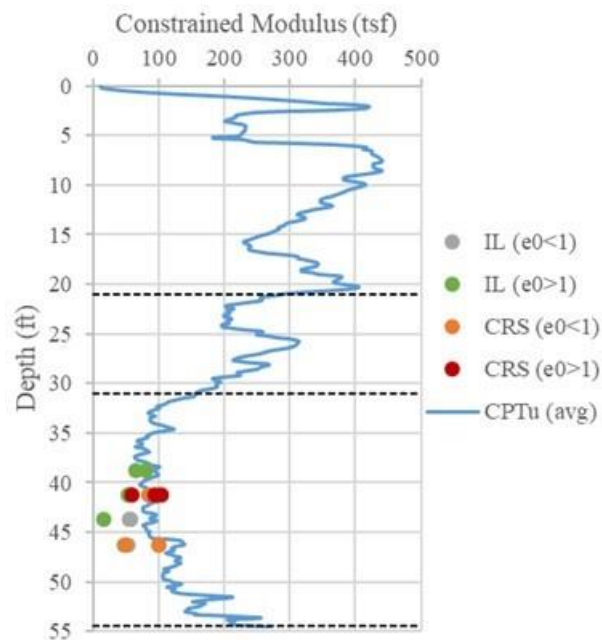


Figure 4-47. Constrained modulus from laboratory and CPTu tests

4.6.6 Shear Wave Velocity and Small-Strain Shear Modulus

Shear wave velocity (V_s) and small-strain shear modulus (G_0) were computed based on CPTu tests. Robertson (2009) stated that V_s can be estimated with relationships using the cone resistance; however, some variability may exist from a real measure of V_s . Recall that G_0 can be easily computed using the relationship $G_0 = \rho V_s^2$. Figure 4-48 presents the variation of shear wave velocity and small-strain shear modulus with depth. V_s values up to 700 ft/s were estimated using the triaxial laboratory tests. Note the wide scatter from the triaxial tests, where values of G_0 up to 950 tsf were measured depending on the exact location of the sample within the soil layer.

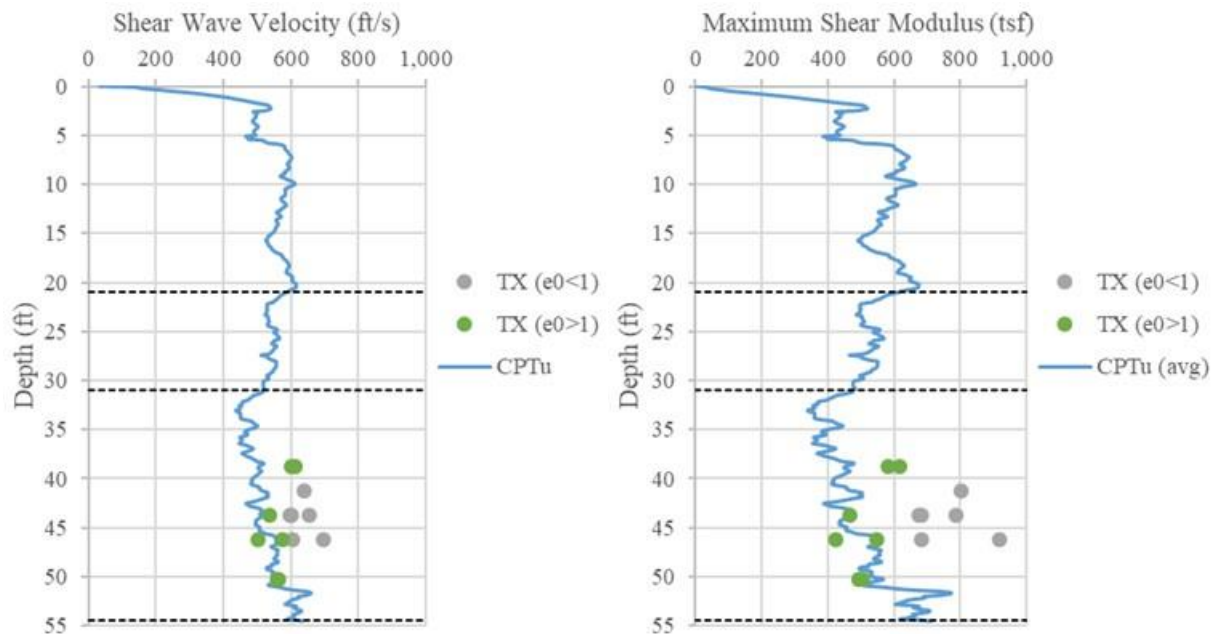


Figure 4-48. Shear wave velocity and maximum shear modulus from laboratory and CPTu tests

4.6.7 Undrained Shear Strength

Undrained shear strength (S_u) was estimated based on the measured excess porewater pressures from the CPTu with a relationship proposed by Lunne et al. (1985). When soft clays are tested with CPTu, the tip resistance may not be very accurate; thus, it is recommended to use the excess porewater pressure to compute the S_u . Figure 4-49 shows the undrained shear strength correlated with CPTu tests when significant excess porewater pressures were measured, along with the triaxial laboratory test results. Note how the TX results match very well the S_u measured with CPTu field tests.

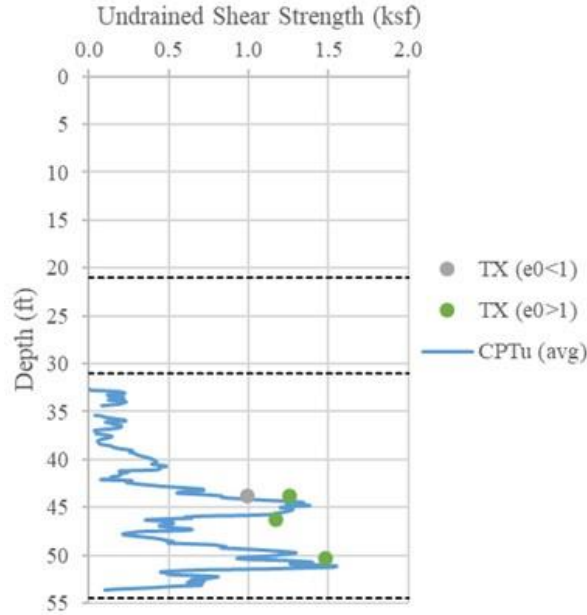


Figure 4-49. Undrained shear strength from laboratory and CPTu

4.6.8 Overconsolidation Ratio

Mayne (2014) proposed a relationship to compute the OCR based on CPTu test results. Figure 4-50 shows the variation over-consolidation ratio with depth along with the CRS and IL laboratory tests. Note how results with $e_0 < 1$ from laboratory tests have closer results to the silt mixture CPT line and laboratory tests with $e_0 > 1$ are closer to the sensitive clay CPT line. Figure 4-50 confirms the capabilities of CPT tests to understand and assess soil profiles. Note how OCR values correlated with CPT tests are reasonably reproduced in the laboratory tests.

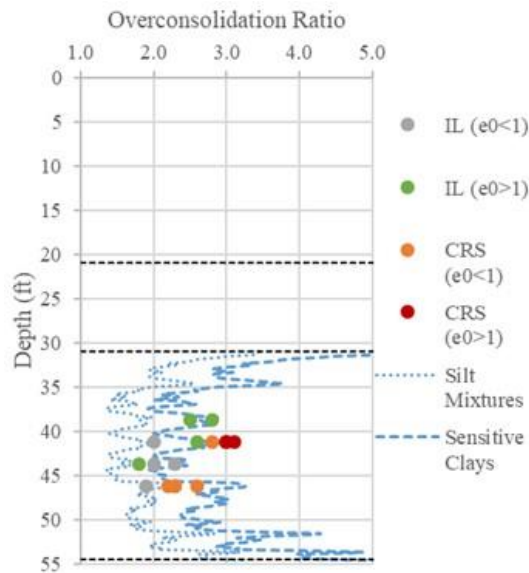


Figure 4-50. Overconsolidation ratio from laboratory and CPTu tests

4.6.9 Pre-consolidation Pressure

Mayne (2014) also suggested a relationship to estimate σ'_p from CPTu tests. Figure 4-51 shows the pre-consolidation pressure computed for CPTu and laboratory tests. Recall that for laboratory tests, σ'_p was estimated by the strain energy method (Becker et al. 1987). Note again how results with $e_0 < 1$ from laboratory tests have closer results to the silt mixture CPT line and laboratory tests with $e_0 > 1$ to sensitive clay CPT line.

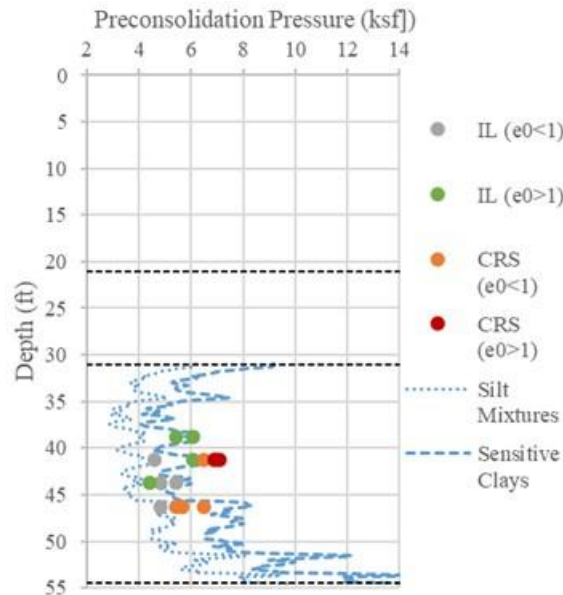


Figure 4-51. Preconsolidation pressure from laboratory and CPTu tests

4.6.10 Coefficient of Earth Pressure at Rest

Mayne (2005) proposed a relationship to estimate the coefficient of earth pressure at rest (K_0) as function of the OCR. Figure 4-52 shows the variation of the coefficient of earth pressure at rest with depth based on CPT and triaxial tests. The stress history of the material as a function of the K_0 value obtained with CPTs must be confirmed with laboratory tests since the results may not be reliable. However, Figure 4-52 shows a good relationship between those two procedures for the soils at that depth.

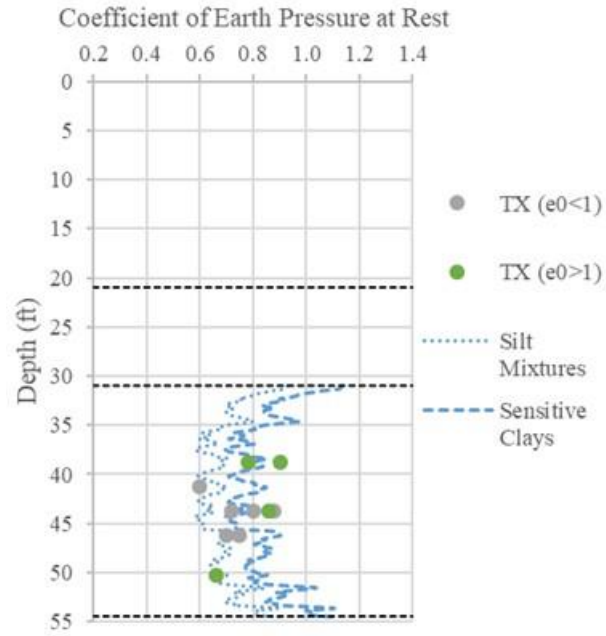


Figure 4-52. Coefficient of earth pressure at rest from laboratory and CPTu tests

CHAPTER 5 RECOMMENDATIONS REGARDING CORRELATIONS AND NUMERICAL MODELING

Differences between observed and computed performance of geotechnical problems are reduced when well-calibrated geotechnical parameters are used in numerical models. With the advances in computational modeling, construction details such as shape of loadings, site-specific soil layering, groundwater modeling, and sequence followed during construction can be implemented in robust numerical platforms without compromising computational efficiency. In this chapter, a compilation of correlations to calculate relative density, friction angle of the soil, small strain shear parameters including shear modulus and shear wave velocity, and coefficient of earth pressure at rest to consider the stress history of the soil, are summarized at the beginning of the chapter. Then, calculations of elastic modulus and immediate settlements are presented using numerous correlations and compared versus the conical load field tests. Numerical simulations of the Schmertmann (1993) conical loading field tests performed at the UCF site, proposed to investigate soil compressibility due to surface loadings, are also conducted and the results are summarized in this chapter. Ground surface settlements, measured at the center of the conical load arrangements using axisymmetric models, are compared versus measured/observed performance as reported in CHAPTER 3.

In the past, elastic-perfectly plastic soil models, such as Mohr-Coulomb, have been used successfully to study stress-strain-strength responses of soils but only when subjected to their ultimate strength under very limited stress paths. For projects involving multiple stress paths, or for projects that mobilize wide ranges of shear strains (γ_s), or simply to evaluate accurately construction-induced ground surface settlements, Mohr-Coulomb-based models tend to oversimplify soil behavior. More advanced constitutive soil models are recommended instead to capture more realistic features of soil response due to construction-induced loadings. In this chapter, two advanced soil models, the Hardening Soil (HS) and Hardening Soil Small-Strain (HSS) models, are used to investigate the soil response to conical load tests. Conical load-induced ground surface settlements, soil stresses, shear strains, and vertical influence zones are computed using the numerical models, and they are presented to describe the soil response observed in the field. Recommendations about geotechnical numerical modeling techniques are issued to calculate geotechnical engineering demand parameters (in particular ground surface settlements) caused by surface loadings for projects in the State of Florida.

5.1 Recommended Correlations for Relative Density Calculation

Tanaka and Tanaka (1998) described the relative density (D_r) as the most important state parameter for granular soil behavior characterization. Comparing the CPT and DMT tests with the SPT test, Tanaka and Tanaka (1998) indicated that the SPT N value is more dependent of the test conditions, such as dropping hammer energy and borehole bottom conditions, than the soil characteristics. The main disadvantage of using correlations for the CPT and DMT tests was the fact that most correlations do not consider size effects, aging, and structure of soils as measured using other advanced laboratory tests performed in natural soil deposits. Tanaka and Tanaka (1998) compared

two CPT and DMT correlations, proposed by Jamiolkowski et al. (1985) and Tanizawa (1990) with high quality frozen samples, and concluded that advanced laboratory test calibrations are valid to be implemented for in situ test correlations. Tanaka and Tanaka (1998) and Robertson and Campanella (1986) pointed out that the only reliable relationship between the D_r and the DMT was via the horizontal stress index (K_D). The relationships between shear modulus at small strains (G_0) and DMT modulus (E_D) or $(q_t - p_{v0})$ from CPT showed a strong dependency with D_r . The following two equations present the correlations proposed by Jamiolkowski et al. (1985) and Tanizawa (1990) used by Tanaka and Tanaka (1998), respectively:

$$D_r = -98 + 66 \log_{10}(q_t/(p'_{v0})^{0.5}) \quad (87)$$

$$D_r = -85.1 + 76 \log_{10}(q_t/(p'_{v0})^{0.5}) \quad (88)$$

where D_r is expressed in percentage and q_t and the effective vertical overburden pressure, p'_{v0} are expressed in tons/m² (=10 kPa) and kgf/cm² (=100 kPa) for Eqs. (87) and (88), respectively.

Figure 5-1 shows the comparison of Eqs. (87) and (88), using frozen samples retrieved from Kemigawa and Ohgishima sands reported by Tanaka and Tanaka (1998). They concluded that both equations underestimated and overestimated the relative density of Kemigawa and Ohgishima sands, respectively. Nevertheless, both equations led to almost identical results.

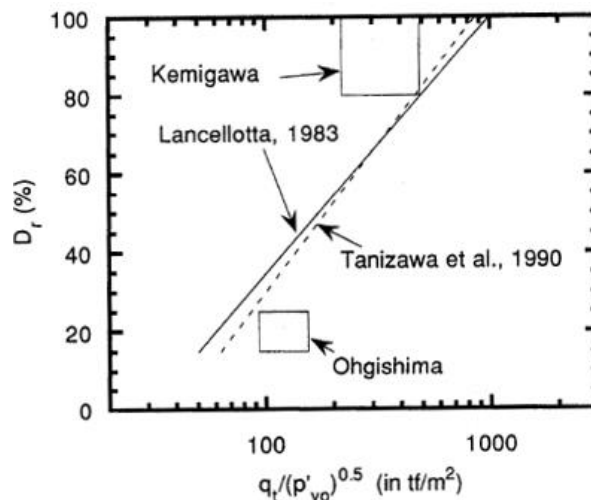


Figure 5-1. Comparison between measured relative density and predicted using CPT correlations (Tanaka and Tanaka 1998)

Although Tanaka and Tanaka (1998) indicated that the process of sedimentation should be studied to understand the discrepancy between correlations, they concluded that both equations obtained from chamber tests can be applied to in situ conditions. In addition to the difficulty associated with determining e_{max} and e_{min} (two critical parameters to compute D_r from a fundamental soil mechanics perspective), research has shown the uncertainty of representing the strain-stress behavior of granular soils only in terms of D_r ; even if this approach has been widely used by

geotechnical engineers for many years (Robertson and Cabal,2015). From several calibration chambers performed in clean quartz sands, it was found that sand density, in situ vertical and horizontal effective stress, and sand compressibility govern the CPT resistance (Robertson and Cabal 2015). The following equation, originally presented by Baldi et al. (1989) and later modified by Robertson and Cabal (2015), includes the effect of compressibility in the CPT resistance as a function of the grain size, grain shape, and mineralogy of sands.

$$D_r = \left(\frac{1}{C_2}\right) \ln\left(\frac{Q_{cn}}{C_0}\right) \quad (89)$$

where:

C_0 and C_2 are soil constants

σ'_{v0} =vertical effective vertical stress

$Q_{cn} = (q_c/p_a)/(\sigma'_{v0}/p_a)^{0.5}$ The normalized CPT resistance, corrected for overburden pressure (defined as Q_{tn} , using net cone resistance, q_n)

p_a = reference pressure of 1 tsf (100 kPa), in same units as q_c and σ'_{v0}

q_c = cone penetration resistance (more correctly, q_t)

Values of $C_0= 15.7$ and $C_2= 2.41$ were given for moderately compressible, unaged and uncemented, predominantly quartz sands (Robertson and Cabal 2015). The authors reported that sands with angular-shaped grains or high mica or carbonates in their mineralogic composition displayed a more compressible response than sands with rounded grains or clean quartz.

Kulhawy and Mayne (1990) stated that most of the research done on CPT had been conducted in calibration chambers, where the variability is smaller than in field because of the controlled laboratory conditions. Kulhawy and Mayne (1990) also discussed the flexibility of the walls in the calibration chamber versus actual field conditions. This effect was included in the following equation proposed by Jamiolkowski et al. (1985). They recommended that the tip resistance (q_c) should be divided by a coefficient K_q to correlate the field and chamber values. K_q is presented in Eq. (90) as follows:

$$K_q = 1 + \frac{D_r - 30}{300} \quad (90)$$

After “correcting” the results obtained from calibration chamber tests, developed for fine and medium dense sands, a linear relationship for D_r^2 in terms of the dimensionless cone tip resistance, Q_{cn} , was presented by Kulhawy and Mayne (1990) and it is shown in this report in Eq. (91). Kulhawy and Mayne (1990) categorized sandy soils according to their level of compressibility as low, medium, and high finding that: (i) low-compressible sands had quartz with very small fine content, (ii) medium-compressible sands had quartz with some feldspar and high fine content, and (iii) high-compressible sands displayed granular shapes with presence of fine-grained soils, mica, and other compressible materials. Kulhawy and Mayne (1990) also found that most of the natural

materials were categorized as medium-to-high compressible sands. The correlation presented in Eq. (91) was derived to exclude stresses above their particle crushing limit (Kulhawy and Mayne 1990).

$$D_r^2 = \frac{Q_{cn}}{305Q_C Q_{OCR} Q_A} \quad (91)$$

where:

- Q_{cn} = $(q_c/p_a)/(\sigma'_{v0}/p_a)^{0.5}$
 = normalized CPT resistance, corrected for overburden pressure (defined as Q_{tn} , using net cone resistance, q_n)
- p_a = reference pressure of 1 tsf (100 kPa), in same units as q_c and σ'_{v0}
- Q_C = Compressibility factor ranges from 0.90 (low compress.) to 1.10 (high compress.)
- Q_{OCR} = Overconsolidation factor = $OCR^{0.18}$
- Q_A = Aging factor = $1.2 + 0.05 \log(t/100)$

Robertson and Cabal (2015) proposed to use of a dividing factor of 350, corresponding to a medium, clean, uncemented, unaged, 1,000-year old quartz sand. For fine and coarse sands values of 300 and 400 were proposed, respectively.

Regarding SPT tests for the determination of relative density, Cubrinovski and Ishihara (2001) showed that SPT N value of sandy materials decreased as the mean grain size (D_{50}) became lower or the fine content became larger. However, Cubrinovski and Ishihara (2001) used the void ratio spread ($e_{max} - e_{min}$) instead of the mean grain size (D_{50}) because of the scatter observed in the gradation properties. Figure 5-2 shows the correlation between D_{50} and ($e_{max} - e_{min}$) for different types of soils as proposed by Cubrinovski and Ishihara (2001). They presented a correlation between N and D_r considering the effects of grain size and fine content using the void ratio range ($e_{max} - e_{min}$) as presented in Eq. (92).

$$D_r = \left[\frac{N(e_{max} - e_{min})^{1.7}}{9} \left(\frac{98}{\sigma'_v} \right)^{1/2} \right]^{1/2} \quad (92)$$

where:

- e_{max} = maximum void ratio
- e_{min} = minimum void ratio
- σ'_v = effective vertical stress in kPa
- N = blow counts at an energy rod ratio of 78%

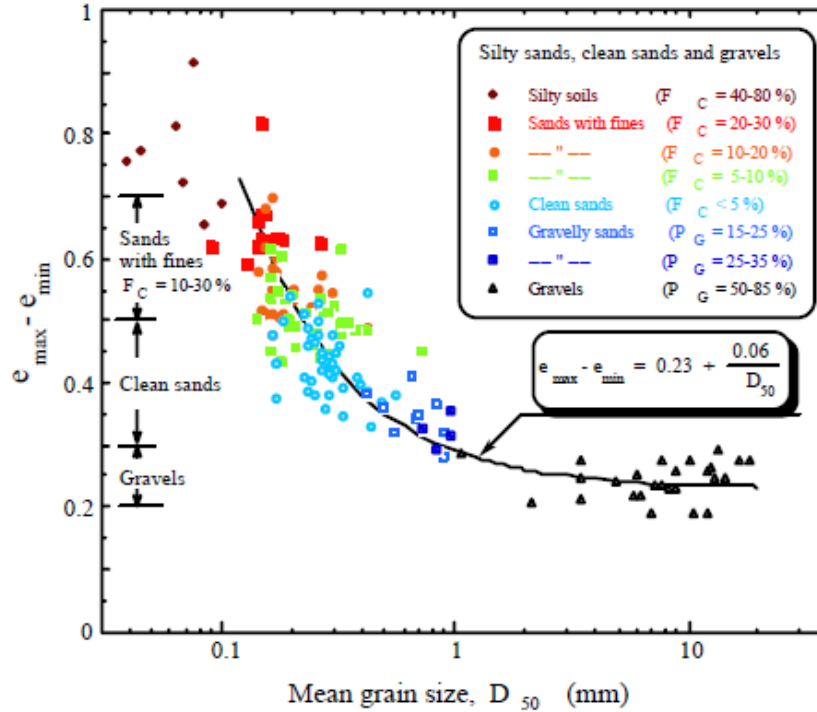


Figure 5-2. Variation of void ratio difference with the mean grain size of soils. From Cubrinovski and Ishihara (2001)

Note that maximum and minimum void ratios of 1.04 and 0.58, respectively were obtained from laboratory tests performed for the soils at the UCF site for surficial layers of soil (i.e., to 15 ft depth), correspond to an $e_{max} - e_{min}$ of approximately 0.5. These values are used for the calculation of relative densities and served as the basis of the constitutive model parameters presented in this report.

Kulhawy and Mayne (1990) reported factors that affected the relationship between D_r and N , which include: the vertical effective stress, stress history of the soil deposit, and sand compressibility. Factors affecting the energy efficiency of the drop hammer onto the drill rod were also presented by Kulhawy and Mayne (1990). They concluded that after correcting the SPT N value for field-related activities (e.g., borehole diameter, sampling method, rod length, among others) and overburden effects, $(N_1)_{60}$ can be used to evaluate the relative density. The proposed relationship between the relative density and $(N_1)_{60}$, presented by Kulhawy and Mayne (1990), considers most factors that affect the correct determination of the relative density. This relationship is presented in Eq. (93).

$$D_r^2 = \frac{C_{ER}C_B C_S C_R C_N N}{C_P C_A C_{OCR}} \quad (93)$$

where the following correction factors are defined as follows:

- C_{ER} = energy ratio
- C_B = borehole diameter
- C_S = sampling method
- C_R = rod length
- C_N = overburden stress
- C_P = particle size
- C_A = aging
- C_{OCR} = Overconsolidation

C_P, C_A, and C_{OCR} are given in Table 5-1.

Table 5-1. Summary of SPT correction factors. From Kulhawy and Mayne (1990)

Effect	Parameter	Correction	
		Term	Value
Particle size	D ₅₀ of sand	C _P	60+25 log D ₅₀ D ₅₀ in mm
Aging	Time (t)	C _A	1.2 + 0.05 log (t/100) t in years
Over-consolidation	OCR= σ'_p / σ'_{v0}	C _{OCR}	OCR ^{0.18}

C_N is given by Eq. (94) suggested by Kulhawy and Mayne (1990) as follows:

$$C_N = \left(\frac{P_a}{\sigma'_{V0}} \right)^{0.5} \quad (94)$$

Since values obtained with Eq. (94) have shown inconsistencies for very low vertical effective stresses, Skempton (1986) suggested a similar equation, but including constant fitting values as presented in Eq. (95):

$$C_N = \frac{2}{(1 + \sigma'_{V0}/P_a)} \quad (95)$$

For the determination of the relative density using the results of DMT field tests, Tanaka and Tanaka (1998) showed that the correlation proposed by Robertson and Campanella (1986) agreed well with laboratory tests performed on high-quality frozen samples. Later, Marchetti et al. (2001) presented an additional correlation relating K_D and the relative density. Figure 5-3 presents all data points used by Marchetti et al. (2001) to correlate both parameters.

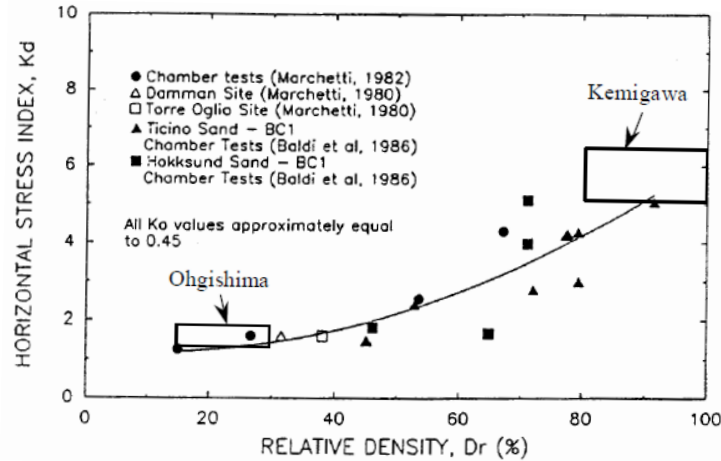


Figure 5-3. Correlation between horizontal stress index from DMT and relative density for uncemented sands. From Marchetti et al. (2001)

The following equation presents the best-fit expression obtained from Marchetti et al. (2001):

$$D_r = 11.7 + \sqrt{1666.7K_D - 1995.6} \quad (96)$$

5.2 Recommended Correlations for Friction Angle (ϕ') Calculation

The determination of the friction angle, ϕ' , is crucial to define strength properties of sandy soils. Robertson and Cabal (2015) pointed out that regardless of current advanced theories on modeling cone penetration processes in sands, the use of correlations based on advanced laboratory and field tests are still widely used. In this report, the following correlations are recommended to determine the friction angle of sands.

The correlation suggested by Robertson and Campanella (1983) is presented in Eq. (97):

$$\tan \phi' = \frac{1}{2.68} \left[\log \left(\frac{q_c}{\sigma'_{v0}} \right) + 0.29 \right] \quad (97)$$

The correlation proposed by Kulhawy and Mayne (1990) for clean, rounded, uncemented quartz sands, also part of Robertson and Cabal (2015) manual, is presented as follows:

$$\phi' = 17.6 + 11 \log(Q_{tn}) \quad (98)$$

Robertson and Cabal (2015) stated that for “low-risk” projects, values of $\phi' = 28^\circ$ for clays and 32° for silts were sufficient. Robertson and Cabal (2015) also presented the following correlation for fine-grained soils, intended for soils in the ranges of: $20^\circ \leq \phi' \leq 40^\circ$ and $0.1 \leq B_q \leq 1.0$.

$$\phi' = 29.5^\circ \cdot B_q^{0.121} [0.256 + 0.336 \cdot B_q + \log Q_t] \quad (99)$$

This equation provided reliable results for normally- to lightly-overconsolidated clays, and only works for positive u_2 recordings from the piezocone.

Hatanaka and Uchida (1996) carried out a series of drained triaxial tests on high-quality samples of sandy soils to determine the friction angle. The authors compared the laboratory test results with empirical equations proposed by several researchers using SPT N -values normalized at an effective overburden pressure of 98 kPa. Hatanaka and Uchida (1996) concluded that the friction angle is a function of the D_r which is highly influenced by the fines content. Six sites composed of sands from the Holocene and Pleistocene volcanic ages were tested by Hatanaka and Uchida (1996). Table 5-2 lists the effective overburden stress, N values, and overburden-corrected N value (i.e., N_1) reported by the authors. Eq. (100) presents the normalization of the N value for an energy efficiency of 78% used in that study.

$$N_1 = N / (\sigma'_V / 98)^{0.5} \quad (100)$$

where:

σ'_V = effective vertical overburden pressure in kPa

The following correlation, proposed by Hatanaka and Uchida (1996), was used in this report to determine the friction angle for the sandy soils found at the UCF site. This equation showed a good correlation with N_1 .

$$\phi' = (20N_1)^{0.5} + 20 \quad (101)$$

Three additional correlations proposed by Peck et al. (1974), Schmertmann (1975), and Marchetti et al. (2001) are presented in the following set of equations.

$$\phi' = 27.1 + 0.3N_{60} - 0.00054 (N_{60})^2 \quad (102)$$

$$\phi' = \tan^{-1} \left[\frac{N_{60}}{12.2 + 20.3 \left(\frac{\sigma'_0}{p_a} \right)} \right]^{0.34} \quad (103)$$

$$\phi' = 28 + 14.6 \log K_D - 2.1 \log^2 K_D \quad (104)$$

Table 5-2. Physical properties of frozen samples tested (Hatanaka and Uchida 1996)

Name	ρ_s g/cm ³	D ₅₀ mm	F _c %	U _C	ρ_d g/cm ³	e	Dr %	N ₇₈ Value	σ'_v kPa	N ₁ Value	ϕ °
IK1	2.73	0.29	1.3-2.4	1.6	1.36	1.00-1.01	34	9.0	68.6	11	36.0
IK2	2.67	0.38-0.40	2.1-4.6	2.2-2.5	1.32	0.99-1.06	57	17	98.0	17	38.2
NA	2.64	0.16-0.21	4.1-5.7	1.6-2.8	1.33	0.89-0.97	81	10	127.4	8.8	32.7
NG1	2.67	0.33-0.45	4.3-9.4	2.8-5.1	1.47	0.74-0.90	74	18	39.2	28	43.4
NG2	2.64	0.43-0.49	7.0-10.4	2.2-6.7	1.39	0.86-0.93	81	15	68.6	18	37.8
NG5	2.72	0.43-0.51	13.0-16.2	2.7-6.0	1.46	0.86-0.89	79	10	137.2	8.5	35.1
KY1	2.47	0.34-0.48	3.6-11.0	4.0-9.3	1.13	0.89-0.99	72	5.7	58.8	7.4	39.0
KY2	2.65	0.41-0.45	1.8-2.9	3.0-3.2	1.37	0.79-0.85	59	5.4	68.6	6.5	31.0
KY3	2.59	0.37-0.47	1.4-2.3	2.7-3.0	1.35	1.12-1.37	59	6.4	78.4	7.2	35.0
KG	2.43	0.19-0.24	3.6-9.6	2.4-2.9	0.92	1.57-1.78	70	11	49.0	16	40.4
KA1	2.48	0.45-0.75	13.5-15.5	14.1-22.3	0.83	1.12-1.28	81	4.5	78.4	5.0	28.0
KA2	2.42	0.15-0.45	9.1-30.4	6.5-13.2	0.89	1.55-1.69	78	4.0	88.2	4.2	30.0

5.3 Recommended Correlations for Small-Strain Shear Modulus Calculation

The dependency of the shear modulus (G) on the strain level has been widely studied in the technical literature. The small strain shear modulus (G_0), which occurs for shear strains (γ) lower than $10^{-3}\%$, plays a very important role in the determination of ground deformations. The stiffness degradation as shear strains are mobilized in geotechnical projects and its numerical consequences have been studied in light of numerical models by numerous researchers. Benz et al. (2009), Davie et al. (2019) proposed the consideration of the stiffness degradation for settlement calculations. The methods to measure G_0 are based on shear wave velocities (V_S) from either advanced laboratory tests or field tests. The most important relationship between G_0 and V_S is given by Eq. (105):

$$G_0 = \rho V_S^2 \quad (105)$$

where:

ρ = mass density of soil ($\rho = \gamma_s/g$)

In the absence of V_s , Kramer (1996) suggested to use Equations (106) and (107) that are highly recommended in this report:

$$G_0 = 625 F(e) OCR^k P_a^{1-n} (\sigma'_m)^n \quad (106)$$

where:

- F(e) = function of the void ratio
= $1/(0.3+0.7e^2)$ (Hardin 1978)
= $1/e^{1.3}$ (Jamiolkowski et al. 1991)
- OCR = overconsolidation ratio
- k = overconsolidation ratio exponent (see Table 5-3)
- σ'_m = mean effective stress = $(\sigma'_1 + \sigma'_2 + \sigma'_3)/3$
- n = stress exponent = 0.5 or computed for individual soils

P_a , σ'_m , and G_0 must be expressed in the same units. The equation can be used to adjust measured G_0 values under different conditions, such as different effective stresses as presented by Kramer (1996).

Table 5-3. Overconsolidated ratio exponent k. After Hardin and Drnevich (1972 b)

Plasticity Index	k
0	0.00
20	0.18
40	0.30
60	0.41
80	0.48
>100	0.50

Seed and Idriss (1970) also investigated the factors affecting the shear modulus on sands, concluding that the modulus values were significantly affected by the shear strain amplitude, confining pressure, and void ratio, and were not as affected by grain size characteristics. Thus, Seed and Idriss (1970) found Eq. (107) which relates G_0 and the confining pressure. This relationship can be used for the determination of constitutive soil parameters for numerical simulations of ground surface settlements in granular soils in Florida.

$$G_0 = 1,000 K_2 (\sigma'_m)^{1/2} \quad (107)$$

where:

- K_2 = function of the relative density
- σ'_m = mean effective stress = $(\sigma'_1 + \sigma'_2 + \sigma'_3)/3$ in psf
- G_0 = low strain shear modulus in psf

K_2 , as a function of the relative density, is presented in Figure 5-4.

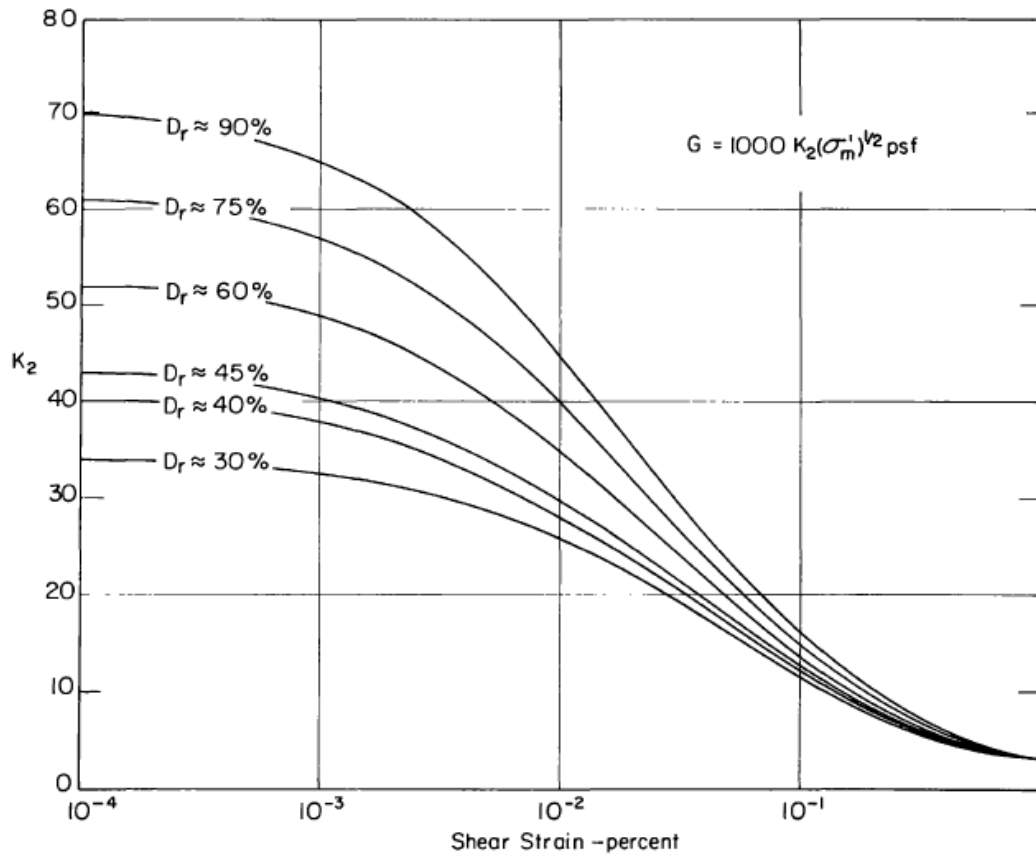


Figure 5-4. Shear moduli for sands at different relative densities. From Seed and Idriss (1970)

For the case of fine grained soil materials, Seed and Idriss (1970) stated that the shear moduli depends on the disturbance, strain amplitude, strength and stiffness. Seed and Idriss (1970) found that the relationships considering those effects in terms of OCR , void ratio (e), σ'_m , and strength parameters are not in good agreement with in situ measurements. Seed and Idriss (1970) reported that: (i) higher soil strength implies larger stiffness, (ii) there is not a wide variation of the ratio E/S_U for saturated clays under static load conditions, and (iii) an approximately linear relationship holds between shear modulus and shear strength at low strain levels. Thus, the variation of G can be normalized with respect to the undrained shear strength of soils S_U .

The soil disturbance was considered using a factor of 2.5 by Seed and Idriss (1970), who stated that detailed information on sampling and testing conditions were not found. In both cases (clays and sands), some useful correlations with field tests were presented by Kramer (1996) and are shown in Table 5-4 that are recommended in this report to be used for the determination of the shear modulus, which is an input for the numerical models that incorporate in their constitutive formulation the soil behavior at small strains.

Table 5-4. Empirical relationships between G_{max} and in situ tests. From Kramer (1996)

In situ test	Relationship	Soil type	References	Comments
SPT	$G_{max} = 20,000 (N_1)_{60}^{0.333} (\sigma'_m)^{0.5}$	Sand	Ohta and Goto (1976), Seed et al. (1986).	G_{max} and σ'_m in lb/ft ²
	$G_{max} = 325 (N)_{60}^{0.68}$	Sand	Imai and Tonouchi (1982).	G_{max} in kips/ft ²
CPT	$G_{max} = 1,634 (q_c)^{0.250} (\sigma'_V)^{0.375}$	Quartz Sand	Rix and Stokoe (1991).	G_{max} , q_c , and σ'_V in kPa Based on field tests in Italy and on calibration chamber tests.
	$G_{max} = 406 (q_c)^{0.695} e^{-1.130}$	Clay	Mayne and Rix (1993)	G_{max} , and q_c , in kPa. Based on field tests worldwide sites.
DMT	$G_{max}/E_D = 2.72 \pm 0.59$	Sand	Baldi et al. (1986).	Based on Calibration Chamber tests.
	$G_{max}/E_D = 2.2 \pm 0.7$	Sand	Bellotti et al. (1986)	Based on field tests.
	$G_{max} = \frac{530}{\left(\frac{\sigma'_V}{p_a}\right)^{0.25}} A K_0^{0.25} (p_a \sigma'_V)^{0.5}$ $A = \frac{\gamma_D/\gamma_W - 1}{2.7 - \gamma_D/\gamma_W}$	Sand, silt, and clay	Hryciw (1990).	G_{max} , p_a , and σ'_V in same units; γ_D is dilatometer-based unit weight of soil; based on field tests

Tanaka and Tanaka (1998) also presented a correlation based on seismic cone tests between G_0 and the parameter $(q_t - p_{v0})$, for NC clays. This correlation is presented in Eq. (108).

$$G_{SC} = G_0 = 50 (q_t - p_{v0}) \quad (108)$$

where:

- q_t = CPT tip resistance in MPa
- p_{v0} = total overburden pressure in MPa

A similar equation for the DMT test was presented by Tanaka and Tanaka (1998) in clays, which is presented in Eq. (109) as a function of the dilatometer modulus.

$$G_{SC} = G_0 = 7.5 E_D \quad (109)$$

where:

- E_D = Dilatometer Modulus in MPa

Figure 5-5 shows the relationship between the ratio G_{SC} (G_0) from seismic cone penetration tests to E_D from DMT tests as a function of K_D for sandy soils reported by Tanaka and Tanaka (1998). For the case of sandy materials, the ratio G_{SC}/E_D decreased with K_D approaching 7.5, which coincided with the value presented in Eq. (109) (Marchetti et al. 2001).

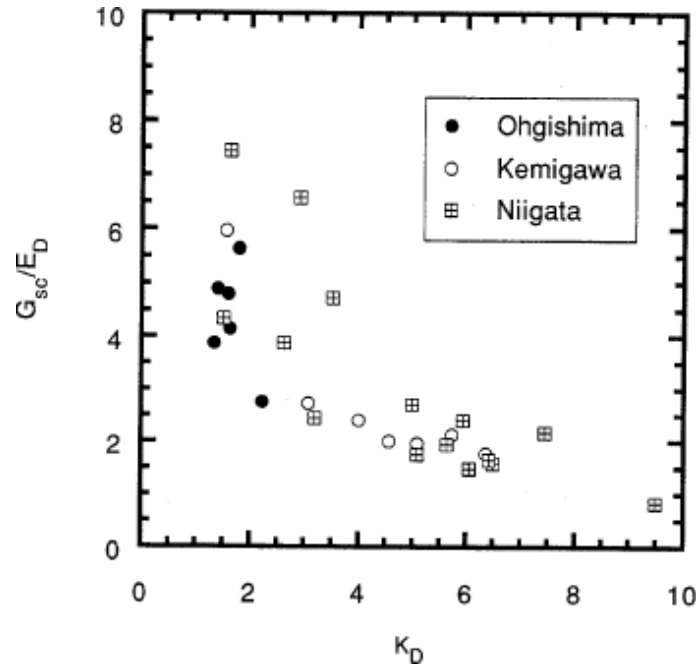


Figure 5-5. Ratio of G_{SC} (G_0) from seismic cone penetration tests to E_D from DMT tests versus K_D for sandy soils. From: Tanaka and Tanaka (1998)

When CPT tests are used for sands, the ratio of G_{SC}/q_t can be described by a nonlinear relationship derived in terms of the ratio $q_t/(p'_{v0})^{0.5}$. The influence of D_r to G_{SC}/E_D and G_{SC}/q_t indicates that when D_r increases, G_{SC}/E_D and G_{SC}/q_t decreases. Numerous researchers have attributed this variation to the fact that K_0 , which is strongly correlated to K_D and E_D , increase with D_r for granular soils.

A different approach was proposed by Robertson and Cabal (2015). They found V_s using correlations from CPT data and G_0 using Eq. (105). Using both values, Robertson and Cabal (2015) proposed the following equation:

$$V_s = [\alpha_{VS}(q_t - \sigma_v)/P_a]^{0.5} \text{ (m/s); } \alpha_{VS} = 10^{(0.55I_c + 1.68)} \quad (110)$$

where:

$$I_c = \text{behavioral CPT index} = \sqrt{[3.47 - \log(Q_{tn})]^2 + [1.22 + \log(F_r)]^2}$$

$$Q_{tn} = \text{Normalized net tip resistance} = \frac{q_t - \sigma_v}{P_a} / \left(\frac{\sigma'_v}{P_a}\right)^n$$

$$n = 0.381 I_c + 0.05 \left(\frac{\sigma'_{vo}}{p_a} \right) - 0.15 \leq 1.00$$

In the previous equation, the calculation requires an iterative procedure for I_c since the variable is also included in the exponent n . This iterative procedure is described by Robertson and Cabal (2015) in the topmost part of the following flowchart:

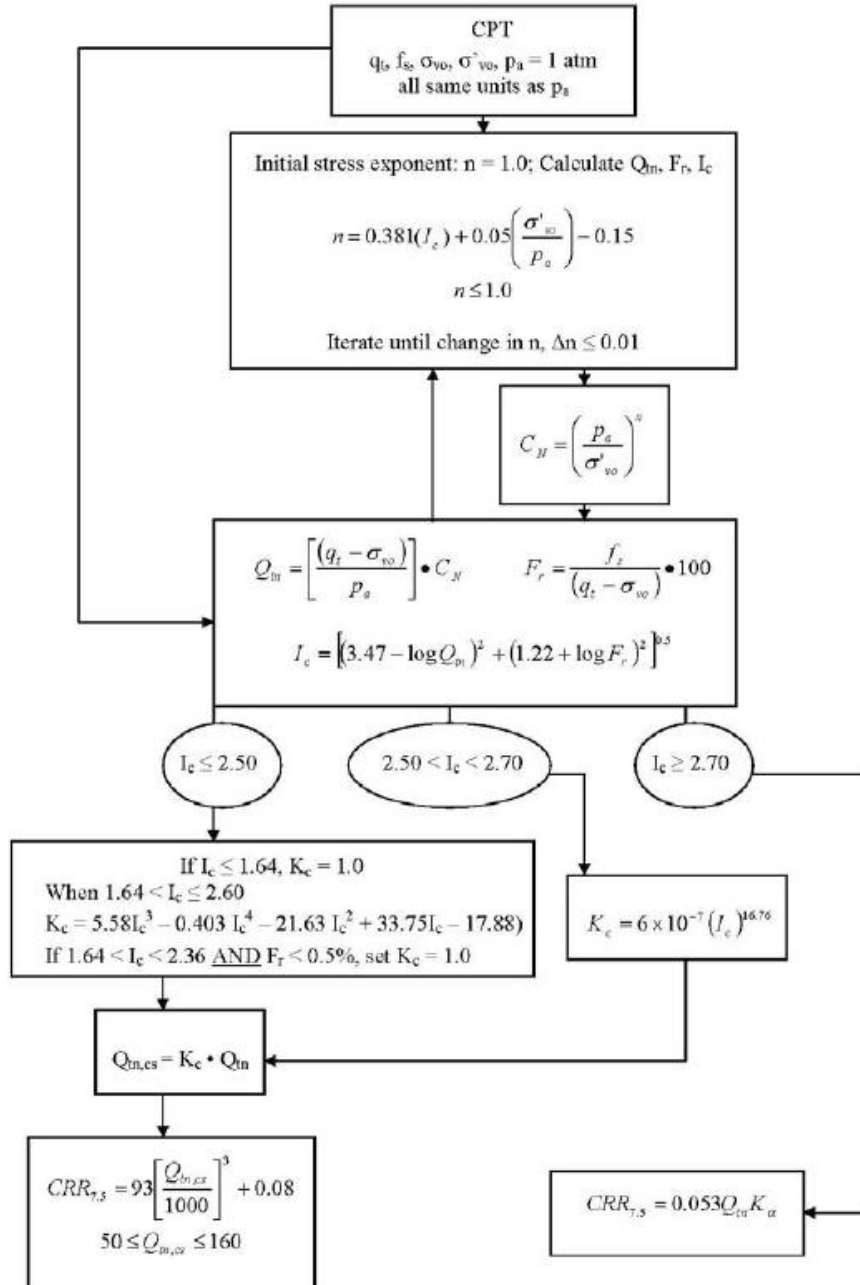


Figure 5-6. Flowchart for evaluation of I_c based on the suggested iterative procedure by Robertson and Cabal (2015)

Dagger et al. (2018) proposed an alternative expression based on regression analyses from tests performed by MDOT as follows:

$$V_s = [10.1 \cdot \log(q_t) - 11.4]^{1.67} \cdot \left(100 \cdot \frac{f_s}{q_t}\right)^{0.3} \quad (\text{m/s}) \quad (111)$$

5.4 Definition of Soil Profile and Parameters

Figure 5-7 illustrates the soil profile obtained using soil representative parameters based on the previous discussions on the correlations presented in this chapter and on the field tests described in CHAPTER 3. Sandy layers found at the project site were mainly composed of fine grained sands with fine contents ranging from 3 to 37% (Chopra et al. 2003). Based on those conditions and the information presented in the figure, the parameters obtained from the recommended correlations were properly adjusted. The field test parameters, initially used to classify the soil, were consistent among the tests performed in this project. The four layers used in the following calculations and numerical simulations are presented in the figure in the following order:

1. The top layer (0-11.5 ft) is a sandy layer with material indexes of $I_c < 2.05$ and $I_D > 1.8$ based on the CPTu and DMT tests (see figure 5-6), respectively, performed at the site. It was defined as a medium-to-dense sand since the tip resistance readings at Cone 1 and Cone 3 areas were closer or higher than 100 TSF. The SPT blow counts showed some variation along the depth, similar to the scatter observed with the CPTu tip resistance. These variations are less noticeable for the location of conical load test 2. A peak value at conical load test 3 coincided with the peak of Q_t in the CPT. From the correlations suggested from the previous section, an overall D_r value of 65% was adopted for that layer. The D_r correlated values using Jamiolkowski et al. (1985) and Tanizawa (1990) correlations provided support for this definition. The D_r correlated using Robertson and Cabal (2015) generated larger values, which were discarded for the analysis. This larger values of D_r can be attributed to the underlying assumptions on the determination of C_0 and C_2 soil constants that were originally recommended for moderately compressible, unaged, and uncemented, predominantly quartz sands since the sand in the field test seemed to be less compressible even in the presence of larger fine contents. This highlights the importance of evaluating several correlations to be used in practice, and with engineering judgement select the most appropriate correlation that fits expected soil behavior that is later confirmed with field tests. The calculations using SPT showed less scatter among the correlations used. A higher value of relative density was correlated using Cubrinovski and Ishihara (2001) and a higher difference was found at the surficial locations. The small vertical effective stress for that shallow layer explains those differences. Comparing the D_r correlated with the information obtained with CPTu and SPT tests, both tests provided similar results. When analyzing the D_r values correlated with the DMT parameters for this specific location, the values were not reliable because of uncertainties in the determination of E_D for similar soils. Thus, only correlations where E_D values were lower than 6 are presented. Regarding the internal friction angle of this layer, the discrepancy between correlations of the same field tests is more noticeable for shallow soils, particularly noticeable for the case of SPT-based correlations. For deeper soils, the scatter between CPTu and SPT reduced. The correlations

between DMT and CPTu parameters are closer above 66 ft depth. Even though there are many correlations that can be used directly to estimate the coefficient of earth pressure at rest (K_0), in this report it is recommended the correlation proposed by Jaky (1944), see Eq. (112). This parameter is very important in numerical analyses since it is used to initialize the initial state of stress acting on the solid elements, estimate the mean principal effective stress (σ'_m) for in situ conditions, account for the stress history of the soil deposit, and calculate the small strain shear modulus. Those are essential parameters when modeling soil behavior.

$$K_{0(NC)} = 1 - \sin\phi' \quad (112)$$

2. The second layer (11.5–31 ft) is defined herein also as a medium-dense sand. As opposed to the parameters computed for the first layer, the correlated parameters exhibit less scatter that can be caused by higher levels of vertical effective stress and thus, higher confining pressures. The relative density adopted for this layer is mostly selected from SPT correlations which coincide with the lowest values from CPT correlated parameters. DMT correlations, similarly as the topmost layer, did not provide reliable estimates due to the large E_D values. The results G_0 were less scattered when using the results of CPTu and SPT tests. The effective friction angle calculations showed moderate but acceptable differences between the correlated values obtained using SPT and CPTu test results. Since different authors presented tables that correlated the CPT tip resistance and SPT blow counts with the relative density and friction angle of the soil, the selection of an average value was finally adopted.
3. The third layer (31.0–52.0 ft) was defined as a silty clay layer. This type of material was selected since the material index from the CPTu and DMT (I_c and I_D) indicated the presence of a fine material. An overall internal friction angle for this layer was adopted as 27° in the following calculations and numerical simulations. That value was adopted based on the recommendation made by Robertson and Cabal (2015), assuming that the mobilized strains are not significant for the type of conical loading applied in this research given the Boussinesq stress influence analyses. The selection of G_0 was determined based on correlations from CPTu and DMT tests.
4. Although the influence zone analyses in the vertical direction, presented later in this chapter, indicated that large stresses from the conical load tests were not expected at large depths, a fourth layer (52.0–65.0 ft) was defined and modeled as a medium-to-dense sandy material.

The following abbreviations are in the following figure of summarized soil profile for the calculations and numerical simulations presented in this chapter.

J. et al_85 (Jamiolkowski et al. 1985), T_90 (Tanizawa 1990), R&C_14 (Robertson and Cabal 2015), K&M_90 (Kulhawy and Mayne 1990), D. et al._18 (Dagger et al. 2018) , R&S_91 (Rix and Stokoe 1991) , S&I_70 (Seed and Idriss 1970), R&C_86 (Robertson and Campanella 1986),

C&I_01 (Cubrinovski and Ishihara 2001), O&G_76 (Ohta and Goto 1976), I&T_82 (Imai and Tonouchi 1982) , H&U_96 (Hatanaka and Uchida 1996), P. et al._74 (Peck et al. 1974), Ba. et al._86 (Baldi et al., 1986), Be. et al._86 (Bellotti et al., 1986), H_90 (Hryciw 1990) , T&T_98 (Tanaka and Tanaka 1998), M. et al. (Marchetti et al. 2001).

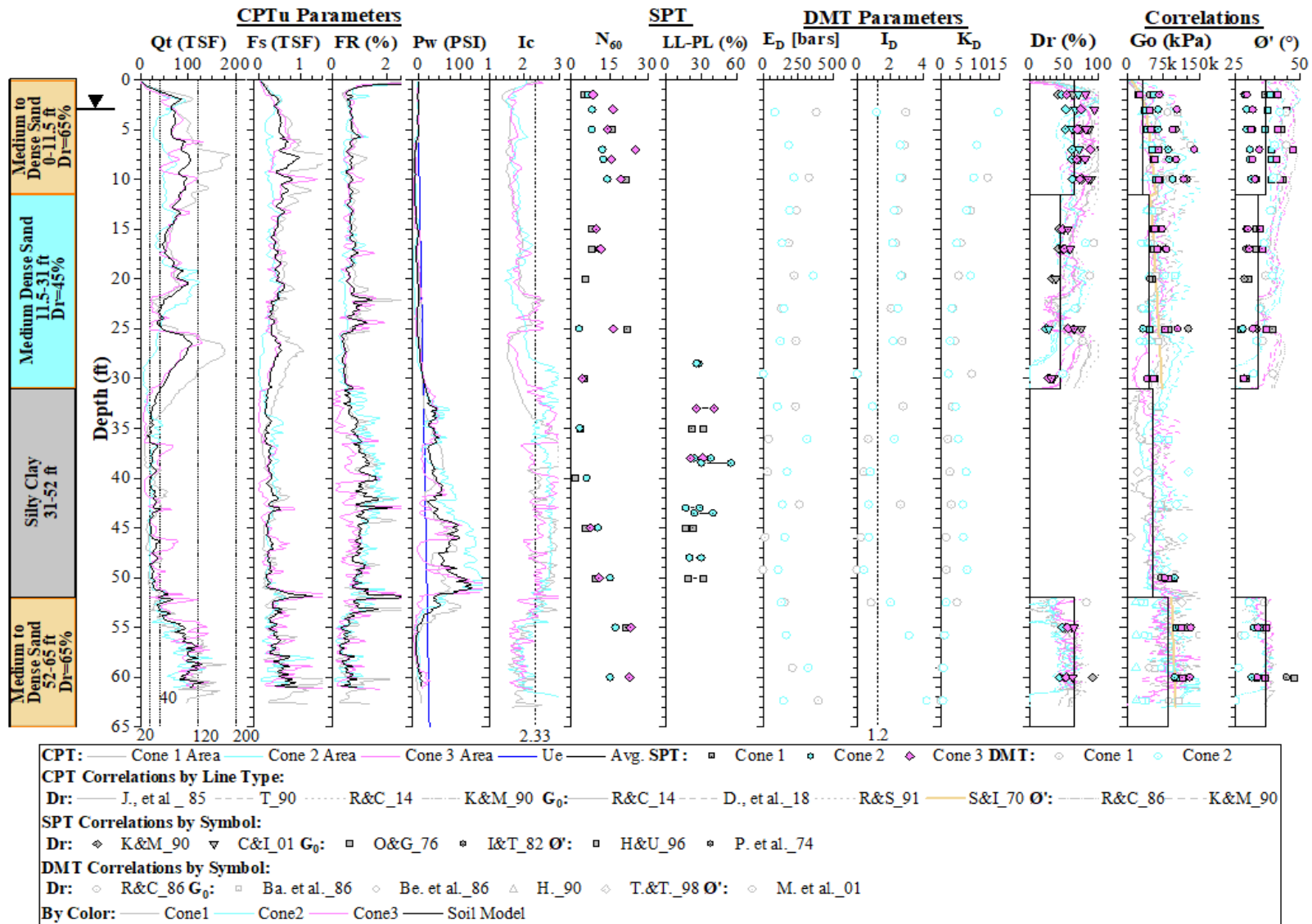


Figure 5-7. Summarized soil profile at the project site showing the results of field tests, soil strength and stiffness parameters defined using the proposed correlations

5.5 Definition of Vertical Stress Influence Zone: Boussinesq Analysis

The incremental vertical and horizontal stress variation calculated for different loading conditions (i.e., point load, linear load, square uniform pressure, circular uniform pressure, among other) were studied by Boussinesq (1885) using the theory of elasticity assuming a homogeneous and semi-infinite half space continuum. In the conical load tests of this study, the pressure applied to the soil does not strictly correspond to any conventional loading applied to the ground surface, thus, the conical load was converted on successive equivalent circular layers of a given thickness, which using the principle of superposition allowed the calculation of variation of pressures with depth. Figure 5-8 presents the variation of the incremental stress with depth. From that figure, the vertical stress influence zone can be estimated to be between 28 and 31 ft, which confirms an influence zone of approximately 30 ft.

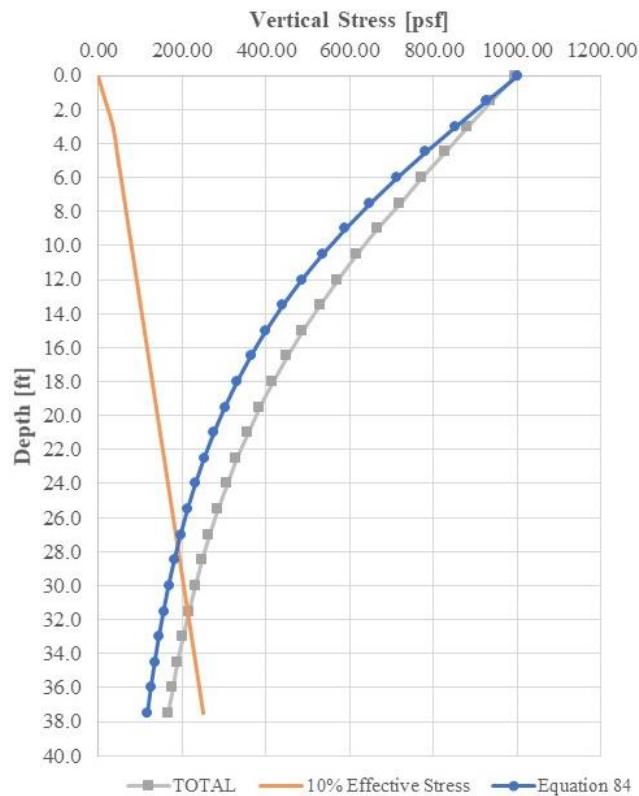


Figure 5-8. Vertical stress profile for the definition of stress influence zone for the conical load arrangement

5.6 Calculation of Elastic Modulus from Published Correlations

Using the soil profile from Figure 5-7 and the influence zone of approximately 30 ft presented in the previous section, the following estimation of Young's modulus is reported for the two topmost stressed granular soil layers that participate in the loading bearing mechanism of the conical load arrangement. The average tip resistance from CPTs and blow counts from SPTs are used into the

correlations. Table 5-5 and Table 5-6 present a summary of the calculated of elastic moduli by using published correlations using SPT and CPT data, respectively. Those values are going to be used as the basis of recommendation for correlations of elastic modulus and calculation of immediate settlements in this project.

Table 5-5. Summarized calculations of elastic modulus for the top two topmost granular soil layers at the project site (using SPT blow counts)

Soil Type	Reference	Equation	Layer 1 [TSF]	Layer 2 [TSF]	Average TSF
Sand	Webb (1969)	$E=4(N + 12)$, ton/ft ²	102	82	89
	Trofimenzov (1974)	$E_s= 350 \log N$, kg/cm ²	396	323	350
		$E_s= 500 \log N$, kg/cm ²	565	462	500
	Chaplin (1963)	$E_s^{4/3} = (44N)$, tsf	120	84	98
	Denver (1982)	$E_s= 7(N)^{0.5}$, MPa	257	203	223
	Clayton et al. (1985)	$E_s= 3.5N$, MPa	473	294	360
$E_s= 40N$, MPa		5,400	3,360	4,117	
	Papadopoulos and Anagnostopoulos (1987)	$E_s= 7.5 + 0.8N$, MPa	183	142	157
Sand with fines	Kulhawey and Mayne (1990)	$E/P_a=5N_{60}$	68	42	51
	Webb (1969)	$E = 3.33 (N + 5)$, tons/ft ² (Clayey saturated sands)	62	45	51
Clean NC Sand	Kulhawey and Mayne (1990)	$E/P_a=10N_{60}$	135	84	103
Clayey sand	Bowles (1996)	$E_s=320(N_{55}+15)$, kPa	95	78	85
Submerged fine to medium sand	Webb (1969)	$E=5(N+15)$, tons/ft ²	143	117	126
Submerged sand	Bowles (1996)	$E_s=250(N_{55}+15)$, kPa	75	61	66
NC Sands	Bowles (1996)	$E_s=500(N_{55}+15)$, kPa	149	122	132
	Bowles (1996)	$=7,000\sqrt{N_{55}}$, kPa	270	215	235
	Bowles (1996)	$E_s=6,000N_{55}$, kPa	890	564	685
Clean fine to medium sands and slightly silty sands	(FHWA-IF-02-034)	$E=700 (N_1)_{60}$, kPa	174	73	110

Table 5-6 Summarized calculations of elastic modulus for the top two topmost granular soil layers at the project site (using CPTu data)

Soil Type	Reference	Equation	Layer 1 [TSF]	Layer 2 [TSF]	W. Avg. [TSF]	
Sand	Buisman (1940):	$E_s = 1.5q_c$	112	83	94	
	Trofimenkov (1964):	$E_s = 2.5q_c$ (lower limit)	188	138	156	
		$E_s = 5q_c$	375	275	312	
	DeBeer (1965)	$E_s = 1.5q_c$	113	83	94	
	Bachelier and Parez (1965)	$E_s = \alpha q_c; \alpha = 0.8$	60	44	50	
		$E_s = \alpha q_c; \alpha = 0.9$	68	50	56	
	Vesić (1970)	$E_s = 2(1 + Dr^2)q_c$	213	132	162	
	Sanglerat et al. (1972)	$q_c < 50$ bars $\alpha = 2$; $q_c > 100$ bars		131	107	116
		$\alpha = 1.5$ Greek Practice				
	DeBeer (1974b)	$E_s = 1.5q_c; q_c > 30$ kg/cm ² $E_s = 3q_c; q_c < 30$ kg/cm ²		113	83	94
Trofimenkov (1974)	$E_s = 3q_c$	225	165	187		
Schmertmann (1970)	$E_s = 2q_c$	150	110	125		
Clean NC Sand	Vesić (1970)	$E = (1 + Dr^2)q_c$	107	66	81	
	No author	$E = 2$ to $4 q_c$	150	110	125	
Clayey sand	Bowles (1996)		225	165	187	
		$E_s = 3$ to $6 q_c$	450	330	375	
	Bachelier and Parez (1965)		285	209	237	
		$E_s = \alpha q_c \alpha = 3.8-5.7$	428	314	356	
Silty sand	No author		75	55	62	
		$E = 1$ to $2 q_c$	150	110	125	
	Bachelier and Parez (1965)	$E_s = \alpha q_c \alpha = 1.3-1.9$	98	72	81	
Submerged sand	Webb (1969)	$E_s = 2.5(q_c + 30)$, tsf	263	213	231	
	Bowles (1996)	$E_s = F q_c$	---	---	---	
		$e = 1.0 \quad F = 3.5$ $e = 0.6 \quad F = 7.0$	525	385	437	
Submerged clayey sand	Webb (1969)	$E_s = 1.67(q_c + 15)$, tsf	150	117	129	
NC Sands	Schmertmann et al. (1978)	$E_s = 2.5q_c \quad L/B = 1$ to 2	188	138	156	
	Bowles (1996)	$E_s = 8,000\sqrt{q_c}$	6,928	5,933	6,302	

The computed values from the previous tables are summarized in Figure 5-9. The figure shows the average correlated values of E (i.e., Young's modulus) from field tests (i.e., CPT, SPT, and DMT) for layers one and two, which are the layers within the vertical stress influence zone.

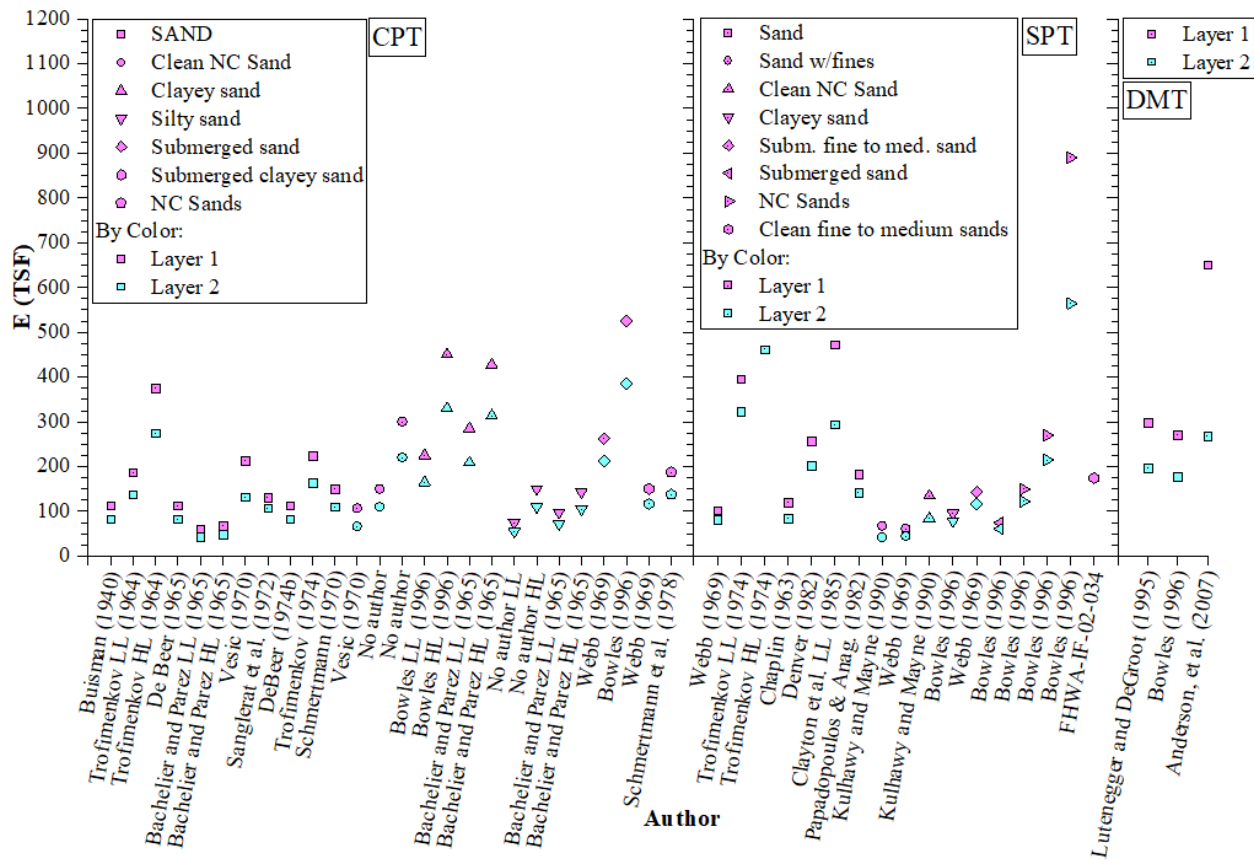


Figure 5-9. Computed values of E for both layers using published correlations with field tests (SPT, CPT, DMT)

Figure 5-10 presents weighted average values for layers one and two, which are compared with the measured values obtained from the conical load test. The weighted average values are based on the incremental vertical stresses that each layer is carrying. For the field measurements (presented as shaded areas in the figure), the calculation was conducted using a uniaxial stress approach that was proposed to estimate the Young's modulus from the conical load tests as a single column of soil. Another method presented in the figure for the calculation of E was based on the theory of elasticity equations. The authors found that the methods developed by Trofimenkov (1964), lower limit, Vesić (1970), and Schmertmann et al. (1978) for the CPT correlations, provided good agreement versus the measured values. Regarding the SPT correlations, most methods provided conservative estimates of the modulus E . The authors attribute this to the fact that the average axial strain along the profile (computed in the order of 0.1% or less) mobilized during the conical load tests are smaller than those that are typically mobilized by field tests including SPTs, CPTs, and DMTs. The definition of soil stiffness greatly depends on the amount of strains mobilized by the given loading conditions, in this case for the conical load arrangement. The authors found that the following correlations for the calculation of elastic modulus provided conservative estimates of the soil stiffness when compared versus those measured with the conical load tests. Using the following correlations, if the input parameters come from reliable field tests, immediate settlements calculations should provide satisfactory results, particularly if those are supplemented and confirmed with well-calibrated numerical models:

- i. Using the results of SPT tests: Webb (1969), Chaplin (1963), Papadopoulos and Anagnostopoulos (1987), Kulhawy and Mayne (1990), Bowles (1996), FHWA – IF – 02-034.
- ii. Using the results of CPT tests: Buisman (1940), DeBeer (1965), Bachelier and Parez (1965), Vesić (1970), Sanglerat et al. (1972), DeBeer (1974), Schmertmann (1970), and Schmertmann (1978).
- iii. Using the results of DMT tests: Lutenegger and DeGroot (1995) and Bowles (1996).

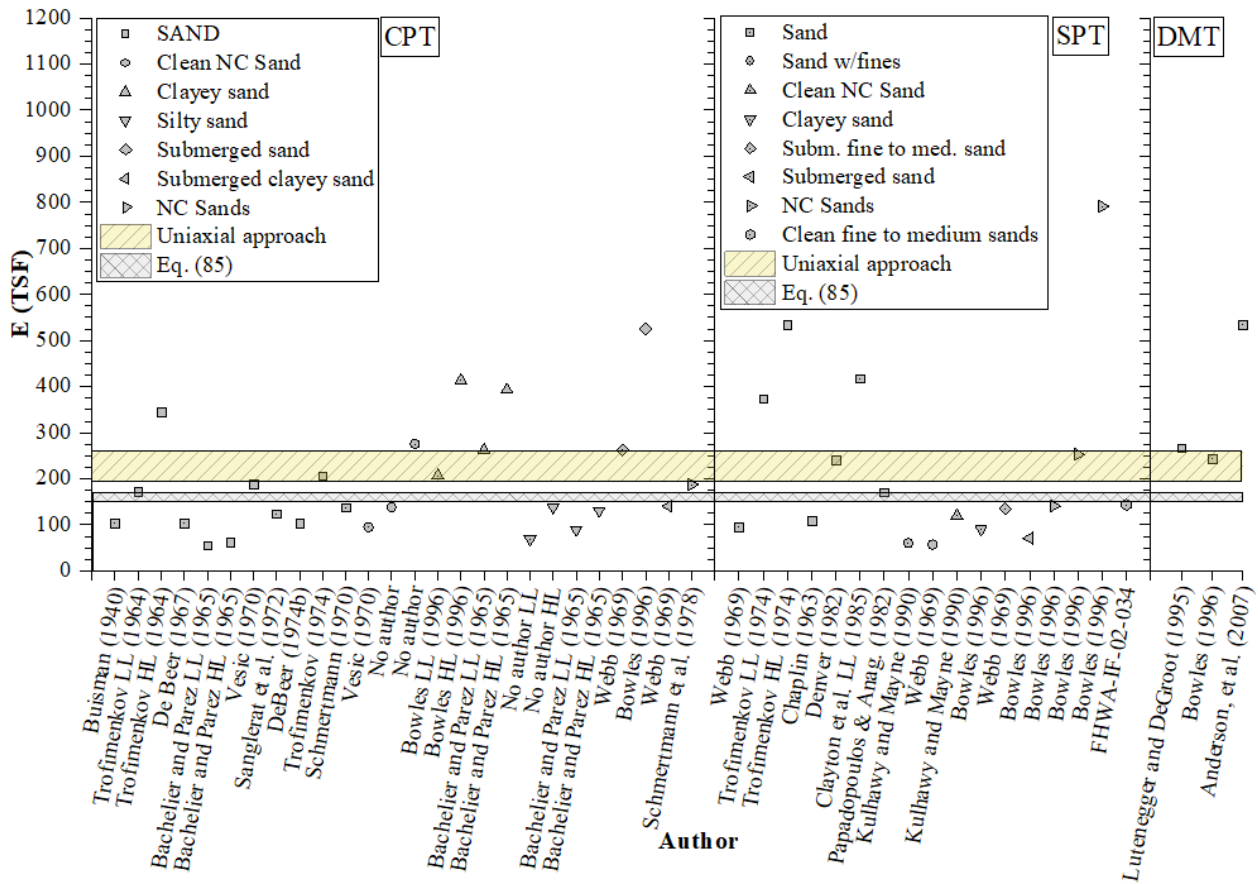


Figure 5-10 Average values of E for the topmost sandy layers one and two compared with the range of Young's modulus measured with the conical load tests

5.7 Immediate Settlement Using Elastic Approaches and Field Test Correlations

Most of the methods available in current practice consider the geometry of the footing (i.e., applied loading) as square or circular. Herein, the stress distribution is converted to an equivalent uniform circular load to calculate immediate settlements. Figure 5-11 shows the results of immediate settlement methods that were presented in CHAPTER 2. Regardless of the influence zone specified for any specific method, an influence zone of 30 ft was adopted as the compressible layer for the following calculations. The Young's moduli adopted for each layer are also shown in the figure,

which were defined from field correlations mainly based on the predominant material type. The conical load testing procedure provided a relatively conservative estimate of the immediate settlements at the project site in relation to those computed with other published methods. The authors recommend the use of this type of test to confirm immediate settlements in geotechnical projects in Florida. Conical load tests constitute a straightforward, fast, and reliable way to confirm the amount of immediate settlements expected in a given project, as long as shallow loading conditions are applied and the expected mobilized strains in the project are in the same order of magnitude as those mobilized during the conical loading (i.e., in the order of 0.1% or less, which implies small strain behavior is important).

It is important to note that the value computed with the DMT-based method use the constrained modulus (M) directly in the calculation, which is based on oedometric compressibility stress paths (i.e., not necessarily the same condition during conical load testing). Using CPTu correlations, the estimations are within the measured threshold and the authors find those methods suitable for the conditions of loading and subsurface presented in this report. The elastic approach methods, which strongly depend on the selection of Young's modulus, showed reasonable correlation with the measured values. Although different assumptions were required for each method based on the theory of elasticity (e.g., soil stiffness and equivalent thickness for the loading material), the estimated values showed reasonably good match with respect to measured values.

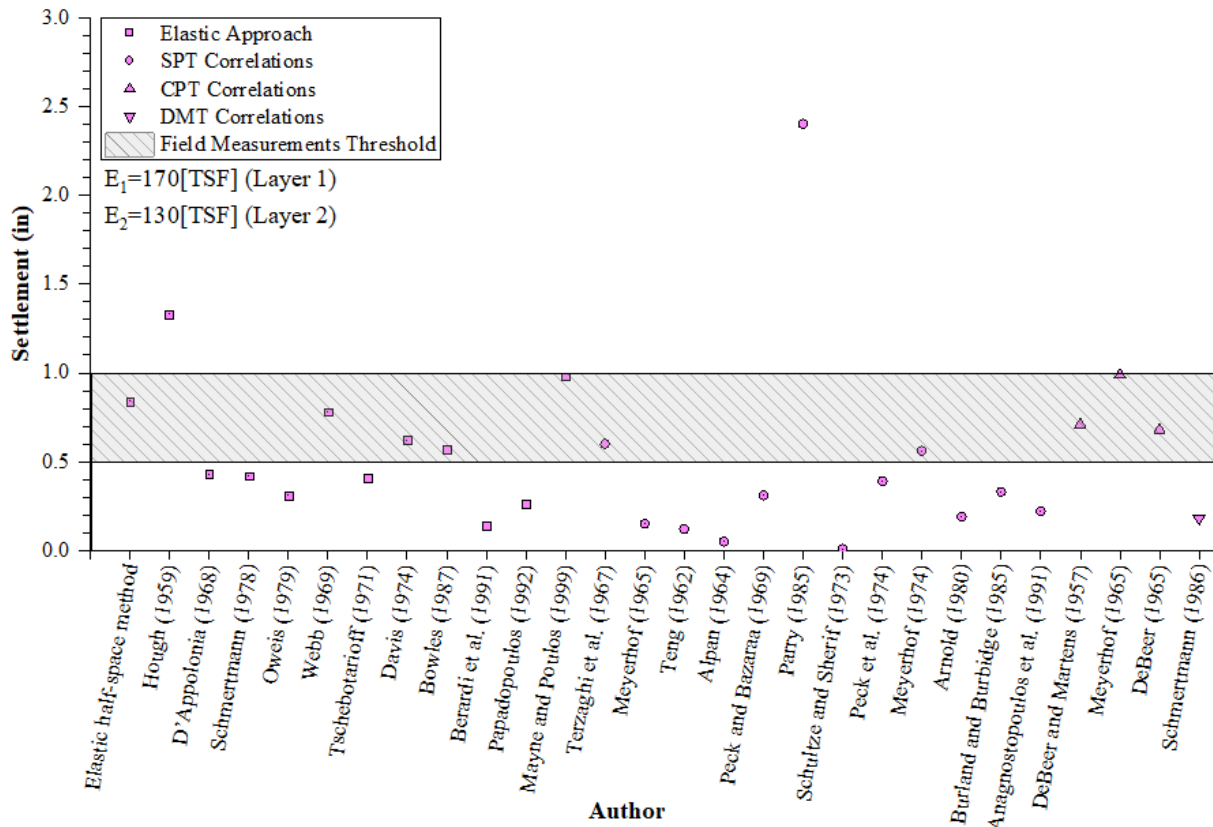


Figure 5-11. Computed immediate settlements using published methods and field test-based methods

5.8 Numerical Finite Element Simulations of Conical Load Tests

PLAXIS2D was the numerical platform selected to simulate the conical loading sequence followed in this project. Figure 5-12 shows the axisymmetric finite element mesh used to reproduce the tests. 15-node type elements were used to increase the number of Gaussian points in the model and to enhance the accuracy of the results. The dimensions adopted for the model were 197 ft (60 m) height by 394 ft (120 m) width. Boundary conditions were set restraining the lateral movement in the vertical boundaries of the model and both vertical and horizontal movements on the horizontal bottom boundary. The left-hand side boundary is considered an axis of symmetry, per definition of “axisymmetric” model. The site-specific location of the water table was also considered in the model. It was located at 3 ft (0.9 m) depth as confirmed with piezometric data and was used to evaluate porewater pressure generation and potential consolidation for a total of 100 days as a result of conical load testing. The initial phase in the model was determined using K_0 conditions to initialize the stress field and match the in situ soil conditions. Then, the loading sequence followed in the field was reproduced in the numerical simulations using sand soil clusters in a total 16 construction loading steps. Figure 5-13 shows a detailed view of the conical loading mesh followed in the model to represent as close as possible the construction steps followed during the conical load tests No. 1 through 3 at the UCF site. The loading material was considered as elastic.

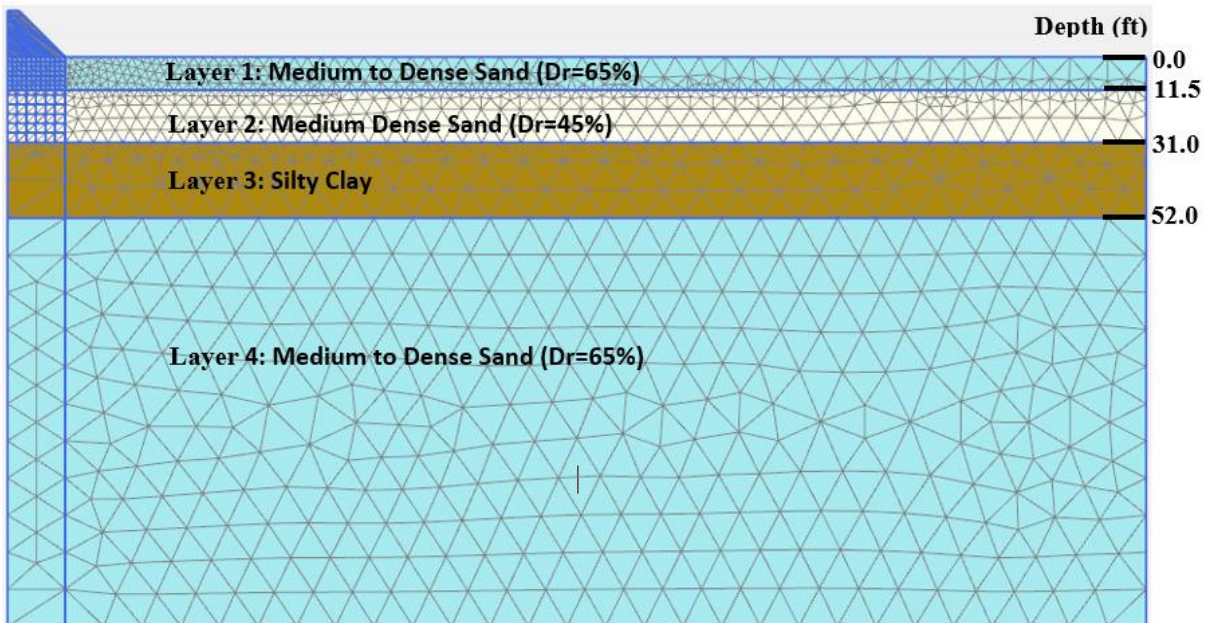


Figure 5-12. Axisymmetric finite element model built in PLAXIS2D to reproduce the conical load tests performed at the UCF site

Two types of soil models, hardening soil and hardening soil small, were used to compare the results of the conical load tests presented in CHAPTER 3. Brinkgreve et al. (2010) stated the importance of a judicious selection of constitutive soil parameters informed with high quality field and laboratory tests to guarantee accurate computation of ground surface settlements using finite element models.

The formulation of both soil models is the hyperbolic relationship between the vertical strain (ϵ_1) and the deviatoric stress (q) in triaxial loading. The hyperbolic relationship is defined with the asymptotic value of the shear strength (q_a) and the initial stiffness (E_i) as is shown in Eq. (113).

$$-\epsilon_1 = \frac{1}{E_i} \frac{q}{1 - q/q_a} \quad \text{for: } q < q_a \quad (113)$$

In the previous equation and following tables, E_i is related to the confining stress-dependent stiffness modulus (E_{50}), and E_{50} is a function of the reference stiffness modulus (E_{50}^{ref}). The reference confining pressure (p^{ref}) was set as 100 stress units default setting in PLAXIS 2D. The cohesion (c), friction angle (ϕ), the minor principal effective stress (σ'_3), and the stress dependency power (m) were defined for sands and silts. For unloading and reloading stress paths, the stress-dependent stiffness modulus E_{ur} is also required. This value is similar to E_{50} , but the only difference is that it requires the reference Young's modulus for unloading and reloading (E_{ur}^{ref}) instead of E_{50}^{ref} . The oedometer loading modulus ($E_{\text{oed}}^{\text{ref}}$) in the soil model is considered as the tangent modulus at the reference pressure (p^{ref}).

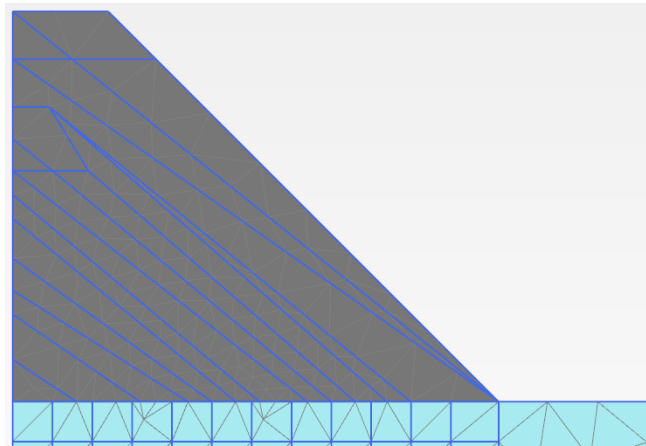


Figure 5-13. Conical loading soil cluster mesh built in a stage construction sequence

The parameters of the hardening soil model (HS) for the topmost alluvium sand materials were computed from the original recommendations issued by the model developers and those proposed by Brinkgreve (2018). The parameters for the fine grained materials are summarized in the conference paper by Nassiri et al. (2020). The HS parameters used for the numerical simulations are summarized in Table 5-7. For the sandy materials, the parameters presented by Brinkgreve (2018) were adjusted according to specific site conditions found at the UCF site. The parameters listed in the table account for the fine content of the sandy soil layers (approximately equal to 30%) and its influence on the stiffness and strength soil properties in relation to other clean sands reported in the technical literature.

Table 5-7. Hardening soil model parameters used in the numerical simulations

Parameter	Unit	HS parameters suggested by Brinkgreve (2018)			Model Parameters in Plaxis 2D Conical Load Modeling		
		Loose	Medium	Dense	Layers 1 & 4 Dr=65%	Layer 2 Dr=45%	Clay
E_{50}^{ref} ($p_{ref} = 100kPa$)	ksf kN/m ²	420 20,000	625 30,000	835 40,000	690 33,000	480 23,000	60 3,000
E_{ur}^{ref} ($p_{ref} = 100kPa$)	ksf kN/m ²	1,250 60,000	1,880 90,000	2,505 120,000	2,170 104,000	1,505 72,000	190 9,000
E_{oed}^{ref} ($p_{ref} = 100kPa$)	ksf kN/m ²	420 20,000	625 30,000	835 40,000	690 33,000	480 23,000	60 3,000
c'	ksf	0	0	0	0	0	0.21
	kN/m ²	0	0	0	0	0	10
φ'	°	30	35	40	36	33	27
ψ	°	0	5	10	7	3	1
v_{ur}	-	0.2	0.2	0.2	0.2	0.2	0.2
m	-	0.5	0.5	0.5	0.5	0.5	1
K_0^{nc}	-	0.5	0.43	0.36	0.41	0.46	0.55
R_f [-]	-	0.9	0.9	0.9	0.9	0.9	0.9

The hardening soil small (HSS) model proposed by Benz (2007), the second soil model evaluated in this report, accounts for the degradation of the soil shear stiffness and captures the stiffness transition from very small to large strains (i.e., small strain soil behavior). The HSS models adequately the entire soil response from the wide range of strains induced by the conical loading tests. Brinkgreve et al. (2010) presented a series of correlations for quartz sands based mostly on the definition of relative density. These correlations were used to determine the constitutive parameters for the HSS model. The calculation of relative density from field tests was conducted following the recommended correlations presented in previous sections of this report.

Table 5-8 lists HSS model parameters used in the numerical model, obtained from the expression presented by Brinkgreve et al. (2010). These expressions are listed in the first column of the table and are considered as first approximation for the calculation of soil parameters, that in addition to other laboratory tests, can be used for practical purposes. Recall that the relative density plays an important role when evaluating ground surface settlements in predominant granular soil conditions. Similarly to the parameters for the HS model, small variations of the calculated stiffness and strength parameters were adjusted to consider the fine content in the granular soil material.

Table 5-8. Hardening soil small model parameters used in the numerical simulations

Equation	Definition	Layers 1 & 4 Dr=65%	Layer 2 Dr=45%	Clay
$E_{50}^{ref} = 60,000Dr/100$ [kN/m ²] (ksf) adopted	Secant stiffness in standard drained triaxial test	39,000 (815) 36,000 (750)	27,000 (565) 25,000 (525)	3,000 (65)
$E_{oed}^{ref} = 60,000Dr/100$ [kN/m ²] (ksf) adopted	Tangent stiffness for primary oedometer loading	39,000 (815) 36,000 (750)	27,000 (565) 25,000 (525)	3,000 (65)

$E_{ur}^{ref} = 180,000Dr/100$ [kN/m ²] (ksf) adopted	Unloading/reloading stiffness.	117,000 (2,445) 108,000 (2,255)	81,000 (1,695) 75,000 (1,565)	9,000 (190)
$G_0^{ref} = 60,000 + 68,000Dr/100$ [kN/m ²] adopted	Reference shear modulus at small strains	104,200 (2,175) 100,000 (2,090)	90,600 (1,895) 90,000 (1,880)	64,000 (1,340)
$m = 0.7 - Dr/320$ [-]	Power for stress-level dependency of stiffness.	0.5	0.56	1
$\gamma_{0.7} = (2 - Dr/100) \cdot 10^{-4}$ [-]	Threshold shear strain	1.35E ⁻⁴	1.55E ⁻⁴	5.00E ⁻⁴
$\varphi' = 28 + 12.5Dr/100$ [°] adopted	Effective angle of internal friction	36	34 33	27
$\psi = -2 + 12.5Dr/100$ [°]	Angle of dilatancy	6	4	1
$R_f = 1 - Dr/800$ [-]	Failure Ratio	0.92	0.94	0.90

Using the parameters listed in Table 5-7 and Table 5-8, sand and clay soil layers were studied numerically using the laboratory testing module included in the numerical platform PLAXIS2D. Two numerically simulated laboratory testing environments were setup using PLAXIS: oedometer and triaxial tests. The numerically simulated laboratory tests were carried out using a representative effective vertical stress (σ'_v) computed in the middle of each layer and assuming a unit weight of 120 pcf. Recall that the water table was located at approximately 3 ft below the ground surface. The relative density used for the cone (i.e., conical loading model presented in Figure 5-13) was defined using sand cone tests at selected loading stages during the test. The measured unit weights for the sand cone tests were discussed in CHAPTER 3. A representative unit weight of 100 pcf was adopted for the numerical model. Table 5-9 lists the earth coefficients at rest, total and effective stresses, and hydrostatic porewater pressures computed at mid-height of each soil layer.

Table 5-9. Parameters used for the numerically simulated laboratory tests

Layer	H (ft)	M.L.D (ft)	σ_v (psf)	U_0 (psf)	σ_v' (psf)	σ_v' (kPa)	K_0	σ_H' (psf)	σ_H' (kPa)
1	11.5	5.75	690.0	171.6	518.4	24.9	0.41	213.7	10.3
2	19.5	21.25	2,550.0	1,138.8	1,411.2	67.7	0.46	642.6	30.8
3	21	41.5	4,980.0	2,402.4	2,577.6	123.7	0.55	1,417.7	68.0
4	13	58.5	7,020.0	3,463.2	3,556.8	170.7	0.41	1,466.2	70.4

Note.- M.L.D. (Mid-layer depth)

For the sandy materials, the numerically simulated triaxial tests were divided into the following two types: (i) isotropically consolidated undrained triaxial compression (CU) test to study the stiffness degradation and assure decoupling of the stiffness matrix for $\Delta\varepsilon_v=0$ (Kim 2011) and (ii) K_0 consolidated- drained triaxial compression (CKD) test to study the behavior of the sands under actual in situ conditions. The computed oedometer and drained triaxial compression tests for the sandy materials are presented in Figure 5-14. The figure shows how the behavior of both soil models was very similar, except by those computed with the HS model which displayed a more dilative behavior. In the figure can be seen that the compressibility of the modeled sandy soils decreased with the increase of vertical effective stress and depth of the soil layer. As expected, layers 1 and 4 had different soil responses despite the fact that input constitutive parameters used for both soils were equal. The confinement pressures, a main variable of the HS and HSS

constitutive relations coded in PLAXIS2D, computed for layer 4 were larger than those for layer 1 (see Table 5-9), resulting in larger strength and stiffness.

Figure 5-15 shows the results of the numerically simulated oedometer and undrained triaxial compression tests carried out for the clayey material (i.e., soil layer 3) using HS and HSS. The numerically simulated oedometer test computed with both soil models had negligible differences. On the other hand, the numerical triaxial test showed noticeable differences between soil models, more evident at small strain levels. Recall that HS model lacks of a constitutive equation to capture small strain soil behavior, and a constant shear stiffness is used to model the wide range of strain levels of soils. Although the deviatoric stress ($\sigma_1 - \sigma_3$) and the excess porewater pressure (Ue) converged to similar values of 2.25 ksf (110 kPa) and 0.45 ksf (21.5 kPa), respectively, the stiffness that the HSS model displayed was larger than the stiffness computed with the HS model.

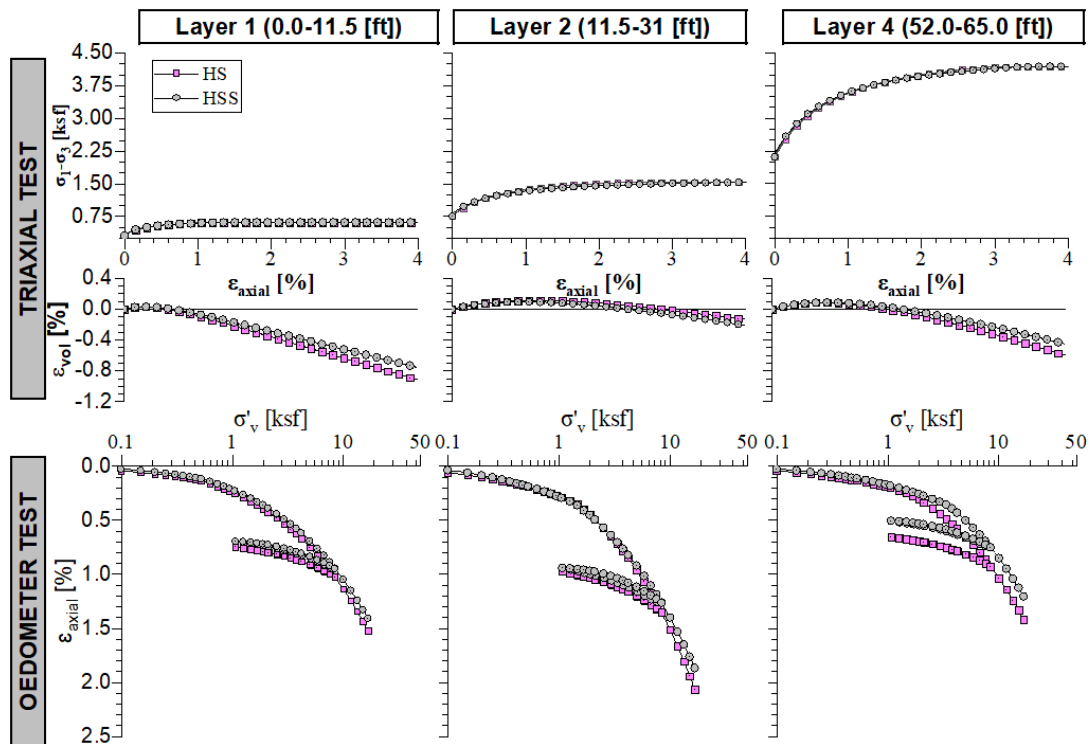


Figure 5-14. Computed response of sandy materials using numerically simulated: (a) drained triaxial compression test and (b) oedometer tests

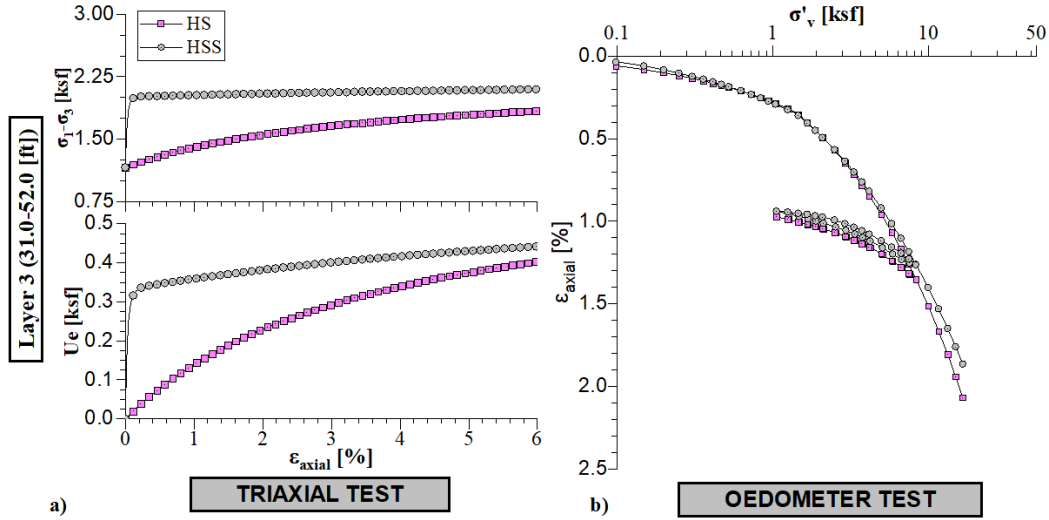


Figure 5-15. Computed clay response numerically simulated: (a) undrained triaxial compression and (b) oedometer tests

Figure 5-16 illustrates the small strain behavior adopted in this report for the determination of the HSS parameters. Figure 5-16a presents the shear stiffness degradation curves computed based on the results from the undrained triaxial compression tests. This was done by assuming that coupling moduli J_v and J_s were very large and a relationship between the deviatoric stress and the secant shear modulus, G_{sec} , can be derived independent of the increase in mean normal effective stress as presented in Eq. (114).

$$\begin{Bmatrix} \Delta \epsilon_{vol} \\ \Delta \epsilon_{sh} \end{Bmatrix} = \begin{bmatrix} 1/K & 1/J_v \\ 1/J_s & 1/3G \end{bmatrix} \begin{Bmatrix} \Delta p' \\ \Delta q \end{Bmatrix} \rightarrow G_{sec} = \frac{\Delta q}{3\epsilon_{sh}} \text{ when } J_v \text{ and } J_s \rightarrow \infty \quad (114)$$

Figure 5-16b presents the stiffness degradation curves normalized with respect to the shear modulus at very small strains, G_0 for soil layers 1 and 2. These curves were computed using the numerically simulated undrained triaxial compression tests. The figure also includes normalized stiffness degradation curves presented by Darendeli (2001) and Ishibashi and Zhang (1993) for a mean normal effective stress, p' , of 20 kPa (417 psf). Negligible differences between computed degradation curves versus those determined from semi-empirical correlations are observed in the figure. The stiffness degradation curves for sandy soils are highly dependent on the confining pressure. This behavior is limited to low values of confinement pressure. According to Guerreiro et al. (2012), confining pressures lower than 4.2 ksf (200 kPa) will yield similar degradation curves.

Based on the previously discussed field correlations, a value of G_{sec} equal to 41,000 kPa and 62,000 kPa was computed for layers 1 and 2, respectively, corresponding to very small shear strain values (i.e., lower than 1×10^{-5}). Computed secant shear moduli reasonably matched those determined using the Seed and Idriss (1970) correlation presented in Eq. (107). Soil parameters were adjusted to account for the fine contents of the sandy materials at the conical loading test location.

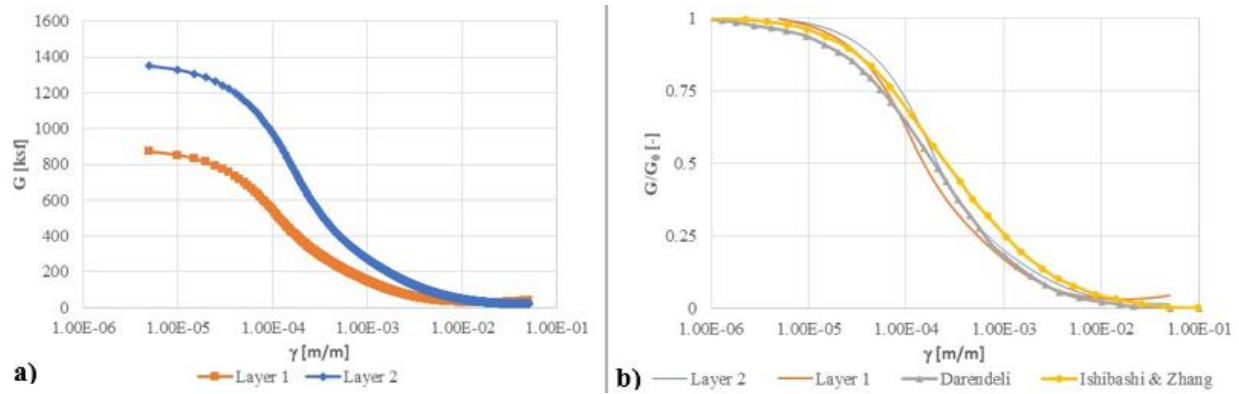


Figure 5-16. Small strain soil behavior: (a) computed shear stiffness degradation curves for layers 1 and 2 and (b) normalized stiffness degradation curves of sandy materials published in the technical literature

In addition, the very small strain shear modulus, G_0 , was verified using the HSS parameters presented in Table 5-8 and the following equation, which denotes the degradation of the shear modulus in terms of the cohesion, friction angle, radial effective stress, reference stress, and stress level dependency constant as proposed in HSS formulation (Brinkgreve 2018).

Table 5-10 lists the parameters needed for the computation of G_0 using the following equation:

$$G_0 = G_0^{ref} \left(\frac{c \cdot \cos\phi - \sigma'_3 \sin\phi}{c \cdot \cos\phi + p^{ref} \sin\phi} \right)^m \quad (115)$$

Table 5-10. Small strain shear modulus parameters computed using HSS model

Layer	H (ft)	σ'_v (psf)	K_0	σ'_H (psf)	m	ϕ	c (psf)	G_0^{ref} (ksf)	G_0 (ksf)	G_0 (kPa)
1	11.5	518.4	0.41	213.7	0.5	36	0	2.10E+03	671.7	32,158.7
2	19.5	1,411.2	0.46	642.6	0.56	33	0	1.88E+03	971.5	46,515.2
3	21	2,577.6	1.00	2,577.6	1	27	209	1.34E+03	1,162.1	55,642.0
4	13	3,556.8	0.41	1,466.2	0.5	36	0	2.10E+03	1,759.3	84,235.6

Table 5-11 lists computed values of G_0 using the numerically simulated triaxial tests and Eq. (115) alongside with the difference between both computed values for layers 1 and 2. Both layers presented differences lower than 25%. This difference is attributed to the adopted p^{ref} value of 100 kPa which is lower than the confinement pressure used in the laboratory testing module of PLAXIS2D.

Table 5-11. Differences between numerically simulated G_{sec} and G_0

Layer	Using Table 5-8		Using PLAXIS 2D		ΔG_0 (kPa)	%
	G_0 (ksf)	G_0 (kPa)	G_{sec} (ksf)	G_{sec} (kPa)		
1	671.7	32,158.7	861.0	41,000.0	8,841.3	21.6
2	971.5	46,515.2	1,302.0	62,000.0	15,484.8	25.0

5.9 Results of the Numerical Simulations

5.9.1 Incremental Vertical Stress Variation due to Conical Load Tests

Figure 5-17 shows contours of cartesian vertical effective stresses using HS and HSS for the final conical loading stage. Both constitutive soil models computed similar distributions of vertical effective stresses throughout the soil layers, with some minor differences observed near the cone and toward the superficial sandy layer. Figure 5-18 shows the variation of vertical effective stresses induced by the conical load test versus depth at the centerline of the model (i.e., axis of symmetry). The results presented in the figure were also computed at the final stage of the conical load test. The figure also shows a 10% in situ vertical effective stress criterion (i.e., $0.1\sigma'_v$), presented to determine the influence zone of the conical loading using the numerical simulations. Both soil models intercept the $0.1\sigma'_v$ at approximately 28 ft (8.5 m). Although the weight and shape of conical loading material used in the numerical models are the same, minor differences were observed in the stress distribution at the ground surface. These differences are attributed to the small strain soil behavior included in the constitutive formulation used by the HSS model. The underlying assumption of the stiffness of the loading material causes changes in the computation of influence zones and stresses at the ground surface as previously discussed by Mayne and Poulos (1999) for soils under similar loading conditions. Conical load-induced settlements largely depend on the stiffness of the loading material, which influences the stress distribution on the underlying soils. These effects were parametrically studied by Nassiri et al. (2020) in the conference paper included in APPENDIX B.

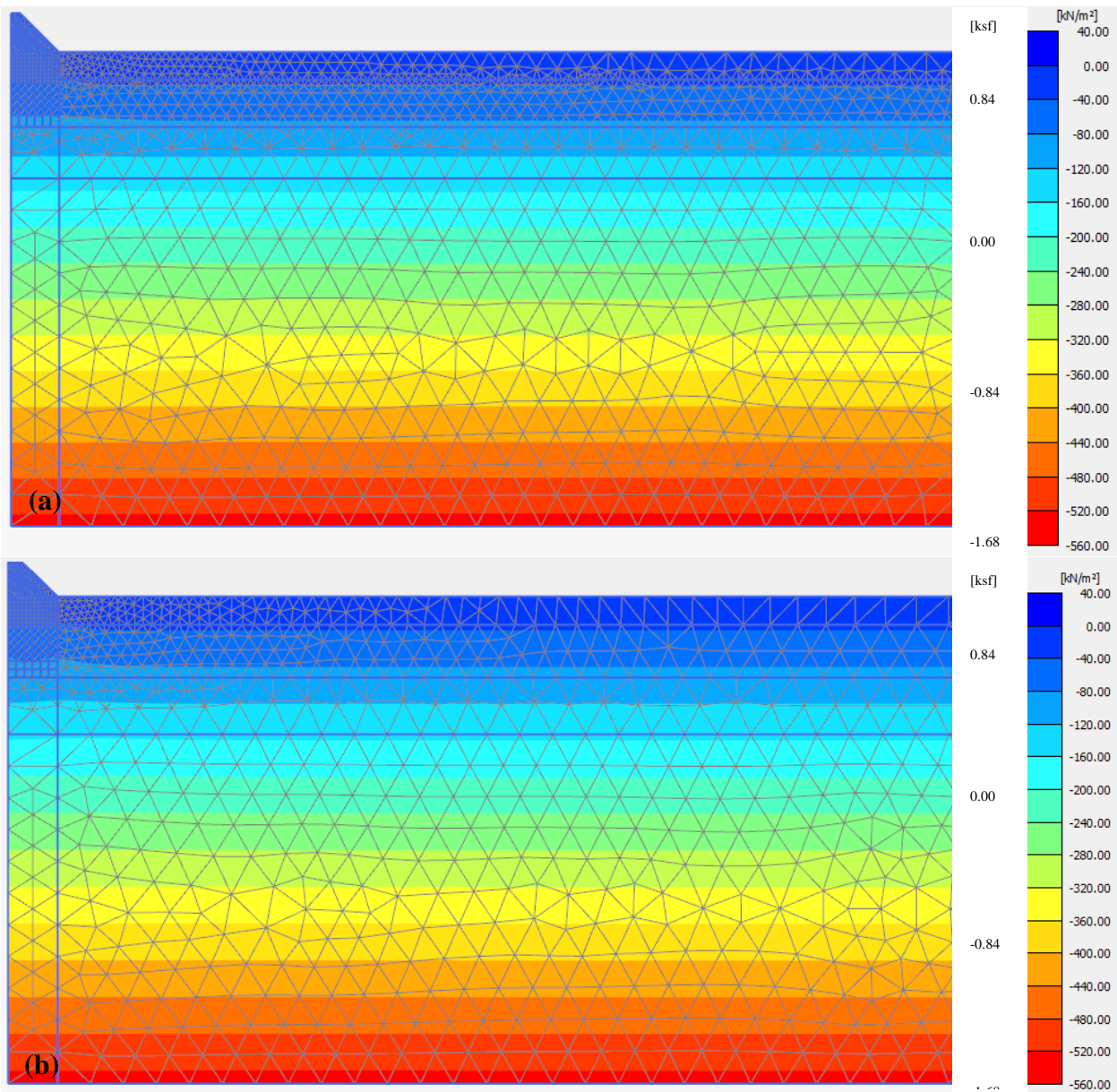


Figure 5-17. Contours of cartesian vertical effective stress at the end of conical load testing (a) results using HS model and (b) results using HSS model

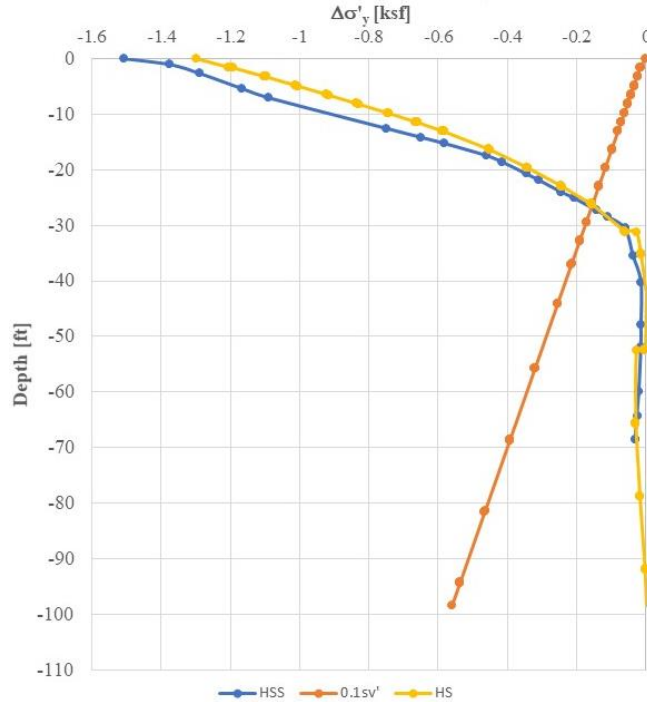


Figure 5-18. Variation of vertical effective stress with depth for the definition of conical load test influence zone with HS and HSS models

5.9.2 Distribution of Vertical Stresses and Settlement at the Ground Surface

Figure 5-19 presents the contact vertical pressure computed with HS and HSS at the final stage of the conical load test varying with the distance from the center of the cone. The figure also shows the vertical contact pressure measured in the field at the centerline of the cone. The variations in vertical pressure are associated with the differences in constitutive formulations adopted by the HS and HSS. Recall that HSS accounts for the small strain soil behavior. Vertical pressures computed with HS and HSS models reasonably matched the measured contact pressure of the conical load; the calculation using the HSS model is closer to the measured value. Note also that the variation of the ground surface pressure is highly dependent of the ratio between loading material and soil stiffness (Mayne and Poulos 1999). The hypothetical case of a rigid loading material was also considered to better understand this relationship between the loading material and the underlying soil. The contact vertical pressure obtained under this hypothetical case was uniformly distributed along the ground surface increasing the influence zone presented in the figure. Further details are presented in Nassiri et al. (2020) included in APPENDIX B.

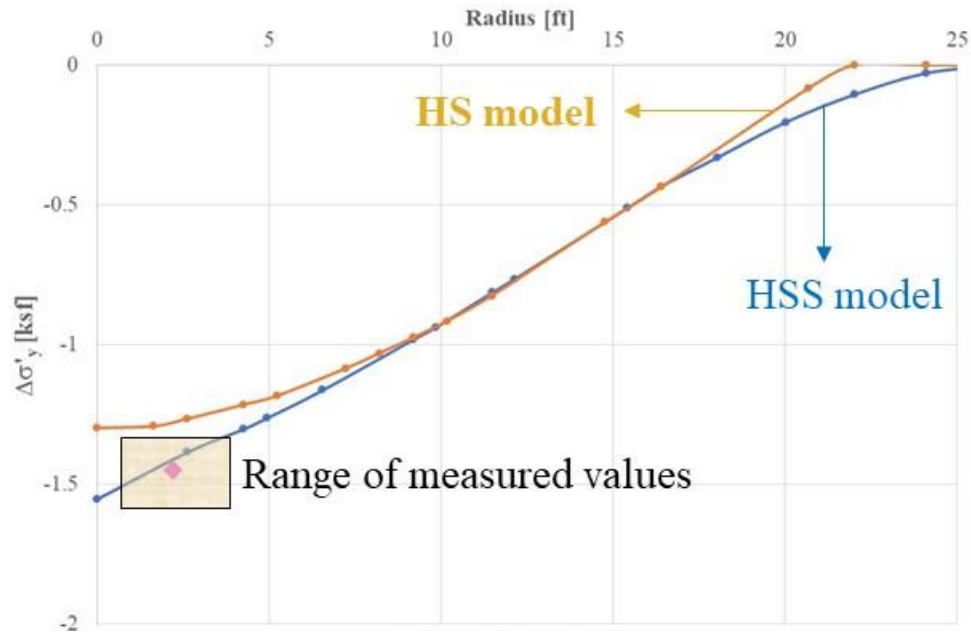


Figure 5-19. Variation of contact vertical stress with distance measured at the centerline of the cone versus that computed with HS and HSS models

Figure 5-20 shows the ground surface settlement troughs computed at the final stage of the conical load test using HS and HSS models. The figure also includes the maximum ground surface settlement measured in the field at the end of the conical load test. Even though the settlement troughs had similar distributions regardless of the model, the maximum ground surface settlement computed using HS model doubled that computed using HSS. The inclusion of small strain soil behavior in the numerical modeling played an important role in the computation of settlements. This effect is better appreciated when computed maximum ground surface settlements with the models are compared with field measurements. The settlement at the centerline of the conical load testing (i.e., approx. 0.75 in) is better predicted with the HSS model. In geotechnical designs, one may argue that the HS model provides a more conservative estimation of settlement.

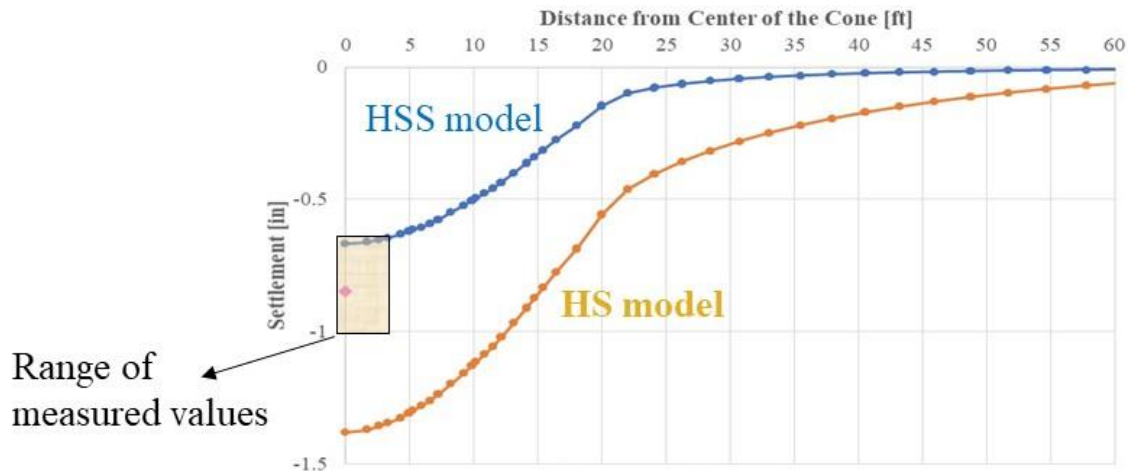


Figure 5-20. Variation of conical load-induced settlement with distance measured at the centerline of the cone versus that computed with HS and HSS models

Figure 5-21 presents contours of vertical strains at the final stage of conical loading. The results are presented for both models: HS and HSS. Larger vertical strains along the depth were computed using the HS model, which confirms its degree of conservatism (see Figure 5-21a). The contribution of the second layer to the overall behavior of the soil due to conical loading is shown in the same figure. Observe the intensity of vertical strain contours in layer 2 on the left-hand side figure. A slight participation of the clay layer in the development of vertical strains is evidenced in the contours with a value of approximately 2.4×10^{-3} computed at the topmost part of the clay layer. This mobilization of vertical strains in the underlying clay does not occur when using the HSS model, as shown in Figure 5-21b. Layers 1 and 2 in the HSS model correctly captured the small strain behavior of the soil causing a stiffer and more realistic response of the soil material. At the center of the cone and at the ground surface, the vertical strain concentration mobilized by conical loading in both models are similar and adopt a value of approximately 5×10^{-3} (or $\epsilon_1 = 0.5\%$). An average value of vertical strains along the conical load test influence zone is 4×10^{-3} and 2×10^{-3} for the results computed with the HS and HSS models, respectively. One more time, larger computed vertical strains were mobilized using the HS model (i.e., certain degree of conservatism was found when ignoring small strain soil behavior). It is important to note that the nonlinearity in the soil response using both models is represented in the constitutive model via a hyperbolic stress-strain relationship as presented in Eq. (113) for a drained triaxial compression test (Brinkgreve 2018). Thus, the larger strains computed using the HS model are a byproduct of a reduced stiffness inherent in the constitutive formulation in relation to more accurate models like HSS that consider small strain soil behavior.

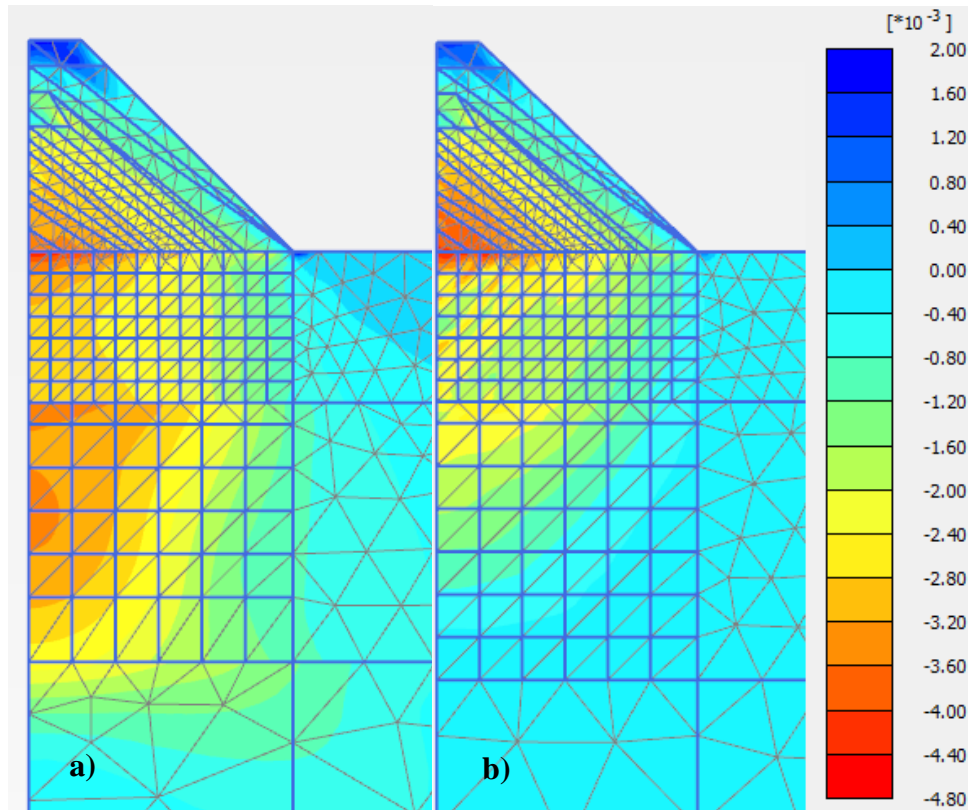


Figure 5-21. Contours of cartesian vertical strains at the final stage of conical loading: (a) results using HS model and (b) results using HSS model

A discussion of the stiffness degradation behavior of soils using the HSS model is presented next. As previously stated, the degradation of the shear modulus in geotechnical projects is a function of the mobilized shear strains caused by the applied loading. Zapata-Medina (2012) explained that the entire degradation curve, also called modulus reduction curve, can be well defined with G_0 and $\gamma_{0.7}$, which are key parameters in the HSS formulation. The level of strains in the soil induced by the construction of different geo-structures coincide with the range of strains that can be reliably measured in advanced laboratory tests (e.g., triaxial tests with internal instrumentation) as is shown in Figure 5-22. For reliable predictions of ground deformations, the very small strain stiffness and its degradation should be considered in the numerical formulation. This is the reason why the authors in general do not recommend Mohr-Coulomb models (i.e., elastic-perfectly plastic formulations) for the calculation of soil deformations since the stress-strain characteristics of soils at strain levels below 0.1% (see that value in Figure 5-22 as a function of the type of structure: foundations, retaining walls, tunnels) cannot be reproduced accurately with such model.

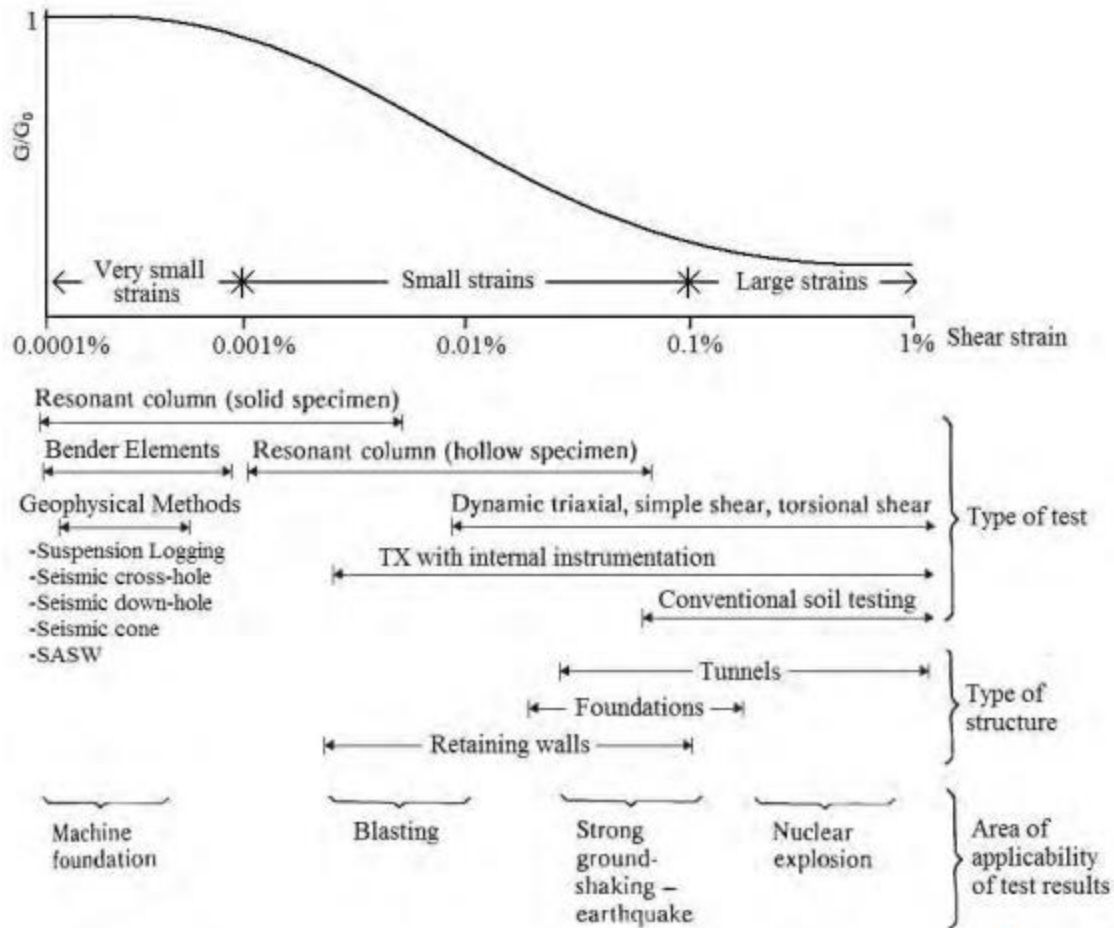


Figure 5-22. Stiffness-strain behavior of soils with typical strain ranges for different testing techniques, geotechnical facilities, and areas of applicability (modified after Atkinson and Salfors, 1991; Mair, 1993 ; Dowding, 2008. From: Zapata-Medina (2012)

Figure 5-23 shows shear strain contours mobilized using both numerical models. Recall that the small strain stiffness behavior just described is not considered in the HS model. Figure 5-23b of mobilized shear strains computed using the HSS model, shows that shear strains approximately vary from 3×10^{-3} (or 0.3%) at the ground surface to approximately zero at a depth of 30 ft (9 m). The higher value, computed at the ground surface, corresponds to a shear modulus of the soil degraded up to $0.1G_0$ at that depth, and $0.2G_0$ at a depth of 16 ft (5 m). This can be demonstrated in the relationship G vs γ schematically shown in Figure 5-22. These analyses are traditionally described in terms of the shear modulus, G , but they can also be described in terms of the Young's modulus, E , by assuming a direct relationship between E , G , and the Poisson's ratio, ν , from the theory of elasticity equation:

$$G = \frac{E}{2(1 + \nu)} \quad (116)$$

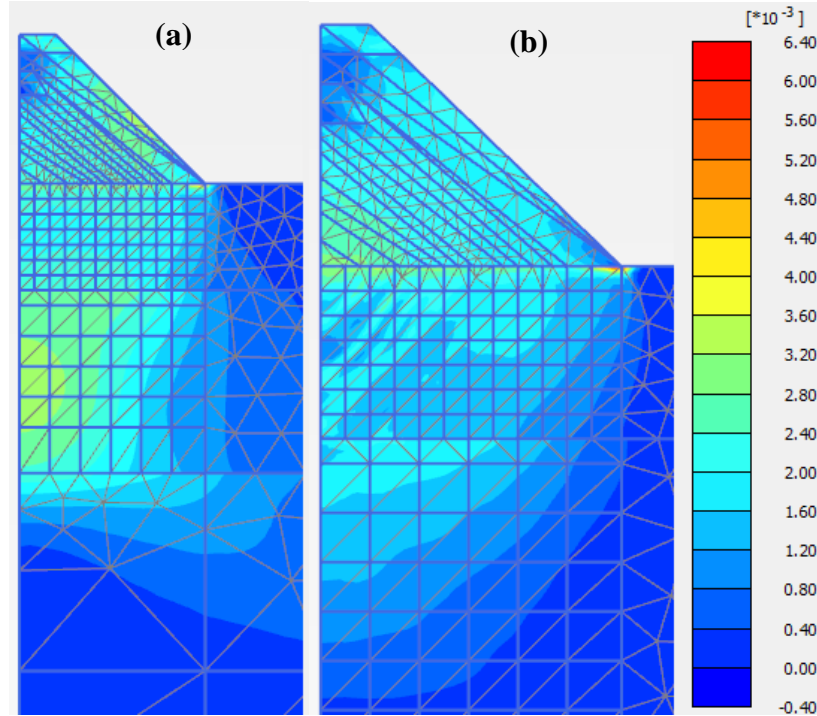


Figure 5-23. Computed shear strain contours induced by conical load testing at final loading stage: (a) results computed with HS model and (b) results computed with HSS model

The computed relative shear stresses (τ_{rel}) for both models are presented in Figure 5-24. Those are defined in the numerical platform as a ratio of the mobilized shear strength, τ_{mob} , and the maximum shear stress, τ_{max} , from a Mohr-Coulomb failure standpoint. The way this is computed in the numerical model is presented in Eq. (117):

$$\tau_{rel} = \frac{\tau_{mob}}{\tau_{max}} = \frac{|\sigma'_1 - \sigma'_3|}{-\frac{\sigma'_1 + \sigma'_3}{2} \sin\phi + c \cos\phi} \quad (117)$$

Figure 5-24 is presented as an indicator of the mobilized stress levels with respect to the failure criterion, which for both models considered herein corresponds to the Mohr-Coulomb failure envelope. The figure shows larger stress concentration values of τ_{rel} for the HS model in relation to those computed with the HSS model. Recall that the geomechanical response is different for both models until failure occurs, even if both models use Mohr-Coulomb as a failure criterion. The figure shows larger plastic strains mobilized by the results computed with the HS model, which leads to a larger ground surface settlement as previously shown in Figure 5-20.

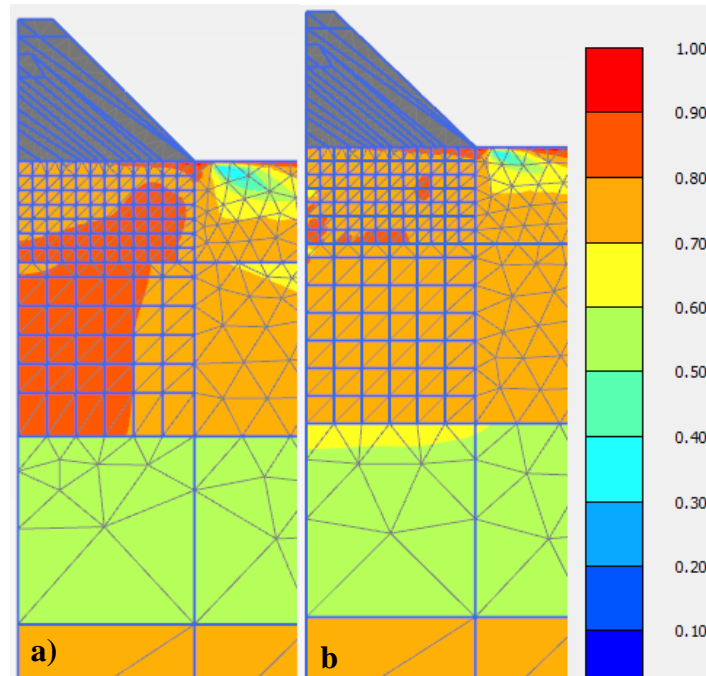


Figure 5-24. Contours of relative shear stresses (τ_{rel}) for the numerical models computed using: (a) HS model and (b) HSS model

5.10 Comparison of Computed Results Versus Field Measurements

Table 5-12 lists the classification of predictions in geotechnical engineering. These categories vary from predictions made before the event, denoted as class A to class C1 for predictions made after the event with some knowledge of available results. In this project, class A prediction models were developed at the early stages of the analyses (see paper APPENDIX B)

Table 5-12. Classification of predictions in geotechnical engineering. From Lambe (1973)

Prediction type	When prediction was made	Results at time prediction made
A	Before event	--
B	During event	Not known
B1	During event	Known
C	After event	Not known
C1	After event	Known

Class A settlement predictions reported by Uribe-Henao et al. (2019) for three constitutive soil models: Mohr-coulomb, Hardening soil, and Hypoplasticity models, ranged from 1 to 1.4 inches. Under the conditions evaluated in Uribe-Henao et al. (2019), the highest settlement was obtained using the Mohr-Coulomb model, while the lowest was reported for the Hypoplasticity model (which also accounts for small strain soil behavior). The variations of measured versus computed settlements presented next correspond to a C1 class prediction according to Lambe (1973).

Figure 5-25 presents the comparison between computed (i.e., using HS and HSS model) and field-measured performance of the three conical load tests. The figure shows the variation of the ground surface immediate settlements in terms of the contact vertical pressures induced by a conical soil arrangement. Recall that the contact vertical pressures were measured using pressure cells placed at approximately 2 ft from the center, while the settlements were measured using average values obtained with settlement plates and confirmed using spider magnets at the cone centerline. The dashed lines labeled as “trendlines” were obtained using second order regressions. Coefficients of correlation, R^2 higher than 0.9 were computed for the three conical load tests. The average response from the three tests labeled as “Trend. Avg.” is shown with a black dashed line. Note that the computed response with the HSS model was closer to the measured values than the computations made with the HS model. The results computed with the HS model overpredicted the overall measured response. The computed maximum settlement with the HS model was approximately 1.4 in (3.5 cm), which is 75% larger than the measured value. This illustrates the point raised by the authors that the computations made with the HSS model represent a more accurate description of the geomechanical response of soils due to conical load testing, but the results with the HS model have some degree of conservatism, as long as the input parameters are calibrated correctly. These differences illustrate the importance of considering the stiffness degradation behavior of soils as small strains are mobilized by constructions. A parametric study shown in APPENDIX B was conducted using the same underlying assumptions and modeling approaches discussed herein. The importance of construction sequence, conical load stiffness, and relative density of the underlying soils on the numerically simulated conical load tests for immediate settlement calculations were parametrically investigated.

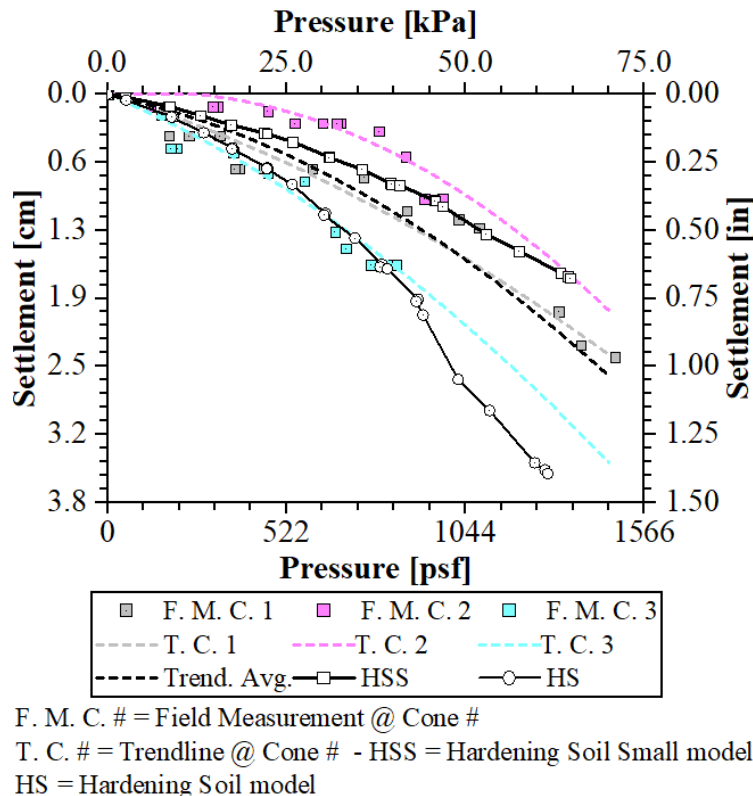


Figure 5-25. Comparison between measured and computed immediate settlements

CHAPTER 6 CONCLUSIONS AND RECOMMENDATIONS

6.1 Research Summary

This report summarized the geotechnical mechanisms that govern immediate settlements measured at the UCF site in Central Florida. The results presented herein provided guidance for practitioners and researchers regarding the most suitable correlations for elastic modulus and immediate settlement procedures that compared well versus measured values with full-scale conical load tests. The report presented a compilation of correlations for modulus elasticity and immediate settlement methods found in the technical literature. Published relationships on the calculation of relative density, friction angle, small strain shear modulus, shear wave velocity, and coefficient of earth pressure at rest are also reviewed in this report. A full-scale field testing and advanced laboratory testing programs were conducted to elucidate field test methods and correlations for the calculation of stiffness parameters for immediate settlement predictions in similar granular soils. Guidance on the calibration of constitutive soil parameters for two soil models: hardening soil and hardening soil small were also presented in this report. The parameters were calibrated from correlations with relative density of the granular soil materials and the models provided a more accurate alternative method for the calculation of immediate settlements.

Recommendations were provided on the proper selection of soil modulus of elasticity at the desired or expected strain levels during field/laboratory testing or during constructions. A detailed analysis was conducted on the piezometric readings related to excess porewater pressure buildup as a result of applied surface loadings from the conical load tests. A clear distinction was issued between changes in the hydrostatic porewater pressures and excess porewater pressures to assess the type and source of settlements. This was done to corroborate not only the extent of vertical stress influence zones due to conical load testing but also to confirm that other time-dependent changes in volume such as consolidation settlements or secondary compression settlements were not measured.

The conclusions drawn herein are only applicable to immediate settlement calculations in similar soils. When consolidation or secondary compression settlements are expected (e.g., generalized presence of clays or organic material in the soil profile), those two components should be added and considered separately. An evaluation of the immediate settlement and soil compressibility responses measured via conical load testing was presented to ultimately conclude that this type of full-scale testing is a soil-structure interaction problem, being the structure the conical load arrangement, where the relative stiffness of the participating components (i.e., soil and structure) play an important role. The interaction of both systems for the calculation of immediate settlements depends greatly on the sequence of loading and strength-stress-strain characteristics of soils and applied loading.

6.2 Concluding Remarks and Recommendations

The following conclusions and recommendations can be drawn from this study:

1. The authors found that the following correlations for the calculation of elastic modulus provided conservative and good estimates of the soil stiffness when compared versus those measured with the conical load tests. Using the following correlations, if the input parameters come from reliable field tests, immediate settlements calculations should provide satisfactory results, particularly if those are supplemented and confirmed with well-calibrated numerical models:
 - Using the results of SPT tests: Webb (1969), Chaplin (1963), Papadopoulos and Anagnostopoulos (1987), Kulhawy and Mayne (1990), Bowles (1996), FHWA – IF – 02-034.
 - Using the results of CPT tests: Buisman (1940), DeBeer (1965), Bachelier and Perez (1965), Vesić (1970), Sanglerat et al. (1972), DeBeer (1974), Schmertmann (1970), and Schmertmann (1978).
 - Using the results of DMT tests: Lutenegeger and DeGroot (1995) and Bowles (1996).
2. The authors found that for the calculation of elastic modulus, and in general for the determination of soil stiffness parameters, the strain level that soil is subjected to causes large impact in the computed settlements since soils reduce their stiffness as a function of the mobilized stresses due to the applied loading. The dependency of the soil stiffness on the strain level, which occurs for shear strains lower than $10^{-3}\%$, plays a very important role in the determination of ground deformations. The inclusion of small strain soil behavior in the numerical framework played an important role in the computation of settlements. This effect was more noticeable when computed maximum ground surface settlement results obtained with the numerical models were compared with field measurements.
3. Excess porewater pressures measured herein did not build up in the sandy soil layers, allowing the conical load sequence to take place by letting dissipation of excess porewater pressures in the silty-sand and sandy-silt layers. Thus, the settlements measured in this report correspond solely to immediate settlements. The numerical models also confirmed that the measured settlements were mostly immediate in nature and are not related to primary or secondary consolidation. The very small range of variation of the inclinometer readings, supports the conclusion that negligible lateral displacements caused by the conical load tests were induced.
4. The authors reported that compressibility of sands with angular-shaped grains with high mica or carbonate contents can display a more compressible response than sands with rounded grains or clean quartz. Sandy soils can be classified according to their level of compressibility as low, medium, and high finding that granular shape and mineralogy can be the cause of their compressibility behavior.
5. The results of properly calibrated geotechnical models reproduced the conical load testing sequence of the full-scale field tests performed at the UCF site reasonably well. The

definition of soil stiffness greatly depends on the amount of strain mobilized by the given loading conditions. The settlement at the centerline of the conical load testing was better predicted (but slightly underpredicted) with the HSS model. The results computed with the HS model overpredicted by approximately 65% the overall measured response. Larger vertical strains were computed using the HS model (i.e., certain degree of conservatism was found when ignoring small strain soil behavior, as long as the input parameters are calibrated correctly). For reliable predictions of ground deformations, the very small strain stiffness and its degradation should be considered in the numerical formulation.

6. The authors recommend the use of the conical load test to confirm immediate settlements in geotechnical projects in Florida. Conical load tests constitute a straightforward, fast, and reliable way to confirm the amount of immediate settlements expected in a given project, as long as shallow loading conditions are applied and the expected mobilized strains in the project are in the same order of magnitude as those mobilized during the conical loading.
7. Numerically simulated oedometer and triaxial tests using HS and HSS showed similar responses to laboratory tests. For the clayey layer, the numerical undrained triaxial compression tests showed noticeable differences between the performance of both soil models, more evident at low strains levels. Even though 100 days were included in the finite element analyses to account for any possible consolidation settlement, the numerical models showed negligible consolidation settlement similar to the observations made in the field that confirmed the very fast dissipation of excess porewater pressures as a result of conical load testing.
8. The soil model parameters that were used in this report, constitute a useful set of parameters that the authors recommend for future use in projects in similar site conditions for the calculation of immediate settlements, mostly in granular soils. Brinkgreve et al. (2010) presented very useful correlations of the parameters for the HSS model with the relative density of the granular soils. These equations can be optimized for local soil conditions and can be adapted to match laboratory testing programs. The recommended parameters for hardening soil (HS) and hardening soil small (HSS) models for future use are presented in the following tables mainly as a function of the relative density of the soil:

Table 6-1. Recommended soil parameters using hardening soil (HS) model

Parameter	Unit	HS parameters suggested by Brinkgreve (2018)		
		Loose Sand	Med. Sand	Dense Sand
$E_{50}^{ref} (p_{ref} = 100kPa)$	ksf (kN/m ²)	420 (20,000)	625 (30,000)	835 (40,000)
$E_{ur}^{ref} (p_{ref} = 100kPa)$	ksf (kN/m ²)	1,250 (60,000)	1,880 (90,000)	2,505 (120,000)
$E_{oed}^{ref} (p_{ref} = 100kPa)$	ksf	420		835

	(kN/m ²)	(20,000)	625 (30,000)	(40,000)
c'	ksf (kN/m ²)	0 (0)	0 (0)	0 (0)
φ'	°	30	35	40
ψ	°	0	5	10
ν_{ur}	-	0.2	0.2	0.2
m	-	0.5	0.5	0.5
K_0^{nc}	-	0.5	0.45	0.4
$R_f [-]$	-	0.9	0.9	0.9

Table 6-2. Recommended equations for hardening soil small (HSS) model in terms of D_r

Equation	Definition
$E_{50}^{ref} = 60,000Dr/100$ [kN/m ²]	Secant stiffness in drained triaxial tests
$E_{oed}^{ref} = 60,000Dr/100$ [kN/m ²]	Tangent stiffness for primary oedometer loading
$E_{ur}^{ref} = 180,000Dr/100$ [kN/m ²]	Unloading/reloading stiffness
$G_0^{ref} = 60,000 + 68,000Dr/100$ [kN/m ²]	Reference shear modulus at small strains
$m = 0.7 - Dr/320$ [-]	Power for stress-level dependency of stiffness
$\gamma_{0.7} = (2 - Dr/100) \cdot 10^{-4}$ [-]	Threshold shear strain
$\varphi' = 28 + 12.5Dr/100$ [°]	Effective angle of internal friction
$\psi = -2 + 12.5Dr/100$ [°]	Angle of dilatancy
$R_f = 1 - Dr/800$ [-]	Failure ratio

9. Vertical effective stresses computed with HS and HSS had similar distributions throughout the soil layers, with some minor differences near the cone centerline and toward the ground surface. Variations in contact vertical pressure were associated with the differences in constitutive formulation adopted by the HS and HSS. Vertical pressures computed with both soil models reasonably predicted the contact pressure of the conical load, where the HSS was the closest to the measured value. Computed settlement troughs using HS and HSS had similar distributions, but maximum ground surface settlements computed using HS model doubled those computed using HSS. The inclusion of small strain soil behavior in the constitutive modeling played an important role in that calculation. This effect was better appreciated when computed maximum ground surface settlements were compared with field measurements, however, the actual measurements exceeded the HSS predictions by 20%. Even though the estimation of soil parameters presented herein were based on correlations with commercially available field tests that are currently performed in the state (mainly SPT, CPT, DMT), valuable information can also be obtained from “seismic” piezocones SCPTu (better known by the authors as “small-strain” piezocones) or other field testing capable of providing information regarding small strain soil behavior in the laboratory (e.g., bender elements in advanced triaxial laboratory tests).

10. Larger vertical strains versus depth were computed using the HS model. Numerical simulations conducted with the HSS model correctly captured the small strain behavior of the soils causing a stiffer, more realistic, response of the material. At the cone centerline and toward the ground surface, the vertical strain concentration mobilized by conical loading in both models were similar. The higher strains computed using the HS model were a byproduct of a reduced stiffness inherent in the constitutive formulation in relation to more accurate models like HSS that consider small strain soil behavior at the stress levels tested.

11. For projects involving multiple stress paths (e.g., excavations, installation of deep foundations, tunnels), or for projects that mobilize wide ranges of shear strains, or simply to evaluate accurately construction-induced ground surface settlements, Mohr-Coulomb-based models tend to oversimplify soil behavior. More advanced constitutive soil models are recommended instead to capture more realistic features of soil response due to construction-induced loadings similar to those tested at this site. In this report, two advanced soil models were used to investigate the soil response due to conical load tests. Conical load-induced ground surface settlements, soil stresses, shear strains, and vertical influence zones were computed using the numerical models and were presented to describe the soil response in terms of immediate settlements.

REFERENCES

AASHTO - LRFD Bridge Design (2017). "American Association of State Highway and Transportation Officials." Washington, DC.

Alpan, I. (1964). "Estimating the settlements of foundations on sands." Civil Eng & Public Works Review/UK/ 59(700).

Anagnostopoulos, A., B. Papadopoulos and M. Kavvas (1991). "Direct estimation of settlements on sand, based on SPT results." Proceedings of the 10th European Conference on Soil Mechanics and Foundation Engineering, Vol. 1, Balkema, Rotterdam, The Netherlands, 293-296.

Andresen, A., and P. Kolstad. (1979). "The NGI 54 Mm Sampler for Undisturbed Sampling of Clays and Representative Sampling of Coarser Materials." In International Symposium of Soil Sampling, 13–21. Singapore.

Arnold, M. (1980). "Prediction of footing settlements on sand." Ground Engineering 13(2).

ASTM D2216. 2010. "Standard Test Methods for Laboratory Determination of Water (Moisture) Content of Soil and Rock by Mass." ASTM.

ASTM D2435. 2011. "Standard Test Methods for One-Dimensional Consolidation Properties of Soils Using Incremental Loading." ASTM.

ASTM D2487. 2017. "Standard Practice for Classification of Soils for Engineering Purposes (Unified Soil Classification System)." ASTM.

ASTM D2488. 2017. "Standard Practice for Description and Identification of Soils (Visual-Manual Procedures)." ASTM.

ASTM D4186. 2012. "Standard Test Method for One-Dimensional Consolidation Properties of Saturated Cohesive Soils Using Controlled-Strain Loading." ASTM.

ASTM D4318. 2017. "Standard Test Methods for Liquid Limit, Plastic Limit, and Plasticity Index of Soils." ASTM.

ASTM D6913. 2017. "Standard Test Methods for Particle-Size Distribution (Gradation) of Soils Using Sieve Analysis." ASTM.

ASTM D7928. 2017. "Standard Test Method for Particle-Size Distribution (Gradation) of Fine-Grained Soils Using the Sedimentation (Hydrometer) Analysis." ASTM.

ASTM D854. 2014. "Standard Test Methods for Specific Gravity of Soil Solids by Water Pycnometer." ASTM.

Atkinson, J. H. and Sallfors, G. (1991). "Experimental determination of soil properties." General Report to Session 1. Proc. 10th ECSMFE, Florence.

Bachelier, M. and L. Parez (1965). "Contribution à l'étude de la compressibilité des sols à l'aide du pénétromètre à cône." Soil Mechanics Foundation Engineering Conference., Montreal, 6th.

Baldi, G., R. Bellotti, V. Ghionna, M. Jamiolkowski and D. Lo Presti (1989). "Modulus of sands from CPT's and DMT's." Congrès international de mécanique des sols et des travaux de fondations. 12.

Baligh, Mohsen M., and Jacques-Noel Levadoux, (1986). "Consolidation After Undrained Piezocone Penetration. II: Interpretation." *Journal of Geotechnical Engineering* 112 (7): 727–45. [https://doi.org/10.1061/\(ASCE\)0733-9410\(1986\)112:7\(727\)](https://doi.org/10.1061/(ASCE)0733-9410(1986)112:7(727)).

Becker, D. E., J. H. A. Crooks, K. Been, and M. G. Jefferies, (1987). "Work as a Criterion for Determining in Situ and Yield Stresses in Clays." *Canadian Geotechnical Journal* 24 (4): 549–64. <https://doi.org/10.1139/t87-070>.

Begemann, H. K. S. (1974). "General report for central and western Europe." In: *Proceedings, European symposium on penetration testing*, Stockholm

Bellotti, R., V. Ghionna, M. Jamiolkowsky, R. Lancellotta and G. Manfredini (1986). "Deformation characteristics of cohesionless soils in insitu tests." *Proceedings, In Situ '86 Geotechnical Special Publication 6*, ASCE, New York: 47-73.

Benz, T. (2007). "Small-strain stiffness of soils and its numerical consequences." Univ. Stuttgart, Inst. f. Geotechnik Stuttgart.

Benz, T., R. Schwab and P. Vermeer (2009). "Small-strain stiffness in geotechnical analyses." *Bautechnik* 86(S1): 16-27.

Berardi, R., M. Jamiolkowski and R. Lancellotta (1991). "Settlement of shallow foundations in sands selection of stiffness on the basis of penetration resistance." *Geotechnical Engineering Congress—1991*, ASCE.

Bjerrum, L. 1967. "Engineering Geology of Norwegian Normally-Consolidated Marine Clays as Related to Settlements of Buildings." *Géotechnique* 17 (2): 83–118. <https://doi.org/10.1680/geot.1967.17.2.83>.

Bogdanovic', L. (1973). "Settlement of stiff structures (silos) founded on soft soil with low penetration resistance." *Transactions, SR Institute of Testing and Materials, Belgrade*, No. 34.

Bowles, J. E. (1987). "Elastic Foundation Settlements on Sand Deposits." *Journal of Geotechnical Engineering*, ASCE, 113(8): 846-860.

Bowles, L. (1996). "Foundation analysis and design." McGraw-hill.

Briaud, J.-L. and R. Gibbens (1997). "Large-scale load tests and data base of spread footings on sand." United States. Federal Highway Administration.

Briaud, J.-L. and R. M. Gibbens (1994). "Predicted and measured behavior of five spread footings on sand." ASCE.

Briaud, J.-L., K. Hossain, J. Barfknecht and J. H. Lee (2000). "Load Settlement Curve Method for Spread Footings on Sand." Publication No. FHWA-RD-2000-XXX, Federal Highway Administration, Washington, D.C.

Brinkgreve, R. (2018). "PLAXIS 2D Manuals. General Information." Tutorial Manual, Reference Manual, Material Models Manual, Scientific Manual. Delft University of Technology & PLAXIS bv, The Netherlands, ISBN13 978(90): 76016.

Brinkgreve, R., E. Engin and H. Engin (2010). "Validation of empirical formulas to derive model parameters for sands." *Numerical methods in geotechnical engineering*: 137-142.

Buisman, A. S. K. (1940). "Groundmechanica." Waltman, Delft, The Netherlands.

Burland, J. B. and M. C. Burbidge (1985). "Settlement of foundations on sand and gravel." *Proceedings of the institution of Civil Engineers* 78(6): 1325-1381.

Canadian Foundation Engineering Manual (2006). Canadian Geotechnical Society, BiTech Publishers Ltd.

Chaplin, T. K. (1963). "The compressibility of granular soils with some applications to foundation engineering." *Proc. Eur. Conf. Soil Me&. Fdn Engng, Wiesbaden*: 215-217.

Cheney, R. S. and Chassie, R. (2000). "Soils and Foundations Workshop Reference Manual." Publication No. FHWA NHI-00 45.

Cho, W., T. Holman, Y. Jung, and R. Finno. 2007. "Effects of Swelling During Saturation in Triaxial Tests in Clays." *Geotechnical Testing Journal* 30 (5): 378–86. <https://doi.org/10.1520/GTJ100797>.

Chopra, M., D. Horhota, F. Townsend, J. B. Anderson and E. Horta (2003). "Site Preparation for a Deep Foundation Test Site at the University of Central Florida." Department of Civil and Environmental Engineering, University of Central Florida.

Christian, J. T. and D. W. Carrier (1978). "Janbu, Bjerrum and Kjaernsli's chart reinterpreted." *Canadian Geotechnical Journal* 15(1): 123-128.

Clayton, C. R. I., M. B. Hababa and N. E. Simons (1985). "Dynamic penetration resistance and the prediction of the compressibility of a fine-grained sand—a laboratory study." *Géotechnique* 35(1): 19-31.

Clayton, C. R. I., D. W. Hight and R. J. Hopper (1992). "Progressive destructuring of Bothkennar clay implications for sampling and reconsolidation procedures." *Géotechnique* 42(2): 219-239.

Coffman, B. (1960). "Estimating the relative density of sands." *Civil Engineering* 30(10): 78-79.

Cubrinovski, M. and K. Ishihara (2001). "Correlation between penetration resistance and relative density of sandy soils."

Cubrinovski, Misko, and Kenji Ishihara. 2002. "Maximum and Minimum Void Ratio Characteristics of Sands." *Soils and Foundations* 42 (6): 65–78. https://doi.org/10.3208/sandf.42.6_65.

D'Appolonia, D. J., E. D'Appolonia and R. F. Brissette (1968). "Settlement of Spread Footings on Sand." *Journal of Soil Mechanics and Foundations Division, ASCE* 94(3): 735-760.

D'Appolonia, D. J., E. D'Appolonia and R. F. Brissette (1970). "Closure: Settlement of spread footings on sand." *Journal of the Soil Mechanics and Foundations Division* 96(2): 754-761.

Dagger, R., D. Saftner and P. Mayne (2018). "Cone Penetration Test Design Guide for State Geotechnical Engineers."

Darendeli, M. B. (2001). "Development of a new family of normalized modulus reduction and material damping curves."

Davie, J. R., T. Liao, M. R. Lewis and J. L. M. Clemente (2019). "Comparison of Estimated Soil Settlements Using Strain-Dependent and High-Strain Elastic Moduli." *Geo-Congress 2019*: 480-489.

DeBeer, E. and A. Martens (1957). "Method of computation of an upper limit for the influence of heterogeneity of sand layers in the settlement of bridges." *Proceedings, 4th International Conference on Soil Mechanics and Foundation Engineering, London.*

DeBeer, E. E. (1965). "Bearing capacity and settlement of shallow foundation on sand." *Proc. Symp. Bearing capacity and settlement of foundations. Duke University, Durham, NC*, 15-33.

Denver, H. (1982). "Modulus of elasticity for sand determined by SPT and CPT."

Dowding, C. H. (2008). "Soil Dynamics." *Northwestern Univ., Evanston, IL. Lecture Notes, Fall 2008.*

Durgunoglu, H. T. and J. K. Mitchell (1975). "Static penetration resistance of soils." *Proc, ASCE Specialty Conf. on In-Situ Measurement of Soil Properties, Raleigh, N.C.*: 151-189.

EPRI (1983). "Transmission Line Structure Foundations for Uplift-Compression Loading, EL-2870." *Electric Power Research Institute, Palo Alto, CA.*

Farrent, T. A. (1963). "The prediction and field verification of settlement in cohesionless soils." *Proceedings of the 4th Australia-New Zealand conference on soil mechanics and foundation engineering.*

Fountain, K. B. 2009. "Origin and Stratigraphic Significance of Kaolinitic Sediments from The Cypresshead Formation: A Sedimentological, Mineralogical and Geochemical Investigation." University of Florida.

Fountain, K. B., D. Cordier, A. Romeo, and B. Shelar. 2009. "The Stratigraphy and Mineral Resource Significance of the North Florida Plio-Pleistocene." St. Augustine, FL.

GeoLogismiki. 2019. "CPeT-IT v.3.0.3.2." Serres, Greece. <https://geologismiki.gr/>.

Gibbs, H. J. and W. G. Holtz (1957). "Research on determining the density of sands by spoon penetration testing." Proc. 4th Int. Conf. on Soil Mechanics and Foundation Engineering.

Gielly, J., P. Lareal and G. Sanglerat (1969). "Correlations between in situ penetrometer tests and the compressibility characteristics of soils." Conference on In-Situ Investigations in Soil and Rock, British Geotechnical Society.

Gifford, D. G., S. Kraemer, J. Wheeler and A. McKown (1987). "Spread footings for highway bridges."

Guerreiro, P., S. Kontoe and D. Taborda (2012). "Comparative study of stiffness reduction and damping curves." 15th World Conference on Earthquake Engineering, Lisbon, CD ROM.

Hardin, B. O. and V. P. Drnevich (1972 b). "Shear modulus and damping in soils: measurement and parameter effects." Journal of Soil Mechanics & Foundations Div. 98(6): 603-624.

Hardin, B. O. (1978). "The nature of stress-strain behavior for soils." From Volume I of Earthquake Engineering and Soil Dynamics-Proceedings of the ASCE Geotechnical Engineering Division Specialty Conference, June 19-21, 1978, Pasadena, California. Sponsored by Geotechnical Engineering Division of ASCE.

Harr, M. E. and C. W. Lovell (1963). "Vertical stress under certain axisymmetrical loadings." Highway Research Record (39).

Hatanaka, M. and A. Uchida (1996). "Empirical correlation between penetration resistance and internal friction angle of sandy soils." Soils and foundations 36(4): 1-9.

Holtz, R. D., T. C. Sheahan., and W. D. Kovacs (2011). "An Introduction to Geotechnical Engineering." ISBN-13: 978-0-13-701132-2, PEARSON.

Horta, Evelio. 2003. "Site Preparation for a Deep Foundation Test Site, at the University of Central Florida." University of Central Florida.

Hough, B. K. (1959). "Compressibility as the basis for soil bearing value." *Journal of the Soil Mechanics and Foundations Division, ASCE*, 85(4): 11-40.

Hryciw, R. D. (1990). "Small-strain-shear modulus of soil by dilatometer." *Journal of Geotechnical Engineering, ASCE*, 116(11): 1700-1716.

Imai, T. and K. Tonouchi (1982). "Correlation of N-value with S-wave velocity and shear modulus." *Proceedings, 2nd European Symposium on Penetration Testing, Amsterdam*: 57-72.

Ishibashi, I. and X. Zhang (1993). "Unified dynamic shear moduli and damping ratios of sand and clay." *Soils and foundations* 33(1): 182-191.

Jaky, J. (1944). "The coefficient of earth pressure at rest." *Journal of the Society of Hungarian Architects and Engineers*: 355-358.

Jamiolkowski, M., C. Ladd, J. Germaine and R. Lancellotta (1985). "New Developments in Field and Lab Testing of Soils." *Proceedings, 11th International Conference on Soil Mechanics and Foundation Engineering*.

Jamiolkowski, M., S. Leroueil and D. C. Lo Presti (1991). "Design parameters from theory to practice." *Int. Conf. on Geotechnical Engineering for coastal development, Port & Harbour Research Institute*.

Janbu, N. (1963). "Soil compressibility as determined by odometer and triaxial tests." *Proc. Europ. Conf. on Soil Mech. Fndn. Engng.*, (pp. 19-25), Essen, Germany..

Janbu, N. (1967). "Settlement calculations based on the tangent modulus concept." *Soil Mechanics*.

Kim, T. (2011). "Incrementally nonlinear responses of soft Chicago glacial clays." *Northwestern University*.

Kenney, T. C. 1964. "Sea-Level Movements and the Geologic Histories of the Post-Glacial Marine Soils at Boston, Nicolet, Ottawa and Oslo." *Géotechnique* 14 (3): 203-30. <https://doi.org/10.1680/geot.1964.14.3.203>.

Kim, T. (2011). "Incrementally nonlinear responses of soft Chicago glacial clays." Northwestern University.

Kimmerling, R. (2002). "Geotechnical Engineering Circular No. 6 Shallow Foundations." United States. Federal Highway Administration. Office of Bridge Technology.

Kramer, S. L. (1996). "Geotechnical earthquake engineering." Pearson Education India.

Kulhawy, F. H. and P. W. Mayne (1990). "Manual on estimating soil properties for foundation design." Electric Power Research Inst., Palo Alto, CA (USA); Cornell Univ., Ithaca, NY (USA).

Ladd, C., and T. Lambe. 1964. "The Strength of 'Undisturbed' Clay Determined from Undrained Tests." In Laboratory Shear Testing of Soils, 342–71. ASTM International. <https://doi.org/10.1520/STP30011S>.

Lade, Poul V., Carl D. Jr. Liggiio, and Jerry A. Yamamuro (1998). "Effects of Non-Plastic Fines on Minimum and Maximum Void Ratios of Sand." Geotechnical Testing Journal 21 (4): 336. <https://doi.org/10.1520/GTJ11373J>.

Lambe, T. (1973). "Predictions in soil engineering." Géotechnique 23(2): 151-202.

Leonards, G. A. and J. D. Frost (1988). "Settlement of Shallow Foundations on Granular Soils." Journal of Geotechnical Engineering 114(7): 791-809.

Lunne, T., H. P. Christoffersen, and T. I. Tjelta. 1985. "Engineering Use of Piezocone Data in North Sea Clays." In Proc. 11th International Conference on Soil Mechanics and Foundation Engineering, San Francisco, August 1985. Vol. 2, (Balkema), 24:907–12. [https://doi.org/10.1016/0148-9062\(87\)90583-3](https://doi.org/10.1016/0148-9062(87)90583-3).

Lunne, T., T. Berre, K. H. Andersen, S. Strandvik, and M. Sjursen (2006). "Effects of Sample Disturbance and Consolidation Procedures on Measured Shear Strength of Soft Marine Norwegian Clays." Canadian Geotechnical Journal 43 (7): 726–50. <https://doi.org/10.1139/t06-040>.

Lutenegger, A. J. and D. J. DeGroot (1995). "Settlement of shallow foundations on granular soils." University of Massachusetts Transportation Center.

Mair, R. J. (1993). "Developments in geotechnical engineering research: applications to tunnels and deep excavations." Unwin Memorial Lecture 1992. Proceedings of Institution of Civil Engineers: Civil Engineering.

Marchetti, S. (1985). "On the field determination of K_0 in sand." Discussion Session No. 2A. XI International Conference on Soil Mechanics and Foundation Engineering. S. Francisco: 2667-2673.

Marchetti, S., P. Monaco, G. Totani and M. Calabrese (2001). "The flat dilatometer test (DMT) in soil investigations." A report by the ISSMGE committee TC16." Proc. In Situ: 41.

Mayne, P. and G. Rix (1993). "G max-qc relationships for clays." Geotechnical Testing Journal, ASTM 16 (1): 54-60.

Mayne, P. W. and H. G. Poulos (1999). "Approximate displacement influence factors for elastic shallow foundations." Journal of Geotechnical and Geo-environmental Engineering 125(6): 453-460.

Mayne, P. W. (2005). "Integrated Ground Behavior: In-Situ and Lab Tests." In Deformation Characteristics of Geomaterials: Recent Investigations and Prospects - International Symposium on Deformation Characteristics of Geomaterials, ISLyon 2003, 155-77.

Mayne, P. W. (2007). "Synthesis on Cone Penetration Test: State-of-Practice. NCHRP Report." Washington, D.C.

Mayne, P. W. (2014). "Generalized CPT Method for Evaluating Yield Stress in Soils." In Geo-Congress 2014 Technical Papers, 1336-46. Reston, VA: American Society of Civil Engineers. <https://doi.org/10.1061/9780784413272.130>.

Meigh, A. C. and B. O. Corbett (1969). "A comparison of in situ measurements in a soft clay with laboratory tests and the settlement of oil tanks." Proc. Conf. In Situ Investigations in Soil and Rocks, Brit. Geotech. Soc., London: 173-179.

Mercado, J. A., L. G. Arboleda-Monsalve, T. S. Butalia and P. J. Amaya (2018). "Compressibility of Fly Ash under K_0 Loading: Strain Rate Effects in Constant Rate of Strain Testing." Coal Combustion and Gasification Products 10(2): 15-22.

Ménard, L. and J. Rousseau (1962). "L'évaluation des tassements, tendances nouvelles." Sols Soils 1(1): 13-29.

Meyerhof, G. (1974). "Penetration testing in countries outside Europe." Proceedings of the European Symposium on Penetration Testing, Stockholm, Sweden:[sn]:40-48.

Meyerhof, G. G. (1965). "Shallow foundations." Journal of Soil Mechanics & Foundations Div 91(Proc. Paper 4275).

Missimer, T. M. 2002. "Late Oligocene to Pliocene Evolution of the Central Portion of the South Florida Platform: Mixing of Siliciclastic and Carbonate Sediments." Tallahassee.

Nassiri, S., S. Savater, L. Arboleda-Monsalve, M. Chopra and L. Jones (2020). "Factors Influencing Immediate Settlements in Central Florida Soils Using Conical Load Tests." Geo-Congress 2020: 350-361. American Society of Civil Engineers. <https://doi.org/10.1061/9780784482780.034>.

NAVFAC, D. M. (1986). "7.02, Foundations & Earth Structures." Department of the Navy, Naval Facilities Engineering Command, Alexandria, VA.

Ohta, Y. and N. Goto (1976). "Estimation of S-wave velocity in terms of characteristic indices of soil." Butsuri-Tanku 29(4): 34-41.

Orange Weather STEM (2019). Retrieve from: <https://orange.weatherstem.com/data?refer=/ucf>

Oweis, I. S. (1979). "Equivalent linear model for predicting settlements of sand bases." Journal of Soil Mechanics and Foundations Division, ASCE, 105(12): 1525-1544.

PANalytical. 2009. "X'Pert HighScore Plus."

Papadopoulos, B. P. and A. G. Anagnostopoulos (1987). "Groundwater effects on settlements estimation." Proc. X European conference on soil mechanics and foundation engineering. Dublin.

Papadopoulos, B. P. (1992). "Settlements of Shallow Foundations on cohesionless soils." Journal of Geotechnical Engineering, ASCE, 118(3): 377-393.

Parry, R. (1985). "A direct method of estimating settlements in sand from SPT values." Golden Jubilee of the International Society for Soil Mechanics and Foundation Engineering: Commemorative Volume: 166.

Peck, R. B. and A. R. Bazaraa (1969). "Discussion of paper by D'Appolonia et al." *Journal of the Soil Mechanics and Foundations Division* 95(3): 305-309.

Peck, R. B., W. E. Hanson and T. H. Thornburn (1974). "Foundation engineering." Wiley New York.

Pirkle, E. C. 1956. "The Hawthorne and Alachua Formations of Alachua County, Florida." *Quarterly Journal of the Florida Academy of Sciences* 19 (4): 197–240.

Poulos, H. G. and E. H. Davis (1974). "Elastic solutions for soil and rock mechanics." John Wiley.

Puri, H. S., and R. O. Vernon. 1972. "Summary of the Geology of Florida." *Earth Science Reviews*. Vol. 8.

Rix, G. J. and K. H. Stokoe (1991). "Correlation of initial tangent modulus and cone resistance." *Calibration Chamber Testing, International Symposium on Calibration Chamber Testing*, A.B. Huang. Elsevier Publishing, New York: 351-362.

Robertson, P. K. and R. Campanella (1983). "Interpretation of cone penetration tests. Part I: Sand." *Canadian geotechnical journal* 20(4): 718-733.

Robertson, P. K. and R. G. Campanella (1986). "Estimating liquefaction potential of sands using the flat plate dilatometer." *Geotechnical Testing Journal* 9(1): 38-40.

Robertson, P. K., J. P. Sully, D. J. Woeller, T. Lunne, J. J. M. Powell, and D. G. Gillespie (1992). "Estimating Coefficient of Consolidation from Piezocone Tests." *Canadian Geotechnical Journal* 29 (4): 539–50. <https://doi.org/10.1139/t92-061>.

Robertson, P. K. (2009). "Interpretation of Cone Penetration Tests — A Unified Approach." *Canadian Geotechnical Journal* 46 (11): 1337–55. <https://doi.org/10.1139/T09-065>.

Robertson, P. K. (2010). "Estimating In-Situ Soil Permeability from CPT & CPTu." In *2nd International Symposium on Cone Penetration Testing*, 1–8.

Robertson, P. K., and K. L. Cabal (2015). "Guide to Cone Penetration Testing for Geotechnical Engineering." 6th Edition. Gregg Drilling & Testing Inc.

Rowe, R. and J. Booker (1981). "The behaviour of footings resting on a non-homogeneous soil mass with a crust. Part II. Circular footings." *Canadian Geotechnical Journal* 18(2): 265-279.

Santagata, M., J. T. Germaine and C. C. Ladd (2005). "Factors Affecting the Initial Stiffness of Cohesive Soils." *Journal of Geotechnical and Geoenvironmental Engineering* 131(4): 430-441.

Sargand, S. M., T. Masada and B. Abdalla (2003). "Evaluation of Cone Penetration Test-Based Settlement Prediction Methods for Shallow Foundations on Cohesionless Soils at Highway Bridge Construction Sites." *Journal of Geotechnical and Geo-environmental Engineering* 129(10): 900-908.

Schiffman, R. (1963). "Discussion to paper by M.E. Harr and C.W. Lovell." *Highway Res. Rec* 39: 78-81.

Schmertmann, J. H. (1970). "Static cone to compute static settlement over sand." *Journal of Soil Mechanics & Foundations Div., ASCE*, 96(SM3):1011-1043.

Schmertmann, J. H. (1975). "Measurement of in situ shear strength, SOA Report." Proceedings, ASCE Special Conference on In Situ Measurement of Soil Properties, Raleigh, NC, 1975.

Schmertmann, J. H., J. P. Hartman and P. R. Brown (1978). "Improved strain influence factor diagrams." *Journal of Geotechnical and Geo-environmental Engineering* 104(Tech Note).

Schmertmann, J. H. (1986). "Dilatometer to compute foundation settlement." *Proc. In Situ test in Geotechnical Engineering, ASCE*: 303-321.

Schmertmann, J. H. (1993). "Conical Test Load Measuring Compressibility." *Journal of Geotechnical Engineering* 119(5): 965-971.

Schultze, E. and K. J. Melzer (1965). "The determination of the density and the modulus of compressibility of non-cohesive soils by soundings." Proceedings of the 6th International Conference on Soil Mechanics and Foundation Engineering.

Schultze, E. and G. Sherif (1973). "Prediction of settlements from evaluated settlement observations for sand." Proceedings Eighth International Conference on Soil Mechanics and Foundation Engineering.

Scott, Thomas M. 1992. "A Geological Overview of Florida." Tallahassee.

Scott, Thomas M. 1988. "The Lithostratigraphy of the Hawthorn Group (Miocene) of Florida." Tallahassee.

Scott, Thomas M. 1990. "The Lithostratigraphy of the Hawthorn Group of Peninsular Florida." Tallahassee.

Scott, Thomas M. 2001. "Text to Accompany the Geologic Map of Florida." Tallahassee.

Seed, H. B. and I. M. Idriss (1970). "Soil moduli and damping factors for dynamic response analysis." EERC.

Seed, H. B., R. T. Wong, I. M. Idriss and K. Tokimatsu (1986). "Moduli and damping factors for dynamic analyses of cohesionless soils." *Journal of Geotechnical Engineering, ASCE*, **112**(11): 1016-1032.

Skempton, A. (1986). "Standard penetration test procedures and the effects in sands of overburden pressure, relative density, particle size, ageing and overconsolidation." *Geotechnique* 36(3): 425-447.

Sowers, G. F. (1979). "Introductory Soil Mechanics & Foundations." *Geotechnical engineering* 92: 114-117.

Tanaka, H. and M. Tanaka (1998). "Characterization of sandy soils using CPT and DMT." *Soils and Foundations* 38(3): 55-65.

Tanizawa, F. (1990). On correlation among cone resistance and shear modulus and angle of shear resistance of Toyoura sand. Proc. of 25th Japan National Conf. on SMFE.

Teh, C. I., and G. T. Houlsby. 1991. "An Analytical Study of The Cone Penetration Test in Clay." *Géotechnique* 41 (1): 17-34. <https://doi.org/10.1680/geot.1991.41.1.17>.

Teng, W. C.-Y. (1962). "FOUNDATION DESIGN."

Terzaghi, K. and R. B. Peck (1948). "Soil Mechanics in Engineering Practice." John Wiley and Sons, New York.

Terzaghi, K., R. B. Peck and G. Mesri (1967). "Soil Mechanics in Engineering Practice, John Wiley & Sons." Inc., New York.

Thomas, D. (1968). "Deep sounding test results and the settlement of spread footing on normally consolidated sands." *Geotechnique* 18(4): 472-488.

Tomlinson, M. (1986). "Foundation Design and Construction." Longman Scientific and Technical London Fifth Edition.

Trofimenkov, Y. G. (1964). "Field methods for testing the structural properties of soils." Building Literature Publishing House, Moscow.

Trofimenkov, Y. G. (1974). "Penetration testing in Western Europe." Proc., European Symp. on Penetration Testing, Stockholm, Sweden.

Tschebotarioff, G. (1971). "Foundations, Retaining and Earth Structures." The Art of Design and Construction and Its Scientific Bases in Soil Mechanics.

U.S. Department of the Navy (1982). "Foundations and earth structures design manual 7.2." Department of the Navy, Naval Facilities Engineering Command, Alexandria, VA.

Upchurch, Sam, Thomas M. Scott, Michael C. Alfieri, Beth Fratesi, and Thomas L. Dobecki, (2019). *The Karst Systems of Florida. Cave and Karst Systems of the World.* Cham: Springer International Publishing. <https://doi.org/10.1007/978-3-319-69635-5>.

Uribe-Henao, A. F., L. G. Arboleda-Monsalve, S. Savater, M. Chopra, and L. Jones, (2019). "Conical Load Test-Induced Settlement in Central Florida Soils: Class A Prediction of Field Performance with Advanced Soil Models." In *Geo-Congress 2019*, 499–508. American Society of Civil Engineers. <https://doi.org/10.1061/9780784482094.046>.

USACE (1990). "Settlement Analysis." Engineer Manual EM 1110-1-1904.

Vail, P. R., and R. M. Jr. Mitchum (1979). "Global Cycles of Relative Changes of Sea Level from Seismic Stratigraphy." In *Geological and Geophysical Investigations of Continental Margins*, edited by J. S. Watkins, L. Montadert, and P. W. Dickerson, 469–72.

Vesić, A. S. (1970). "Research on bearing capacity of soils." *Foundation Engineering Handbook*, 142.

Webb, D. (1969). "Settlement of structures on deep alluvial Sandy sediments in Durban, South Africa. In situ investigations in soil and rocks." Proc. of Conf. Organized by the Brit. Geotechn. Soc., London.

Wickremesinghe, D. S., and R. G. Campanella (1991). "Statistical Methods for Soil Layer Boundary Location Using the Cone Penetration Test." In 6th International Conference on Application of Statistics and Probability in Civil Engineering, 636–44. CERRA-ICASP6.

Zapata-Medina, D. G. (2012). "Evaluation of dynamic soil parameter changes due to construction-induced stresses." Northwestern University.

APPENDIX A
SURVEY RESULTS OF THE CURRENT PRACTICE IN FLORIDA

A survey was developed using the Qualtrics platform available through the University of Central Florida. It was then disseminated as a link to a list of geotechnical engineers compiled using the attendance at GRIP meetings and other sources for contact information for consultants in Florida.

The survey is presented below:

UCF is currently conducting a research study funded by the Florida Department of Transportation (FDOT) on the calculation of immediate settlement and the use of elastic moduli from correlations with field and/or laboratory testing.

We would like to request you to provide us with some information related to your approach to this task. Please be assured that your responses are voluntary and will be confidential. All responses will be compiled and analyzed as a group.

Question 1: For the design of shallow foundations, which procedure or equation do you most often use for the calculation of immediate settlement in Florida soils? Please select all that apply and provide any relevant information about reference manuals or links in the last box below.

- General elastic solutions (e.g. Steinbrenner, 1934, Terzaghi, 1943 etc.)
- Terzaghi and Peck (1948, 1967)
- Peck (1974)
- Meyerhof (1956, 1965, 1974)
- Schmertmann (1970, 1986)
- Bowles (1968, 1987)
- Robertson (1991)
- Mayne and Poulos (1999)
- AASHTO LRFD (2017)
- Canadian Foundation Manuals
- Other Procedure or Equation, please specify _____
- Additional Details _____

Question 2: Which correlations and/or values do you use for elastic modulus of the soil in the methods specified in Question 1? Please enter text below or provide information about reference manuals with pages or relevant links.

Question 3: Do you use any specific correlations for elastic modulus of the soil with field tests?
Please select all that apply

- SPT
- CPT
- PMT
- DMT
- Other, please specify _____

Question 4: For those identified in Question 3, please provide information about any reference, or manuals with page numbers, or relevant links in the box below. If more than one is identified, which do you use with greatest confidence?

Question 5: Which of the following approaches do you use to perform your calculations of immediate settlement?

- Hand Calculations on Paper
- In-house Spreadsheets
- Commercial Software
- Other, please specify _____

Question 6: Do you perform any additional laboratory and/or field tests to check your selection of elastic modulus and immediate settlement values? If the answer is Yes, please provide information about the tests performed in the last box below.

- Yes
- No

Question 7: If the answer to Question 6 is Yes, please provide information about the tests performed in the box below.

Question 8: Do you run any numerical models to calculate or verify your immediate settlement (e.g. finite elements, finite difference, discrete elements)?

- Yes
- No

Question 9: If the answer to Question 8 is Yes, please select the type of constitutive soil model used and provide any details in the text box below.

- Mohr-Coulomb
- Von Mises
- Drucker-Prager
- Lade and Duncan
- Modified Cam-clay
- Hardening Soil Model
- Any advanced models (e.g. Hypoplasticity, Bounding Surface Plasticity, PM4Sand, 3 Surface Kinematic
- Other, please specify _____
- Additional details _____

Question 10: Do you feel that the existing method you use to calculate elastic modulus and immediate settlement is conservative? Please select one of the following choices -

- Very Conservative
- Moderately Conservative
- Not conservative
- Other, please comment _____

End of survey

The responses received are summarized in the following figures.

Q1: For the design of shallow foundations, which procedure or equation do you most often use for the calculation of immediate settlement in Florida soils? Please select all that apply and provide any relevant information about reference manuals or links in the last box below.

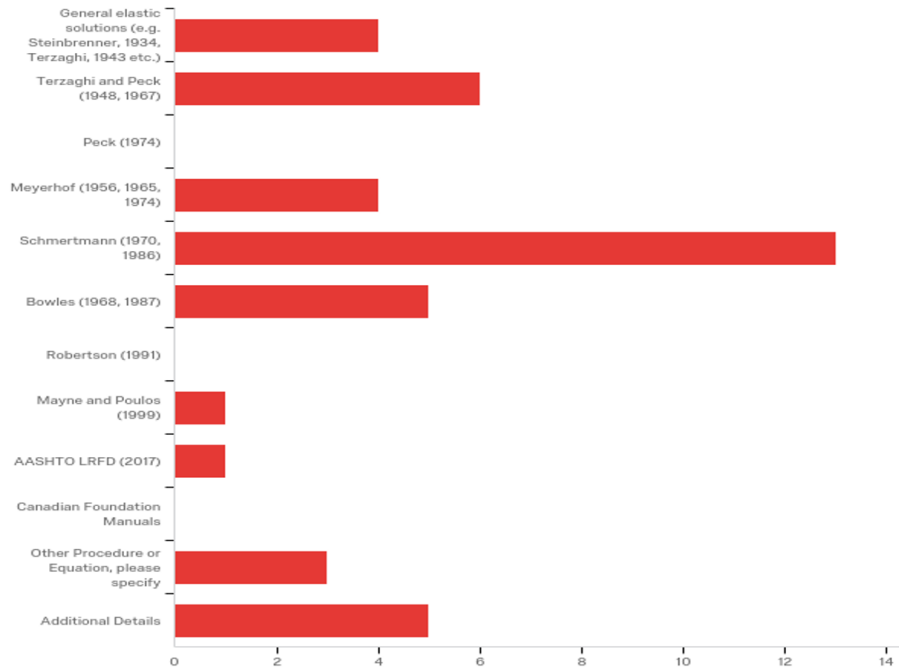


Figure A-1. Responses received for question 1.

Q2: Which correlations and/or values do you use for elastic modulus of the soil in the methods specified in Question 1? Please enter text below or provide information about reference manuals with pages or relevant links.

Selected Answers-

- Bowles formulas
- Soils and Foundations FHWA HI-88-009 Figure 13
- $E = 8N$ (tsf)
- SPT and CPT correlations and data from pressuremeter testing
- Correlations presented in the [FB-MultiPier Soil Parameter Tables](#)
- $M = 30 * N_{\text{manual}}$ (tsf): Schmertmann, J.H. (1988)
- Please see FHWA-IF-02-034, Table 28 and Table 29
- Young's Modulus (elastic modulus) (1984) by Robertson and Campanella
- GeoStudio 2007 Sigma/W for further settlement analysis for larger structures, which does require Elastic Modulus as input

Figure A-2. Responses received for question 2.

Q3: Do you use any specific correlations for elastic modulus of the soil with field tests? Please select all that apply.

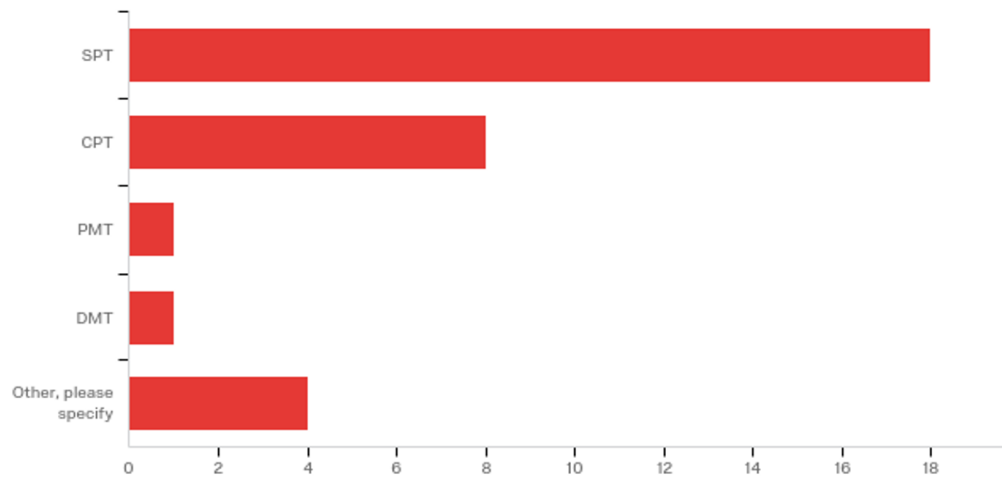


Figure A-3. Responses received for question 3.

Q4: For those identified in Question 3, please provide information about any reference, or manuals with page numbers, or relevant links in the box below. If more than one is identified, which do you use with greatest confidence?

Selected Answers:

- Bowles P. 189
- Soils and Foundations FHWA HI-88-009 Figure 13 (page 170)
- SPT and CPT data
- $E=(100,000*OCR^{0.5})+24000N60$ (sands) $E=(50,000*OCR^{0.5})+12000N60$ (clayey, silty sands)
- AASHTO recommendations
- For SPT, please see FHWA-IF-02-034, Table 28 and Table 29
- EM 1110-1-1904
- Using the Bowles 1996 Foundation Analysis and Design (5th Edition) tables, we converted the soil density descriptions to approximate SPT N-values

Figure A-4. Responses received for question 4.

Q5: Which of the following approaches do you use to perform your calculations of immediate settlement?

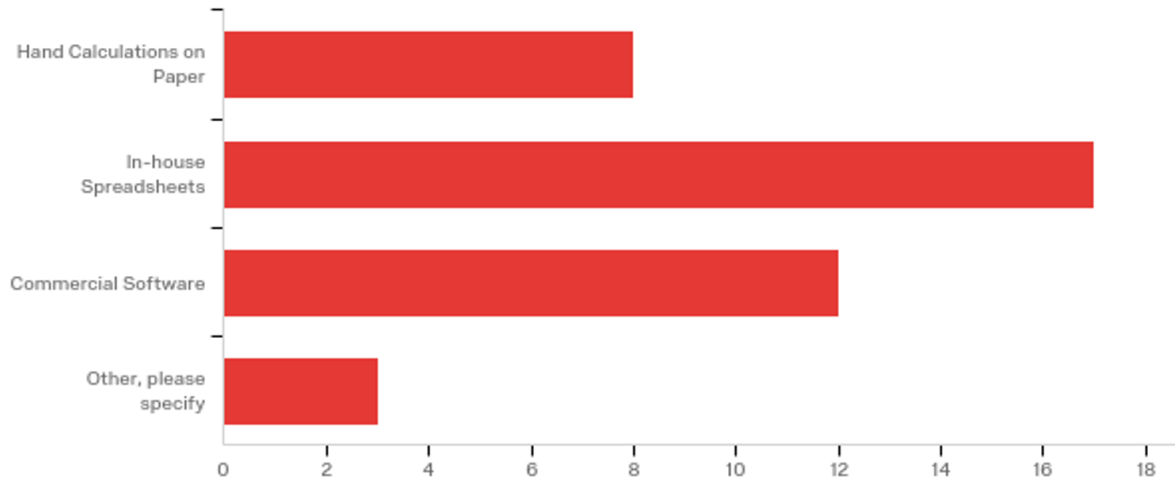


Figure A-5. Responses received for question 5.

Q6: Do you perform any additional laboratory and/or field tests to check your selection of elastic modulus and immediate settlement values? If the answer is Yes, please provide information about the tests performed in the last box below.

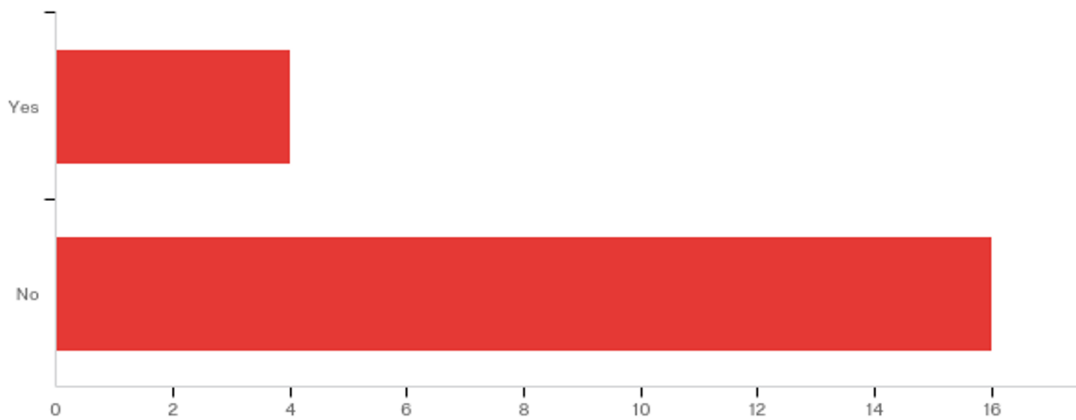


Figure A-6. Responses received for question 6.

Q7. If the answer to Question 6 is Yes, please provide information about the tests performed in the box below.

Unconfined Compression

Settlement performance from survey data and static load test data

On occasion, we perform DMT. Not very often, though. Often difficult to convince clients to pay for it.

Figure A-7. Responses received for question 7.

Q8. Do you run any numerical models to calculate or verify your immediate settlement (e.g. finite elements, finite difference, discrete elements)?

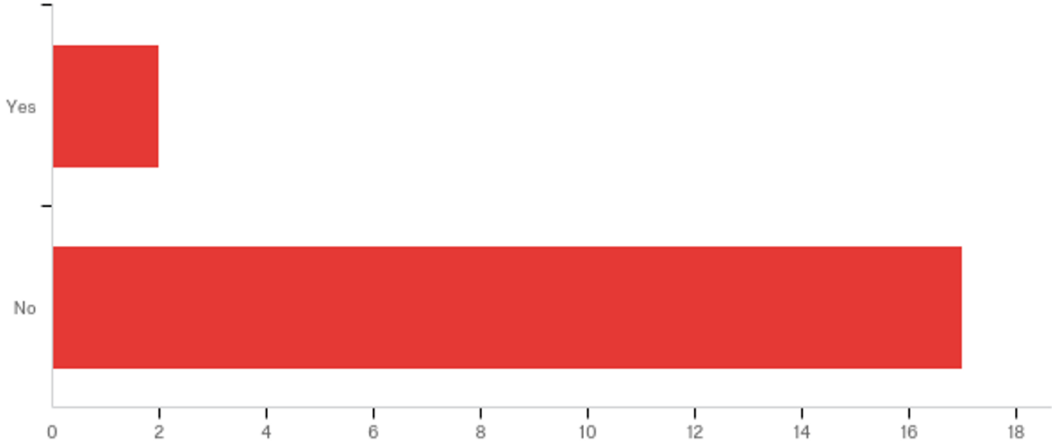


Figure A-8. Responses received for question 8.

Q9. If the answer to Question 8 is Yes, please select the type of constitutive soil model used and provide any details in the text box below.

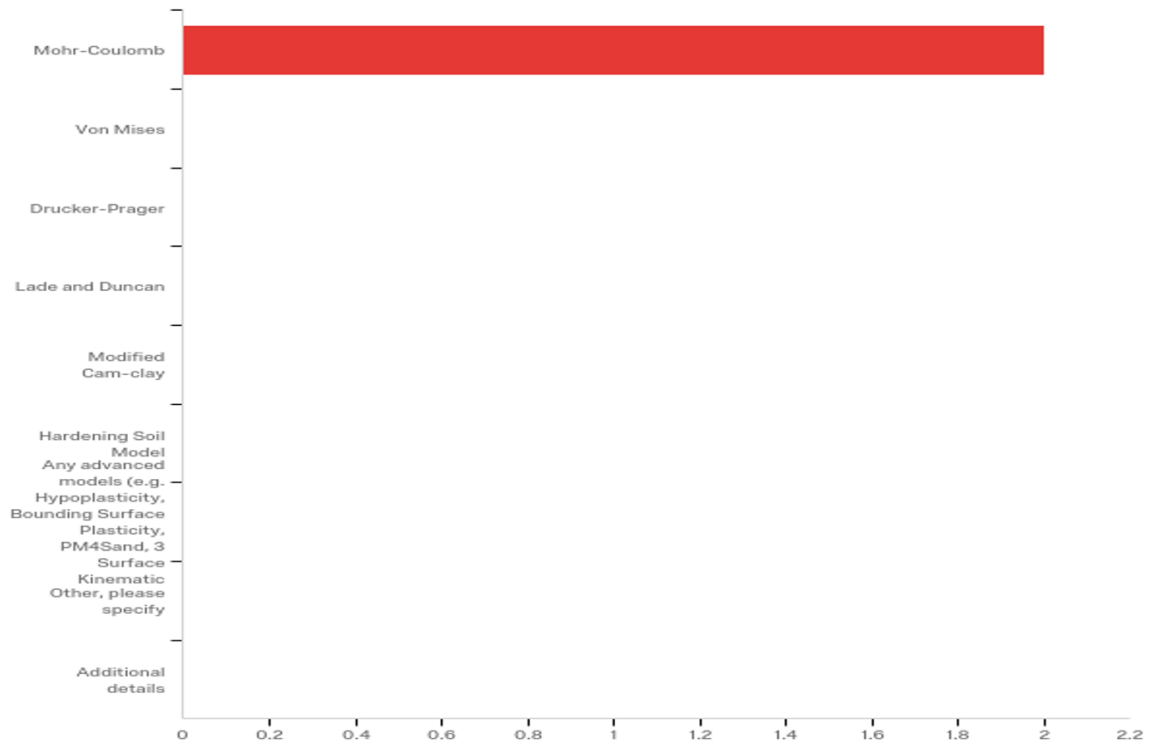


Figure A-9. Responses received for question 9.

Q10: Do you feel that the existing method you use to calculate elastic modulus and immediate settlement is conservative?

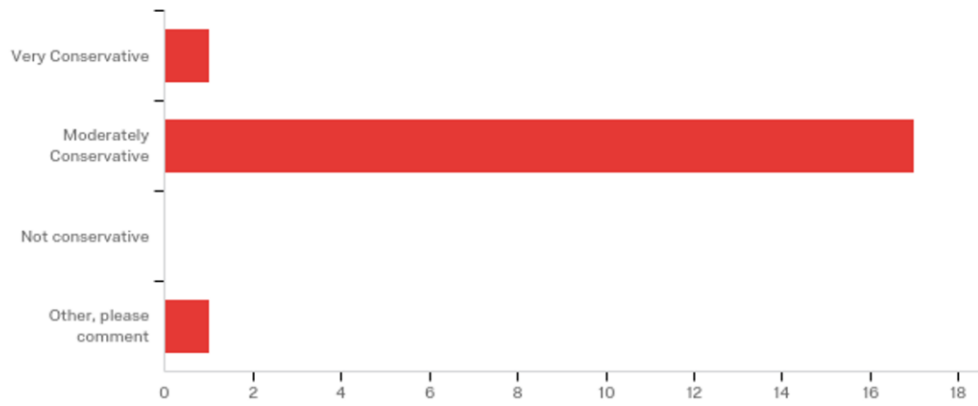


Figure A-10. Responses received for question 10.

APPENDIX B
PAPERS PRESENTED AT GEO-CONGRESS-ASCE

- **Conical Load Test-Induced Settlement in Central Florida Soils: Class A Prediction of Field Performance with Advanced Soil Models**
- **Factors Influencing Immediate Settlement in Central Florida Soils Using Conical Load Tests**

Conical Load Test-Induced Settlement in Central Florida Soils: Class A Prediction of Field Performance with Advanced Soil Models

A. Felipe Uribe-Henao¹; Luis G. Arboleda-Monsalve²; Sergio Savater³; Manoj Chopra⁴; and Larry Jones⁵

¹Research Assistant, Dept. of Civil, Environmental, and Construction Engineering, Univ. of Central Florida, Orlando, FL 32816, USA. E-mail: afuribeh@knights.ucf.edu

²Assistant Professor, Dept. of Civil, Environmental, and Construction Engineering, Univ. of Central Florida, Orlando, FL 32816, USA. E-mail: Luis.Arboleda@ucf.edu

³Research Assistant, Dept. of Civil, Environmental, and Construction Engineering, Univ. of Central Florida, Orlando, FL 32816, USA. E-mail: marinsergio81@knights.ucf.edu

⁴Professor, Dept. of Civil, Environmental, and Construction Engineering, Univ. of Central Florida, Orlando, FL 32816 USA. E-mail: Manoj.Chopra@ucf.edu

⁵State Geotechnical Engineer, Florida Dept. of Transportation, 605 Suwannee St., Tallahassee, FL 32399, USA. E-mail: Larry.Jones@dot.state.fl.us

ABSTRACT

A class “A” prediction of conical test-induced settlements in Central Florida soils is conducted using one conventional Mohr-Coulomb and two advanced hardening soil and hypoplasticity constitutive models. A conical load test is performed by constructing a cone-shaped mound of soil on the ground surface, placed over a center plate to measure settlement arising from the self-weight of the conical soil arrangement. Constitutive soil parameters for the numerical models presented in this paper are determined from previous case histories with similar expected soil behavior based on field test records. A conical load test is modeled using the finite element numerical software PLAXIS 2D to predict the evolution of the settlement during the construction of a conical load test. Results obtained from the numerical model showed that predicted settlements for the Central Florida soil conditions ranged from 24 to 36 mm. Given the soil conditions, excess pore water pressures generated from the construction of the conical load were negligible.

INTRODUCTION

The calculation of immediate settlements for embankments and shallow foundations require the use of accurate stiffness parameters. The most common method to determine soil modulus in practice is by means of correlations with the results of field tests such as: standard penetration test (SPT), cone penetration test (CPT), dilatometer test (DMT), pressuremeter test (PMT), or geophysical seismic wave propagation tests. There are many correlations that can be used to define stiffness parameters for settlement calculations, which yield a wide range of results due to the uncertainties in measuring accurate soil stiffness in the field and the laboratory (Kulhawy and Mayne 1990). Even if the soil elastic modulus is known with a large degree of confidence, there are numerous methods to predict settlements which yield a wide range of results. The accuracy of these methods for Central Florida-specific soil conditions is planned to be evaluated by means of a conical field load test at three different test sites located at the University of Central Florida (UCF) campus. This effort will consist on a Class “A” prediction presented in this paper followed by a conical field load test. This concept was introduced by Lambe (1973) to describe geotechnical behavior predicted before knowing actual behavior, which denotes a vital phase of

design in geotechnical practice.

Schmertmann (1993) was the first proponent of a conical load test to measure soil compressibility on a scale between *in situ* plate and full-scale embankment tests. A conical load test is advantageous because of its full-scale nature; typically loads ranging from 400 to 1,000 kips (1,780 to 4,450 kN) can be applied which results in a large influence zone in terms of vertical stresses generated at great depths. From this test, useful and realistic compressibility information parameters can be obtained for the calculation of settlements. The site has been geotechnically characterized using 10 field CPTu and 2 SPT. This data is used to reproduce soil behavior via preliminary numerical simulations. Constitutive soil models of Hardening Soil, Mohr-Coulomb, and Hypoplasticity Sand and Clay were employed to perform a “Class A” type prediction of the evolution of settlements at the proposed site where a full-scale surcharge load conical test will be developed. Constitutive soil parameters were determined numerically using the laboratory test module of PLAXIS 2D taking as baseline other soils with similar geotechnical characteristics in terms of shear strength, dilation, and compressibility presented by Arboleda-Monsalve (2014), Zapata-Medina (2007), Gallant (2015), and Blackburn (2005).

CONICAL LOAD TEST-INDUCED SETTLEMENT

The conical load test-induced settlement proposed by Schmertmann (1993) is used to measure soil compressibility on a scale between *in situ* plate and full-scale embankment tests. The test consists of constructing a cone-shaped mound of soil on the ground surface, placed over a center plate to measure settlement arising from the self-weight of the conical soil arrangement. Schmertmann (1993) performed this test to evaluate the compressibility of a 6-m thick layer of construction debris and granular materials. The test was performed by increasing the height and base diameter of the cone in four stages until a height of 4.3 m and a diameter of 12.2 m were reached; equivalent to an accumulated loading of 2,600 kN. Once the construction of the cone was completed, the conical load test-induced settlements were recorded for 100 days and a maximum settlement of 41 mm was measured beneath the cone. For those soil conditions, Schmertmann observed rapid excess pore water pressure dissipation due to the conical distribution of the surcharge (i.e., mostly immediate settlements were measured). The author concluded that the ratio of the compressible layer thickness to conical test diameter defines the influence of radial drainage on the consolidation of underlying soils; e.g., small ratios led to 1-D consolidation, whereas large ratios led to anisotropic consolidation (Schmertmann 1993). In the present paper, a class “A” prediction of a conical load test-induced settlement is presented using advanced constitutive soil models.

Figure 1 presents a plan view of the project site including the locations of field tests and a schematic view of a conical load test that will be accomplished in the area. The site is part of an ongoing experimental program developed by the Florida Department of Transportation (FDOT) at the UCF that started in the early 2000s (Chopra et al. 2003). The main objective has been to evaluate axial and lateral capacities of deep foundations and issue site-specific immediate settlement recommendations to be used by practitioners in the state of Florida. Eight field tests, including the two SPTs shown in Figure 1, were performed near the projected location of the cone (denoted with dashed lines in the figure). These tests provided sufficient information for the determination of a generalized soil profile and soil parameters to be used in the numerical simulations presented in this paper. The CPTs denoted in the figure as CPTu-1 through 3 were performed at the project site near the projected location of the conical load test. The projected conical load test will consist on building a 12.2 m-diameter cone made of a controlled granular

fill placed at the angle of repose of the soil until a height of 4.3 m (14ft) reached in successive increments completed in about a week. The soil cone will induce a total weight of approximately 3,150 kN (700 ksi) on the ground surface over an area of 117 m².

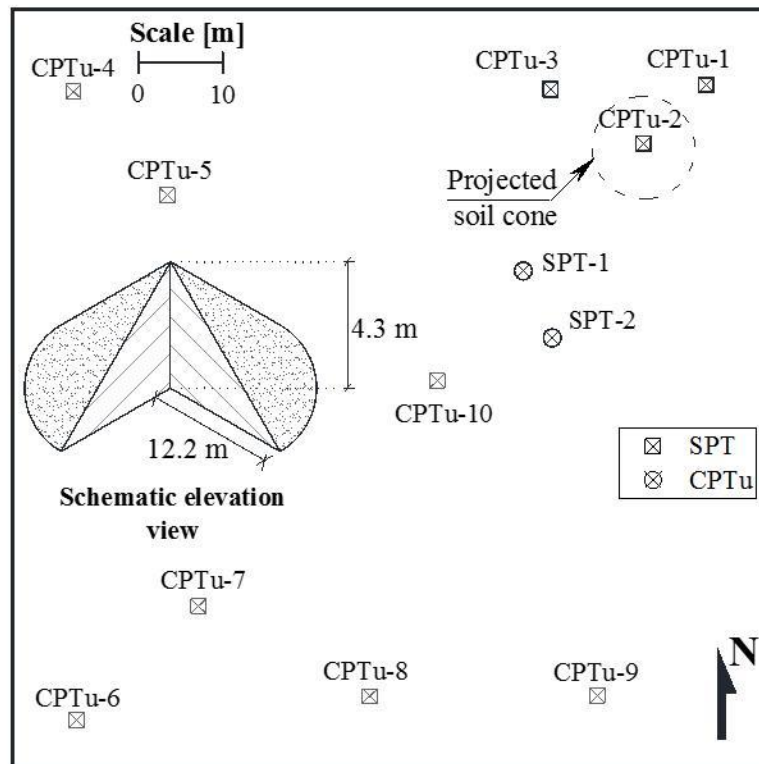


Figure 1. Plan view of project site and projected location of a conical load test.

Figure 2 shows the summarized soil profile obtained from the analysis of 3 CPTu and 2 SPT field tests. The soil profile consists of a surficial 4.5-m layer of poorly graded medium-dense sand deposits geologically identified from the Pleistocene age, which transitions to dense within the same soil layer. The estimated average relative density of the material is 70%. This layer is followed by a medium-dense sand from depths between 5 and 11 m. This sandy layer presents an estimated average relative density of 50%. More contractive than dilative behavior during shearing is expected for that layer in relation to the topmost layer. Underlying the sandy layers, a 3-m thick silty clay was found with undrained shear strengths ranging between 80 and 100 kPa and estimated overconsolidation ratio of 5 based on correlations of the stress history of clayey soils with CPT data (Kulhawy and Mayne 1990). The deepest soil layer consists of a 3.5-m thick layer of very dense sand. The groundwater table at the site was found at a depth of 0.9 m.

NUMERICAL MODEL

A two-dimensional numerical analysis using PLAXIS 2D (2018) was conducted to predict conical load test induced-settlements using three constitutive soil models: one conventional-Mohr Coulomb and three advanced- Hardening soil (1999) and Hypoplasticity sand (von Wolfersdorff 1996) and clay models (Mašin 2014). Hypoplasticity, as opposed to Mohr-Coulomb and Hardening soil, uses a constitutive relation derived in terms of a single tensorial equation that defines the directional triaxial stress probes and stiffness degradation of the material instead of defining complex yield functions, consistency rules, or plastic potential

functions. The version of the model used herein incorporates the intergranular strain concept proposed by Niemunis and Herle (1997) and Mašin (2014) capturing small-strain stiffness non-linearity, recent stress history effects, and stress-strain-strength behavior of compressible clay and sand deposits. Further details can be found in Arboleda-Monsalve (2014) and Gallant (2015).

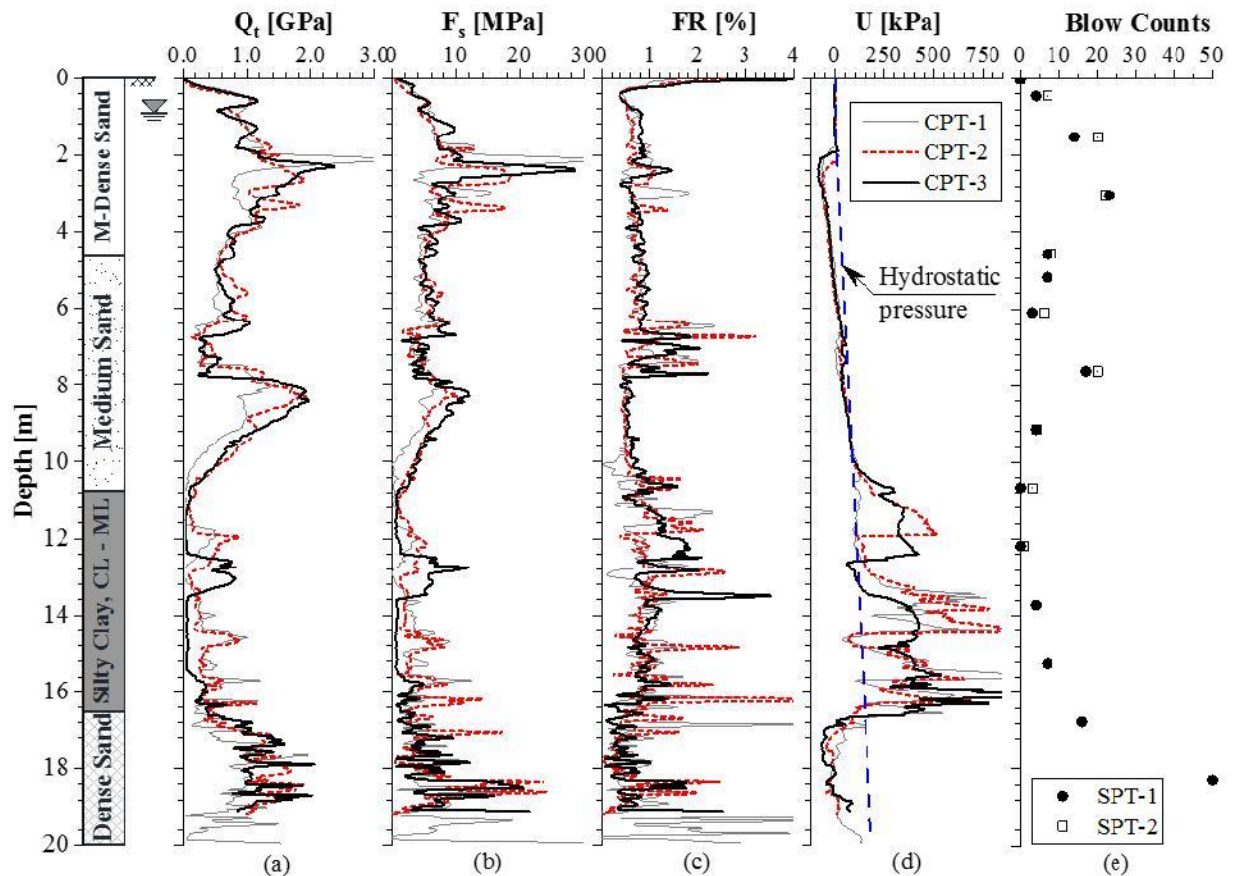


Figure 2. Summarized soil profile and field test records.

Tables 1 through 3 list the Mohr-Coulomb, Hardening Soil, and Hypoplasticity sand constitutive soil parameters employed to describe the soil behavior at the projected location of the soil cone (see Figure 2). These parameters were selected to best represent the soil behavior as measured in the field tests. They were obtained from soils with similar behavior in terms of shear strength, dilation, and compressibility as reported by Blackburn (2005), Zapata-Medina (2007), Gallant (2015), and Arboleda-Monsalve (2014). Hypoplasticity clay parameters are not presented in the paper due to space limitations and can be found in Arboleda-Monsalve (2014).

Figure 3 presents numerically simulated soil tests performed using the built-in laboratory test module of PLAXIS 2D for the three sandy layers found in the soil profile. In the figure, triaxial compression tests and oedometer tests were computed using the constitutive soil parameters listed in Tables 1-3. This is performed to study expected soil behavior at the elemental scale level. Triaxial compression tests were K_0 -consolidated and sheared under drained conditions. In spite of the differences in the formulation and capabilities of the constitutive soil models, the soil parameters were selected to minimize the differences in computed volumetric strains and deviatoric stresses. The parameters were also selected to obtain similar dilative behavior

regardless of the soil model employed to match expected behavior of the subsurface soils. The computed results with Mohr-Coulomb were more contractive than those computed with Hypoplasticity sand and Hardening soil models. Oedometer tests were computed with one unload and reload cycle for each sandy layer, obtaining reasonable differences between each soil model.

Table 1. Constitutive soil parameters for the Mohr-Coulomb soil model.

Parameter	Description	Units	Sandy layers			Silty Clay
			Dense	M-Dense	Medium	
E'	Effective young's modulus	kPa	19000	10000	7000	104.4
ν	Poisson ratio		0.3	0.3	0.3	0.2
E_{oed}	Oedometer modulus	kPa	25580	13460	9423	116
C_{ref}	Reference cohesion	kPa	1	1	1	21
ϕ	Friction angle	deg	40	35	30	38
ψ	Dilatancy angle	deg	12	14	5	1

Table 2. Constitutive soil parameters for the Hardening soil model.

Parameter	Description	Units	Sandy layers			Silty Clay
			Dense	M-Dense	Medium	
E_{50}^{ref}	Secant modulus at 50% strength for primary at reference pressure	kPa	14370	7185	7185	244
E_{oed}^{ref}	Tangent modulus for primary compression at reference pressure	kPa	14370	7185	7185	73
E_{ur}^{ref}	Elastic unloading/reloading at reference pressure	kPa	43110	21560	21560	731
p^{ref}	Reference pressure	kPa	100	100	100	100
e_{init}	Initial void ratio		0.6	0.7	0.8	1
m	Stress dependent stiffness		0.3	0.3	0.3	0.94
C_{ref}	Reference cohesion	kPa	1	1	1	1
ϕ	Friction angle	deg	40	35	30	38
ψ	Dilatancy angle	deg	15	13	5	5

Figure 4 shows the results of two computed soil tests obtained using the constitutive parameters listed in Tables 1-3 for an overconsolidated silty clay. K_0 -consolidated triaxial compression tests sheared under undrained conditions were computed using PLAXIS 2D as presented in Figure 4a. Figure 4b shows results obtained for the oedometer tests with a unload and reload cycle. Constitutive parameters determination efforts were directed to minimize the differences in computed excess pore pressures and deviatoric stresses. However, differences in compressibility were found for Mohr-Coulomb, which had a more compressible behaviour than Hypoplasticity and Hardening soil model.

CLASS "A" PREDICTION OF A CONICAL LOAD TEST-INDUCED SETTLEMENTS

Figure 5 illustrates the axisymmetric finite element model used for the predictions of conical

load test-induced settlements. The figure shows the soil layers employed to numerically simulate the subsurface conditions and the dimensions used for the soil cone modeled with a soil cluster of linear-elastic material. The subsurface soil conditions were modeled employing soil elements using the abovementioned constitutive models (Tables 1-3). Soil clusters for each layer were defined using 15-node triangular elements to provide high-quality stress results with 12 gauss integration points and a fourth order interpolation for displacements.

Table 3. Constitutive soil parameters obtained using Hypoplasticity sand.

Parameter	Description	Sandy layers		
		Dense	M-Dense	Medium
ϕ	Critical state friction angle	35	32	30
h_s	Granular hardness [GPa]	200	200	200
N	Exponent for pressure sensitive of a grain skeleton	0.28	0.28	0.28
e_{do}	Minimum void ratio at zero pressure	0.58	0.58	0.58
e_{co}	Critical void ratio at zero pressure	1.096	1.096	1.096
e_{io}	Maximum void ratio at zero pressure	1.315	1.315	1.315
α	Exponent for the transition between peak and critical stresses	0.25	0.25	0.25
β	Exponent for stiffness dependency on pressure and density	1.4	1.4	1.4
R	Size of the elastic range	1×10^{-3}	1×10^{-3}	1×10^{-3}

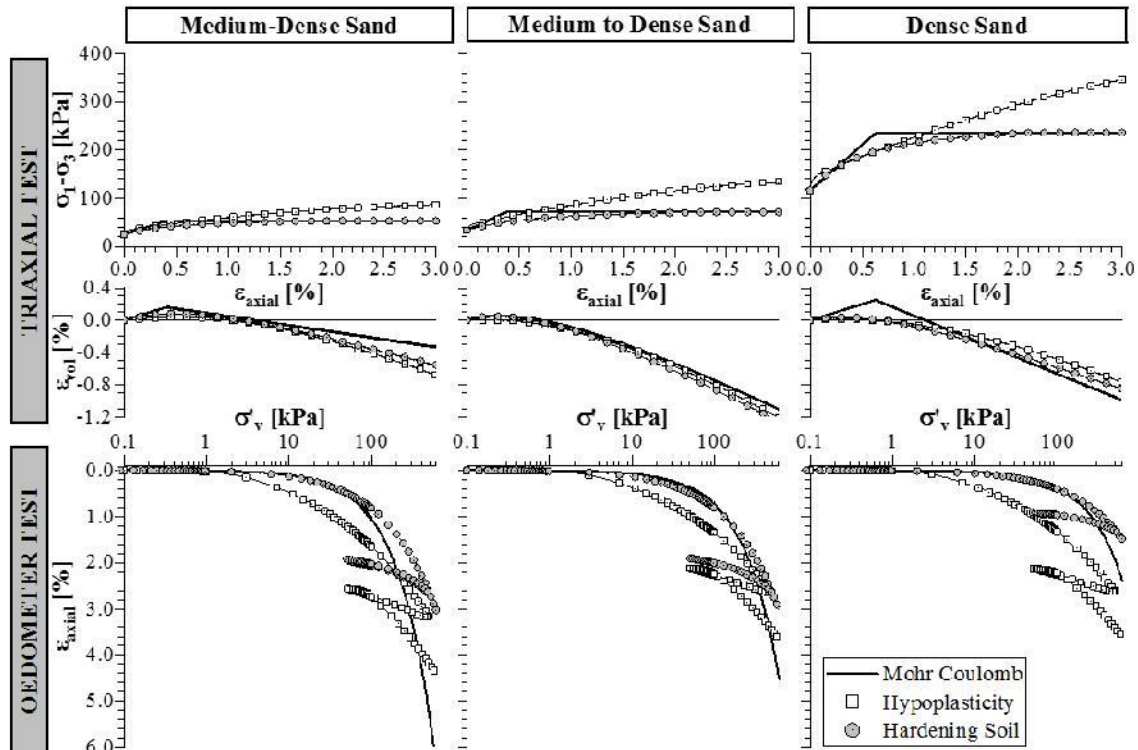


Figure 3. Computed triaxial compression and oedometer tests for the sandy layers.

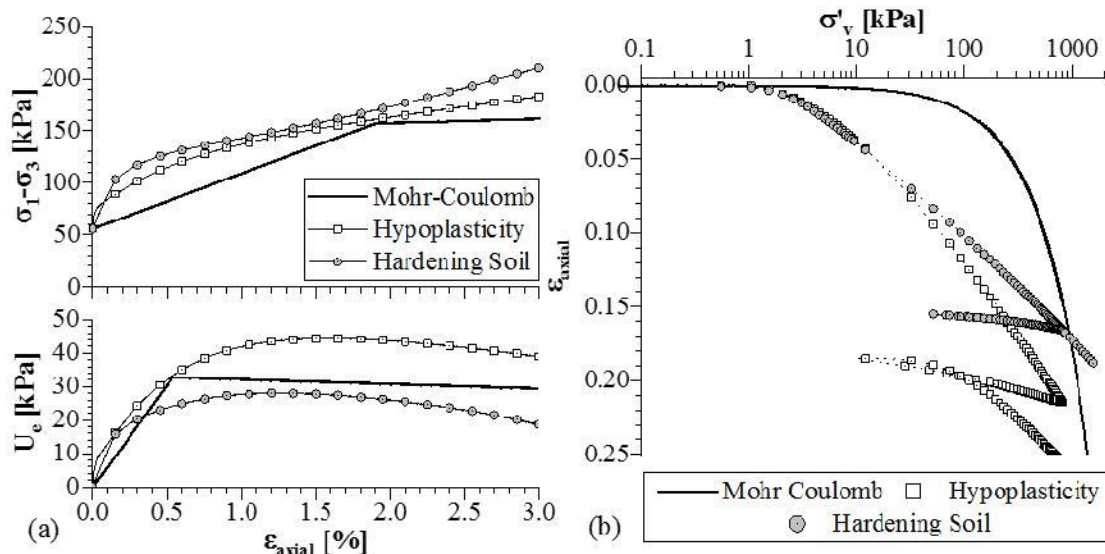


Figure 4. Computed behavior for the silty clay layer: a) triaxial compression tests and b) oedometer tests.

The following assumptions were made for these “Class A” type prediction models (Lambe 1973): i) the unit weight of the soils used for the conical loading is 19 kN/m^3 , ii) the loading applied with the soil cone is flexible, iii) the loading is applied incrementally by adding 0.33 m (1 ft) of soil in a stage construction scheme in the numerical model using plastic stages followed by consolidation stages of approximately one day per increment, iv) the conical load tests is completed when the height of the cone reaches 4.3 m; v) a final consolidation stage of 87 days is added so that any excess pore water pressure build-up is dissipated.

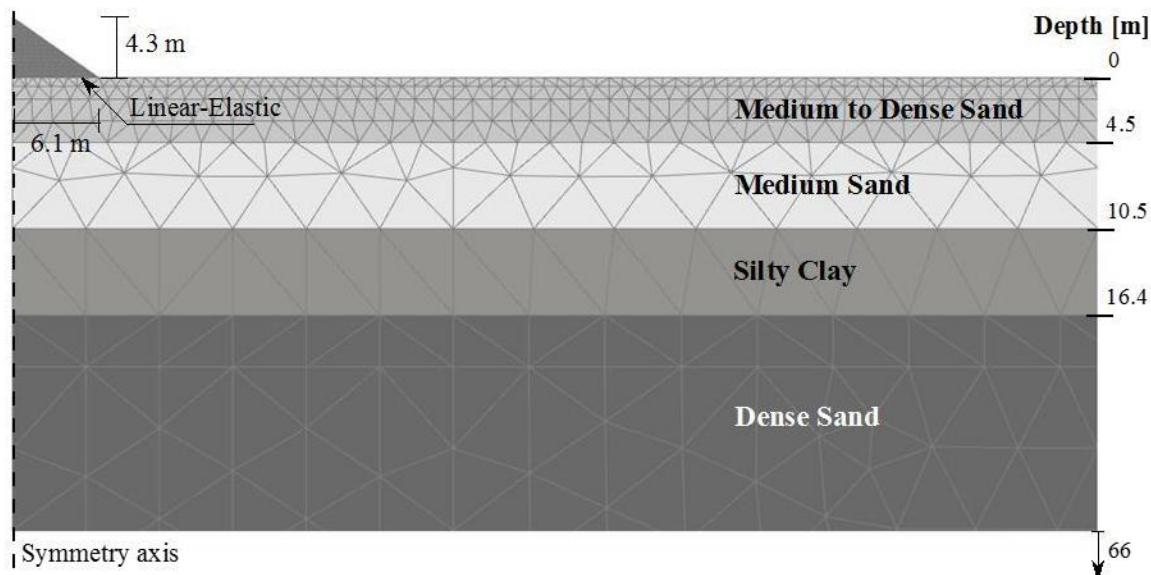


Figure 5. Axisymmetric finite element model built in PLAXIS 2D

Figure 6 presents the predicted results using the finite element model for the conical load test. Figure 6a shows the distribution of the vertical effective stresses with depth for different cone height stages. The soil cone was modeled to be flexible to better represent the real surcharge

conditions associated with the cone construction. This assumption led to vertical effective stresses up to 70% larger than those estimated using methods based on the theory of elasticity (i.e., Boussinesq 1885). The influence zone in the vertical (i.e., depth) direction because of the application of the cone loading is approximately 10 m. This was determined as the depth corresponding to an increase in total vertical stress ($\Delta\sigma$) induced by the cone lower than 10% of the vertical effective stress at that given depth. The soil layers below that point are no longer participating in the settlement calculation.

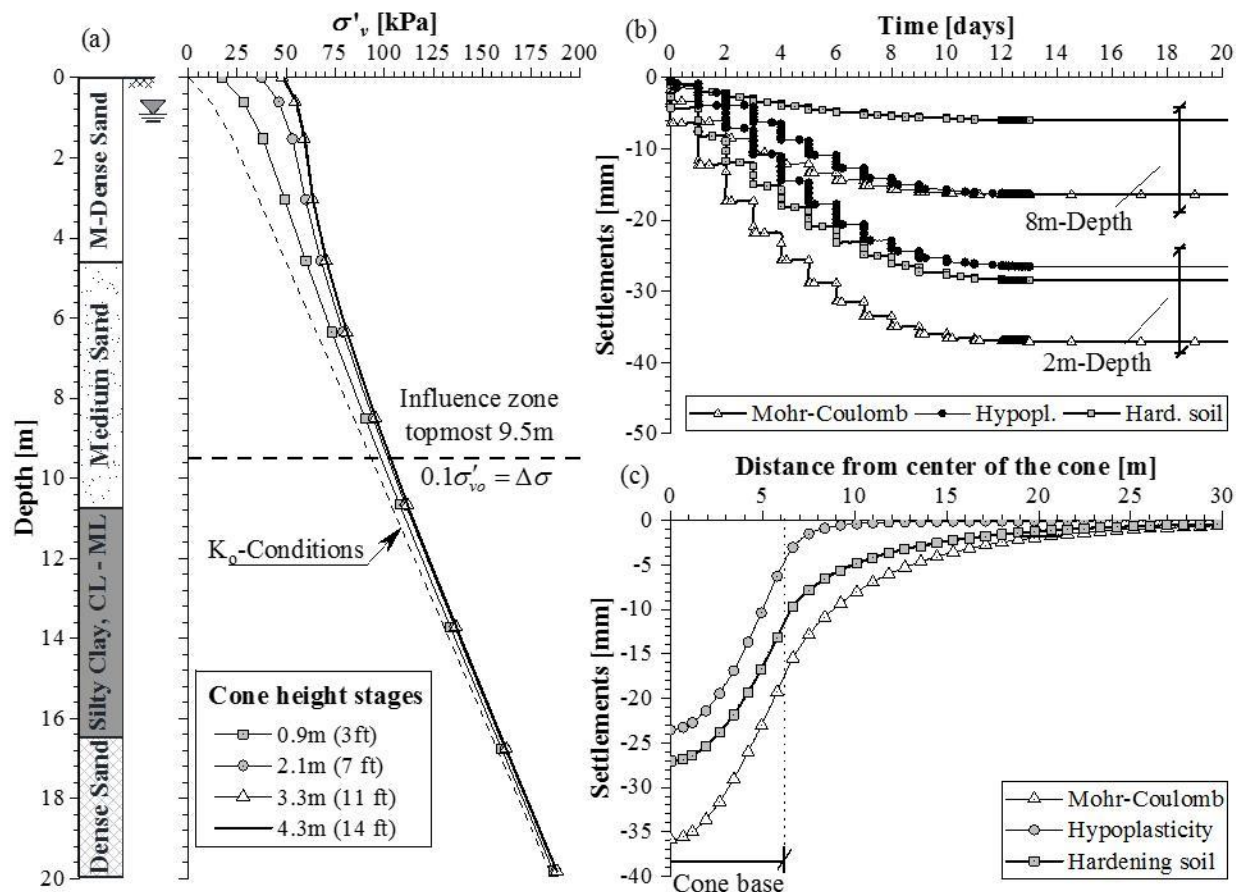


Figure 6. Computed results of the conical load test: a) vertical effective stress varying with depth; b) evolution of settlements with time; and c) conical load test-induced settlements.

The evolution of settlements with time of a point located in the center of the cone and at 2 m and 8 m below the ground surface are presented in Figure 6b for each constitutive soil model. As expected, most settlements occurred between the first and fifth day of the cone construction which corresponds to 73% of the conical loading. Excess pore water pressure generation was computed with the numerical model but given the relatively large hydraulic conductivities of the soils at the projected project site, these values were very small (i.e., less than 1 kPa) causing negligible consolidation settlements after the last cone construction day (i.e., day 14). Note also that the settlements computed with Mohr-Coulomb model at 2 m below the ground surface were approximately 10 mm greater than those computed with Hardening soil and Hypoplasticity at the end of the cone construction. Differences between Mohr-Coulomb and Hypoplasticity were negligible near the influence zone threshold (i.e., 8 m depth). Figure 6c presents the computed conical load-induced settlements, where a maximum settlement of 40 mm was obtained.

Differences in settlements are attributed to model capabilities to capture changes in volume in vertical direction.

Figure 6c shows the computed ground surface settlement trough at the end stage of the cone construction (4.3 m or 14 ft). The maximum predicted ground surface settlements ranged from approximately 25 to 35 mm, being those computed using Mohr-Coulomb the largest predicted settlements. This is attributed to the fact that Mohr-Coulomb displayed the most contractive behavior estimated with the laboratory test module of PLAXIS 2D (see Figure 3). Recall that constitutive parameter determination efforts were directed to model the dilative rather than the contractive behavior of the sandy layers.

SUMMARY AND CONCLUSION

Based on the results of the finite element model, the following conclusions can be drawn: i) the computed vertical effective stresses with the numerical model, which model the inherent flexibility of the soil cone, were greater than those preliminary estimated using conventional methods based on the theory of elasticity; ii) it is expected that the influence zone in the vertical (i.e., depth) direction because of the application of the cone loading will be approximately 10 m; iii) excess pore water pressure generation during the construction of the soil cone was very small, and thus long-term time-dependent effects associated with a conical load test for the Central Florida soil conditions are negligible; and iv) maximum predicted ground surface settlements ranged from 24 to 36 mm, where Mohr-Coulomb showed the largest amount of predicted settlements, while Hardening soil and Hypoplasticity predicted lower values. These results are associated with the fact that Mohr-Coulomb displayed the most contractive behavior estimated with the laboratory test module of PLAXIS 2D.

ACKNOWLEDGMENTS

Financial support was provided by the Florida Department of Transportation, Grant No. BDV24 TWO 977-29. The support of the funding agency is greatly appreciated. The opinions, findings, and conclusions expressed in this publication are those of the authors and do not necessarily those of the Florida Department of Transportation or the U.S. Department of Transportation.

REFERENCES

- Arboleda-Monsalve, L. G. (2014). "Performance, instrumentation and numerical simulation of One Museum Park West Excavation." Doctoral dissertation, Northwestern University.
- Blackburn, J. T. (2005). "Automated remote sensing and three-dimensional analysis of internally braced excavations." Doctoral dissertation, Northwestern University.
- Boussinesq, J. (1885). *Application des potentiels à l'étude de l'équilibre et du mouvement des solides élastiques...* Gauthier-Villars.
- Chopra, M., Horhota, D., Townsend, F. C., Anderson, J. B., and Horta, E. (2003). *Site preparation for a deep foundation test site at the Univ. of Central Florida*. Department of Civil and Environmental Engineering, University of Central Florida.
- Gallant, A. P. (2015). "A field and numerical evaluation of blast densification at a test section." Doctoral dissertation, Northwestern University.
- Kulhawy, F. H., and Mayne, P. W. (1990). *Manual on Estimating Soil Properties for Foundation Design (No. EPRI-EL-6800)*. *Electr. Power Res. Inst.*, Geotechnical Engineering Group, Palo

- Alto, CA (USA); Cornell Univ., Ithaca, NY (USA).
- Lambe, T. W. (1973). "Predictions in soil engineering." *Géotechnique*, 23(2), 151–202.
- Mašin, D. (2014). "Clay hypoplasticity model including stiffness anisotropy." *Géotechnique*, 64(3), 232–238.
- Niemunis, A., and Herle, I. (1997). "Hypoplastic model for cohesionless soils with elastic strain range." *Mech. Cohesive-Frictional Mater.*, 2(4), 279–299.
- Plaxis. (2018). "PLAXIS 2D 2018." Delf, Netherlands.
- Schanz, T., Vermeer, a, and Bonnier, P. (1999). "The hardening soil model: formulation and verification." *Beyond 2000 Comput. Geotech. 10 years PLAXIS Int. Proc. Int. Symp. beyond 2000 Comput. Geotech. Amsterdam Netherlands 1820 March 1999*, (June 1999), 281.
- Schmertmann, J. H. (1993). "Conical test load measuring compressibility." *J. Geotech. Geoenviron. Eng.*, 119(5), 965–971.
- von Wolffersdorff, P. A. (1996). "Hypoplastic relation for granular materials with a predefined limit state surface." *Mech. Cohesive-Frictional Mater.*, 1(3), 251–271.
- Zapata-Medina, D. G. (2007). "Semi-empirical method for designing excavation support." Master thesis, University of Kentucky.

Factors Influencing Immediate Settlements in Central Florida Soils Using Conical Load Tests

Sina Nassiri¹; Sergio Savater²; Luis Arboleda-Monsalve³; Manoj Chopra⁴; and Larry Jones⁵

¹Research Assistant, Dept. of Civil, Environmental, and Construction Engineering, Univ. of Central Florida, Orlando, FL, USA. E-mail: sina.nssr@knights.ucf.edu

²Research Assistant, Dept. of Civil, Environmental, and Construction Engineering, Univ. of Central Florida, Orlando, FL, USA. E-mail: marinsergio81@knights.ucf.edu

³Assistant Professor, Dept. of Civil, Environmental, and Construction Engineering, Univ. of Central Florida, Orlando, FL, USA. E-mail: Luis.Arboleda@ucf.edu

⁴Professor, Dept. of Civil, Environmental, and Construction Engineering, Univ. of Central Florida, Orlando, FL, USA. E-mail: Manoj.Chopra@ucf.edu

⁵State Geotechnical Engineer, Florida Dept. of Transportation, Tallahassee, FL, USA. E-Mail: Larry.Jones@dot.state.fl.us

ABSTRACT

Calculation of immediate settlement plays a very important role in the design of foundations and geostructures when they are supported in granular soils. Soil strength and stiffness mechanisms associated with immediate settlements can be studied via full-scale load tests following Schmertmann (1993) conical load test method, which has been proven successful and practical to study settlements in granular soil deposits. The test consists of constructing a conical mound of granular fill placed at its angle of repose to create an approximate 12.3 m diameter 4.2 meter-high cone. This paper presents first the site characterization of a site near the University of Central Florida campus mainly in terms of CPTs, SPTs, and DMTs. These tests were used to calibrate constitutive soil model parameters for finite element models intended to recreate the conical load sequence. Numerical simulations using hardening soil and hardening soil enhanced with small strains constitutive models were developed to simulate the loading sequence of a Schmertmann conical load test and draw conclusions regarding the variables involved in the problem: stiffness and construction sequence of the conical loading, stage construction sequence of loading, relative density and stiffness of supporting granular soils, and horizontal influence zones.

INTRODUCTION

Analysis and design of geostructures require accurate identification and characterization of soil strata via field tests since collecting high-quality laboratory data on undisturbed soil samples (e.g., using block sampling techniques) is challenging in weakly cemented sandy soils. Thus, geotechnical engineers rely on *in situ* tests such as Cone Penetration Test (CPT), Standard Penetration Test (SPT), Dilatometer Test (DMT), or Pressuremeter Test (PMT) to accurately estimate representative soil parameters. Numerous studies have been conducted to estimate soil settlement using directly the results of field data (e.g., Robertson and Campanella 1988; Anagnostopoulos *et al.* 1991). The results of field tests have been widely used in practice for the determination of soil strength and compressibility parameters to be used for the calculation of settlement (Hough 1959, Terzaghi and Peck 1967, Meyerhof 1965, 1974, D'Appolonia 1969, Schmertmann 1970, 1986, Oweiss 1979, Bowles 1987, Papadopoulos 1992, Mayne and Poulos 1999). Alternative full-scale field tests have also been developed to avoid the excessive use of

correlations to feed the abovementioned methods, including field plate settlement tests, in situ footing testing programs, and the method used in this research: conical load tests (Schmertmann 1993, Anderson *et al.* 2007, O'Loughlin and Lehane 2010).

The Schmertmann (1993) conical load field testing method was originally proposed to investigate soil compressibility. The method consisted of a gradually constructed cone-shaped mound of soil placed on the ground surface as short and long term soil stresses and ground movements are continuously monitored. This type of test has been classified as an intermediate level test between field plate load tests and full-scale embankment tests. Conical load tests represent a reliable field test procedure that at a relatively low construction cost can accurately provide insight into the *in situ* compressibility characteristics of soils, rather than indirectly determining soil parameters only on the basis of strength field tests such as SPT, CPT, DMT, or PMT. This paper elucidates and studies in detail the variables that influence the settlement/compressibility response of soils when measured via conical load testing and ultimately concludes that this type of full-scale testing is an example of a soil-structure interaction problem, being the structure the conical load arrangement, where the relative stiffness of the participating component play an important role. In this test, the interaction between both systems, soils and conical load arrangement, depend greatly on the sequence of loading and strength-stress-strain characteristics of soils and applied loading. By means of well-calibrated geotechnical models, this paper reproduces the conical load testing sequence of a series of conical load tests performed at the UCF campus (Arboleda-Monsalve *et al.* 2019) which are numerically simulated to determine the variables involved in the determination of ground surface settlements.

PLAXIS 2D is a commercial finite element software that has been commonly used in practice to simulate the behavior of geotechnical structures (e.g., Blackburn 2005; Zapata-Medina 2007; Arboleda-Monsalve 2014). Using the results of field tests, finite element input parameters can be determined and numerical models can be built to compute representative engineering demands for new designs, for quantification of performance of existing geotechnical structures, or to extend parametrically (i.e., study the variables involved) the reach of geotechnical field or laboratory testing programs. Two aspects associated to numerical modeling techniques need to be accounted for in practice to provide valuable insight of soil behavior: i) a comprehensive field investigation program for the accurate knowledge of initial soil stress states and ii) adequate calibration of constitutive soil input parameters. Conventional elastic-perfectly plastic soil models (e.g., Mohr-Coulomb) have been widely used to study strength limit state responses in numerous geotechnical applications (e.g., Anderson *et al.* 2007) but the model lacks of robustness and oversimplifies soil behavior when dealing with ground deformation assessments for projects that mobilize rather complex stress paths and wide ranges of shear strains (γ_s). Thus, more advanced soil models are recommended to capture more realistically soil behaviors for accurate estimation of ground movements. In this research, two advanced soil models, including small strain soil behavior, are used to study parametrically the abovementioned effects.

In order to make a reliable prediction of soil response to applied loadings, a combination of methods was adopted in this study: Based on site-specific SPT, CPT_u, and DMT tests, compressibility characteristics of the soil mass at the test site were investigated and the results were analyzed in numerically simulated laboratory testing environments. A 2D PLAXIS model is developed in this paper based on the results of a full-scale field test to investigate the compressibility soil behavior subjected to a Schmertmann (1993) type conical load test. Because of space limitations, only a brief comparison of field versus computed results is presented since

this paper is intended to elucidate the main variables involved in the soil-structure interaction mechanisms of the geomechanical response of soils due to full-scale conical load tests. Further details of the experimental program are provided in Arboleda-Monsalve *et al.* (2019). Ground surface settlements and vertical and horizontal influence zones are calculated herein using Hardening Soil (HS) and Hardening Soil Small Strain (HSS) models. This parametric evaluation provides a range of settlements for each adopted constitutive soil model, studies the importance of modeling adequately the conical loading construction sequence, and highlights the pivotal role that small strain behavior plays in the results of numerical simulations in geotechnical engineering.

GEOTECHNICAL SITE CHARACTERIZATION

A rectangular 100 m by 100 m site located at the University of Central Florida Arboretum was selected to study the variables that influence conical load testing. Subsurface soil stratigraphy and geotechnical characteristics were defined from ten Piezocone Tests (CPTu), five Standard Penetration Tests (SPT), and three Dilatometer Tests (DMT) performed until a depth of approximately 20 m was reached. Tests were conducted by Florida Department of Transportation (FDOT) to investigate site-specific soil parameters. This study defines input soil parameters determined from the proposed subsurface conditions to be used in numerical simulations so that the most important geotechnical variables involved in the program can be studied.

Note: Abbreviations used in the figure: K&M (CPT)= Kulhawy and Mayne (1990) CPT correlation. R&C (CPT)= Robertson and Campella's (1983) CPT correlation. DMT= Dilatometer test results by TC16 DMT report (2001). Peck (SPT)= Peck et al. (1974) SPT correlation. J (CPT)= Jamiolkowski et al. (2001) CPT correlation. ω = water content. Mf (SPT), SPT= Meyerhof (1956) SPT correlation. PWP= porewater pressure and P_w = porewater pressure from CPT result. M (CPT)= Mayne (2005) CPT correlation. Guide (CPT)= CPT Guide (2015) 6th edition. I&T (SPT)= Imai and Tonouchi (1982) Young's Modulus based on SPT. R&S (CPT)= Rix and Stokoe (1991) shear modulus CPT correlation.

Figure 1 shows the summarized soil profile and computed stiffness parameters via published correlations. The soil conditions are summarized in four layers: The superficial layer, ground surface to approximately 5 m in depth (L1), is a poorly-graded medium-dense sand deposit geologically identified from the Pleistocene age with water content and relative density of approximately 20% and 50%~70%, respectively. Based on the field test results, internal friction angle was determined as 40°, and further laboratory tests indicated that the *in situ* void ratio and specific gravity are 0.7 and 2.59, respectively. This layer (L1), transitioned to a poorly-graded sand with medium density (40%~50%), lower internal friction angle (i.e., approximately 35°) and thickness of 5 m (L2). More contractive than dilative behavior from this layer was expected. This layer was followed by a silty clay layer (L3) of 6 m in thickness. The deepest layer (L4) consisted of a 3.5-meter thick dense sand and the field tests were terminated at the bottom of the layer. According to the observation wells and piezometric data, the groundwater table was located at 0.9 m from the ground surface.

Based on the data provided by the test results, soil parameters were calculated. The internal friction angle was calculated based on correlations by Peck et al. (1974), Kulhawy and Mayne (1990), Robertson and Campella (1983), and TC16 DMT report (2001). Based on the CPT and SPT results and adopting correlations by Meyerhof (1956), Kulhawy, Mayne (1990), and Jamiolkowski et al. (2001), and were used to calculate *in situ* relative density. Other parameters such as Young's and shear moduli were calculated based on correlations by using Imai and

Tonouchi (1982), Rix and Stokoe (1991), Mayne (2006), and CPT guide 2015 6th edition.

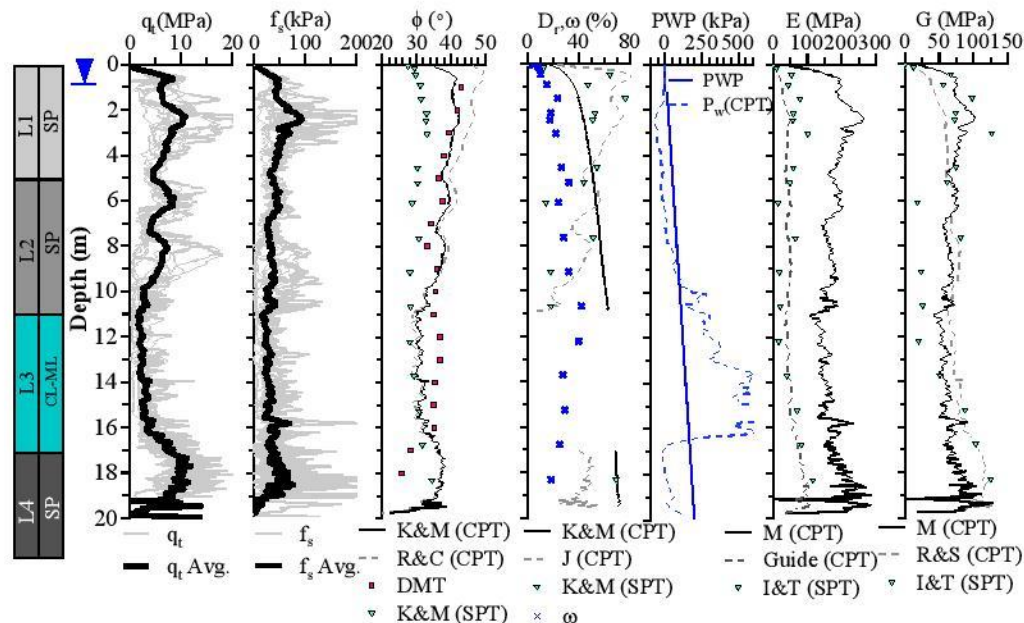


Figure 1. Summarized soil profile based on CPT, SPT, and DMT.

Note: Abbreviations used in the figure: K&M (CPT)= Kulhawy and Mayne (1990) CPT correlation. R&C (CPT)= Robertson and Campella's (1983) CPT correlation. DMT= Dilatometer test results by TC16 DMT report (2001). Peck (SPT)= Peck et al. (1974) SPT correlation. J (CPT)= Jamiolkowski et al. (2001) CPT correlation. ω= water content. Mf (SPT), SPT= Meyerhof (1956) SPT correlation. PWP= porewater pressure and P_w= porewater pressure from CPT result. M (CPT)= Mayne (2005) CPT correlation. Guide (CPT)= CPT Guide (2015) 6th edition. I&T (SPT)= Imai and Tonouchi (1982) Young's Modulus based on SPT. R&S (CPT)= Rix and Stokoe (1991) shear modulus CPT correlation.

DETERMINATION OF SOIL PARAMETERS

To simulate of the Schmertmann (1993) conical load test in PLAXIS 2D, the Hardening Soil (HS) and Hardening Soil Small Strain (HSS) model were selected. The constitutive formulation of the HS model was developed by Schanz et al. (1999), uses the same strength parameters of Mohr-Coulomb, but the soil stiffness is defined more accurately by adding three input parameters: E₅₀ representing secant stiffness modulus at 50% of the failure deviatoric stress, E_{oed} which is a one-dimensional compression modulus, and E_{ur} to account for unloading-reloading material stiffness. The HS model considers the stress-dependency (p') of stiffness moduli through a parameter "m". In this study, based on recommendation taken from Janbu (1963) and Duncan and Chang (1970) for sand and clay layers, the parameter "m" was determined as 0.5 and 1.0, respectively.

An extension was introduced to the model to consider soil stiffness degradation. The Hardening Soil Small Strain (HSS) incorporated the change in shear stiffness ratio G/G₀ versus shear strains based on Hardin and Dmnech (1972) degradation curves. Table 1 presents the input parameters using the HSS model. The parameters were determined from the results of field tests and were verified to match expected dilative or contractive soil behavior at an elemental

scale level as a function of the relative density of each soil.

Table 1. Input Parameters for the HSS Model

<i>Param</i>	<i>Description</i>	<i>Unit</i>	<i>L1</i>	<i>L2</i>	<i>L3</i>	<i>L4</i>
E_{50}^{ref}	Secant stiffness in drained triaxial test	MPa	20	15	3	23
E_{oed}^{ref}	Tangent stiffness from oedometric loading	MPa	20	15	3	23
E_{ur}^{ref}	Unloading/Reloading stiffness	MPa	61	45	9	70
m	Stress -level dependency stiffness factor	-	0.5	0.5	1	0.5
e_{init}	Initial void ratio	-	0.7	0.8	1	0.6
c'_{ref}	Effective cohesion	kPa	1	1	10	1
ϕ'	Effective internal friction angle	deg	40	35	35	43
Ψ'	Dilatancy angle	deg	10	8	1	12
K_0	K_0 value for normally consolidated soil	-	0.35	0.42	1	0.3 6
P_{ref}	Reference stress	kPa	100	100	100	10 0
ν	Poisson's ratio	-	0.3	0.3	0.25	0.3 60
D_r	Relative density	%	50~70	40~50	-	~8 0
$\gamma_{0.7}$	Shear strain threshold	-	5e-05	1e-04	5e-04	3e- 04
G_0^{ref}	Shear modulus at small strain	MPa	100	86	64	11 6

Sand cone soil parameters were measured by standard laboratory tests, sand cone tests (compaction test). The parameters values were found to be relatively similar to the layer L2. The sandy soil used for the conical load was modeled using Mohr-Coulomb constitutive soil model with Young's modulus and Poisson's ratio of 15 MPa and 0.3, respectively. The internal friction angle was assumed as 28 degrees. Soil parameters was assessed via PLAXIS virtual soil test feature. Figure 2a shows the computed results of the drained triaxial compression tests (TXC) for the sandy layers under K_0 - consolidated conditions selected to match soil properties of the soil in field. There is negligible difference in computed behavior between the results for L1 and L2; both displayed contractive behavior. Larger difference were computed for L4, since the combination of large confining pressures and high relative density, soil dilation was expected. Silty clay layer (L3) was also simulated under K_0 -consolidated undrained triaxial compression conditions (Figure 2b). Based on virtual oedometer test (OED), stress path plotted and as expected, constrained oedometric axial strains for L3 was larger than those computed for the granular soils.

NUMERICAL SIMULATION OF CONICAL LOAD TESTS

Figure 3 shows the axisymmetric finite element model developed in PLAXIS 2D with 15-node element type. The model dimensions were 70 m (height) to 150 m (width). On side boundaries, the lateral movements were constrained while vertical movements allowed. Initialization of the stress field was generated under K_0 conditions. Then, the conical loading

sequence was applied by incrementally activating sand cone soil clusters in 7 steps until a height of 4.2 m was reached. Soil behavior due to conical loading applied by the sand cone was analyzed using plastic analysis stages followed by 30-day consolidation stages in the numerical environment.

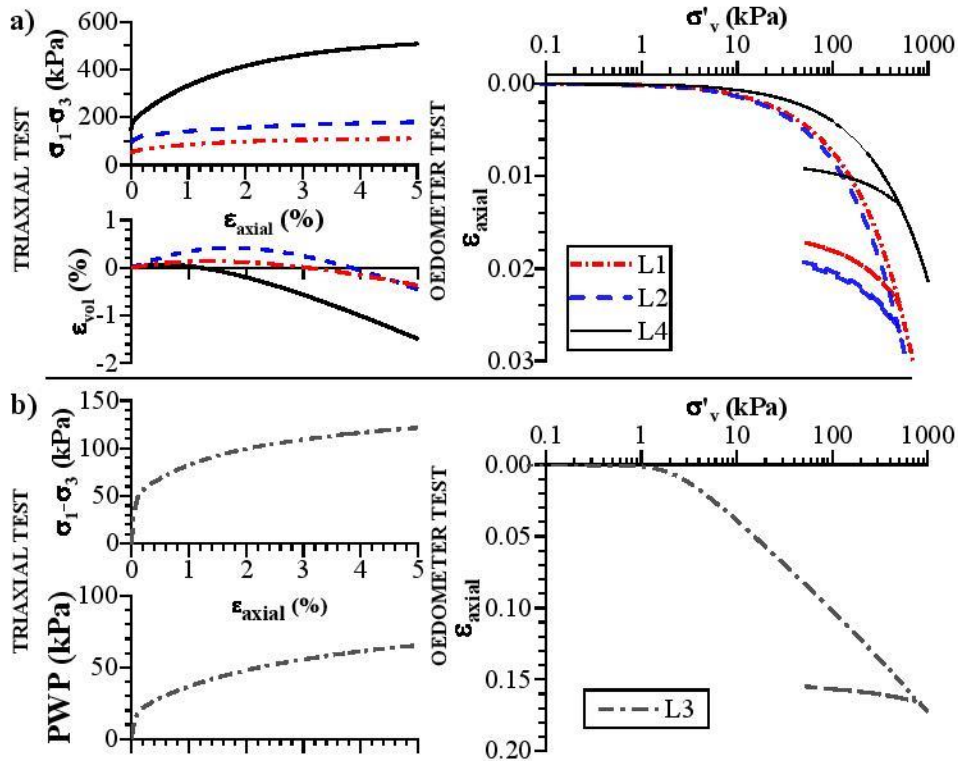


Figure 2. Computed results of TXC and OED tests for: a) L1, L2, L4 and b) L3.

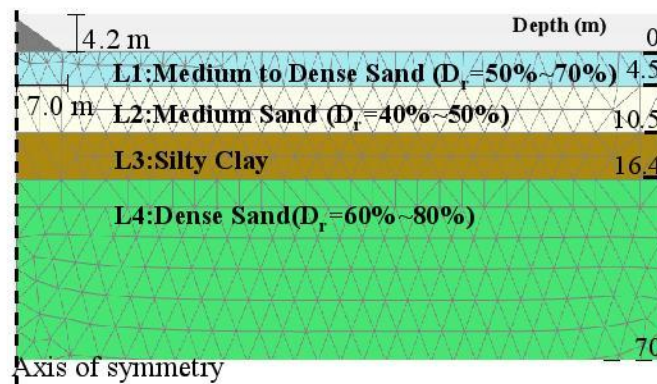


Figure 3. Model geometry: axisymmetric finite element model constructed in PLAXIS 2D

Figure 4 shows the effect of relative density of the surficial soil in the computed settlement. The best estimate of the relative density of layer L1 was from 50% to 70% (labeled in the figure as “natural soil” condition) which triggered a maximum settlement with the HSS model of approximately 20mm. Parametrically, by increasing the relative density of this layer by 20%, computed settlement decreased by 50%. Conversely, by decreasing the relative density by 20%, the computed settlements doubled. In the aforementioned soil models, relative densities were controlled by changing initial void ratios in the input values and the importance of a judicious

selection of the soil relative density is evident.

To demonstrate the importance of small strains on the computation of the settlement trough, the small-strain portion of the HSS model was switched off (i.e., HS model parameters matched those of the HSS model, except of those that controlled the small strain soil behavior). This way, the computed settlement increased three times those computed with the HSS model. This result was expected since the HS model was forced to completely ignore the large soil shear stiffness at the very small to small strain range. Given that it is not an accurate comparison, HS model parameters were independently calibrated (i.e., not only switching off small strain parameters). This way, stiffness parameters of the newly calibrated HS model E_{50} , E_{oed} , and E_{ur} were found to be four times those used for the HSS model. Both models, HSS and HS, now matched relatively well in terms of the magnitude of settlement, but larger differences were computed in the computed horizontal influence zones (defined as the distance from the center of the cone at which negligible settlements occurs, approximately 2-3 mm). In the HSS model, negligible settlement was noticed approximately 7 m from the center of the cone whereas for HS model, this magnitude is 11 m. If one calculates distortions from both models (i.e., slope of the settlement troughs), very large differences are noted in the computed values. Results with the HSS model predict larger distortion levels in relation to those computed with the HS model which evidences the importance of small strain soil behavior, not necessarily on the magnitude of settlements but in the computed influence zones and computed distortions from the settlement troughs.

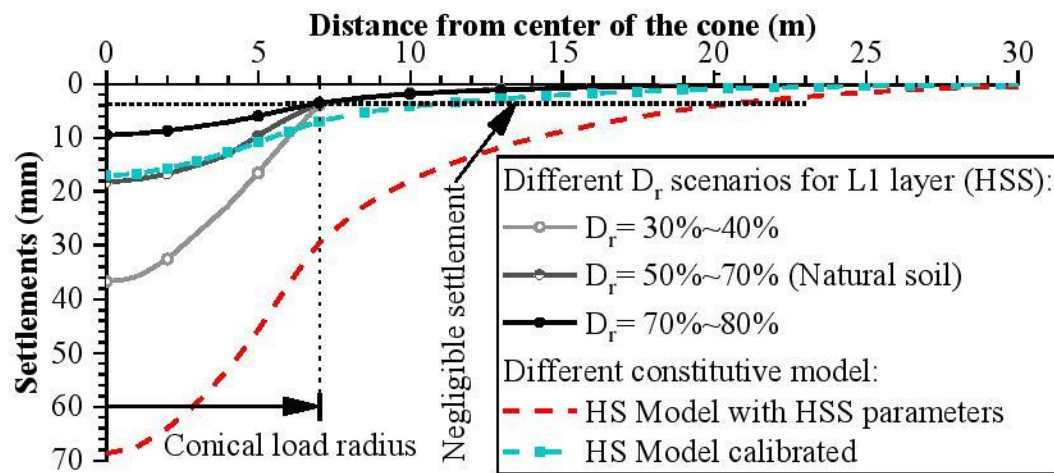


Figure 4. Effect of soil model and D_r selection of topmost layer on computed settlements

In Figure 5, the effects of conical loading material properties are parametrically varied leaving the supporting soil parameters unchanged. This is accomplished with the HSS model in terms of the computed settlement trough. In the figure, the variables changed for the conical loading material are the loading/construction sequence and the stiffness at which the loading material is placed. The loading/construction sequence was studied by adopting a diagonal and a horizontal loading path. For the conical loading stiffness, the material was assumed either as a “loosely deposited material” or a “compacted material.” This was accomplished numerically by varying the elastic properties of the conical loading in the computer model. The results showed how the conical loading sequence influences the computed settlements. By increasing the stiffness of the cone (see blue lines versus black lines), settlement decreases by approximately 40% which highlights how the conical loading stiffness (or in general, the stiffness of a

foundation or embankment for example) plays a very important role in the computed results. In terms of the horizontal influence zones, the computed variations are not critical since in every case, approximately negligible settlement (i.e., 3 mm) were computed at 8 m from the center of the cone.

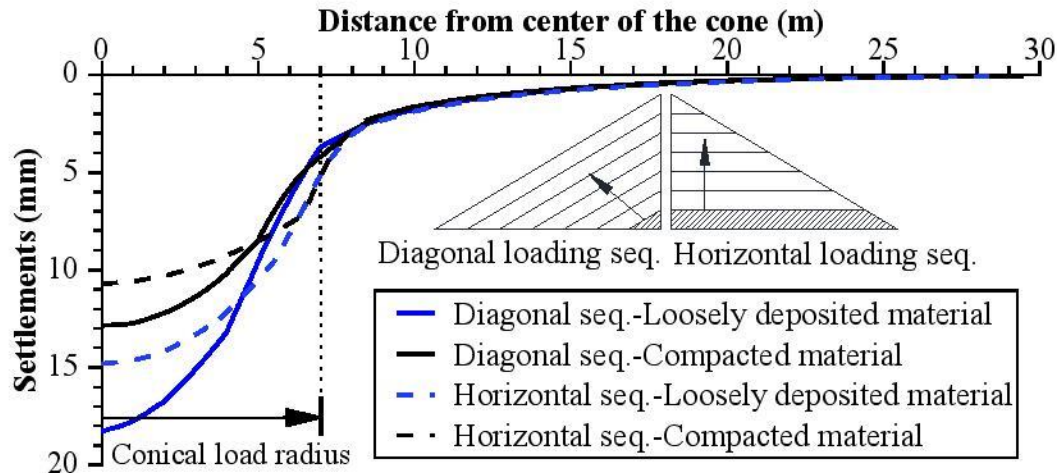


Figure 5. Effect of conical load construction method and stiffness on computed settlement with the HSS model

Figure 6 shows the relative shear stresses (defined in PLAXIS as a ratio of applied shear stress to soil shear strength) of the subsurface soil layers due to conical loading for different combinations of relative density of the topmost layer (L1), assumed constitutive soil model, and loading sequence. Regardless of the model or assumed parameters, conical loading mobilizes the shear strength of the material in a similar form beyond the *in situ* Ko-consolidated state of the material, where differences in the computed relative shear stress (τ_{rel}) below layer L2 (depth 11 m) were negligible. This notion was also confirmed from a Boussinesq-type analysis of the proposed conical loading in terms of the influence zone but in the vertical direction. Negligible differences in the τ_{rel} were computed regardless of the adopted topmost soil relative density or constitutive soil model used or conical loading sequence followed, which demonstrates that in terms of mobilized strength, every model provided similar results but noticeable differences were computed in terms of deformations and distortions.

Figure 7 provides summarized information regarding a validation conical load field test performed. The figure briefly shows the instrumentation layout and photographs of the conical load test performed at the project site. Porewater pressures and conical load pressures were continuously measured with piezometers and stress cells, respectively. Evolution of settlements in the center of the cone were measured using magnetic extensometers and vibrating wire settlement transducers. Lateral movements along the depth at the edge of the conical load were also monitored with an inclinometer to determine if soil wedge effects were caused laterally by the conical loading. The figure summarizes a comparison between field measurements and computed results with the HS and HSS models. The conical loading sequence adopted in the numerical model was determined to match the field test. Each data point in the figure represents a loading increment. Because of space limitations, further details about the conical load field testing are not provided in this paper but the figure indicates that there is a reasonable agreement between the field and computed results in this study.

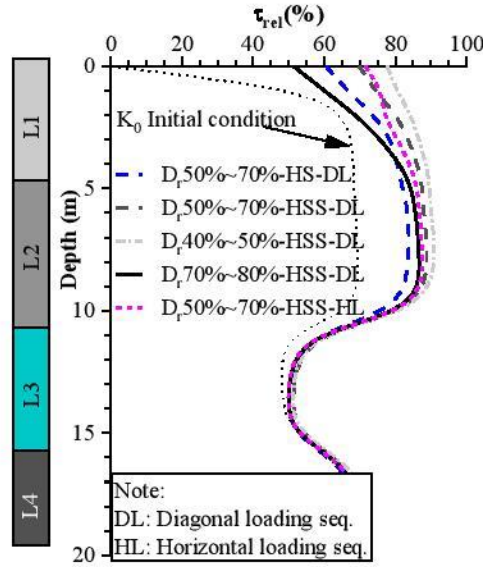


Figure 6. Variation of computed relative shear stress versus depth to show effects of topmost soil relative density, adopted constitutive soil model, and conical load sequence.

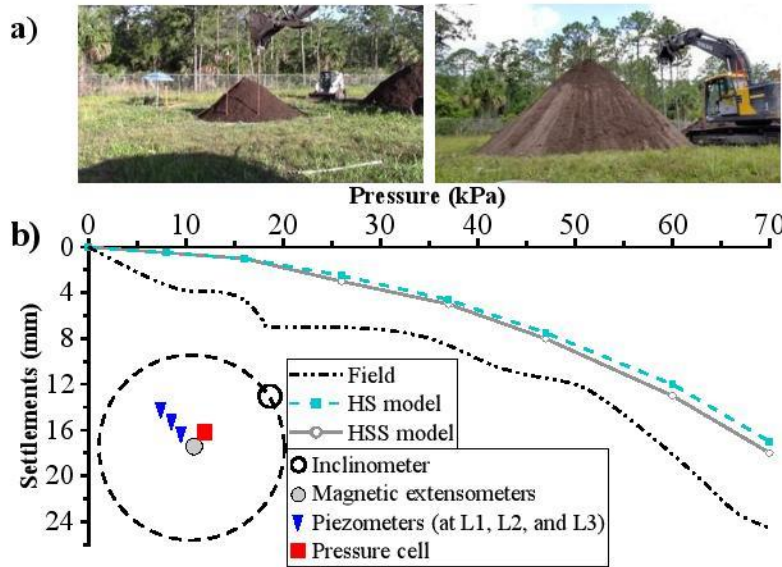


Figure 7. Conical loading field test results: a) sand cone construction and b) comparison computed versus measured settlements as conical loading is applied.

CONCLUSION

In this study, the effect of subsurface soil relative density, soil constitutive model, sand cone loading stiffness, and construction sequence on settlement on sandy soil on central Florida was investigated. The investigation was conducted by simulating the Schmertmann conical load test and validate the model by full scale, field test. Based on the simulation results, increasing the relative density of the top layer of soil by 20% from its natural relative density, settlement reduced by 50%. Also, decreasing the relative density by 20%, doubled the settlement. The results indicate that although settlement in HS and HSS model were relatively similar, HS model caused less distortion close to the sand cone edge. This notion is an evidence for importance of

small strain soil behavior.

The effect of sand cone properties such as stiffness and construction sequence was investigated by defining four scenarios which were the combination of loosely deposited versus compacted material, and diagonal versus horizontal loading, respectively. The results of these scenarios indicated horizontally loading the cone material caused less settlement, but larger distortion. Also, noticeably less settlement was computed when the cone was simulated via stiff material. Study of relative shear stress in soil layers in depth variations showed that the vertical influence zone of the cone is about 11 m since the differences between relative density in K_0 condition and the end of the test is minuscule in the depth lower than the mentioned depth. Regardless of the soil constitutive model, relative density, and cone properties, similar relative shear stress was computed, however the variations in deformations and distortions were significant.

ACKNOWLEDGMENTS

Financial support of the project was provided by the Florida Department of Transportation (FDOT), Grant No. BDV24 TWO 977-29. The support of the funding agency is greatly appreciated.

REFERENCES

- Anagnostopoulos, A. G., Papadopoulos, B. P., and Kawadas, M. J. (1991). "Direct estimation of settlements on sand, based on SPT results." *Proc., 10th Eur. Conf. Soil Mech. Found. Engrg.*, Vol. 1, Balkema, Rotterdam, The Netherlands, 293–296.
- Anderson, J., Townsend F., and Rahelison, L., (2007). "Load testing and settlement prediction of shallow foundation." *Journal of Geotechnical and Geoenvironmental Engineering*, 1492-1502
- Arboleda-Monsalve, L. (2014). "Performance, instrumentation and numerical simulation of One Museum Park West Excavation." *Doctoral dissertation*, Northwestern University.
- Arboleda-Monsalve A. G., Chopra, M., Marin-Savatier, S., Nassiri, S., "BDV24 977-29: Comparison of Standard Penetration Test (SPT) N-value with Alternative Field Test Methods in Determining Moduli for Settlement Predictions" State Materials Office, FDOT, Gainesville, FL.
- Blackburn, J. (2005). "Automated remote sensing and three-dimensional analysis of internally." *Doctoral dissertation, Northwestern University.*
- Bowles, J.E. (1987). "Elastic Foundation Settlements on Sand Deposits." *Journal of Geotechnical Engineering*, ASCE, Vol. 113, No. 8, pp. 846-860.
- D'Appolonia, D. J., D'Appolonia, E., and Brissette, R. F. (1970). "Settlement of Spread Footings on Sand." *Journal of the Soil Mechanics and Foundation Division*, ASCE, Vol. 96, SM2, pp. 754-761.
- Duncan, J., and Chang, C. (1970). "Nonlinear analysis of stress and strain in soils." *Soil Mechanics and Foundation Division*, 7513-7526.
- Hardin, B., and Drnevich, V., (1972). "Shear modulus and damping in soils: Design equations and curves." *Journal of the Soil Mechanics and Foundations Division*, 667-692.
- Hough, B.K. (1959). "Compressibility as the Basis for Soil Bearing Value." *Journal of Soil Mechanics and Foundations Division*, ASCE, Vol. 85, No. Issue 4, pp. 11-39.
- Imai, T., and Tonouchi, K. (1982). "Correlation of N-value with S-wave velocity and shear modulus." *Proc. 2nd European Symp. Of Penetration Testing*, (pp. 57-72). Amsterdam.

- Jamiolkowski, M., LoPresti, D., and Manassero, M. (2001). "Evaluation of relative density and shear strength of sands from CPT and DMT." *Geotechnical Special Publication*, 201-238.
- Janbu, N. (1963). "Soil compressibility as determined by oedometer and triaxial test." *European Conference on Soil Mechanics and Foundation Engineering*, (pp. 19-25). Essen, Germany.
- Kulhawy, F., and Mayne, P. (1990). "*Manual on estimating soil properties for foundation design.*" Report EL-6800, Electric Power Institute.
- Marchetti, S. (1985). "Determination of K_0 in sand." *XI ICSMFE, Panel Presentation*, (pp. 2667-2673). S. Francisco.
- Mayne, P. (2006). "In situ test calibrations for evaluating soil parameters." *Characterisation and Engineering Properties of Natural Soils conference*, 1601-1652.
- Mayne, P., and Poulos, H. (1999). "Approximate displacement influence factors for elastic shallow foundations." *Journal of Geotechnical and geo-environmental engineering*, ASCE, Vol. 125, No 6, pp. 453-460.
- Meyerhof, G. (1956). "Penetration Tests and Bearing Capacity of Cohesionless Soils." *Journal of the Soil Mechanics and Foundations Division*, 1-19.
- Meyerhof, G.G. (1965). "*Shallow Foundations.*" *Journal of the Soil Mechanics and Foundation Division*, ASCE, Vol. 91. No. SM2, pp. 21-31.
- Meyerhof, G. G. (1974). "*General Report: State-of-the-Art of Penetration Testing in Countries Outside Europe.*" *Proceedings of the 1st European Symposium on Penetration Testing*, Vol. 2.1, pp. 40-48.
- O'Loughlin, C. D., and Lehane, B. M. (2003). "Measurement and prediction of deformation patterns beneath strip footings in sand." *Proc., Int. BGA Conf. on Foundations, Thomas Telford, London, 705-714.*
- Oweiss, I.S. (1979). "*Equivalent Linear Model for Predicting Settlements of Sand Bases.*" *Journal of the Geotechnical Engineering Division*, ASCE, Vol. 105, No. GT12, pp 1525-1544.
- Papadopoulos, B.P. (1992). "*Settlement of Shallow Foundations on Cohesionless Soils.*" *Journal of Geotechnical Engineering*, ASCE, Vol. 118, No.3, pp. 377-393.
- Peck, R., Hanson, W., and Thornburn, T. (1974). "*Foundation Engineering.*" New York: John Wiley and Sons.
- Plaxis. (2018). "*PLAXIS 2D 2018 Material Manual.*" Delft, Netherland.
- Rix, G., and Stokoe, K. (1991). "*Correlation of initial tangent modulus and cone penetration resistance.*" *1st International Symposium on Calibration Chamber Testing/ ISOCCT1*, (pp. 351-362). New York.
- Robertson, P., and Cabal, K. (2015). "*Guide To Cone Penetration Testing*". 6th Edition.
- Robertson, P., and Campanella, R. (1983). "Interpretation of cone penetration tests." *Canadian Geotechnical Journal*, 718-733.
- Robertson, P., and Campanella, R. (1988). "*Guidelines for geotechnical design using CPT and CPTu data.*" Rep. No. FAWA-PA-87-014-84-24, Federal Highway Administration, Washington, D.C.
- Schanz, T., Vermeer, A., and Bonnier, P. (1999). "The hardening soil model: formulation and verification." *Beyond 2000 Comput. Geotech.* Amsterdam: 10 years PLAXIS Int. Proc.
- Schmertmann, J.H. (1970). "*Static Cone to Compute Static Settlement Over Sand.*" *Journal of the Soil Mechanics and Foundation Division*, ASCE, Vol. 96, No. SM3, pp. 1011-1043.
- Schmertmann, J.H. (1986). "*Dilatometer to Compute Foundation Settlement.*" *Use of Insitu Tests in Geotechnical Engineering*, ASCE, pp. 303-321.

Page intentionally left blank.